Hydrotreatment of Biomass and Waste Derived Hydrothermal and Pyrolysis Liquid Intermediates for the Production of Fuels and Lubricants

by

Poulami Roy

A dissertation submitted to the Graduate Faculty of
Auburn University
in partial fulfillment of the
requirements for the Degree of
Doctor of Philosophy

Auburn, Alabama
December 10, 2022

Keywords: Hydrotreatment, Heterogeneous catalysis, Biochar catalyst, Biolubricants, Hydrothermal liquefaction, Pyrolysis

Approved by

Sushil Adhikari, Chair, Professor, Department of Biosystems Engineering
Oladiran Fasina, Professor, Department of Biosystems Engineering
Robert L. Jackson, Professor, Department of Mechanical Engineering
Tae-Sik Oh, Assistant Professor, Department of Chemical Engineering

Abstract

Extensive use of crude oil resources in producing fuel, energy, and chemicals to sustain the growing world population has led to the depletion of natural resources and the release of greenhouse gas emissions leading to global warming and climate change. There is an indispensable need to maintain the development of lignocellulosic biomass and waste resources for biofuel and bioproduct conversion, as this could be the answer to energy security and the use of various domestic natural resources. The objectives of this dissertation were based on the perceived need to develop biofuels and high value bioproducts such as biolubricants from waste precursors and biomass produced from hydrothermal liquefaction (HTL) and pyrolysis after hydrotreatment over different heterogeneous catalyst supports.

First, hydrotreatment of non-edible vegetable oil (*Brassica Carinata*) was carried out over biochar-supported catalysts. These catalysts were developed from nickel (Ni) - and cobalt (Co)-nitrates and hydroxide salts. Nitrate-based (from water-soluble salts) and hydroxide-based (from water-insoluble salts) catalysts of Ni and Co were prepared via wetness impregnation and aqueous dispersion methods, respectively. The synchroton method showed nitrate-sourced metals were primarily dispersed in the pores, while the hydroxide-sourced metals were distributed mainly on the catalyst surface. The C=C saturation and cracking of triglycerides, decarboxylation, and hydrogenation of aromatic structures appeared to be dominant on the hydroxides of transition metals, taking place on the catalyst surface. However, methanation and dehydrogenation (thus aromatization) seemed to be a pore phenomenon, catalyzed more than nitrate-based catalysts. A reaction network was proposed based on chemical analysis of upgraded carinata oil and erucic acid model compound. Catalytic cracking followed by hydrotreatment performed better in fuel properties than other approaches in this study.

Since biochar-supported Co and Ni catalysts successfully hydrotreated carinata oil to produce biofuel, especially Co-produced better results than Ni. This further motivated us to utilize the same biochar support in the present study and introduce a bimetallic (cobalt and molybdenum) component instead of a monometallic (cobalt) component on the support and hydrotreat a mixture of oils (HTL algae and carinata) instead of only carinata. Therefore, in the present study, sulfided and unsulfided bimetallic (CoMo) catalysts on two supports (Douglas fir biochar support (DF) and alumina support (Al)) were used for hydrotreating a blend of HTL algae biocrude and carinata oil. Four types of catalysts were used: 1) alumina-supported CoMo (denoted as CoMo/Al, 2) sulfided alumina-supported CoMo (denoted as S-CoMo/A, 3) Douglas fir biochar (DF)-supported CoMo (denoted as CoMo/DF), and 4) sulfided DF-supported CoMo (denoted S-CoMo/DF). The main objective of this study was to understand the synergistic effect of the blending and the order of reactivity for different supports in terms of hydrodeoxygenation (HDO), hydrodenitrogenation (HDN), hydrodesulfurization (HDS) and hydrodemetallization (HDM). Results showed a synergistic effect when HTL algae biocrude and carinata oil blends are hydrotreated. The yield of the upgraded blend (UB) oils retrieved over the alumina catalyst was higher than the individual hydrotreated parent oils. For example, a 9% and 5% increase in yield was noted compared to the average of individual hydrotreated parent oils. The upgraded blends had higher heating value (syngas) was higher irrespective of the support type. The UB produced from sulfided CoMo/Al exhibited superior HDO activity primarily by decarbonylation. This was apparent in increased heating value, carbon addition, higher octane number, and lower total acid number than the oils obtained from the biochar-supported catalysts. Sulfided CoMo/DF catalyzed cracking reactions, which lowered the viscosity, followed by high HDN and HDS activity compared to the commercial catalyst. The two supports showed different sorption behaviors.

Interestingly, CoMo/DF had an effective sorption mechanism that helped increase metal removal from the oil. Additionally, presulfiding and DF support exhibited positive results in less coke formation. In brief, biochar supports have higher acidic sites, inorganic mineral oxides, ion exchange capacity, high surface area, pore structure and connectivity. All of these make a substantial contribution to its unique catalytic behavior.

This further motivated us to explore the alumina and DF biochar supports and carinata oil as one of the blending feedstocks for the hydrotreatment of more complex pyrolysis oil this time. Additionally, there needs to be more understanding of pyrolysis oil and vegetable oil/animal fat behavior when subjected to hydrodeoxygenation under different catalyst supports. Hence, this research aimed to assess the co-hydrotreatment of fast pyrolysis oil and carinata oil or poultry fat to identify synergistic effects, if any. Overall, the blended hydrotreated oil produced from biochar support showed a better positive synergistic effect in carbon and hydrogen addition, oxygen removal, HHV and viscosity. Biochar-supported catalysts demonstrated higher jet fuel fraction consisting mainly of paraffin and the lowest amount of light and heavy diesel. Oxygen was predominantly removed via dehydrogenation and methylation reactions, consuming more hydrogen. Alumina-supported catalysts removed oxygen predominantly via decarboxylation and decarbonylation reactions. A lower amount of coke formation was seen for biochar support. Large oxygen-containing functional groups, inorganic mineral oxides, high surface area, pore structure and acid sites make biochar-support catalysts better HDO catalysts compared to alumina-supported catalysts. On the other hand, blending the pyrolysis oil with poultry fat yielded better bio-oil quality over carinata oil due to the presence of C15 hydrocarbons. In summary, pyrolysis oil blended with poultry fat and hydrotreated using biochar support catalysts was more successful in

HDO activity and improving overall bio-oil quality than alumina-supported catalyst and carinata oil.

There is a need to support the biofuel sector by utilizing waste materials for its production and finding uses for co-products through an integrated approach. Due to bio-oils diverse composition, other applications of it are emerging, such as foams, resins and most importantly, biolubricants, a product with increasing global demand. Given the hydrocarbon chain number produced from the above objectives, these products can also be used as lubricants. This study produced four hydrocarbon biolubricants (HBL) via a hydrotreatment process. Two samples were produced using hydrothermal liquefaction (HTL) of algae (HAL) and sewage sludge (HSS), whereas the other two samples were from nonedible oil (carinata; HCA) and animal fat (poultry fat; HPF) and were evaluated for their tribological properties and compared with mineral base oil (MBO). These potential biolubricants samples had viscosity indices (VI) ranging from 197 to 254, pour points (PP) from -10℃ to -20℃, and Noack volatilities between 16% to 23%. The coefficient of friction (COF) for HAL and HSS was lower than MBO, HPF, and HCA, but the wear was high. Large amounts of oxygenates and olefins imparted higher viscosity index and pour points to HPF. Even though both HSS and HAL demonstrated higher amounts of paraffin, they exhibited lower thermo-oxidative stability, poor pour point, and higher volatility than other samples. HPF had the lowest wear, highest viscosity index and pour point but higher COF. In contrast, volatility and COF were predominantly dependent on cyclic structures, unsaturation, and heteroatoms. The results indicated that the hydrotreated bio-oil produced from HTL biocrude and waste precursors could be considered eco-friendly hydrocarbon biolubricants blend stock.

Acknowledgments

I would like to express my profound gratitude and deepest appreciation to my supervisor Dr. Sushil Adhikari for his unwavering support, invaluable guidance, and continuous feedback throughout my entire time at Auburn University. Without his support and encouragement this dissertation would not have seen the light of the day. I am equally thankful and gratefully indebted to Dr. Hossein Jahromi for his valuable suggestions to improve my dissertation and his time to coach me. I would also like to express my thankfulness to my colleague Tawsif Rahman for his invaluable assistance around the laboratory. I sincerely acknowledge the unflagging help from Dr. Oladiran Fasina for allowing me to use his lab space. My deepest thankfulness to Dr. Robert L. Jackson for permitting me to use his lab space and providing valuable suggestions to improve my dissertation. I would also like to extend my gratitude to Dr. Tae-Sik Oh for helping us with catalyst characterization. I would also like to thank Dr. Mark Hoffman for serving as the university reader.

I would like to recognize Alabama Agricultural Experiment Station and the Hatch program (ALA014-1-19068) of the National Institute of Food and Agriculture, U.S. Department of Agriculture and the Alabama Department of Economic and Community Affairs (ADECA-1ARDEF22 02) for supporting my study. Additionally, I would like to thank Dr. Austin Hagan for securing hexane-extracted Brassica carinata oil and Mrs. Courtney Garnder of Charles Miller Jr. Poultry Research and Education Center for providing poultry fat used in this study. My sincere acknowledgement goes to Dr. Zou Finfrock at Argonne National Laboratory, Chicago Illinois, Dr. El Barbary Hassan from Mississippi State University, Dr. Michael Miller from Life Sciences Department, Dr. Masoud Mahjouri-Samani from Electrical and Computer Engineering and Dr. Laura Bilenkar from Geosciences Department from Auburn University for helping me with my samples characterization.

I am thankful to all my past and present members of Dr. Adhikari's research group, my friends in Auburn and my extended family in the USA. I also extend my heartfelt gratitude to all technicians and research engineers in the Department of Biosystems Engineering at Auburn University for their invaluable assistance in conducting the experiments. I would also like to thank the Biosystems Engineering, Mechanical Engineering, Chemical Engineering, Electrical and Computer Engineering, Life Sciences and Geosciences Department for giving me this opportunity to pursue my doctoral degree. Finally, I express my sincere thanks to my parents, brother, sister - in-law and my nephew, for providing me with unfailing support and encouragement throughout my years of study.

Table of Contents

List of Tables

List of Figures

List of Abbreviations

AD	Aqueous deposition method
ASC	Alumina supported catalysts
BCA/AL	Hydrotreated blend of pyrolysis oil and carinata oil over cobalt molybdenum catalyst supported on alumina
BCA/DF	Hydrotreated blend of pyrolysis oil and carinata oil over cobalt molybdenum catalyst supported on Douglas fir biochar support.
BL/BLs	Biolubricant/Biolubricants
BPF/AL	Hydrotreated blend of pyrolysis oil and poultry fat over cobalt molybdenum catalyst supported on alumina
BPF/DF	Hydrotreated blend of pyrolysis oil and poultry fat over cobalt molybdenum catalyst supported on Douglas fir biochar support.
BSC	Biochar supported catalysts
CA/AL	Hydrotreated carinata oil over alumina supported catalyst
CA/DF	Hydrotreated carinata oil over biochar supported catalyst
CC	Catalytic cracking carried out under N_2 gas
CC-HYD	Catalytic cracking followed by hydrotreatment carried under H_2 gas
CFP	Cold flow properties
COF	Coefficient of friction
CoMo/Al	Cobalt molybdenum supported on alumina
CoMo/Al	Cobalt molybdenum supported on alumina
CoMo/DF	Cobalt molybdenum supported on Douglas Fir biochar
CoMo/DF	Cobalt molybdenum supported on Douglas Fir biochar
$CONO_3$/DF	Cobalt nitrate metal impregnated in biochar support
CoOH/DF	Cobalt hydroxide metal deposited on the biochar support
DF	Douglas fir biomass
DF	Douglas fir biochar support
HAL	Hydrotreated algae bio-oil produced from hydrothermal liquefaction process
HBL	Hydrocarbon biolubricants
HCA	Hydrotreated carinata bio-oil
HPF	Hydrotreated poultry fat bio-oil
HSS	Hydrotreated sewage sludge bio-oil from hydrothermal liquefaction process
HTL	Hydrothermal liquefaction

HYD	Direct hydrotreatment carried out under H_2 gas
HYD	Hydrotreatment/hydrogenation
IP	Wetness impregnation method
MBO	Mineral base oil
$NINO_3$/DF	Nickel nitrate metal impregnated in biochar support
NiOH/DF	Nickel hydroxide metals deposited on the biochar support
OS	Oxidative stability
PF/AL	Hydrotreated poultry fat over alumina supported catalyst
PF/DF	Hydrotreated poultry fat over biochar supported catalyst
PP	Pour point
PY/AL	Hydrotreated pyrolysis oil over alumina supported catalyst
PY/DF	Hydrotreated pyrolysis oil over biochar supported catalyst
RDF	Reduced Douglas fir biochar
S-CoMo/Al	Sulfided cobalt molybdenum supported on alumina
S-CoMo/DF	Sulfided cobalt molybdenum supported on Douglas Fir biochar
TAN	Total acid number
TGA	Thermogravimetric analysis
UA	Upgraded/hydrotreated algae oil
UB	Upgraded/hydrotreated blend of algae and carinata oil
UBO	Upgraded/hydrotreated blended oil
UC	Upgraded/hydrotreated carinata oil
VI	Viscosity index

CHAPTER

1 INTRODUCTION

1.1 Background

The detrimental effects of climate change are cumulative and gradual [1]. The climate change crisis could take years, decades or even centuries to be noticeable. Therefore, to prepare ourselves for an impending global climate crisis, we need to secure energy from sources that can be continuously replenished. Renewable and enormous waste resources must be valorized to generate biofuels and bioproducts to complement fossil-based sources. This, in turn, can promote jobs and innovation and boost the economy. Long-distance transportation of low-density feedstock needs to be minimized. Thus, there is a need to promote the utilization of local biomass resources. Valorization of these resources in local biorefineries can help to produce energy, biofuel and bioproducts [2]. According to the labor organization, about 24 million new green jobs will be generated by 2030 [4]. Therefore, local and international cooperation must be established to synergistically unite competencies and shared goals to accelerate the transition to a bio-based, greener future [2].

As an intelligent and adaptive species, we must find solutions and strategies to lower global carbon dioxide (CO_2) emissions (energy-related) to zero by 2050 and limit global temperature rise to 1.5℃. Biofuels, which lower CO_2 emissions by at least 50% compared to fossil fuels, are crucial to reducing this sector's environmental footprint [5]. Ethanol and biodiesel are 1st and 2nd generation biofuel technology, while cellulosic and algae-based are 3rd and 4th generation biofuels. Even after 20 years of development, biofuel cost continues to be higher than fossil fuel cost, with

the effect of slowing down the rate of commercialization of bio-based conversion processes. Issues such as diverse feedstock, handling issues, conversion strategies, and upgrading processes, among others, have contributed to this relatively high biofuel cost. One solution to lowering the biofuel cost is to utilize waste materials and the co-products from the conversion process using an integrated approach. Due to its diverse composition, bio-oil applications, such as foams, resins and, most importantly, bio-lubricants, are emerging. One strategy for addressing this challenge is to generate valuable co-products alongside biofuels [6]. Co-products produced from bio-oil include bio-alcohols, bio-lubricants, bio-solvents, bio-based acids, bio-surfactants, bioplastics, and others [7]. The bio-lubricant sector is garnering rapid incentives due to its exceptional 'environmental benignity' [7], and the market size is projected to grow from USD 2.0 billion in 2020 to USD 2.4 billion by 2025. A key component of developing a diverse, robust, and resilient bioeconomy is the establishment of integrated biorefineries, where biomass is converted into fuels, power, and chemicals. Chemicals and materials produced alongside biofuels can improve the overall economics of the refinery process [9].

1.2 Research Objectives

The core objective of this research was to develop new catalytic pathways for the conversion of renewable and waste feedstocks such as hydrothermal liquefaction (HTL) sewage sludge biocrude, HTL algae biocrude, poultry fat, non-edible oil, pyrolysis oils and their blends to biofuel and biolubricants and to understand the chemistry of heterogeneous feedstocks over alumina and carbon supported catalysts. This study has four specific sub-objectives to meet the core objective of this study proposed herein.

1.2.1 Performance of biochar-assisted transition metal catalysts during hydroprocessing of vegetable oil for transportation fuels.

The first objective is a comparative study between two different catalyst synthesis methods: the wetness impregnation method and the aqueous deposition method on biochar-supported catalysts to hydrotreat inedible vegetable oil (Brassica Carinata).

1.2.2 Understanding the effects of feedstock blending and catalyst support on hydrotreatment of algae HTL biocrude with non-edible vegetable oil

In the second objective, bimetallic salts (CoMo) on two types of support (Al_2O_3 and Douglas fir biochar), either sulfided by H_2S gas or un-sulfided, were used for hydrotreating a blend of carinata and hydrothermal liquefied (HTL) algae biocrude. This study evaluated the synergistic effects and also studied the order of reactivity for different supports in terms of hydrodeoxygenation (HDO), hydrodenitrogenation (HDN), hydrodesulfurization (HDS) and hydrodemetallization (HDM).

1.2.3 Overview of support effects in hydrotreating a blend of pyrolysis oil with triglycerides.

The third objective was an extension of the second objective, where a more complex bio-oil produced from pyrolysis was hydrotreated with a blend of two different sources of triglycerides, such as non-edible vegetable oil and poultry fat. Hydrodeoxygenation was studied over different catalyst supports.

1.2.4 Hydrocarbon biolubricants from hydrotreated renewable and waste derived liquid intermediates

Finally, in the last objective, hydrotreated bio-oils produced from poultry fat, sewage sludge, algae, and an inedible oil were tested for their tribological properties at the boundary lubrication regime.

The overall conclusions of the parts and recommendations for future work are summarized in Chapter 7.

1.3 References

[1] "Covid map: Coronavirus cases, deaths, vaccinations by country," *BBC News*, Jul. 05, 2022. Accessed: Sep. 30, 2022. [Online]. Available: https://www.bbc.com/news/world-51235105.

[2] C. C. Schmitt, F.G. Fonseca, M.M Fraga, S. Karp , "Thermochemical and Catalytic Conversion Technologies for the Development of Brazilian Biomass Utilization," *Catalysts*, vol. 11, no. 12, Art. no. 12, Dec. 2021, doi: 10.3390/catal11121549.

[3] "Addressing climate change post-coronavirus | McKinsey." https://www.mckinsey.com/capabilities/sustainability/our-insights/addressing-climate-change-in-a-post-pandemic-world (accessed Sep. 30, 2022).

[4] Martin, "Green economy could create 24 million new jobs," *United Nations Sustainable Development*, Apr. 03, 2019. https://www.un.org/sustainabledevelopment/blog/2019/04/green-economy-could-create-24-million-new-jobs/ (accessed Sep. 30, 2022).

[5] "Committed to the Future of Bioenergies," *TotalEnergies.com*. https://totalenergies.com/group/energy-expertise/exploration-production/committed-future-bioenergies (accessed Sep. 22, 2021).

[6] "Moving toward the future with sustainable biofuels," *Neles.com*. https://www.neles.com/insights/blogs/2020/moving-toward-the-future-with-sustainable-biofuels/ (accessed Sep. 22, 2021).

[7] R. and M. ltd, "Biolubricants - Global Market Trajectory & Analytics." https://www.researchandmarkets.com/reports/1824122/biolubricants_global_market_trajectory_and (accessed Sep. 22, 2021).

[8] T. Cordero-Lanzac, J. Rodríguez-Mirasol, T. Cordero, and J. Bilbao, "Advances and Challenges in the Valorization of Bio-Oil: Hydrodeoxygenation Using Carbon-Supported Catalysts," *Energy Fuels*, vol. 35, no. 21, pp. 17008–17031, Nov. 2021, doi: 10.1021/acs.energyfuels.1c01700.

[9] "Bioproduct Basics," *Energy.gov*. https://www.energy.gov/eere/bioenergy/bioproduct-basics (accessed Nov. 19, 2022).

CHAPTER

2 LITERATURE REVIEW

2.1 Introduction

Currently, 80% of energy is produced from fossil fuels, with energy consumption projected to increase to 16,000 million tons of oil equivalent by 2040 [1]. However, the projected share of renewable resources will be only 30% by the end of 2040 [2]. Therefore, there is an urgent need to develop a sustainable energy model that ensures energy security, mitigates climate change, and helps develop novel bio-products. In this scenario, biomass can play a pivotal role in producing biofuels, biochemicals, and bio-products. Moreover, it can help in the management of agricultural and forest waste as well. Figure 2.1 shows a biorefinery scheme where bioproducts can be produced alongside biofuels [1], [3], [4]. The figure demonstrates the conversion of lignocellulosic biomass into energy, chemicals, and materials via thermochemical conversion (gasification, pyrolysis. hydrothermal liquefaction) and biochemical conversion processes (anaerobic digestion).

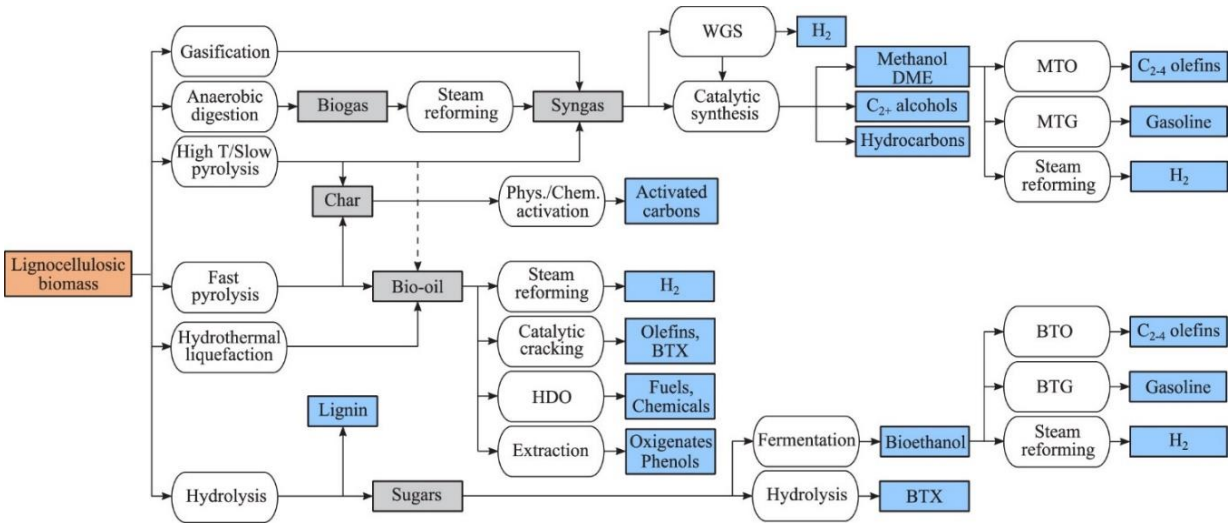

Figure 2.1 Biorefinery scheme and routes for the valorization of lignocellulosic biomass [1] (Legends: HDO=hydrodeoxygenation, BTX= benzene, toluene and xylene, MTO= methanol to olefin MTG=methanol to gas, DME= Dimethyl ether, BTO=bioethanol to olefin BTG= bioethanol to gas).

2.2 Thermochemical processes

Pyrolysis (fast and slow), gasification, and hydrothermal liquefaction (HTL) are some of the possible routes for biomass valorization, as shown in Figure 2.1. Pyrolysis of biomass has been studied extensively by many authors. This process produces bio-oil, char, and non-condensable gas. The yield of bio-oil depends on pyrolysis conditions and process parameters. The three types of pyrolysis process are defined below [5]– [7]:

- Slow pyrolysis: low temperature (300℃), low heating rate (1 K s-1): 35% oil, 35% char and 30% gas.
- Intermediate pyrolysis: moderate temperature (500℃) and moderate heating rate (1-10 K s-1): 50% oil, 20% char and 30% gas.
- Fast pyrolysis: moderate temperature (500℃) and fast heating rate (> 10 K s-1): 75% oil, 12% char and 13% gas.

In contrast, HTL is performed for feedstock with high water content at lower temperatures and higher pressure than pyrolysis [8]. Water acts as a solvent and reactant. It is done near its critical point (Tc= 374℃ Pc= 22.1 Mpa), which leads to a low dielectric constant and increased solubility of the organic phase [9]. Depolymerization of biomass, decomposition of biomass monomers by cleavage, dehydration, decarboxylation, and deamination, followed by recombination of reactive fragments [1]. In terms of the yield, a study reported that bio-oil yield from HTL decreased from 67% (mass fraction) at 220℃ to 59% (mass fraction) at 310℃. In contrast, the bio-oil yield from pyrolysis increased from 53% at 400℃ to 60% at 550℃ for algae feedstock (*Chlamydomonas reinhardtii*) [5]. An overall lower amount of water, nitrogen and oxygen content was seen in HTL bio-oil compared to pyrolysis bio-oil.

2.3 Requirement for Bio-Oil Upgrading

Bio-oil and biocrude produced from either pyrolysis or HTL process have considerable amounts of moisture, heteroatoms (oxygen, nitrogen, sulfur), heavy metals and oxygenated compounds (carboxylic acids and alcohols). Unprocessed bio-oils consist of 15-30% moisture in the feedstock, which decreases its heating value and delays the ignition. Sulfur and nitrogen in the bio-oil release SO_X and NO_X upon combustion, respectively [10]–[12]. Condensation and polymerization reactions occur in the presence of carboxylic acids, increasing the bio-oil acidity and viscosity and decreasing the bio-oil heating value. Apart from acids, other oxygenated compounds such as phenolics, furans, ketones, aldehydes, polyols and alkali and alkaline earth metals like Na, K, Ca and Mg make bio-oil highly unstable and impart high wear to engines, refineries, fuel pumps meters and piping systems respectively [10], [13], [14]. These properties make bio-oil/biocrude unsuitable for "drop-in" transportation fuel.

Therefore, to reduce the oxygen, nitrogen and sulfur, the bio-oil must undergo an upgradation process. Various catalytic upgradation routes are used, namely hydrotreatment, hydrocracking, catalytic cracking, esterification, and transesterification. In contrast, non-catalytic routes are emulsification, solvent addition, supercritical fluid addition, and electrochemical stabilization (Figure 2.2) [15]. The hydrotreatment (HYD) route is majorly used among all the routes. Removal of oxygen, nitrogen, sulfur, and metals is termed hydrodeoxygenation (HDO), hydrodenitrogenation (HDN), hydrodesulfurization (HDS) and hydrodemetallization (HDM) (Figure 2.3) [16].

2.4 Hydrodeoxygenation process to produce green diesel

Green diesel is a type of upgraded bio-oil, and it is produced from edible and non-edible vegetable oils or waste cooking oils. Figure 2.4 shows the reaction mechanism, and it can be seen

that at first, a saturation of double bonds in aliphatic chains of triglycerides takes place, followed by cleavage of C-O bonds. This produces propane molecules and three fatty acids. Subsequently, by HDO, decarbonylation (DCO), and decarboxylation (DOCx) reactions, intermediate oxygenated products such as fatty alcohol and aldehyde are produced. Then, light hydrocarbons or even waxes are formed depending on the catalyst and operating conditions. CO_2 and CO gas are formed, followed by methanation and water gas shift reactions. These reactions are undesirable since it increases the consumption of hydrogen.

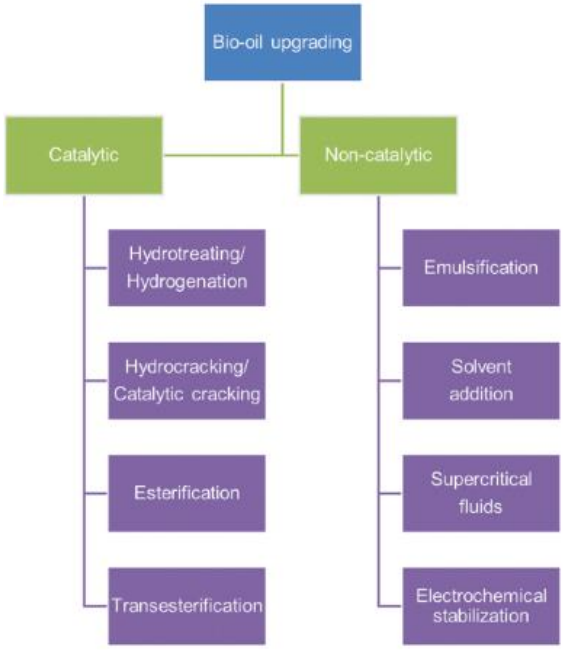

Figure 2.2 Catalytic and noncatalytic techniques used for bio-oil upgrading [10].

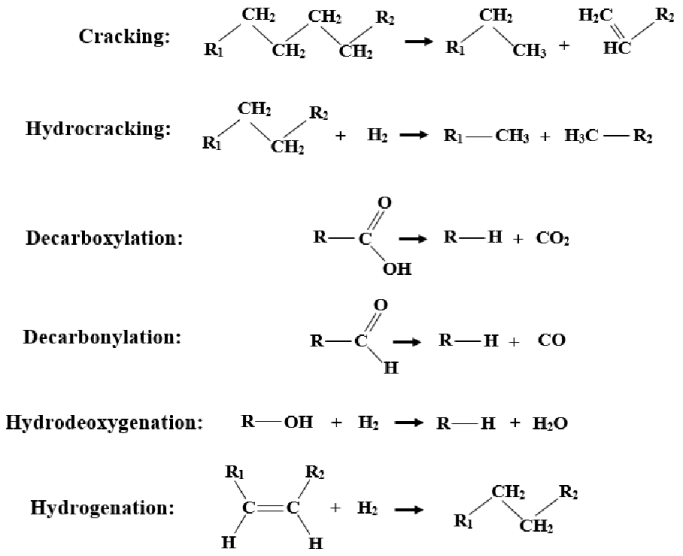

Figure 2.3 Reactions associated with catalytic HDO process [18].

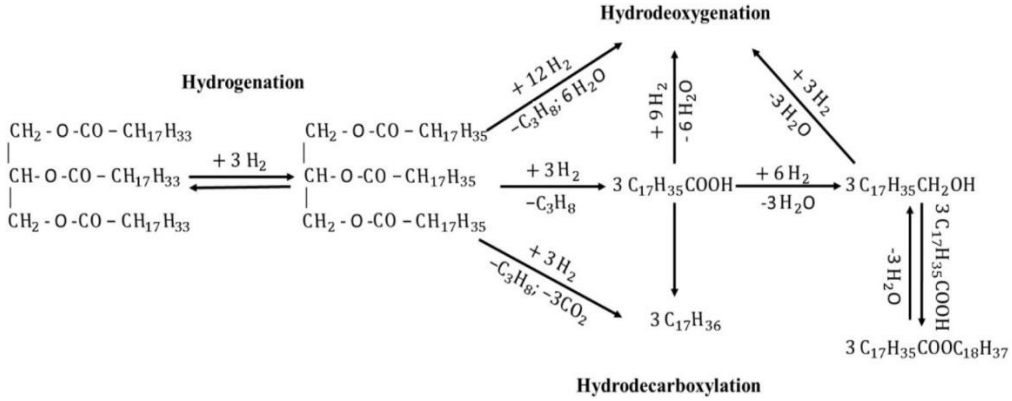

Figure 2.4 Reaction scheme for the conversion of triglycerides into hydrocarbons [19].

2.5 Effects of process parameters on hydrotreatment

The commonly investigated temperature for HYD is between 250-400℃. Since HDO is an exothermic process, temperatures above 450℃ are not desirable, and it even tends to form coke and eventually catalyst deactivation [17], [20]. Ramesh et al. [21] carried out catalytic HDO of jojoba oil over NiMoS/ mesoporous zirconia silica and found that increasing the temperature over 350℃ resulted in lower yield but higher hydrocarbon production. High hydrogen pressure (10-30

MPa) and high temperature are necessary for the catalytic HYD process [22]. High H_2 pressure ensures good H_2 solubilization and stabilizes unstable high molecular weight fractions [17], [23]. Pourzolfaghar et al. [23] investigated that varying the H_2 volumetric flow from 0 ml/min to 900 ml/min for HDO of phenol over Zn/SiO_2 at 500℃ increased the conversion from 30% to 80% at 150 ml/min. However, above 150 ml/min, the phenol and the oil yield were reduced due to the saturation of the catalyst surface by H_2 adsorption. Also, high H_2 pressure can limit the coke formation. A weight hourly space velocity (WHSV) or shorter contact time lowers HDO efficiency. A study by Ramesh et al. [17], [24] reported that increasing WHSV from 0.5h to 2h for HDO of jatropha oil (350℃ and 30 bar) the yield reduced from 95% to 65% and selectivity reduced from 30% to 15% for C17 hydrocarbons.

Solvents can be categorized into H_2 bond donors (methanol, ethanol, propanol, and butanol), H_2 bond acceptor (acetone, ethyl acetate and tetrahydrofuran), hydrocarbon (hexane) and water [28], [39]. The solvent's polarity and polarizability dictate the reactants' absorption strength and the final bio-oil yield and quality. Solvents are used as a hydrogen donor to replace costly H_2 gas during HYD treatment. Ethanol solvent was used in a study for HDO of fast pyrolysis of bio-oil at 350℃ over Ru/C [25]. The usage of the solvent resulted in an increase in HHV from 21 MJ/kg to 38 MJ/kg, a reduction in molecular weight and ethanol helped in the reduction of polymerization reactions.

2.6 Hydrotreating catalysts

Mixed sulfides of CoMo, NiMo or NiW supported on γ alumina are generally used for hydrotreatment reactions. Sulfided NiMo is preferred for HDN and HDO, while CoMo is excellent for HDS activity [26], [27]. For sulfided CoMo and sulfided NiMo supported over alumina, the Co and Ni act as a promoter and donates an electron to the Mo atom, which weakens the bond

between Mo and S that creates an S vacancy site, and this is reported to be an active site during HDO process [26], [28]. Increasing the concentration of Ni or Co does not increase the number of sulfur vacancies but creates more vacancies with higher HYD activity compared to unpromoted molybdenum sulfide catalysts [18], [29]. Unlike fossil fuels, biomass has limited to zero sulfur; therefore, during HYD, the sulfur form of CoMo and NiMo cannot be maintained, and these are transformed into corresponding oxide forms. Adding sulfur to the system causes sulfur leaching in the biofuel and subsequent catalyst poisoning [30], [31]. Apart from metal sulfide and oxide catalysts, noble metals such as Pt, Pd, Rh and Ru have a higher catalytic activity or hydrogenation activity than transition metal sulfided catalysts. Wild shut et al. [32] achieved a 60% deoxygenation rate for crude pyrolysis oil at 350℃ for 60 min over Pd/C [17]. However, noble metals are sensitive to sulfur poisoning and have a higher price than transition metals, which has restricted their commercialization. Furthermore, metal phosphides and metal carbides are also developed for the HYD of bio-oils.

2.7 Active phase of catalysts

Active sites of catalysts have been a matter of great discussion. The function and location of Co or Ni is the central area of debate. The Co-Mo-S model is widely accepted now among other models. Ratnasamy and Sivanskar first proposed this model, and the first experimental evidence was based on IR studies by Topsee [26], [33], [34]. The structural models for Co-Mo-S are based on the ratio of Co to Mo, and the commercial catalysts lie between both extremities (Figure 2.5A). Figure 2.5A shows that other species exist besides Co-Mo-S, such as bulk Co sulfide, unpromoted MoS_2 and $CoAl_2O_3$ interacting species. Two different Co-Mo-S structures are proposed by different authors [27], [35], [36] based on the low and high activity forms. Type I is for low activity, and type II is for high activity. Based on catalyst preparation methods, activation, support

types, presence of additives and metal loading, single and multiple slabs of Co-Mo-S structures were reported in the literature [37]. Single slabs type I Co-Mo-S were seen for alumina-supported catalysts. In this type, the slab interacts strongly with the support via Mo-O-Al linkages at the edges [27], [34], [36]. Co-Mo-S I is incompletely sulfided due to remaining Mo-O-Al linkages to the support. The linkages are formed due to interaction between the Mo and alumina OH groups during the calcination process, leading to the formation of oxygen-bridged monolayer slabs that are difficult to completely sulfide [37]. One of the merits of strong interaction is beneficial for high MoS2 dispersion [38].

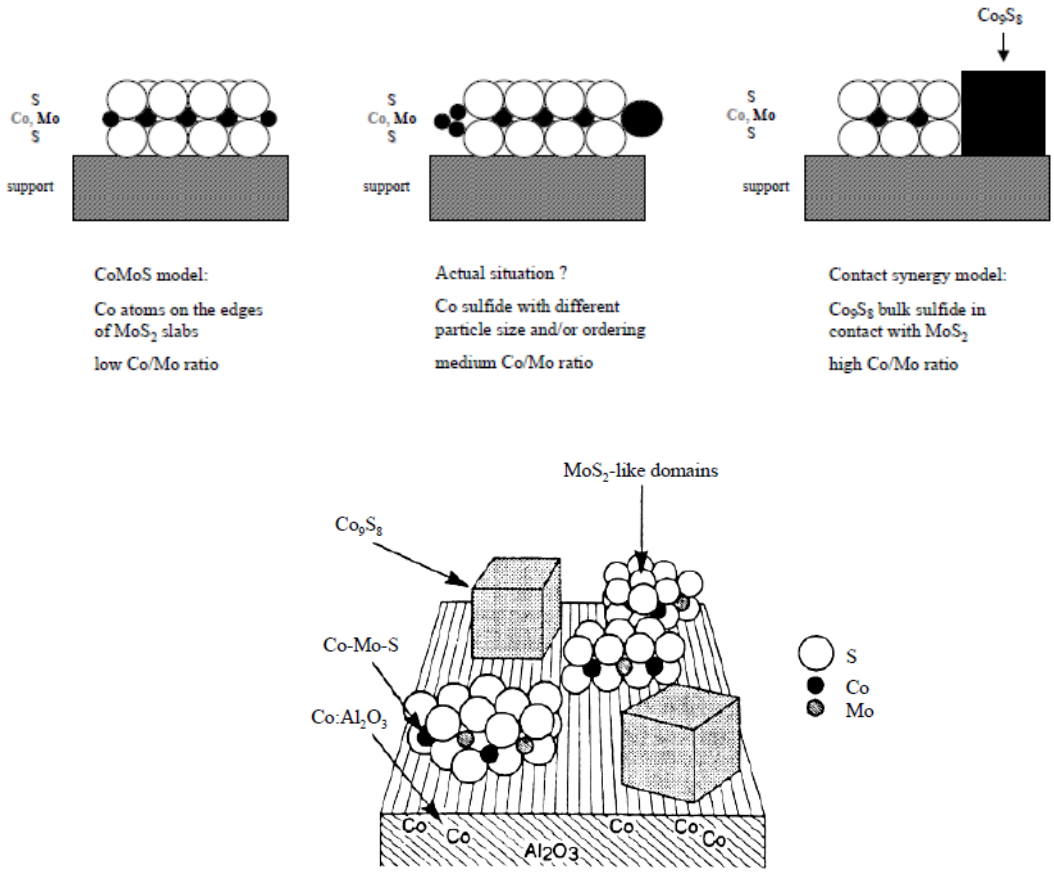

Figure 2.5 (A) Relation between different proposed models for the active phase in CoMo catalysts (B) Schematic picture of different phases present in a sulfided alumina supported CoMo catalyst [26].

While in Co-Mo-S II (multi slabs), the phases are fully sulfided and consist of stacked MoS2 particles that interact weakly with the support via Van der Waals interactions [38]. The degree of staking in MoS2 can be controlled by support type and catalyst preparation parameters and methods. Co-Mo-S II is twice more active than Co-Mo-S I during HDS of thiophene [26], [39]. Sulfided CoMo and NiMo catalysts supported on activated carbon demonstrated superior HDS activity compared to alumina because of the type II CoMoS phase [38], [40], [41].

2.8 Catalyst Supports

Promoters such as Cobalt or Nickel on molybdenum sulfide supported on alumina are used as industrial hydrotreating catalysts [42]. Alumina has excellent textural and mechanical properties, high thermal stability, contains acidic and basic sits and is cheap [43], [44]. However, it was reported that alumina is not an inert carrier and depending on the catalyst preparation conditions, the promoter reacts with the support to form $CoAl_2O_4$($NiAl_2O_4$). Increasing the sulfiding temperature, the Co-Mo-S I phase changes to Co-Mo-S II for alumina support [45]. Therefore, the strong interactions have urged the researchers to develop other supports.

Carbon supports are preferable because of their surface inertness, which facilitates sulfidation, reduction, and calcination. Apart from that, some of its advantages are high thermal conductivity, tunable pore structure, surface chemistry, high metal dispersion, large specific surface area and controlled volume [38]. Carbon supports stabilize CoMoS active phase [38], [46]. This support allows for the modification of functional groups by bonding extra heteroatoms on their surface [47]. These functional groups on carbon support can act as an anchoring site for the active phases or act as an active phase during catalytic reactions [47]. Activated carbons, biochar, multiwalled carbon nanotubes and nanofibers are being used as a support [42], [39],[31],[47]. More recently, uniform carbon structures such as ordered mesoporous carbons, carbon spheres and

graphene have been the subject of increasing interest [32]. CoMo supported on carbon was more active in HDS of DBT and 4,6 DMDBT than alumina. Incorporating both supports can decrease the interaction between the phases. However, carbon supports are not used in industries because of their low density, low mechanical strength, small micropore volume, non-uniformity in shape and size and high-pressure drop-in reactors [47]. Also, weak interaction with the support can cause metal sintering that causes loss of catalytic activity; hence surface modifications are necessary. Among different carbon supports, biochar-supported catalysts are attractive because it is environmentally friendly, followed by an excellent geometric effect (size, morphology), electronic effect (charge transfer), interfacial reactivity and finally, the support acting as an active site [48], [49].

Biomass can be converted into biochar via pyrolysis, hydrothermal carbonization, activation, and template methods. It is rich in oxygenated functional groups such as OH and COOH. It helps anchor metals impregnated in it via the wet process, sol-gel method, and vapor deposition method, among others [49]. Large pore size and high specific surface area help in the absorption of the reactants and dispersion of the metals. For example, the catalytic conversion of 4 nitrophenols to 4 aminophenols can be done within 3 min by Pd/ biochar from sawdust compared to commercial Pd/C and the conversion rate increased by 33% for Pd/biochar [49], [50]. The oxygen content of the biochar reduces the hydrophobicity compared to activated carbon supports. Many oxygenated functional groups produce acidic sites during the reduction process and help hydrogenate C=O bonds [48],[49]. However, biochar has a limited surface area and underdeveloped pores, which needs activation.

2.9 Catalyst Deactivation

Catalyst deactivation is the most technical critical barrier faced during the hydrotreatment process (Figure 2.6). Deactivation occurs due to poisoning, coking, support pore blockage, thermal degradation, and sulfide loss [17], [49]. Deactivation can be temporary or permanent and depends on the catalyst type and operating conditions. *Poisoning* is the chemisorption of reactants or impurities on the active sites. For example, complete hydrodemetallization is often tricky, so metals in low concentration can cause poisoning. For instance, it was reported that vanadium could be deposited on $CoMo/Al_2O_3$ and $NiMo/ Al_2O_3$ at 1mgh-1 kg-1 [55]. Vanadium competes with Ni and Co and active sites, forms V5S8 and VMO4S8, and blocks the pores [55]. Similarly, Fe, which is present in abundant renewable feedstocks, form species such as FeMoO4, CoFe2O4, NiFe2O4 and FeAl2O4 [57]. Coking is defined as the coverage or blocking of active sites and micropores due to strong chemisorption of carbonaceous materials as a monolayer and physical adsorption of carbon particles as multilayers [18], [52]. Reduction in surface area, pore volume and catalyst structure disintegration occur due to coke buildup. It is a faster reaction, and 30% of catalyst pores can be blocked during the initial stage of HDO [18], [55], [56]. Olefins and aromatics are the main precursors for coke formation [18], [57], [58]. A possible mechanism for coke formation is illustrated in Figure 2.6. Phenolics are the main precursors for coke formation, but high temperatures above 450°C also favor coke formation. The acidity of catalysts is a significant factor in coke formation [17], [59]. High temperature can cause catalyst deactivation via three processes: 1) growth of active metal phases results in loss of dispersion, 2) support pore collapse, and 3) transformation of active phase to inactive phases due to cold phase chemical reactions [18], [52]. The last two processes are known as sintering, which can happen during catalyst preparation, reduction, presence of hot spots or regeneration [60]. Therefore, prevention is necessary.

To prevent coke formation, it is necessary to co-feed the bio-oil with a hydrogen donor solvent such as methanol, ethanol, and tetralin. The solvents can help dilute the phenolics or other reaction intermediates, ultimately preventing polymerization reactions. The literature has reported that using an activated carbon-supported catalyst helps remove oxygen at low H_2 consumption, and it has a strong resistance to coke formation. Compared to alumina support, the hydrophobic nature of activated carbon support can restrict catalyst deactivation by restricting metal particles do not come in contact with water. HYD experiments conducted at low temperatures (<350℃) and high partial pressure of hydrogen can reduce coke deposition [17], [18], [61].

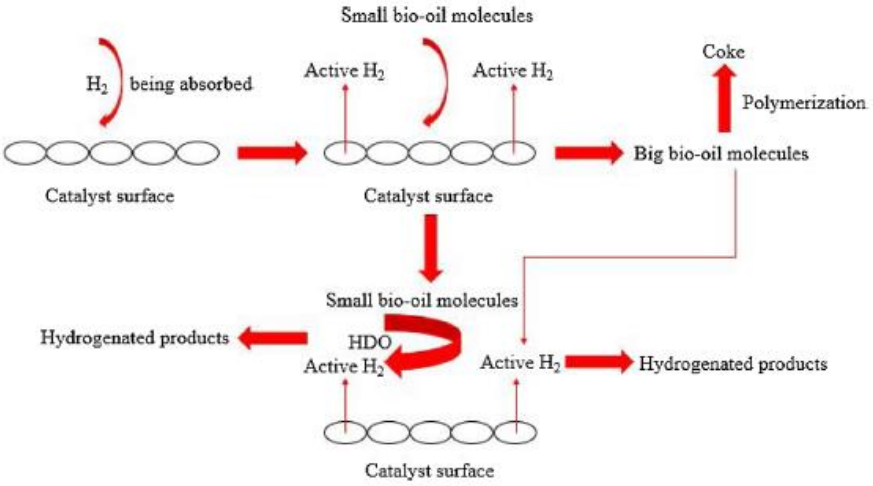

Figure 2.6 A possible reaction mechanism for the coke formation during catalytic HDO of bio-oil. [17], [62].

2.10 References

[1] T. Cordero-Lanzac, J. Rodríguez-Mirasol, T. Cordero, and J. Bilbao, "Advances and Challenges in the Valorization of Bio-Oil: Hydrodeoxygenation Using Carbon-Supported Catalysts," *Energy Fuels*, vol. 35, no. 21, pp. 17008–17031, Nov. 2021, doi: 10.1021/acs.energyfuels.1c01700.

[2] D. Guban, I. K. Muritala, M. Roeb, and C. Sattler, "Assessment of sustainable high temperature hydrogen production technologies," *Int. J. Hydrog. Energy*, vol. 45, no. 49, pp. 26156–26165, Oct. 2020, doi: 10.1016/j.ijhydene.2019.08.145.

[3] F. Cherubini, “The biorefinery concept: Using biomass instead of oil for producing energy and chemicals,” *Energy Convers. Manag.*, vol. 51, no. 7, pp. 1412–1421, Jul. 2010, doi: 10.1016/j.enconman.2010.01.015.
[4] G. Dragone, A. A. J. Kerssemakers, J. L. S. P. Driessen, C. K. Yamakawa, L. P. Brumano, and S. I. Mussatto, “Innovation and strategic orientations for the development of advanced biorefineries,” *Bioresour. Technol.*, vol. 302, p. 122847, Apr. 2020, doi: 10.1016/j.biortech.2020.122847.
[5] C. Hognon *et al.*, “Comparison of pyrolysis and hydrothermal liquefaction of Chlamydomonas reinhardtii. Growth studies on the recovered hydrothermal aqueous phase,” *Biomass Bioenergy*, vol. 73, pp. 23–31, Feb. 2015, doi: 10.1016/j.biombioe.2014.11.025.
[6] A. V. Bridgwater, “Review of fast pyrolysis of biomass and product upgrading,” *Biomass Bioenergy*, vol. 38, pp. 68–94, Mar. 2012, doi: 10.1016/j.biombioe.2011.01.048.
[7] S. S. Toor, L. Rosendahl, and A. Rudolf, “Hydrothermal liquefaction of biomass: A review of subcritical water technologies,” *Energy*, vol. 36, no. 5, pp. 2328–2342, May 2011, doi: 10.1016/j.energy.2011.03.013.
[8] L. J. Guo, Y. J. Lu, X. M. Zhang, C. M. Ji, Y. Guan, and A. X. Pei, “Hydrogen production by biomass gasification in supercritical water: A systematic experimental and analytical study,” *Catal. Today*, vol. 129, no. 3, pp. 275–286, Dec. 2007, doi: 10.1016/j.cattod.2007.05.027.
[9] I. Pavlovič, Ž. Knez, and M. Škerget, “Hydrothermal Reactions of Agricultural and Food Processing Wastes in Sub- and Supercritical Water: A Review of Fundamentals, Mechanisms, and State of Research,” *J. Agric. Food Chem.*, vol. 61, no. 34, pp. 8003–8025, Aug. 2013, doi: 10.1021/jf401008a.
[10] S. Nanda, F. Pattnaik, V. B. Borugadda, A. K. Dalai, J. A. Kozinski, and S. Naik, “Catalytic and Noncatalytic Upgrading of Bio-Oil to Synthetic Fuels: An Introductory Review,” in *ACS Symposium Series*, vol. 1379, A. K. Dalai, D. B. Dadyburjor, Y. Zheng, A. Duan, W. L. Roberts, and S. Nanda, Eds. Washington, DC: American Chemical Society, 2021, pp. 1–28. doi: 10.1021/bk-2021-1379.ch001.
[11] A. R. K. Gollakota, M. Reddy, M. D. Subramanyam, and N. Kishore, “A review on the upgradation techniques of pyrolysis oil,” *Renew. Sustain. Energy Rev.*, vol. 58, pp. 1543–1568, May 2016, doi: 10.1016/j.rser.2015.12.180.
[12] S. K. Nayak, B. Nayak, P. C. Mishra, M. M. Noor, and S. Nanda, “Effects of biodiesel blends and producer gas flow on overall performance of a turbocharged direct injection dual-fuel engine,” *Energy Sources Part Recovery Util. Environ. Eff.*, vol. 0, no. 0, pp. 1–20, Nov. 2019, doi: 10.1080/15567036.2019.1694101.
[13] M. D. Kass., “Stability, Combustion, and Compatibility of High-Viscosity Heavy Fuel Oil Blends with a Fast Pyrolysis Bio-Oil,” *Energy Fuels*, vol. 34, no. 7, pp. 8403–8413, Jul. 2020, doi: 10.1021/acs.energyfuels.0c00721.
[14] G. Lyu, S. Wu, and H. Zhang, “Estimation and Comparison of Bio-Oil Components from Different Pyrolysis Conditions,” *Front. Energy Res.*, vol. 3, 2015, Accessed: Oct. 01, 2022. [Online]. Available: https://www.frontiersin.org/articles/10.3389/fenrg.2015.00028
[15] Y. Shi, E. Xing, K. Wu, J. Wang, M. Yang, and Y. Wu, “Recent progress on upgrading of bio-oil to hydrocarbons over metal/zeolite bifunctional catalysts,” *Catal. Sci. Technol.*, vol. 7, no. 12, pp. 2385–2415, Jun. 2017, doi: 10.1039/C7CY00574A.

[16] Y. Li , “Coke formation on the surface of Ni/HZSM-5 and Ni-Cu/HZSM-5 catalysts during bio-oil hydrodeoxygenation,” *Fuel*, vol. 189, pp. 23–31, Feb. 2017, doi: 10.1016/j.fuel.2016.10.047.
[17] M. Zhang, “A review of bio-oil upgrading by catalytic hydrotreatment: Advances, challenges, and prospects,” *Mol. Catal.*, vol. 504, p. 111438, Mar. 2021, doi: 10.1016/j.mcat.2021.111438.
[18] H. Ojagh, “Hydrodeoxygenation (HDO) Catalysts Characterization, Reaction and Deactivation Studies,” Ph.D., Chalmers Tekniska Hogskola (Sweden), Sweden. Accessed: Oct. 01, 2022. [Online]. Available: https://www.proquest.com/docview/2393720953/abstract/C0B0BEB08C3D4010PQ/1
[19] A. K. Noriega, A. Tirado, C. Méndez, G. Marroquín, and J. Ancheyta, “Hydrodeoxygenation of vegetable oil in batch reactor: Experimental considerations,” *Chin. J. Chem. Eng.*, vol. 28, no. 6, pp. 1670–1683, Jun. 2020, doi: 10.1016/j.cjche.2019.12.022.
[20] T. M. H. Dabros *et al.*, “Transportation fuels from biomass fast pyrolysis, catalytic hydrodeoxygenation, and catalytic fast hydropyrolysis,” *Prog. Energy Combust. Sci.*, vol. 68, pp. 268–309, Sep. 2018, doi: 10.1016/j.pecs.2018.05.002.
[21] A. Ramesh, P. Tamizhdurai, and K. Shanthi, “Catalytic hydrodeoxygenation of jojoba oil to the green-fuel application on Ni-MoS/Mesoporous zirconia-silica catalysts,” *Renew. Energy*, vol. 138, pp. 161–173, Aug. 2019, doi: 10.1016/j.renene.2019.01.076.
[22] M. Gholizadeh, “Effects of temperature on the hydrotreatment behaviour of pyrolysis bio-oil and coke formation in a continuous hydrotreatment reactor,” *Fuel Process. Technol.*, vol. 148, pp. 175–183, Jul. 2016, doi: 10.1016/j.fuproc.2016.03.002.
[23] H. Pourzolfaghar, F. Abnisa, W. M. A. Wan Daud, and M. K. Aroua, “Gas-phase hydrodeoxygenation of phenol over Zn/SiO2 catalysts: Effects of zinc load, temperature, weight hourly space velocity, and H2 volumetric flow rate,” *Biomass Bioenergy*, vol. 138, p. 105556, Jul. 2020, doi: 10.1016/j.biombioe.2020.105556.
[24] A. Ramesh, P. Tamizhdurai, P. Santhana Krishnan, V. Kumar Ponnusamy, S. Sakthinathan, and K. Shanthi, “Catalytic transformation of non-edible oils to biofuels through hydrodeoxygenation using Mo-Ni/mesoporous alumina-silica catalysts,” *Fuel*, vol. 262, p. 116494, Feb. 2020, doi: 10.1016/j.fuel.2019.116494.
[25] S. Ahmadi, E. Reyhanitash, Z. Yuan, S. Rohani, and C. (Charles) Xu, “Upgrading of fast pyrolysis oil via catalytic hydrodeoxygenation: Effects of type of solvents,” *Renew. Energy*, vol. 114, pp. 376–382, Dec. 2017, doi: 10.1016/j.renene.2017.07.041.
[26] L. Coulier, “Hydrotreating model catalysts : from characterization to kinetics,” Phd Thesis 1 (Research TU/e / Graduation TU/e), Technische Universiteit Eindhoven, Eindhoven, 2001. doi: 10.6100/IR548074.
[27] J. Speight, “A review of: ‘Hydrotreating Catalysis Science and Technology’ Topsoe, H., Clausen, B.S., and Massoth, F.E., Springer-Verlag New York, 1996. ISBN No. 3-540-60380-8 Price not available at time of review,” *Fuel Sci. Technol. Int.*, vol. 14, no. 10, pp. 1465–1465, Nov. 1996, doi: 10.1080/08843759608947653.
[28] L. Medici and R. Prins, “The Influence of Chelating Ligands on the Sulfidation of Ni and Mo in NiMo/SiO2Hydrotreating Catalysts,” *J. Catal.*, vol. 163, no. 1, pp. 38–49, Sep. 1996, doi: 10.1006/jcat.1996.0303.
[29] E. Furimsky, “Catalytic hydrodeoxygenation,” *Appl. Catal. Gen.*, vol. 199, no. 2, pp. 147–190, Jun. 2000, doi: 10.1016/S0926-860X(99)00555-4.

[30] M. Attia, S. Farag, and J. Chaouki, “Upgrading of Oils from Biomass and Waste: Catalytic Hydrodeoxygenation,” *Catalysts*, vol. 10, no. 12, Art. no. 12, Dec. 2020, doi: 10.3390/catal10121381.
[31] M. Saidi, F. Samimi, D. Karimipourfard, T. Nimmanwudipong, B. C. Gates, and M. R. Rahimpour, “Upgrading of lignin-derived bio-oils by catalytic hydrodeoxygenation,” *Energy Environ. Sci.*, vol. 7, no. 1, pp. 103–129, Dec. 2013, doi: 10.1039/C3EE43081B.
[32] J. Wildschut, I. Melián-Cabrera, and H. J. Heeres, “Catalyst studies on the hydrotreatment of fast pyrolysis oil,” *Appl. Catal. B Environ.*, vol. 99, no. 1, pp. 298–306, Aug. 2010, doi: 10.1016/j.apcatb.2010.06.036.
[33] P. Ratnasamy and S. Sivasanker, “Structural Chemistry of Co-Mo-Alumnina Catalysts,” *Catal. Rev.*, vol. 22, no. 3, pp. 401–429, Jan. 1980, doi: 10.1080/03602458008067539.
[34] N.-Y. Topsøe and H. Topsøe, “Characterization of the structures and active sites in sulfided Co□MoAl2O3 and Ni□MoAl2O3 catalysts by NO chemisorption,” *J. Catal.*, vol. 84, no. 2, pp. 386–401, Dec. 1983, doi: 10.1016/0021-9517(83)90010-6.
[35] J. A. R. van Veen, E. Gerkema, A. M. van der Kraan, and A. Knoester, “A real support effect on the activity of fully sulphided CoMoS for the hydrodesulphurization of thiophene,” *J. Chem. Soc. Chem. Commun.*, no. 22, pp. 1684–1686, Jan. 1987, doi: 10.1039/C39870001684.
[36] H. Topsøe and B. S. Clausen, “Active sites and support effects in hydrodesulfurization catalysts,” *Appl. Catal.*, vol. 25, no. 1, pp. 273–293, Aug. 1986, doi: 10.1016/S0166-9834(00)81246-4.
[37] A. Stanislaus, A. Marafi, and M. S. Rana, “Recent advances in the science and technology of ultra low sulfur diesel (ULSD) production,” *Catal. Today*, vol. 153, no. 1, pp. 1–68, Jul. 2010, doi: 10.1016/j.cattod.2010.05.011.
[38] G. Dhillon, “HYDROTREATING TUNGSTEN CATALYST FOR PRODUCTION OF GREEN DIESEL FROM BIODIESEL,” p. 84.
[39] G. Kishan, L. Coulier, V. H. J. de Beer, J. A. R. van Veen, and J. W. Niemantsverdriet, “Preparation of highly active NiW hydrotreating modelcatalysts with1,2-cyclohexanediamine-N,N,N′N′-tetraacetic acid (CyDTA) as a chelating agent,” *Chem. Commun.*, no. 13, pp. 1103–1104, Jan. 2000, doi: 10.1039/B003272G.
[40] A. E. Coumans and E. J. M. Hensen, “A model compound (methyl oleate, oleic acid, triolein) study of triglycerides hydrodeoxygenation over alumina-supported NiMo sulfide,” *Appl. Catal. B Environ.*, vol. 201, pp. 290–301, Feb. 2017, doi: 10.1016/j.apcatb.2016.08.036.
[41] M. Wang, M. He, Y. Fang, J. Baeyens, and T. Tan, “The Ni-Mo/γ-Al2O3 catalyzed hydrodeoxygenation of FAME to aviation fuel,” *Catal. Commun.*, vol. 100, pp. 237–241, Sep. 2017, doi: 10.1016/j.catcom.2017.07.009.
[42] M. Breysse, P. Afanasiev, C. Geantet, and M. Vrinat, “Overview of support effects in hydrotreating catalysts,” *Catal. Today*, vol. 86, no. 1, pp. 5–16, Nov. 2003, doi: 10.1016/S0920-5861(03)00400-0.
[43] Y. Wang, T. He, K. Liu, J. Wu, and Y. Fang, “From biomass to advanced bio-fuel by catalytic pyrolysis/hydro-processing: Hydrodeoxygenation of bio-oil derived from biomass catalytic pyrolysis,” *Bioresour. Technol.*, vol. 108, pp. 280–284, Mar. 2012, doi: 10.1016/j.biortech.2011.12.132.
[44] S. N. Naik, V. V. Goud, P. K. Rout, and A. K. Dalai, “Production of first and second generation biofuels: A comprehensive review,” *Renew. Sustain. Energy Rev.*, vol. 14, no. 2, pp. 578–597, Feb. 2010, doi: 10.1016/j.rser.2009.10.003.

[45] P. M. Cox, R. A. Betts, C. D. Jones, S. A. Spall, and I. J. Totterdell, "Acceleration of global warming due to carbon-cycle feedbacks in a coupled climate model," *Nature*, vol. 408, no. 6809, Art. no. 6809, Nov. 2000, doi: 10.1038/35041539.
[46] A. N. Varakin, V. A. Salnikov, M. S. Nikulshina, K. I. Maslakov, A. V. Mozhaev, and P. A. Nikulshin, "Beneficial role of carbon in Co(Ni)MoS catalysts supported on carbon-coated alumina for co-hydrotreating of sunflower oil with straight-run gas oil," *Catal. Today*, vol. 292, pp. 110–120, Sep. 2017, doi: 10.1016/j.cattod.2016.10.031.
[47] M. J. Valero-Romero, M. Á. Rodríguez-Cano, J. Palomo, J. Rodríguez-Mirasol, and T. Cordero, "Carbon-Based Materials as Catalyst Supports for Fischer–Tropsch Synthesis: A Review," *Front. Mater.*, vol. 7, 2021, Accessed: Oct. 01, 2022. [Online]. Available: https://www.frontiersin.org/articles/10.3389/fmats.2020.617432
[48] I. C. Gerber and P. Serp, "A Theory/Experience Description of Support Effects in Carbon-Supported Catalysts," *Chem. Rev.*, vol. 120, no. 2, pp. 1250–1349, Jan. 2020, doi: 10.1021/acs.chemrev.9b00209.
[49] S. Wang, H. Li, and M. Wu, "Advances in metal/ biochar catalysts for biomass hydro-upgrading: A review," *J. Clean. Prod.*, vol. 303, p. 126825, Jun. 2021, doi: 10.1016/j.jclepro.2021.126825.
[50] S.-F. Jiang, L.-L. Ling, Z. Xu, W.-J. Liu, and H. Jiang, "Enhancing the Catalytic Activity and Stability of Noble Metal Nanoparticles by the Strong Interaction of Magnetic Biochar Support," *Ind. Eng. Chem. Res.*, vol. 57, no. 39, pp. 13055–13064, Oct. 2018, doi: 10.1021/acs.iecr.8b02777.
[51] P. M. Mortensen, "Deactivation of Ni-MoS2 by bio-oil impurities during hydrodeoxygenation of phenol and octanol," *Appl. Catal. Gen.*, vol. 523, pp. 159–170, Aug. 2016, doi: 10.1016/j.apcata.2016.06.002.
[52] C. H. Bartholomew, "Mechanisms of catalyst deactivation," *Appl. Catal. Gen.*, vol. 212, no. 1, pp. 17–60, Apr. 2001, doi: 10.1016/S0926-860X(00)00843-7.
[53] D. Kubička and J. Horáček, "Deactivation of HDS catalysts in deoxygenation of vegetable oils," *Appl. Catal. Gen.*, vol. 394, no. 1, pp. 9–17, Feb. 2011, doi: 10.1016/j.apcata.2010.10.034.
[54] E. Furimsky and F. E. Massoth, "Deactivation of hydroprocessing catalysts," *Catal. Today*, p. 116, 1999.
[55] A. Fonseca, P. Zeuthen, and J. B. Nagy, "13C n.m.r. quantitative analysis of catalyst carbon deposits," *Fuel*, vol. 75, no. 12, pp. 1363–1376, Oct. 1996, doi: 10.1016/0016-2361(96)00106-8.
[56] M. Marafi and A. Stanislaus, "Effect of initial coking on hydrotreating catalyst functionalities and properties," *Appl. Catal. Gen.*, vol. 159, no. 1, pp. 259–267, Oct. 1997, doi: 10.1016/S0926-860X(97)00066-5.
[57] E. E. Wolf and F. Alfani, "Catalysts Deactivation by Coking," *Catal. Rev.*, vol. 24, no. 3, pp. 329–371, Jan. 1982, doi: 10.1080/03602458208079657.
[58] S. A. W. Hollak, K. P. de Jong, and D. S. van Es, "Catalytic Deoxygenation of Fatty Acids: Elucidation of the Inhibition Process," *ChemCatChem*, vol. 6, no. 9, pp. 2648–2655, 2014, doi: 10.1002/cctc.201402290.
[59] S. Cheng, L. Wei, X. Zhao, and J. Julson, "Application, Deactivation, and Regeneration of Heterogeneous Catalysts in Bio-Oil Upgrading," *Catalysts*, vol. 6, no. 12, Art. no. 12, Dec. 2016, doi: 10.3390/catal6120195.

[60] J. A. Moulijn, A. E. van Diepen, and F. Kapteijn, “Catalyst deactivation: is it predictable?: What to do?,” *Appl. Catal. Gen.*, vol. 212, no. 1, pp. 3–16, Apr. 2001, doi: 10.1016/S0926-860X(00)00842-5.
[61] Å. Wrammerfors, *Catalyst Deactivation by Coke Formation. A Study of the Carbonaceous Layer on a Used Hydrogenation Catalyst*. 1993. Accessed: Oct. 01, 2022. [Online]. Available: https://research.chalmers.se/en/publication/1458
[62] S. Kadarwati , “Coke formation during the hydrotreatment of bio-oil using NiMo and CoMo catalysts,” *Fuel Process. Technol.*, vol. 155, pp. 261–268, Jan. 2017, doi: 10.1016/j.fuproc.2016.08.021.

CHAPTER

3 PERFORMANCE OF BIOCHAR ASSISTED CATALYSTS DURING HYDROPROCESSING OF NON-EDIBLE VEGETABLE OIL: EFFECT OF TRANSITION METAL SOURCE ON CATALYTIC ACTIVITY

Abstract

Biochar-supported catalysts were developed from nickel (Ni) - and cobalt (Co)- nitrates and hydroxides and tested for the hydrotreatment of carinata oil. Nitrate-based (from water-soluble salts) and hydroxide-based (from water-insoluble salts) catalysts of Ni and Co were prepared via wetness impregnation and aqueous dispersion methods, respectively. The catalysts were characterized using various tools such as, confocal XRF, BET specific surface area analyzer, NH_3-TPD, and SEM-EDS. Synchroton method showed nitrate-sourced metals were dispersed mostly in the pores while, the hydroxide-sourced metals were distributed mainly on the catalyst surface. C=C saturation and cracking of triglycerides, decarboxylation, and hydrogenation of aromatic structures appeared to be dominant on the hydroxides of transition metals, hence took place on catalyst surface. Methanation and dehydrogenation (thus aromatization), however, seemed to be a pore phenomenon, catalyzed more over nitrate-based catalysts. A reaction network was proposed based on chemical analysis of upgraded carinata oil and erucic acid model compound. Catalytic cracking followed by hydrotreatment performed better in terms of fuel properties than other approaches in this study.

Keywords: *Biochar catalysts; surface activity; pore activity; confocal XRF imaging; transition metals; hydrotreatment.*

**This work has been published in Energy Conversion and Management, vol, 252, 15 January 2022,115131.*

3.1 Introduction

The commonly used method for preparing heterogeneous catalysts is incipient wetness impregnation [1],[2]. This method uses the capillary action where the aqueous media containing the dissolved metal salts get absorbed into the pores of the catalyst support [3]. The concentration of impregnated metal depends on the mass transfer within the pores. Therefore, larger pore volume of the catalyst is advantageous for reducing mass transfer limitations [4]. However, a larger pore volume and diameter can be detrimental because they can accelerate deactivation mechanism by sintering [4]. Other catalyst synthesis methods, such as sol-gel, co-precipitation and precipitation are studied in literature, and each method can lead to different catalytic performances, due to different physiochemical properties and reactivity with the support [5]. A comparison between sol-gel and wetness impregnation method with Ni/Al_2O_3 for hydrodeoxygenation of canola oil showed that acidity of the catalyst using the impregnation method was lower and produced C_9-C_{14} alkanes in the diesel range. Catalysts produced from impregnation was less stable, had non-uniform particles and low metal-support interaction compared to sol-gel [6]–[8]. Metal particle's size is an important factor for example, the size of the supported metal crystallites of Ni supported on zeolites was a contributing factor for hydrotreatment of stearic acid and algal oil in a batch reactor [9]–[12]. Co-precipitation and precipitation showed smaller Ni crystals compared to impregnation even after two cycles of recycling runs. However, different preparation methods did not affect the chemical composition of the upgraded oil.

Apart from the catalyst synthesis method, catalyst support and its properties such as surface area, chemical and mechanical stability, dispersion of metals on the surface, low affinity for coke formation are highly desirable [13]–[15]. Previous researchers have suggested that porous carbons such as biochar [16], [17], activated carbon [18] and carbon nanotubes [19] have all the properties

of a robust catalyst support discussed above and are most suitable and effective supports for hydrotreatment [20]–[22].

Non-noble monometallic types of specially Fe [23], Ni [24], Mo [25] and Co [26], [27] are used for hydrotreatment of vegetable oil for its hydrogenolysis ability [5], [13]. Among them, Ni-based catalyst has been extensively used due to its low cost, good electrical properties, and high performance for the hydrotreatment of triglycerides to produce hydrocarbon fuels [8], [13], [27], [28]. According to Gamal et al. [13], catalysts having Co metal salts have acid and base sites which proved to be beneficial for hydrotreatment of palm oil [29], triolein [30] and stearic acid [20] . Co supported on activated carbons produced green diesel, but it had unsaturated components [13], [20]. While, another study, demonstrated the ability of Co supported on activated carbons to produce 90% of green diesel from hydrotreatment of palm oil [13], [31].

Although extensive studies have been conducted in the last decade for understanding the role of catalysts prepared especially via wetness impregnation method for the hydrotreatment of vegetable oil and/or fatty acids to green diesel and/or biodiesel over monometallic Ni and Co over different supports, there remain ambiguous knowledge gaps in surface and pore activity [8]. There is a gap in understanding the role of biochar when it is used with active metals in bulk phase or as a support. Salts containing nitrate ion (NO_3^-) are generally water-soluble, easing the mass transfer, thus, metal dispersion on catalyst support. The solubility of hydroxides of transition metals, however, is limited due to the increasingly large ionization energies that result from removing electrons from the metal cation. Due to the insolubility of transition metal hydroxides, these metals are expected to precipitate, deposit, or anchor on active sites of support surface. Also, some metal particles might not interact with the support and remain as a bulk mixture. Unlike, wetness impregnation method, which is primarily a pore phenomenon, and is used to avoid deposition of

catalyst particles on the external surface, the aqueous deposition (AD) method is expected to be a surface phenomenon in which metal active phase gets deposited on the surface or available in the bulk phase.

The objective of this research was to conduct a comparison study between two catalyst synthesis methods namely, wetness impregnation method (IP) and aqueous deposition (AD) on biochar supported catalysts to hydro-treat inedible vegetable oil. IP is well-established catalysis synthesis method, where the water-soluble metallic salts penetrate the pores. In AD, the water-insoluble metallic salts deposit on the surface, with negligible occupancy inside the pores.

Carinata oil was chosen as a feedstock in this study. Several studies and decades-long research have established carinata oil for its potential as biodiesel [24], [32]–[34], green diesel [35],[36] and via catalytic hydrothermolysis process. Carinata oil is even successfully tested as an aviation drop-in-fuel [37]. On the other hand, biocrude primarily from pyrolysis and hydrothermal liquefaction of biomass is a complex mixture of oxygenated organic compounds, heteroatoms, water, and it is highly viscous, corrosive, and unstable [38],[39]. Therefore, the seemingly less complex well-established carinata oil feedstock was used in this study to test the role of biochar as a support for hydrotreating carinata oil. Catalyst pore and surface reaction mechanism was studied in detail over nitrate salts of nickel and cobalt prepared by IP, and hydroxides of nickel and cobalt prepared by AD, respectively. Douglas fir (DF) biomass was utilized to prepare biochar catalyst support, and then the effect of three upgrading approaches was studied according to the previous research [40]. Subsequently, erucic acid was used as a model compound to understand the reaction mechanism and the nickel nitrate catalyst supported on the biochar support was compared with commercial Ni/C over the same process parameters.

3.2 Material and Methods

3.2.1 Materials

Carinata oil was obtained from Applied Research Associates, Inc. (provided by Agrisoma Biosciences, Inc, Gatineau, Quebec, Canada). High purity nitrogen and hydrogen gases were purchased from Airgas Inc. (Opelika, AL, USA). The H_2 gas used for hydrotreatment is of ultra-high purity grade (99.999 mole%). For reduction, we used hydrogen (10 mole%) and nitrogen balance with an analytical uncertainty of +/-2%. DF biomass was hammer milled (passed 1.68 mm) and was obtained from Forest Concepts, LLC (Auburn, Washington, USA). DF biomass was used in catalyst preparation without any further size reduction. Nickel (II) nitrate hexahydrate (99 wt.% crystalline), cobalt nitrate hexahydrate (99 wt. % crystalline), nickel (II) hydroxide (95% pure) and cobalt (II) hydroxide (95% pure) were purchased from Sigma–Aldrich (St. Louis, MO, USA) and was used as received.

3.2.2 Catalyst preparation

Nickel nitrate hexahydrate ($Ni(NO_3)_2.6H_2O$) and cobalt nitrate hexahydrate ($Co(NO_3)_2.6H_2O$) were used to prepare catalysts via incipient wetness impregnation method. Nickel hydroxide ($Ni(OH)_2$) and cobalt hydroxide ($Co(OH)_2$) catalysts were prepared by the aqueous deposition method. In both the processes, hammer milled Douglas Fir (DF) biomass (20 g) was mixed with 350 ml deionized water. To this slurry, calculated amount of each metal salt was added to give 10% metal loading in the final catalyst. The metallic salts mixed with DF biomass slurry was stirred at 80℃ for 4 h to obtain a thick mixture. The mixture was then dried at 105°C overnight to obtain catalyst precursors. The pH of the salt slurries is reported in the appendix (Table A1). The precursors were then activated by reduction using 10% hydrogen (H_2) and 90% (N_2) at their respective reduction temperatures (Figure 3.1) with a residence time of 1 h. The

$NiNO_3$/DF, $CoNO_3$/DF, NiOH/DF, and CoOH/DF denote nickel nitrate, cobalt nitrate, nickel hydroxide and cobalt hydroxide salts supported on DF biochar, respectively. RDF denotes the reduced DF or the bare support. From Figure 3.1 A-D, four sharp decomposition peaks could be noticed at 405℃, 401℃, 415℃ and 405℃ for $NiNO_3$/DF. $CoNO_3$/DF, NiOH/DF, and CoOH/DF precursors respectively. These temperatures are close to the DF decomposition temperature at 445℃ as discussed in detail in the appendix Figure A1 (A-D). While the shift from 445°C (in bare support) to 401-415°C could be due to metal addition, all these peaks correspond to decomposition of the biomass support. Figure 3.1 A-D shows the decomposition peaks of the calcined salt as well. In order to minimize the loss of the support, the reduction was done at temperature between the precursor and the calcined salt's decomposition temperature.

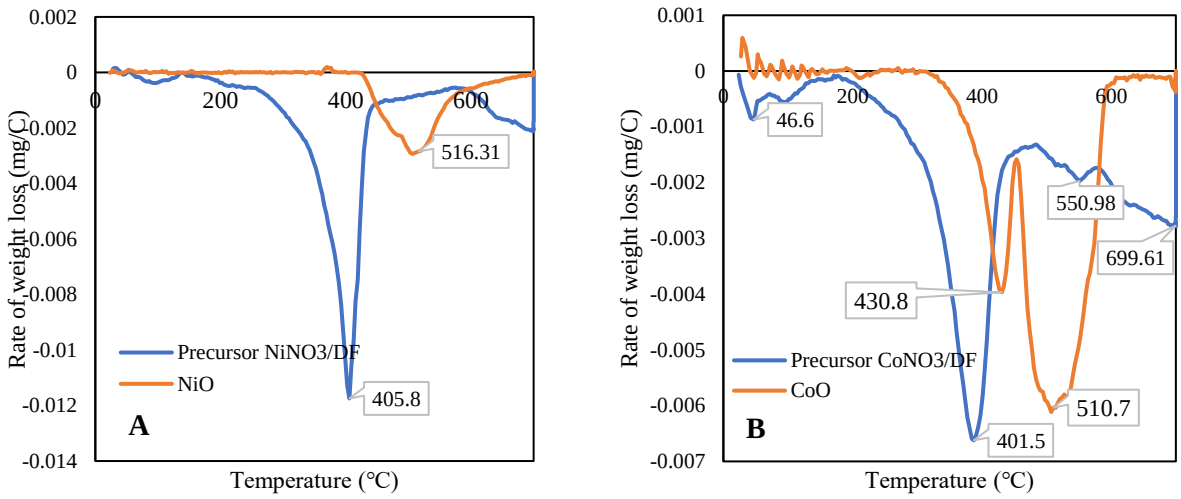

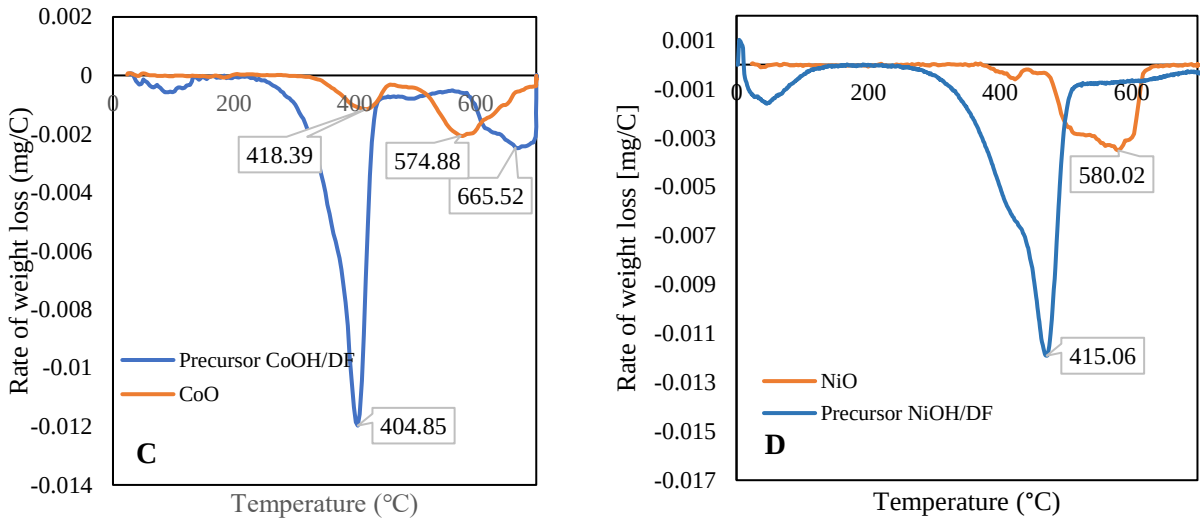

Figure 3.1 DTG-TPR analyses of (A) Precursor $NiNO_3$/DF and calcined nickel nitrate hexahydrate, (B) Precursor $CoNO_3$/DF and calcined cobalt nitrate hexahydrate, (C) Precursor CoOH/DF and calcined cobalt hydroxide and (D) Precursor NiOH/DF and calcined nickel hydroxide.

Blank experiments showed that RDF reduction temperatures of 450°C and 500°C did not have a significant influence on support activity. The RDF and $NiNO_3$/DF precursors were reduced at 450°C. From Figure 1A, the two decomposition peaks of precursor $NiNO_3$/DF and calcined $NiNO_3$.6H20 were 406°C and 516°C, respectively. Therefore, the catalyst was reduced at 450°C in order to minimize the loss of the support. Calcined $CoNO_3.6H_20$ showed two decomposition peaks at 431°C and 511°C, while the precursor showed 401°C, therefore the catalyst was reduced at 500°C (Figure 3.1 B). Similarly, calcined $Co(OH)_2$ salt showed decomposition peaks at 419°C and 575°C, while the precursor had decomposition temperature at 405°C, and it was reduced at 500°C, as well (Figure 3.1 C). Calcined Ni(OH)2 showed two decomposition peaks at 420°C, and 580°C and the precursor showed a decomposition temperature at 415°C, therefore it was reduced at 500°C. Additionally, the oxidative and thermal loss on the fresh and spent catalysts were done by carrying out TGA experiments under air and nitrogen, respectively details of which are discussed in appendix (Figure A2; A-I).

3.2.3 Catalyst characterization

Metal composition in the catalysts was measured using the inductively coupled plasma-optical emission spectrometry (ICP-OES) of the fresh catalysts at Soil and water testing services, UGA. Confocal X-ray fluorescence imaging (CXRF) analysis of fresh catalysts was conducted at beamline 20ID at the Advanced Photon Source (APS) at the Argonne National Laboratory (Lemont, Illinois, USA). The monochromatic micro-focused incident beam size (I0) was ~2*2 μm^2 [41]–[43]. The CXRF data were obtained for DF, RDF, Ni and Co catalysts at an incident beam energy (I0) of 9000 eV and 9200 eV for Ni and Co, respectively [44]. Single element Si-drift vortex detector was placed perpendicular to the incident beam and was used to collect the spectra. A germanium collimating channel array optic unit (Ge) was placed in front of the Si-drift detector to complete the confocal set-up [41], [45]–[48]. The depth resolution of the optic was ~2 μm, the confocal volume was 8 μm^3, and the working distance was ~1.5 mm^4 [44]. Data processing and visualization were completed in 2D Qscan Plot v5 and PyMCA. More details of the setup and method is provided elsewhere [48], [49]. Specific surface area (Brunauer–Emmett–Teller; BET equation) of the biochar supported catalysts (0.3 g) was measured using N_2-adsorption-desorption isotherm in an adsorption analyzer (Autosorb-iQ, Quantchrome Instruments, USA). Detailed procedure is explained in our previous study [40]. Detailed chemisorption macro steps could be found in our previous study [50]. Biochar supported fresh catalysts (0.1 g) were packed in a quartz U-tube, placed between ceramic wool layers. These samples were degassed at 140℃ for 30 min under Ammonia (NH_3) temperature programmed desorption was used to estimate the acid strength sites (Autosorb-iQ, Quantchrome Instruments, USA). Biochar supported fresh catalysts (0.1 g) were packed in a quartz U-tube, placed between ceramic wool layers. These samples were degassed at 140℃ for 30 min under helium atmosphere, saturated with NH_3 for 15 min at 100℃,

then flushed with helium at 100℃ for 30 min, followed by desorption with helium to 900℃ at 20℃/min. The desorption of NH_3 was recorded with a TCD detector (16x attenuation). Raman spectroscopy was conducted using a Horiba HR spectrometer with a 1200 grooves mm^{-1} grating and a laser excitation wavelength of 532 nm with 3.4 mW power and accumulation time of 5 s to capture the data. Detailed procedure is explained elsewhere [40]. An X-ray diffractometer (AXRD, Proto manufacturing, MI, USA) pattern was obtained by employing CuKα radiation (λ = 1.5418 Å), operated at 40 kV and 30 mA. The morphology was characterized by scanning electron microscopy (SEM) using Zeiss EVO50 (Carl Zeiss Microscopy, New York, USA) at different magnification with a voltage of 20 kV and a working distance of 7 to 10 mm. Detailed procedure is explained in our previous study [40].

3.2.4 Hydroprocessing experiments

The hydroprocessing experiments were conducted using a 100 mL Parr 4598 bench top reactor. The oil to catalyst mass ratio was maintained at 70:1 i.e., 35 g of carinata oil and 0.5 g of catalyst for each experiment. Our previous study [40] motivated us to use carbon supported catalysts for hydrotreatment of non-edible vegetable oil to understand the reaction mechanism. Since the motivation of the current study was to understand the catalytic reaction pathway when biochar/ carbon is used as support, we did not study the role of parameters such as temperature, time, H_2 gas pressure and catalyst to oil ratio. We used the same parameters and experimental design from our previous publication and tried to understand the role of carbon (biochar) as a support for hydrotreating carinata oil since Ni on carbon support produced better results compared to other supports studied.

The experimental design consisted of:

1) Catalytic cracking (**CC**) - In this step, the experiment was carried out at 400℃ with a residence time of 75 min with 500 psi of nitrogen cold pressure.

2) Direct hydrotreatment (**HYD**) - For these set of experiments, 1000 psi of H_2 was charged into the reactor initially, and the reaction was performed at 400℃ with a residence time of 75 min.

3) Catalytic cracking followed by hydrotreatment (**CC-HYD**) - The cracked oil from the first step (CC) was mixed with 0.5 g of fresh catalyst. The reaction was carried out at 400℃ with an initial hydrogen loading of 1000 psi with a residence time of 75 min once the temperature reached 400℃.

Apart from the above catalytic and non-catalytic experiments, model compound (erucic acid) experiments were also performed. All experiments had a heating rate of 20℃/min and a stirring speed of 600 rpm.

For catalytic cracking (CC), the same $CoNO_3$/DF and $NiNO_3$/DF catalysts (that were used for hydrotreatment; HYD) were used to crack the carinata oil. For example, if CC was carried out using $NiNO_3$/DF, the same catalyst was used for the next CC-HYD step. All the CC, HYD and CC-HYD experiments were conducted in triplicates. Among the characterizations, BET surface area, TAN, elementary composition and ash content were conducted in triplicates. While HHV, viscosity, NH_3-TPD, TGA, TG-TPR, GC-MS, XRD, and Raman spectroscopy were conducted in duplicate.

3.2.5 Analysis of products

The gas samples were analyzed using a micro-GC. Hydrogen consumption was calculated using the following equation [40], [51].

$$H_2\ consumption\ \left(\frac{mole\ H_2}{kg\ HEBCO}\right) = \left(n_{iH2} - x_{fH2}.n_{ftot}\right) \times \frac{1}{35\ g\ HEBCO} \times \frac{1000g}{1kg} \quad (1)$$

where n_{iH2} was the initial number of moles of hydrogen, x_{fH2} was the final mole fraction of hydrogen and n_{ftot} was the total number of moles of gas at the end of the experiment that was approximated using the ideal gas equation.

For mass-balance purpose, the liquid and solid reaction products were weighed. The liquid products along with the solid products were centrifuged using DYNAC centrifuge (Clay Adams, Parsippany, NJ, USA) for 15 min at g-force of 2147. The total mass of gaseous products was estimated by difference. The liquid, gas, and solid product were calculated using following equations [40]:

$$Y_{liquid}(\%) = \frac{w_l}{w_f} \times 100 \quad (2)$$

$$Y_{wax}(\%) = \frac{(w_s - w_c)}{w_f} \times 100 \quad (3)$$

where w_f was the combined mass of the feed of carinata oil and the consumed hydrogen (g).w_l was the mass of the liquid product (g). w_s was the weight of total waxy residue (g) and w_c was the weight of the catalyst (g).

The total acid number (TAN) of oil samples were measured by titration method (ASTM-D664-07) using a Mettler Toledo T50 Titrator. The kinematic viscosity and density of each sample were measured at 40℃ using a viscometer (SVM 3001, Anton Paar, Austria). Elemental analysis (CHNS/O) was measured of each oil sample using an elemental analyzer (Elementar Vario MICRO, Ronkonkoma, NY, USA). The higher heating value of oil samples were determined using a calorimeter (IKA Model C2000, Wilmington, NC, USA). The chemical composition of the upgraded oil samples was analyzed by an Agilent Technologies 7890A Gas Chromatograph (GC)

system coupled with a mass spectrometry (MS). Detailed procedure is discussed in our previous study [12], [40].

3.3 Results and discussion

3.3.1 Catalyst characterization

The ICP analysis in the Table 3.1 shows catalyst had approximately 10 wt.% of Ni and Co as expected by the metal loading on the biochar for nitrate catalysts. Ni and Co catalysts prepared by the AD synthesis process had lower metal loading of 8.2 and 8.6 wt.% transition metal, respectively, slightly lower than expected value of 10 wt.%. This could be due to lack of homogenous mixing of the bulk phase metals in biochar but also sampling issues while analyzing the metals. However, most of the metal was still present in the final catalyst suggesting surface doping or physical mixing of biochar with the metals. Detailed ICP analysis of the DF, RDF, carinata oil, upgraded oils and the catalysts are provided in the appendix (Table B2; A-B). To evaluate possible metal leaching from the catalyst into the oil, ICP analysis was performed on selected upgraded oil samples. No leaching of heavy metal ions was observed according to the ICP results in the upgraded oil irrespective of the treatment and the catalyst type. Therefore, two different catalyst synthesis method were successful to stop the loss of active species from the solid to the liquid medium. Therefore, none of the metals were poorly bounded to the surface of the biochar or washed away from the solid to the liquid. The catalysts were loaded with 10% metal on the biochar. Approximately, 10% of Ni and Co were present in the nitrate-based catalysts, while around 9% metal loading was observed for the case of hydroxide salts. This could be due to lack of homogenous mixing of the bulk phase metals in biochar but also sampling issues while analyzing the metals. However, most of the metal was still present in the final catalyst suggesting successful surface doping or physical mixing of biochar with the metals.

Table 3.1 ICP analysis of catalysts and upgraded carinata oil and semi-quantification of acidic sites based on NH3-TPD analysis (for detailed metal analysis, refer to Tables S2-A and S2-B in supporting information).

Samples		Metal (wt. %)		Acid sites (Area %)	
		Ni	Co	Moderate	Strong
Catalyst	$NiNO_3$/DF	10.9	<0.01	13.9	86.1
	$CoNO_3$/DF	<0.01	10.8	24.1	75.9
	NiOH/DF	8.2	<0.01	9.2	90.8
	CoOH/DF	<0.01	8.6	9.6	90.4
	RDF	NA*		10.7	89.3
Upgraded oil	$NiNO_3$-HYD	0.05	<0.01	NA*	
	$CoNO_3$-HYD	<0.01	0.01		
	NiOH-HYD	0.02	<0.01		
	CoOH-HYD	<0.01	0.006		

Figure 3.2-A and 3.2-B show the NH_3-TPD profiles of nitrate-based and hydroxide-based catalysts, respectively. NH_3-TPD analysis was carried out to evaluate the distribution of acid sites such as weak (<200℃), moderate (>200℃ and <400℃) and strong (>400℃). According to Ndlela et.al. [52], the weak acidic sites correspond to desorption of loosely bound ammonia, while ammonia desorption at temperature greater than 400℃ corresponds to strong acidic sites. A medium intensity desorption peak at higher temperature was observed for RDF, this could be due to the support's acidity containing oxygen functional groups.

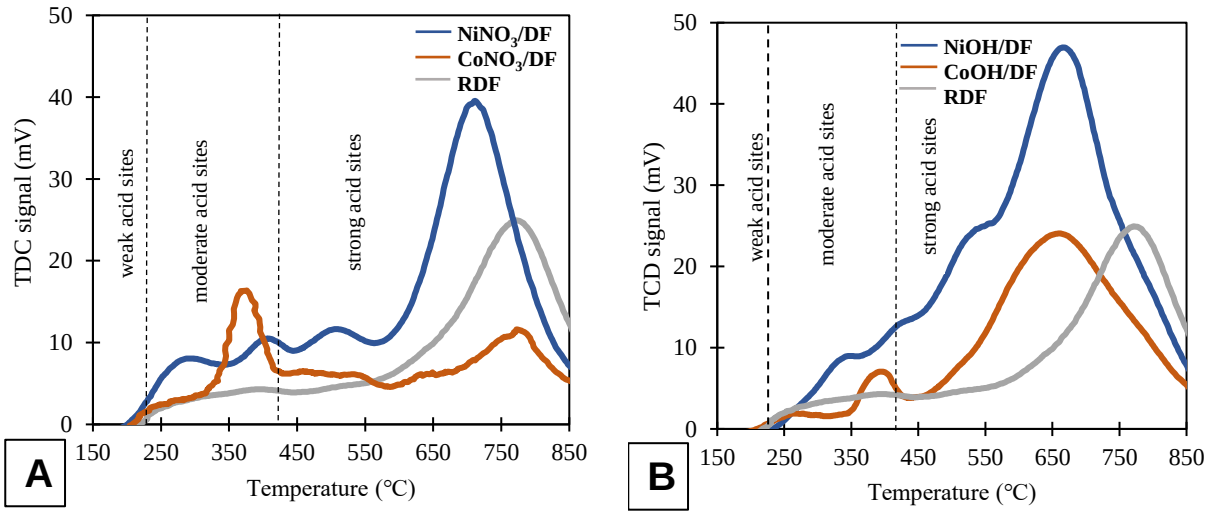

Figure 3.2 TPD of $NiNO_3$/DF, $CoNO_3$/DF, NiOH/DF, CoOH/DF and RDF.

The acidic material of a carbon supports may depend on the presence of carboxylic, hydroxide, phenol and lactone groups [53]. $CoNO_3$/DF exhibited a sharp desorption peak at 375°C, located on the moderate acid site and a lower intensity broad desorption peak at 750°C under strong acidic site. $NiNO_3$/DF showed three broad desorption peaks at different temperatures, indicating a broad distribution of moderate and strong acid sites. The introduction of acidic metals on the biochar support introduced medium strength acidic sites [52], [54]. CoOH/DF exhibited a broad desorption peak at 650°C and a small desorption peak under moderate acidic site, a stark contrast to $CoNO_3$/DF. Even though both the Co salt catalysts showed peaks in the strong acidic sites, the intensity of CoOH/DF was much higher than $CoNO_3$/DF. Since the same trend was observed in the case of Ni catalysts, this could be due to the AD synthesis method, where majority of the metals were deposited on the surface rather than in the pores. Both NiOH and CoOH catalysts have strong acid sites at lower temperature than their nitrate counterparts do. Notably, the concentration of strong acid sites at lower-end temperature (380-550°C) in both NiOH and CoOH catalysts was much more than their nitrate counterparts in the same temperature range. This could be due to

insolubility of hydroxide salts that may had resulted in close-to-surface deposition of transition metals (more evidence provided under CXRF characterization). In other words, in the case of nitrate catalysts, since the water-soluble nitrate salts could penetrate deeper through the catalyst structure, most of the strong acid sites were probably formed inside the catalyst pores, thus, showed up at higher-end temperatures (550-850°C). Furthermore, Ni is more electronegative than Co, hence it has more acidic sites and it is seen from Figure 3.2, that intensity of Ni desorption peaks irrespective of salt source was higher compared to Co [55]–[57]. Semi-quantification of acidic sites (Table 1) also supports higher concentration of acid sites in Ni than Co catalysts. While the concentration of moderate and strong acids was not influenced significantly after Co doping on the DF support, according to Table 1 a backward shift in maximum desorption peak in strong acid region was observed in both CoOH/DF and NiOH/DF compared to the bare support. This could further support more surface activity than pore activity that is directly correlated to catalyst synthesis method.

The BET specific surface area of catalysts in descending order CoOH/DF> $CoNO_3$/DF>NiOH/DF>$NiNO_3$/DF>RDF are presented in Table 2.1. Micropore volume was obtained with the Barrett, Joyner, and Halend (BJH) method considering the pore width was within the mesoporous range (2-50) nm. Total pore volume was obtained at P/P0 = 0.99. Mesopore volumes were calculated by subtracting the micropore volume from the total pore volume. The BET specific surface area of Co in both acidic and basic salts showed much higher compared to Ni and DF support (Table 2.1). This phenomena is also observed by other authors in the literature [58]–[60]. This is primarily due to the smaller molecular diameter of Co compared with Ni. However, the possibility of more nanoparticle formation might have played a role in increased BET in the case of Co catalysts. The source of transition metal (hydroxide) did seem to have a

significant influence on the BET surface area, with CoOH/DF being the highest and NiOH/DF being higher than $NiNO_3$/DF. It is possible that during the preparation of the catalysts at the slightly basic pH of the aqueous suspension of biomass and metal compounds (pH data are presented in Table A1 in appendix), well-dispersed metal hydroxides are formed, which during reduction, convert to metals with a well-developed porous structure with higher BET surface area than metal nitrates. CoOH/DF showed highest micropore volume, followed by $CoNO_3$/DF which confirms with the surface area measurements. All the catalysts showed micro and mesopores, with majority of the pores less than 2nm. We can see from Table 2.1 that RDF had the lowest surface area and once it was treated with either OH or NO_3-based metals, it created higher surface area, which increased the BET surface area along with pore volume, micro and mesopores. Biomass consists of both acidic and basic sites, however from Table A1 (appendix) it could be seen that DF biomass has more acidic sites than basic sites due to its acidic slurry (pH 4.7). When OH salt was added via aqueous deposition method on the DF biomass, the pH of the OHs (metallic salt+ water) which were 8.3 (for CoOH) and 8.7 (for NiOH) were reduced to 5.8 (for $CoNO_3$) and 6.1 (for $NiNO_3$) respectively, which was between the DF pH (4.7) and the metallic salt + water pH (8.3 and 8.7). This could be due to neutralization reaction. If neutralization reaction took place (see Figure A3.A), it is assumed to be removing acidic sites from the surface of the support and in this way, it might have increased the BET surface area and the pore volume. Hence, CoOH/DF and NiOH/DF showed higher BET surface area than their nitrate counterparts (Table 2). In the case of NO_3 salt, the pH was 5.8 (for $CoNO_3$) and 6.1(for $NiNO_3$), when DF biomass was added it produced more acidic pH (3.3; for $NiNO_3$ and 4.01; for $CoNO_3$). When the acidity of the metallic salt, biomass and water was increased, the basic sites got neutralized with the newly added NO_3 salt. Therefore, it might have increased the BET surface area, pore volume, however, not as high as hydroxides.

According to the Figure A3.A and A3.B, higher BET surface and pore volume could be seen for the hydroxides.

$CoNO_3$/DF and CoOH/DF exhibited H4 type of hysteresis, which indicates broad pore size distribution (Figure 3.3). These are usually seen in hierarchical carbons that contain micro, meso, and macro pores. These pores have slit like opening, narrow and internal spaces are not regular in shape [50], [61]. Both Co catalysts showed micro and meso pores, with majority of the pores less than 6nm (Figure 3.3). Similarly, $NiNO_3$/DF and NiOH/DF exhibited H3 type of hysteresis. H3 hysteresis loop is observed in aggregates, which are disordered lamellar mesopores of plate like particles that gives rise to slit or wedge-shaped pores.

Table 3.2 Physisorption and chemisorption data of the catalysts and the support.

	Physisorption			
Samples	**Specific surface area (m^2/g)**	**Total pore Volume (cc/g)**	**Micropore**	**Mesopore**
$NiNO_3$/DF	113±8	0.09	0.04	0.05
NiOH/DF	197±7	0.13	0.03	0.09
$CoNO_3$/DF	307±10	0.19	0.04	0.14
CoOH/DF	383±13	0.30	0.15	0.14
RDF	19±5	0.09	0.01	0,08
	Chemisorption			

	Active metal surface area (m^2/g)	Percent metal dispersion	Average crystallite size (nm)
$NiNO_3$/DF	1.2	14.3	11.2
NiOH/DF	1.8	18.3	28.8
$CoNO_3$/DF	1.5	17.7	24.5
CoOH/DF	2.7	20.1	13.4

Table 3.2 gives the active metal surface area, metal dispersion and average crystallite size of the four catalysts determined from the H_2-chemisorption. In Table 3.2, Co catalyst irrespective of the salt source showed higher metal dispersion (20.1% and 18.6%) and active metal surface area (2.7 and 1.8 m^2/g) compared to their Ni counterparts. Average crystallite size was highest for $CoNO_3$/DF (28.8 nm) followed by NiOH/DF (24.5nm) and lowest for $NiNO_3$/DF (14.3 nm). In the case of spent catalysts, the active metal surface area decreased for all the catalysts, this could be due to coke deposits on the surface [62]. The average crystallite size was higher than the fresh catalyst, that might have occurred due to agglomeration [63] .

CXRF analysis was conducted to indicate spatial distribution of Ni, and Co present within the catalyst particle at the surface (0 μm) and at a depth of 30 μm. The information depth of elements studied here depends on three factors: a) composition and density of the sample, b) intensity and energy of the incident x-ray beam, and c) energy of the characteristic fluorescence beam of each elements [49], [64]. For example, the CXRF signal of those elements was detectable up to 30 μm from the surface (Figure 4). Large differences in Co distribution compared to Ni are

evident at 30 µm and at surface. The map of Co intensity for $CoNO_3$/DF indicate Co distribution showed a honey cone-like pattern across the basic structure and inside the pores.

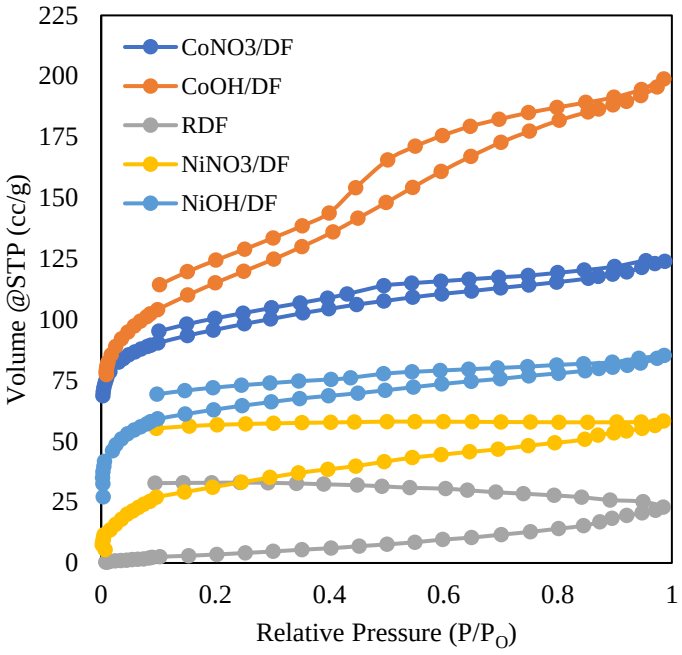

Figure 3.3 N_2 adsorption-desorption isotherms and pore size distribution of the catalysts and support.

For nitrate catalysts, the intensity of red color at higher depth (30 µm) is clearly higher than on the surface (0 µm) that is assumed to be due to the penetration of soluble nitrate salts inside the catalyst pores. For hydroxide catalysts, the microscope scanned along the length of the biochar particle, and it was observed that the concentration of the metals was higher on the surface, while the red or yellow regions seem to disappear at greater depths as seen in Figure 3.4. All of these conclusions show that the hydroxide metals were deposited more on the biochar surface since the salts were insoluble in water during catalyst preparation, while the nitrate metal particles were seen mostly within the biochar cavities due to their solubility in water. This could be due to the AD synthesis

method where the hydroxide salts were deposited on the surface or were present in a bulk phase. On the other hand, for the nitrate catalysts, metals were impregnated into the biochar pores.

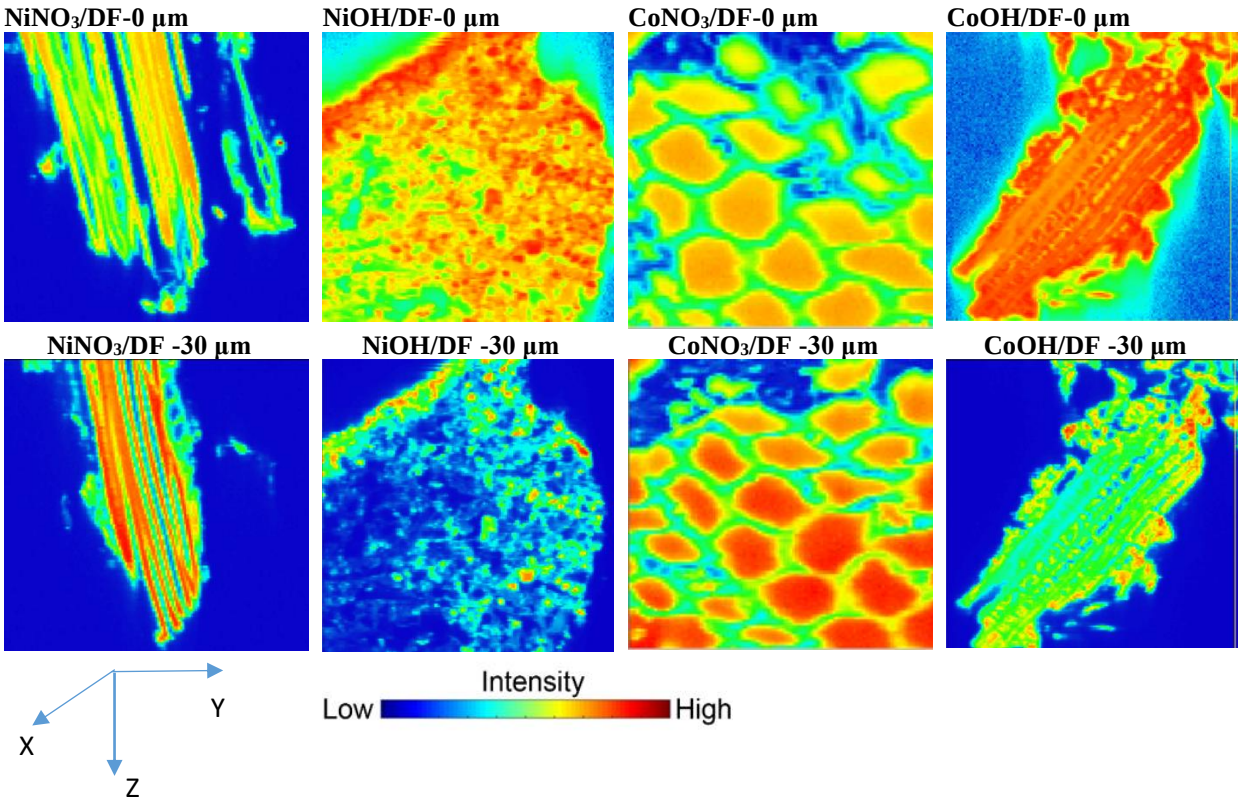

Figure 3.4 CXRF imaging showing distribution of Ni and Co at 0µm and 30µm imaging depth.

The surface morphology of the catalysts is presented in Figure 3.5. For the $NiNO_3$/DF, the Ni particle sizes could be in the form of polycrystalline arrangements attached on the cellulosic structure of the biochar [65], [66] (Figure 3.5a). NiOH/DF (Figure 3.5c) stacked to from chaotic arrangement and an amorphous surface texture could be seen, that may be due to deposition of the active metal salts on the biochar surface. CoOH/DF (Figure 3.5d) showed deposition of the metal salts on the surface. Reduced DF biochar exhibited vertically aligned ordered arrays of micro channels, resembling structures of raw wood [50], [67]–[69] (Figure 5e).

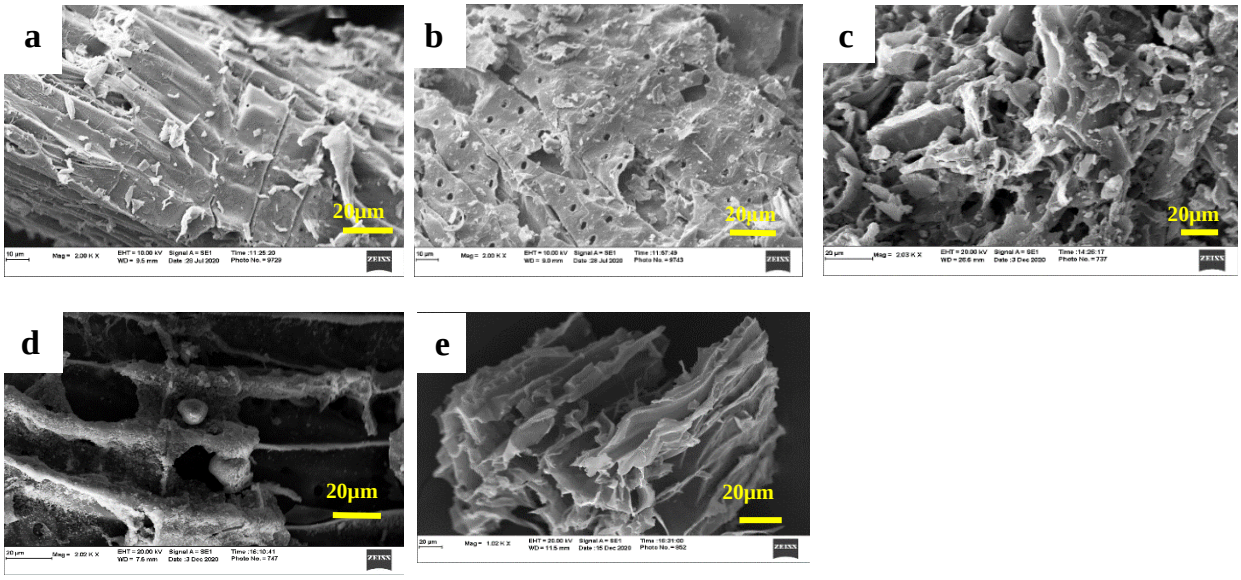

Figure 3.5 SEM images of: a) $NiNO_3$/DF, b) $CoNO_3$/DF, c) NiOH/DF, d) CoOH/DF catalysts, and e) RDF support.

All the catalysts showed significant disordered (D) and graphitic (G) carbon Raman bands regardless of the metallic salt source and support (Figure A4; appendix). The relative intensity of the D-band to G-band (I_D/I_G) is often used to measure the degree of graphitization or crystallinity [70]. The degree of crystallinity for the catalysts in increasing order were 0.838< 0.839< 0.857< 0.875< 0.873 for $CoNO_3$/DF< CoOH/DF< NiOH/DF< $NiNO_3$/DF < RDF, respectively. While catalyst preparation method or metal source did not seem to influence I_D/I_G, Co catalysts suggested slightly less crystallinity than Ni catalysts. All ratios were lower than 1, which indicated lower disordered carbon structure, or the graphitization was dominant across all the catalysts.

3.3.2 Catalyst activity under HYD treatment

The distribution of fatty acids present in the carinata oil is discussed in the previous paper [40]. Erucic acid, a C_{22} fatty acid with one double bond, was the major component with ~40 wt. % in the crude carinata oil. The elemental composition, HHV, dynamic viscosity, and density of crude carinata oil are listed in Table 3. Crude carinata oil consisted of 70.4% carbon, 11.3% of hydrogen, and 17.9% of oxygen and trace amount of nitrogen. The physiochemical

characterization, along with hydrogen consumption and other gas production are reported in Table 3. Only H_2, N_2, CH_4, CO_2 and CO were quantified by the micro-GC, and the balance gas mainly consisted of C_2-C_4 gases. Figure A5 in appendix shows the reactor pressure profile during the HYD experiments. Two major parameters were believed to influence the reactor pressure after the heating period: hydrogen consumption and gas production. Gas production appeared to dominate hydrogen consumption on the RDF.

At the first glance it looks like that RDF has a better catalytic activity comparted to the metal-loaded DF, however, three more experiments at longer reaction time (300 minutes) were performed to get a deeper insight in the deoxygenation pathway. RDF, $CoNO_3$/DF and CoOH/DF were selected to hydrotreat carinata oil for 300 minutes (5h). Results of these reactions are presented in Table A3 (appendix). These results suggested that the oil underwent hydrodeoxygenation on RDF within 75 minutes of the experiment instead of cracking. The intrinsic acidity of the RDF support could have helped in reducing the oxygen content to 5.9%, however, the oxygen content did not change much after the long reaction time. This could suggest rapid deactivation of acid centers on RDF. The metal-loaded catalysts on the other hand, did not do much deoxygenation within the 75 minutes but cracked the oil molecules (thus lowered the viscosity). Once the viscosity was reduced, significant deoxygenation took place on both Co catalysts. Therefore, this could suggest that transition metal species prolonged the catalyst life. In other words, RDF could deoxygenate and hydrocrack the oil to some extent, but it deactivated faster than the Co catalysts. On Co catalysts, hydrocracking seemed to take place before hydrodeoxygenation. On the other hand, the CoOH/DF showed a 75% decrease in oxygen content (1.8 wt.%) and 35% decrease in the dynamic viscosity (10.3 cp @40°C) lower compared to 75 mins experiment. Similarly, for $CoNO_3$/DF, the oxygen content was 2.5 wt.% and dynamic

viscosity was 8.2 cp, which are considerably lower compared to 75 mins experiment as shown in Table 3.3. This indicates that, the metal in the support lasts much longer than RDF and undergoes deoxidation and cracking by knocking out catalyst poisoning materials, which the RDF support was unable to do so.

On $NiNO_3$/DF catalyst, gas production and hydrogen consumption were about the same because the pressure profiles tended to level off with minor fluctuations after the heating period. Hydrogen consumption dominated gas production in the case of CoOH/DF, and both nitrate-derived catalysts, while these catalysts consumed much more hydrogen than CoOH/DF. This could suggest that most hydrogen-consuming reactions (i.e., methanation reaction) took place within the pores while cracking reactions (i.e., decarboxylation) likely happened on catalyst surface. Because CoOH/DF also produced a relatively high amount of methane, we believe that BET specific surface area played an equally important role as pore Co in methanation reaction. Methanation of carbon dioxide on transition metals is a reversible reaction, thus, the final CO_2 and CH_4 concentrations depend on equilibrium constants. Overall, there should be a trade-off between the location of active sites, BET specific surface area, and the equilibrium constant to determine the final methane and CO_2 concentrations. Hydrogen consumption and gas yield over each catalyst are reported in Table 3.3 and Figure 3.6, respectively. From Figure 3.6, RDF had the lowest liquid yield (63.5 %) and highest wax (13.1%) under HYD process. High acidity (Figure 3.2) of the biochar support helped in formation of active sites [26], [71] and low BET surface area (Table 3.2) also contributed to this, since the large triglyceride molecules could not penetrate the biochar support. High wax production (~13%) suggested that even without a catalyst, some hydrogenation reaction took place on the RDF biochar support and rapid hydrogenation of the C=C in the triglycerides. RDF without an active metal catalyst had the lowest hydrogen consumption (2%),

lowest methane (6%) and carbon dioxide (3.8%) emission in the HYD process. Highest gas yield (23.3%) was observed on RDF, followed by hydroxide and nitrate catalysts (Figure 3.6). Both metallic and acid centers are needed for

Table 3.3 Physiochemical characterization of crude and upgraded carinata oil after HYD upgrading.

Properties	Carinata oil	Catalyst				
		RDF	$NiNO_3$/DF	$CoNO_3$/DF	NiOH/DF	CoOH/DF
Oil						
Elemental composition (wt.%)						
C	70.4±1.70	80.8±0.81	78.8±1.01	77.5±1.49	79.7±0.52	78.9±1.83
H	11.3±0.01	12.0±0.11	12.0±0.08	12.4±0.37	12.2±0.24	11.9±0.27
N	0.7±0.40	0.02±0.01	0.08±0.03	0.06±0.01	0.02±0.00	0.08±0.00
S	<0.01	0.05±0.03	0.11±0.01	0.12±0.02	0.02±0.01	0.06±0.03
Ash	<0.01	1.19±0.81	1.20±0.42	1.85±0.72	1.00±1.24	1.66±0.51
O[1]	17.9±1.10	5.9±2.46	7.8±2.01	8.06±1.10	7.06±1.33	7.4±0.81
HHV (MJ/kg)	40.6±0.40	43.4±1.22	41.6±0.58	42.9±1.46	42.2±0.32	42.0±1.28
Density (kg/m^3)	0.9±0.00	0.9±0.00	0.9±0.05	0.8±0.05	0.8±0.05	0.8±0.05
Dynamic viscosity 40 ^oC (cP)	44.6±0.03	38.3±3.22	19.1±1.18	18.2±2.12	14.1±1.35	16±0.54
Gas product analysis						
H_2 consumption (mol/kg)	NA	2.09±1.79	2.51±0.30	2.79±0.11	2.11±0.23	2.41±1.12
CH_4 (mol%)	NA	6.1±0.81	13.4±1.17	19.4±0.31	6.2±1.77	17.3±0.5
CO_2 (mol%)	NA	3.8±1.32	7.6±0.56	8.4±0.24	24.8±2.20	6.1±0.14
Balance (mol%)	NA	30.8±1.50	21.8±3.00	17.4±1.84	23.2±2.36	20.0±1.45

NA= Not applicable [1]Oxygen determined by difference.

hydrocracking [63]. While nitrate-based catalysts in general suggested higher acidity than hydroxide counterparts did (Figure 3.2), higher gas yield in the case of hydroxide catalyst are assumed be due to surface activity of the catalysts. As suggested by CXRF analysis (Figure 3.4), the active metals were dispersed more on the surface rather than inside the pores in hydroxide catalysts. Thus, the oil molecules could have a higher chance of interaction with the active metals. This might have caused more cracking than hydro(deoxy)genation on the surface, due to presence and easy availability of higher concentration of active metals. Since cracking was more pronounced on the surface of the hydroxide catalyst, hydrogen consumption to hydrotreat the oil

molecules were also lower compared to nitrate catalysts. While this conclusion requires further research, at this time it appears to suggest that the contribution of metallic sites in catalyzing hydrocracking reaction might have dominated the catalyst acidity in in the case of hydroxide-based catalysts.

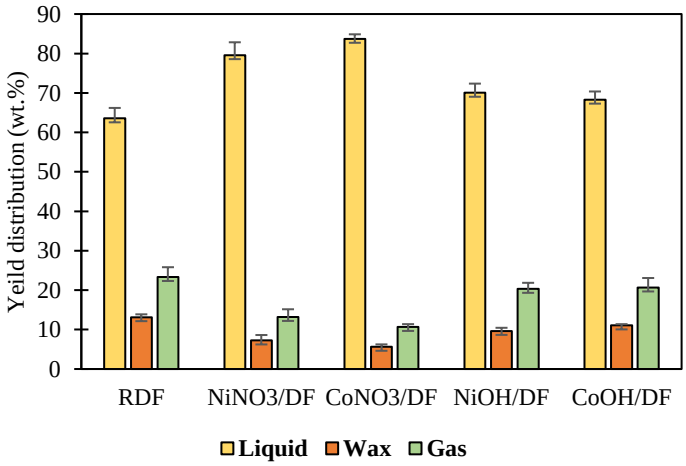

Figure 3.6 Product yield distribution after upgrading of carinata oil via HYD.

This trend is seen in Table 3, where the hydrogen consumption of hydroxide catalysts was 2.11 mol/kg and 2.41mol/kg for Ni and Co, respectively, compared to 2.51mol/kg and 2.79 mol/kg of nitrate catalysts for Ni and Co, respectively. Dynamic viscosity of the hydroxide catalysts was lower compared to nitrate catalysts (Table 3.3), and this is due to cracking of oil molecules. This further supported that the oil did not undergo hydrotreatment as expected, but instead underwent cracking reaction which produced smaller molecules that reduced the viscosity. These results support our hypothesis that pronounced cracking took place on the surface of hydroxide catalysts compared to pores of the nitrate catalysts. In the case of RDF, the viscosity reduced 14% from the crude carinata oil, which could be due to the help of acidic support along with the thermal effect from the reactor. Moreover, nitrate catalysts had higher liquid yield, lower gas yield and higher viscosity. This supports that nitrate-based catalysts had lower cracking inside the pores. In

addition, upgraded oils over hydroxide-based catalysts had slightly lower oxygen content than nitrate catalysts. The higher amount of CO_2 in the gas phase over NiOH/DF catalyst may be an indication of increased decarboxylation on catalyst surface. The CO_2 from decarboxylation reaction could then underwent methanation; however, methanation reaction appeared to be catalyzed more by the pore activity according to gas analysis data in Table 3.3. Methanation was highest for $CoNO_3$/DF (19.4 mol%) and CoOH/DF (17.3 mol%), and this suggests, higher BET surface area (Table 3.2) of these catalysts might have helped in diffusion of hydrogen gas into the pores and caused methanation, because Co catalysts had much higher BET specific surface area regardless of the metal source. Decarboxylation is a reaction in which CO_2 is produced, but it can be then consumed at the same time to produce CH_4 gas. Therefore, it is difficult to distinguish between surface activity, pore activity, and the effect of BET specific surface area on CO_2 reaction chain. Also, it was difficult to differentiate whether the CO_2 formed from the water gas shift reaction or from decarboxylation route as proposed by other researchers [72]. From Table 3.3, it is seen that there was no CO emission for the catalysts studied; it is unknown whether decarbonylation was the reaction pathway for the DF biochar supported catalysts to upgrade crude carinata oil. However, it could be possible that the CO produced via decarbonylation underwent secondary reaction with H_2 to produce CH_4 [73]. Considerable amount of ash is seen in Table 3 for the upgraded oil, this could be due to suspended catalysts in the oil centrifugation was carried out after hydrotreatment. Ultra-filtration might be needed for complete separation of the catalyst from the oil. This could have introduced metals in the upgraded oil as seen in the ICP data (Table A2; A-B). The GC-MS results of the upgraded carinata oil is shown in Figure 3.7 were quantified for top seventy-five peaks out of more than hundred peaks depending on the catalyst. The detailed semi-quantification of the top seventy-five peaks is provided in Tables A4-A12 in the appendix.

The GC-MS-detectable compounds were divided into paraffin, olefins, cyclic and oxygenated compounds. The RDF support showed selectivity towards C_9-C_{23} hydrocarbons which were mostly paraffin and olefins, followed by C_5-C_{26} cyclic and oxygenated compounds.

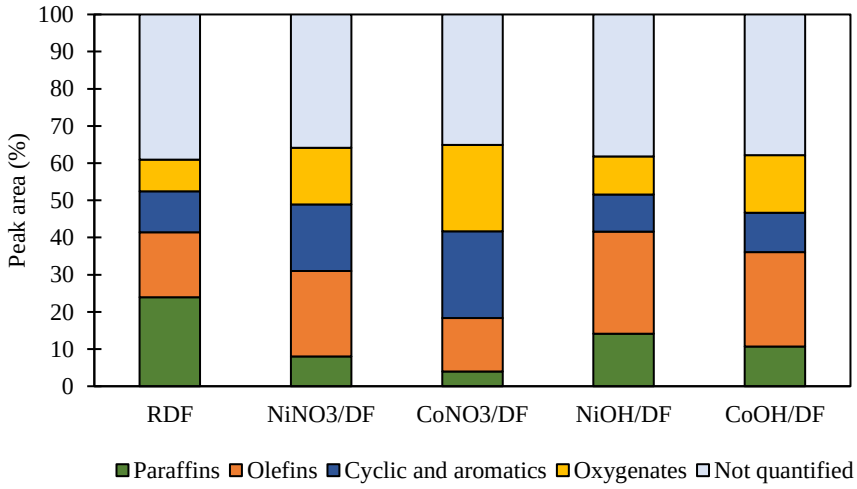

Figure 3.7 Semi quantification and classification of upgraded carinata oil products based on top seventy- fifty GC-MS peaks under HYD treatment.

From Figure 3.7, olefins have the highest peak area in the hydroxide catalysts and that could be a product from the cracking of oil molecules. Therefore, olefins in the upgraded oil could be formed from the active metals occupying the surface or in the bulk phase. Cyclic and aromatics occupy a larger peak area in the nitrate catalysts. This shows that, aromatization is mostly catalyzed by the metals occupying the pores, thus a pore activity phenomenon. In other words, olefin, and aromatic production both require dehydrogenation of parent oil molecules, however, as further discussed under reaction mechanism, a higher level of dehydrogenation is needed for aromatization reaction than in dehydrogenation of paraffins. This could support that dehydrogenation reaction takes place on both surface and pores while the degree of dehydrogenation inside the pores are higher. As a result, more aromatics are formed over nitrate-catalysts than hydroxide-catalysts, while more olefins were produced over hydroxide-catalysts. From Table 3, nitrate catalysts consumed higher

amount of H_2 gas during HYD process, especially $CoNO_3$/DF. Consequently, cyclic and aromatics was the highest in this catalyst, and this may confirm the hypothesis that the aromatization might have occurred within the pores of the catalysts, which had the highest BET surface area as well. Dehydrogenation of olefins can produce aromatization products on carbon support as shown in our previous study [40], although such reaction was not expected to take place under the experimental conditions (i.e. >1000 psi operating H_2 pressure). Furthermore, some unsaturated and/or aromatic compounds could be formed due to the electron impact ionization and fragmentation during GC-MS analysis [51], which signifies the need for more chemical characterization using other techniques. Additionally, CoOH/DF had the lowest amount of H_2 (11.9 wt.%) in the upgraded oil, and lowest amount of cyclic and aromatics (10.7%). In terms of oxygenates in the upgraded oil, $CoNO_3$/DF had the highest peak area percentage of 24%, which agrees with the highest oxygen content (10%) of the upgraded oil presented in Table 3.4. $NiNO_3$/DF and CoOH/DF showed similar oxygen contents (9.1%) in the upgraded oil, as well as in the oxygenated compounds (15%) shown by the GC. Similarly, NiOH/DF, which had the lowest oxygen content (8.08%) in the upgraded oil, also showed lowest oxygenated compounds (10.2%) in the oil as well.

3.3.3 Reaction mechanism

Erucic acid was used as a model compound for carinata oil, and it was tested under similar upgrading experimental conditions as carinata oil over $CoNO_3$/DF and CoOH/DF. Understanding the reaction pathway was the motivation to perform erucic acid experiments. GC-MS analyses results of the top seventy-five compounds of upgraded liquid products derived from erucic acid, (Figure A2). From previous results, it was understood that cracking reactions are more favored on the catalyst surface than the pores. Since erucic acid may represent cracked carinata oil, obtained

data suggest that hydrogenation of C=C bonds is facilitated through catalyst pores because more paraffins were identified on $CoNO_3$/DF catalyst. Therefore, a longer reaction time in hydrotreatment of the actual carinata oil may result in higher concentration of paraffins. Under CC treatment, more olefins and more aromatics were produced over $CoNO_3$/DF suggesting that aromatization and dehydrogenation reactions were likely pore phenomena. Based on the chemical analysis of products from erucic acid and carinata oil upgrading experiments, a simplified reaction network was proposed as shown in Figure 3.8.

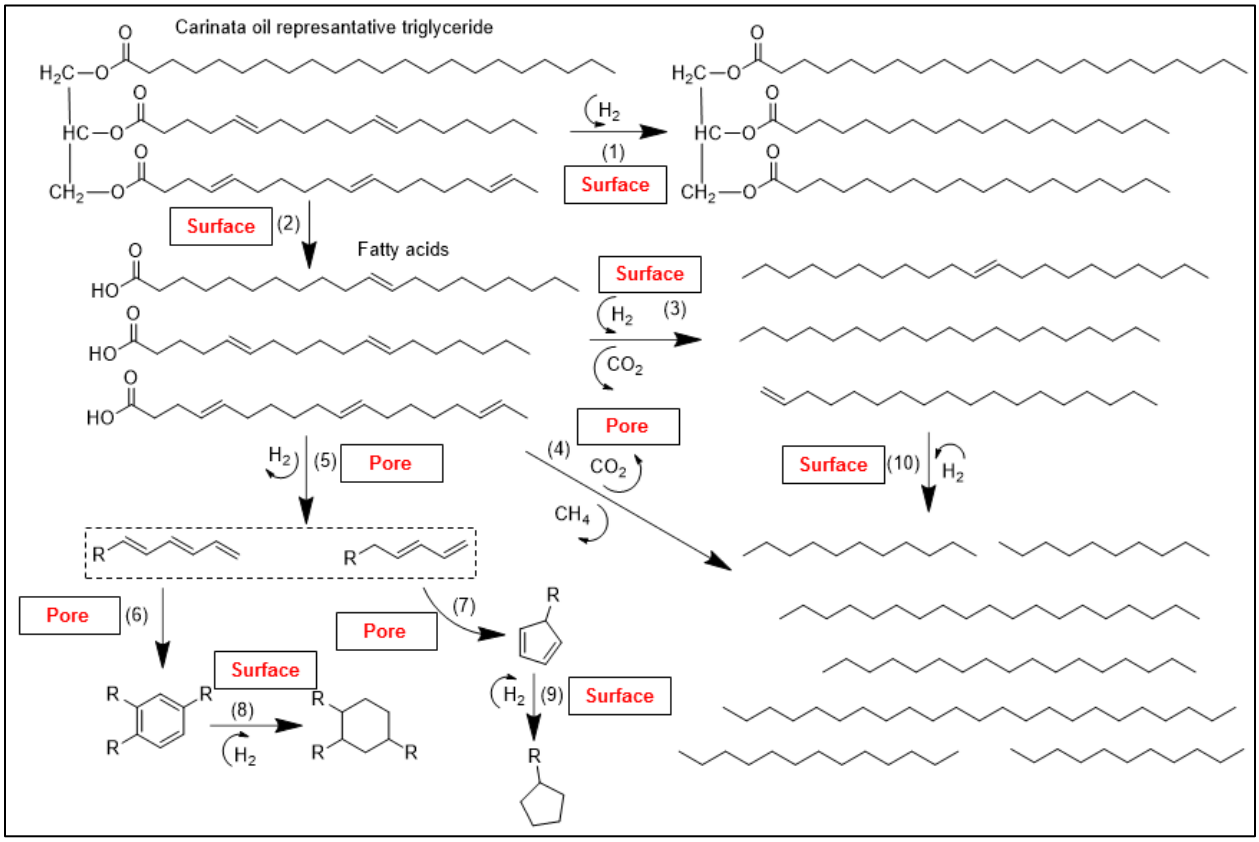

Figure 3.8 Proposed reaction pathway for hydrotreatment of carinata oil over Erucic acid.

Pathway (1) is the saturation (hydrogenation) of triglycerides that resulted in high-yield wax production after HYD. This pathway was more dominant on the catalyst surface. Pathway (2) is the cracking of triglycerides into their FFA building blocks. This route seemed to be favored more

on the catalyst surface. Pathway (3) represents decarboxylation, and partial hydrogenation of FFAs. Both reactions were more dominant on hydroxides of transition metals, hence, on catalyst surface. Besides, methanation of CO_2 is a dominant gas-phase reaction along with this route that is shown in pathway (4). As mentioned previously, higher concentration of methane over both nitrate-based catalysts could be an indication of pore phenomena. Pathway (5) is dehydrogenation of FFAs, appeared to be more significant in nitrate-based catalysts. In our previous study, we found that the dehydrogenation pathway produces multiple C=C double bonds along the aliphatic chains. These unstable compounds would then produce aromatization products (routes (6) and (7)) [40], [74]. Aromatization reactions took place in catalyst pores. As a result, aromatic and cyclic alkylated hydrocarbons are found in upgrading products. Pathways (8) and (9) are the hydrogenation of aromatic structures that seemed to be a surface phenomenon. Nevertheless, it is important to emphasize that reaction labels (surface vs. pore) does not mean a clear boundary between surface and pore catalytic activity. In other words, the pore and surface catalytic activity indeed overlapped, however, labels show the dominant site that catalyzed the associative reaction.

3.3.4 Effect of CC & CC-HYD treatments and comparison with Ni/C

Reactor pressure during the hydrotreatment step in CC-HYD of carinata oil using nitrate-based catalysts is showed in appendix (Figure A6) and GC-MS analysis of the upgraded oil (Figure A7). Co showed much higher hydrogen consumption after the heating period until 45 minutes compared with Ni. After 45 minutes gas production appeared to dominate hydrogenation on $CoNO_3$/DF. The $NiNO_3$/DF catalyst, however, showed continued decreasing trend in reactor pressure throughout the experiment. The final pressures on these two catalysts were nearly the same after 75 minutes of residence time. In the case of CC approach, $NiNO_3$/DF produced the highest liquid yield (80%) compared to $CoNO_3$/DF (70%). Even though, the liquid yield

percentage of $NiNO_3$/DF is higher than $CoNO_3$/DF, but according to GC-MS data, $NiNO_3$/DF had a higher percentage of hydrocarbons with carbon numbers lower than C_{17} and $CoNO_3$/DF had a higher percentage of hydrocarbons with carbon numbers higher than C_{16}. These results suggested that $NiNO_3$/DF had superior cracking ability compared to $CoNO_3$/DF. During CC-HYD step, the results reversed, with highest liquid yield for $CoNO_3$/DF (89.3%), followed by $NiNO_3$/DF (86.7%), with similar wax yield (Figure 3.9).

The physiochemical characterization, along with hydrogen consumption and other gas product analyses are reported in Table 4. The hydrogen consumption in this study varied between 2.0 to 3.1 mol/kg of bio-oil (Tables 3 and 4) irrespective of catalyst type or hydrotreatment (CC, HYD or CC-HYD), which was relatively low. The H_2 generation during CC reactions (N_2 atmosphere) of $NiNO_3$/DF and $CoNO_3$/DF were 5.7 mol% and 11.6 mol%. $CoNO_3$/DF and $NiNO_3$/DF generated 8.4 mol/kg and 6.7 mol/kg of CH_4 gas, while 6.2 mol/kg and 7.6 mol/kg of CO_2 was generated during CC reactions. Since, there was availability of H_2 gas, it helped in more CH_4 gas formation than CO_2 gas.

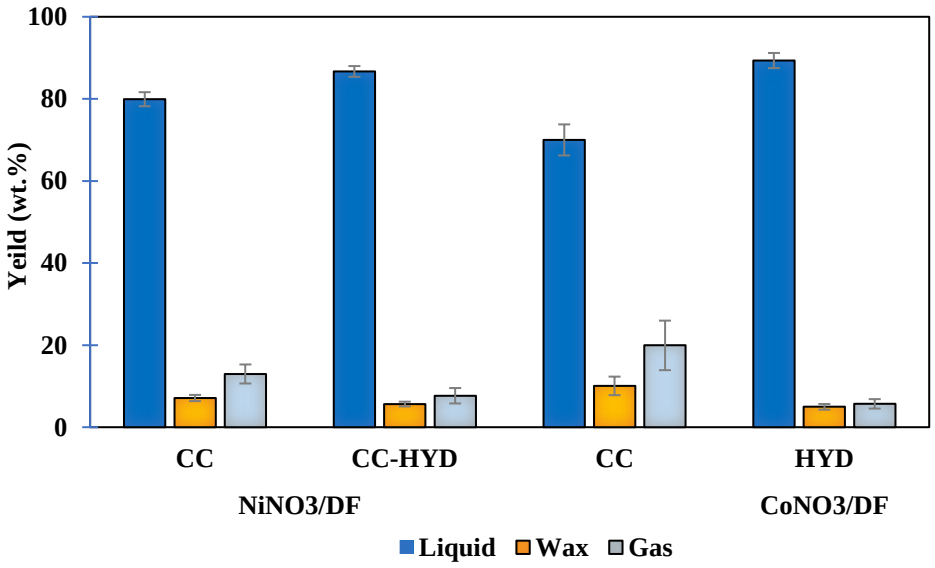

Figure 3.9 Liquid, solid and gas yield for nitrate catalysts under CC and CC-HYD.

In CC-HYD process, the H_2 consumption was the highest for $CoNO_3$/DF (3.13%; Table 3.4). The high H_2 consumption in the CC-HYD process could be due to ease of hydrogenation of the cracked oil molecules. For CC-HYD treatments, the TAN was 15.4 and 19.1 for $CoNO_3$/DF and $NiNO_3$/DF catalysts, respectively. To understand the effect of reaction parameter (time), the $CoNO_3$/DF catalyst for HYD treatment was hydrotreated for 180 minutes, when the TAN drastically reduced to 9.32 mgKOH/g from 15.4 mgKOH/g. The TAN numbers could be significantly reduced with the use of longer reaction time for complete conversion of carboxylic acids to hydrocarbons. The heating value of crude carinata oil was 40.6 MJ/kg, while the upgraded oil under CC-HYD treatment for $CoNO_3$/DF and $NiNO_3$/DF were approximately 44 MJ/kg. These results are quite comparable to jet fuel HHV of about 42-47 MJ/kg. Viscosity of an upgraded oil depends on the number of smaller molecules that are produced during cracking reaction from large molecules. The viscosity of $CoNO_3$/DF-derived oil (6.1cP) was lower than $NiNO_3$/DF oil (8.3cP), that could be due to enhanced cracking of oil molecules by the $CoNO_3$/DF compared to $NiNO_3$/DF. From the GC-MS results (Figure S5), the CC oil by $CoNO_3$/DF showed 5% of paraffin and 32% of olefins, while $NiNO_3$/DF showed 9% and 29% respectively. The higher amount of olefins and lower amount of paraffin in the CC oil in the case of $CoNO_3$/DF, could be due to the high dehydrogenation that resulted in 11.6 mol% hydrogen in the gas phase. The H_2 and O_2 in the upgraded oil was highest (14.9 %) and lowest (3.3 %) for $NiNO_3$/DF. In terms of oxygenates, both the catalysts showed similar concentration (8%), this matches with the similar oxygen content (3%) in the upgraded oil as well. In our prior study [40], commercial Ni supported on activated carbon (Ni/C) was used for hydro treating carinata oil. Liquid yields over $NiNO_3$/DF under HYD and CC-HYD treatment were 4.6 and 14.2% higher compared to commercial Ni/C catalyst under

same condition. The TAN after CC-HYD for Ni/C was 67% more compared to $NiNO_3$/DF. Similarly, the viscosity was 10.7 cP compared to 8.3 cP for the present study. However, the oxygen content in the oil was slightly lower 2.7 % compared to 3.3%. The paraffin yield was 19% higher compared to biochar based $NiNO_3$/DF.

Table 3.4 Physiochemical characterization of upgraded carinata oil after CC-HYD upgrading.

Properties	Carinata oil	Catalyst	
		$NiNO_3$/DF	**$CoNO_3$/DF**
Oil properties			
Elemental composition (wt.%)			
C	70.40±1.70	81.28±1.13	81.87±1.52
H	11.30±0.01	14.91±0.33	14.4±0.12
N	0.70±0.40	0.03±0.00	0.01±0.00
S	<0.01	0.62±0.11	0.12±0.02
Ash	<0.01	2.16±0.20	1.98±0.14
O[1]	17.91±1.17	1.05±0.52	1.6±2.32
HHV (MJ/kg)	40.61±0.45	44.14±0.57	44.30±1.16
TAN (mgKOH/g)	0.00	19.18±1.00	15.4±0.22
Density (kg/m^3)	0.90±0.00	0.7±0.05	0.80±0.00
Dynamic viscosity 40 °C (cP)	44.61±0.03	8.3±2.2	6.1±1.5
Gas product analysis	NA		
H_2 consumption (mol/kg)	NA	3.01±0.41	3.13±1.58
CH_4 (mol%)	NA	16.4±1.00	22.7±1.12
CO_2 (mol%)	NA	1.85±2.17	5.15±1.48
Balance (mol%)	NA	19.71±3.10	16.90±3.53

NA= Not applicable [1]Oxygen determined by difference.

The DF-based catalyst did not produce carbon monoxide (CO) irrespective of its treatment or salt source, unlike commercial Ni/C. During catalytic cracking (CC), hydrogen produced was 5.7 mol% over $NiNO_3$/DF in comparison to <0.1 mol% for Ni/C. From the Raman spectroscopy, the I_D/I_G ratio was lower than 1 for $NiNO_3$/DF, which could be due to near graphite like carbon structures compared to amorphous structures of Ni/C. The BET surface area of commercial Ni/C was 1500 m^2/g, which was 92.4% more than the lab-made DF biochar support with Ni impregnation.

3.4 Conclusion

In this study, two catalyst preparation methods were applied to the transition metals assisted with biochar for hydrotreating carinata oil. CXRF analysis showed that by AD synthesis method, OH-sourced metals occupied the surface, while NO_3-sourced metals were dispersed mostly inside the pores. The nature of the metal, catalyst BET specific surface area, and catalyst preparation method played major role in and carinata upgrading and methanation reaction. Regardless of the catalyst preparation method, methanation appeared to take place mostly inside the pores, as supported by higher H_2 consumption, CH_4 gas production, and lower gas yield over the nitrate-based catalysts. While cracking reactions and decarboxylation took place on the catalyst surface based on the lower viscosity, lower H_2 consumption, and higher gas yield on hydroxide-based catalysts. Methanation was the highest for $CoNO_3$/DF followed by CoOH/DF, both exhibited higher BET surface areas, suggesting that methanation was a pore phenomenon. Both surface and the pore of the catalyst played the role in olefin formation, while aromatization was catalyzed by metals occupying the pores. Under catalytic cracking (CC) reaction, more H_2 was generated under $CONO_3$/DF compared to $NiNO_3$/DF. Under CC-HYD treatment, the upgraded carinata oil had lowest TAN (~15 mgKOH/g), viscosity (~6 cP) and highest HHV (~44 MJ/kg) compared to the other two treatments. $NiNO_3$/DF had lower BET specific surface area than commercial Ni/C. However, the TAN and viscosity were lower over biochar supported catalyst, while oxygen content, and liquid yield were higher under similar CC-HYD treatments on biochar supported catalysts than the commercial catalyst. Finally, a reaction network was proposed based on chemical analysis of the upgraded **carinata oil and erucic acid model compound.**

3.5 References

[1] S. I. Al-Resayes *et al.*, "List of contributors," in *Metal Oxides in Energy Technologies*, Y. Wu, Ed. Elsevier, 2018, pp. xi–xiii. doi: 10.1016/B978-0-12-811167-3.09994-6.

[2] G. A. Alsultan, N. Asikin-Mijan, H. V. Lee, A. S. Albazzaz, and Y. H. Taufiq-Yap, "Deoxygenation of waste cooking to renewable diesel over walnut shell-derived nanorode activated carbon supported CaO-La2O3 catalyst," *Energy Convers. Manag.*, vol. 151, pp. 311–323, Nov. 2017, doi: 10.1016/j.enconman.2017.09.001.

[3] P. Munnik, P. E. de Jongh, and K. P. de Jong, "Recent Developments in the Synthesis of Supported Catalysts," *Chem. Rev.*, vol. 115, no. 14, pp. 6687–6718, Jul. 2015, doi: 10.1021/cr500486u.

[4] Y. He *et al.*, "Influence of catalyst synthesis method on selective catalytic reduction (SCR) of NO by NH3 with V2O5-WO3/TiO2 catalysts," *Appl. Catal. B Environ.*, vol. 193, pp. 141–150, Sep. 2016, doi: 10.1016/j.apcatb.2016.04.022.

[5] M.-Y. Choo *et al.*, "Deposition of NiO Nanoparticles on Nanosized Zeolite NaY for Production of Biofuel via Hydrogen-Free Deoxygenation," *Materials*, vol. 13, no. 14, Art. no. 14, Jan. 2020, doi: 10.3390/ma13143104.

[6] A. Afshar Taromi and S. Kaliaguine, "Hydrodeoxygenation of triglycerides over reduced mesostructured Ni/γ-alumina catalysts prepared via one-pot sol-gel route for green diesel production," *Appl. Catal. Gen.*, vol. 558, pp. 140–149, May 2018, doi: 10.1016/j.apcata.2018.03.030.

[7] F. Bimbela, J. Ábrego, R. Puerta, L. García, and J. Arauzo, "Catalytic steam reforming of the aqueous fraction of bio-oil using Ni-Ce/Mg-Al catalysts," *Appl. Catal. B Environ.*, vol. 209, pp. 346–357, Jul. 2017, doi: 10.1016/j.apcatb.2017.03.009.

[8] N. Hongloi, P. Prapainainar, and C. Prapainainar, "Review of green diesel production from fatty acid deoxygenation over Ni-based catalysts," *Mol. Catal.*, p. 111696, Jun. 2021, doi: 10.1016/j.mcat.2021.111696.

[9] B. Peng, Y. Yao, C. Zhao, and J. A. Lercher, "Towards Quantitative Conversion of Microalgae Oil to Diesel-Range Alkanes with Bifunctional Catalysts," *Angew. Chem. Int. Ed.*, vol. 51, no. 9, pp. 2072–2075, 2012, doi: 10.1002/anie.201106243.

[10] L. A. M. Hermans and J. W. Geus, "Interaction Of Nickel Ions With Silica Supports During Deposition-Precipitation," in *Studies in Surface Science and Catalysis*, vol. 3, B. Delmon, P. Grange, P. Jacobs, and G. Poncelet, Eds. Elsevier, 1979, pp. 113–130. doi: 10.1016/S0167-2991(09)60208-1.

[11] P. Wang *et al.*, "Enhancement of biogas production from wastewater sludge via anaerobic digestion assisted with biochar amendment," *Bioresour. Technol.*, vol. 309, p. 123368, Aug. 2020, doi: 10.1016/j.biortech.2020.123368.

[12] P. Wang *et al.*, "Sorption and recovery of phenolic compounds from aqueous phase from sewage sludge hydrothermal liquefaction using bio-char," *Chemosphere*, p. 131934, Aug. 2021, doi: 10.1016/j.chemosphere.2021.131934.

[13] M. Safa Gamal, N. Asikin-Mijan, M. Arumugam, U. Rashid, and Y. H. Taufiq-Yap, "Solvent-free catalytic deoxygenation of palm fatty acid distillate over cobalt and manganese supported on activated carbon originating from waste coconut shell," *J. Anal. Appl. Pyrolysis*, vol. 144, p. 104690, Nov. 2019, doi: 10.1016/j.jaap.2019.104690.

[14] N. Kaewtrakulchai, R. Kaewmeesri, V. Itthibenchapong, A. Eiad-Ua, and K. Faungnawakij, "Palm Oil Conversion to Bio-Jet and Green Diesel Fuels over Cobalt Phosphide on Porous

Carbons Derived from Palm Male Flowers," *Catalysts*, vol. 10, no. 6, Art. no. 6, Jun. 2020, doi: 10.3390/catal10060694.
[15] A. Jain, V. Ong, S. Jayaraman, R. Balasubramanian, and M. P. Srinivasan, "Supercritical fluid immobilization of horseradish peroxidase on high surface area mesoporous activated carbon," *J. Supercrit. Fluids*, vol. 107, pp. 513–518, Jan. 2016, doi: 10.1016/j.supflu.2015.06.026.
[16] H. Li *et al.*, "Biochar supported Ni/Fe bimetallic nanoparticles to remove 1,1,1-trichloroethane under various reaction conditions," *Chemosphere*, vol. 169, pp. 534–541, Feb. 2017, doi: 10.1016/j.chemosphere.2016.11.117.
[17] C.-C. Tran, D. Akmach, and S. Kaliaguine, "Hydrodeoxygenation of vegetable oils over biochar supported bimetallic carbides for producing renewable diesel under mild conditions," *Green Chem.*, vol. 22, no. 19, pp. 6424–6436, 2020, doi: 10.1039/D0GC00680G.
[18] J. de Barros Dias Moreira, D. Bastos de Rezende, and V. Márcia Duarte Pasa, "Deoxygenation of Macauba acid oil over Co-based catalyst supported on activated biochar from Macauba endocarp: A potential and sustainable route for green diesel and biokerosene production," *Fuel*, vol. 269, p. 117253, Jun. 2020, doi: 10.1016/j.fuel.2020.117253.
[19] A. Alsultan, N. Mijan, H. Lee, U. Rashid, A. Islam, and Y. H. Taufiq-Yap, "A Review On Thermal Conversion of Plant Oil (Edible and Inedible) Into Green Fuel Using Carbon-Based Nanocatalyst," *Catalysts*, vol. 9, Jan. 2019, doi: 10.3390/catal9040350.
[20] N. Asikin-Mijan, H. V. Lee, G. Abdulkareem-Alsultan, A. Afandi, and Y. H. Taufiq-Yap, "Production of green diesel via cleaner catalytic deoxygenation of Jatropha curcas oil," *J. Clean. Prod.*, vol. 167, pp. 1048–1059, Nov. 2017, doi: 10.1016/j.jclepro.2016.10.023.
[21] L. N. Silva, I. C. P. Fortes, F. P. de Sousa, and V. M. D. Pasa, "Biokerosene and green diesel from macauba oils via catalytic deoxygenation over Pd/C," *Fuel*, vol. 164, pp. 329–338, Jan. 2016, doi: 10.1016/j.fuel.2015.09.081.
[22] E. Santillan-Jimenez, T. Morgan, J. Lacny, S. Mohapatra, and M. Crocker, "Catalytic deoxygenation of triglycerides and fatty acids to hydrocarbons over carbon-supported nickel," *Fuel*, vol. 103, pp. 1010–1017, Jan. 2013, doi: 10.1016/j.fuel.2012.08.035.
[23] "Promotional effect of Fe on performance of Ni/SiO 2 for deoxygenation of methyl laurate as a model compound to hydrocarbons - RSC Advances (RSC Publishing) DOI:10.1039/C4RA07932A."
https://pubs.rsc.org/en/content/articlehtml/2014/ra/c4ra07932a (accessed Aug. 28, 2021).
[24] C. Miao *et al.*, "Hydrothermal catalytic deoxygenation of palmitic acid over nickel catalyst," *Fuel*, vol. 166, pp. 302–308, Feb. 2016, doi: 10.1016/j.fuel.2015.10.120.
[25] N. Krobkrong, V. Itthibenchapong, P. Khongpracha, and K. Faungnawakij, "Deoxygenation of oleic acid under an inert atmosphere using molybdenum oxide-based catalysts," *Energy Convers. Manag.*, vol. 167, pp. 1–8, Jul. 2018, doi: 10.1016/j.enconman.2018.04.079.
[26] H. Zhang, H. Lin, and Y. Zheng, "The role of cobalt and nickel in deoxygenation of vegetable oils," *Appl. Catal. B Environ.*, vol. 160–161, pp. 415–422, Nov. 2014, doi: 10.1016/j.apcatb.2014.05.043.
[27] A. Srifa, K. Faungnawakij, V. Itthibenchapong, and S. Assabumrungrat, "Roles of monometallic catalysts in hydrodeoxygenation of palm oil to green diesel," *Chem. Eng. J.*, vol. 278, pp. 249–258, Oct. 2015, doi: 10.1016/j.cej.2014.09.106.
[28] M. Ameen, M. T. Azizan, A. Ramli, S. Yusup, and B. Abdullah, "The effect of metal loading over Ni/γ-Al2O3 and Mo/γ-Al2O3 catalysts on reaction routes of hydrodeoxygenation of

rubber seed oil for green diesel production," *Catal. Today*, vol. 355, pp. 51–64, Sep. 2020, doi: 10.1016/j.cattod.2019.03.028.
[29] N. Asikin-Mijan *et al.*, "Promoting deoxygenation of triglycerides via Co-Ca loaded SiO2-Al2O3 catalyst," *Appl. Catal. Gen.*, vol. 552, pp. 38–48, Feb. 2018, doi: 10.1016/j.apcata.2017.12.020.
[30] J. M. Crawford, C. S. Smoljan, J. Lucero, and M. A. Carreon, "Deoxygenation of Stearic Acid over Cobalt-Based NaX Zeolite Catalysts," *Catalysts*, vol. 9, no. 1, Art. no. 1, Jan. 2019, doi: 10.3390/catal9010042.
[31] M. S. Gamal, N. Asikin-Mijan, W. N. A. W. Khalit, M. Arumugam, S. M. Izham, and Y. H. Taufiq-Yap, "Effective catalytic deoxygenation of palm fatty acid distillate for green diesel production under hydrogen-free atmosphere over bimetallic catalyst CoMo supported on activated carbon," *Fuel Process. Technol.*, vol. 208, p. 106519, Nov. 2020, doi: 10.1016/j.fuproc.2020.106519.
[32] R. Seepaul *et al.*, "Brassica carinata: Biology and agronomy as a biofuel crop," *GCB Bioenergy*, vol. 13, no. 4, pp. 582–599, 2021, doi: 10.1111/gcbb.12804.
[33] C. Zhao, P. Lv, L. Yang, S. Xing, W. Luo, and Z. Wang, "Biodiesel synthesis over biochar-based catalyst from biomass waste pomelo peel," *Energy Convers. Manag.*, vol. 160, pp. 477–485, Mar. 2018, doi: 10.1016/j.enconman.2018.01.059.
[34] J.-M. Jung, J.-I. Oh, K. Baek, J. Lee, and E. E. Kwon, "Biodiesel production from waste cooking oil using biochar derived from chicken manure as a porous media and catalyst," *Energy Convers. Manag.*, vol. 165, pp. 628–633, Jun. 2018, doi: 10.1016/j.enconman.2018.03.096.
[35] S. L. Douvartzides, N. D. Charisiou, K. N. Papageridis, and M. A. Goula, "Green Diesel: Biomass Feedstocks, Production Technologies, Catalytic Research, Fuel Properties and Performance in Compression Ignition Internal Combustion Engines," *Energies*, vol. 12, no. 5, Art. no. 5, Jan. 2019, doi: 10.3390/en12050809.
[36] B. H. H. Goh *et al.*, "Progress in utilisation of waste cooking oil for sustainable biodiesel and biojet fuel production," *Energy Convers. Manag.*, vol. 223, p. 113296, Nov. 2020, doi: 10.1016/j.enconman.2020.113296.
[37] S. George *et al.*, "A regional inter-disciplinary partnership focusing on the development of a carinata-centered bioeconomy," *GCB Bioenergy*, vol. 13, no. 7, pp. 1018–1029, 2021, doi: 10.1111/gcbb.12828.
[38] T. Rahman, H. Jahromi, P. Roy, S. Adhikari, E. Hassani, and T.-S. Oh, "Hydrothermal liquefaction of municipal sewage sludge: Effect of red mud catalyst in ethylene and inert ambiences," *Energy Convers. Manag.*, vol. 245, p. 114615, Oct. 2021, doi: 10.1016/j.enconman.2021.114615.
[39] S. Wang, H. Yuan, Y. Wang, and R. Shan, "Transesterification of vegetable oil on low cost and efficient meat and bone meal biochar catalysts," *Energy Convers. Manag.*, vol. 150, pp. 214–221, Oct. 2017, doi: 10.1016/j.enconman.2017.08.020.
[40] H. Jahromi *et al.*, "Production of green transportation fuels from Brassica carinata oil: A comparative study of noble and transition metal catalysts," *Fuel Process. Technol.*, vol. 215, p. 106737, May 2021, doi: 10.1016/j.fuproc.2021.106737.
[41] Y. Feng, P. Liu, Y. Wang, W. Liu, Y. Liu, and Y. Z. Finfrock, "Mechanistic investigation of mercury removal by unmodified and Fe-modified biochars based on synchrotron-based methods," *Sci. Total Environ.*, vol. 719, p. 137435, Jun. 2020, doi: 10.1016/j.scitotenv.2020.137435.

[42] W. Liu *et al.*, "Aqua regia digestion cannot completely extract Hg from biochar: A synchrotron-based study," *Environ. Pollut.*, vol. 265, p. 115002, Oct. 2020, doi: 10.1016/j.envpol.2020.115002.
[43] P. Liu *et al.*, "Evaluation of mercury stabilization mechanisms by sulfurized biochars determined using X-ray absorption spectroscopy," *J. Hazard. Mater.*, vol. 347, pp. 114–122, Apr. 2018, doi: 10.1016/j.jhazmat.2017.12.051.
[44] P. Liu, C. J. Ptacek, D. W. Blowes, Y. Z. Finfrock, M. Steinepreis, and F. Budimir, "A Method for Redox Mapping by Confocal Micro-X-ray Fluorescence Imaging: Using Chromium Species in a Biochar Particle as an Example," *Anal. Chem.*, vol. 91, no. 8, pp. 5142–5149, Apr. 2019, doi: 10.1021/acs.analchem.8b05718.
[45] Y. Feng *et al.*, "Distribution and speciation of iron in Fe-modified biochars and its application in removal of As(V), As(III), Cr(VI), and Hg(II): An X-ray absorption study," *J. Hazard. Mater.*, vol. 384, p. 121342, Feb. 2020, doi: 10.1016/j.jhazmat.2019.121342.
[46] C. Su *et al.*, "Chemical processes of Cr(VI) removal by Fe-modified biochar under aerobic and anaerobic conditions and mechanism characterization under aerobic conditions using synchrotron-related techniques," *Sci. Total Environ.*, vol. 768, p. 144604, May 2021, doi: 10.1016/j.scitotenv.2020.144604.
[47] P. Liu, C. J. Ptacek, D. W. Blowes, Y. Z. Finfrock, and R. A. Gordon, "Stabilization of mercury in sediment by using biochars under reducing conditions," *J. Hazard. Mater.*, vol. 325, pp. 120–128, Mar. 2017, doi: 10.1016/j.jhazmat.2016.11.033.
[48] P. Liu, C. J. Ptacek, D. W. Blowes, and Y. Z. Finfrock, "Mercury distribution and speciation in biochar particles reacted with contaminated sediment up to 1030 days: A synchrotron-based study," *Sci. Total Environ.*, vol. 662, pp. 915–922, Apr. 2019, doi: 10.1016/j.scitotenv.2019.01.148.
[49] P. Liu, C. J. Ptacek, D. W. Blowes, and Y. Zou Finfrock, "A beam path-based method for attenuation correction of confocal micro-X-ray fluorescence imaging data," *J. Anal. At. Spectrom.*, vol. 32, no. 8, pp. 1582–1589, 2017, doi: 10.1039/C7JA00148G.
[50] K. Harun, S. Adhikari, and H. Jahromi, "Hydrogen production via thermocatalytic decomposition of methane using carbon-based catalysts," *RSC Adv.*, vol. 10, no. 67, pp. 40882–40893, 2020, doi: 10.1039/D0RA07440C.
[51] H. Jahromi, S. Adhikari, P. Roy, M. Shelley, E. Hassani, and T.-S. Oh, "Synthesis of Novel Biolubricants from Waste Cooking Oil and Cyclic Oxygenates through an Integrated Catalytic Process," *ACS Sustain. Chem. Eng.*, Sep. 2021, doi: 10.1021/acssuschemeng.1c03523.
[52] S. S. Ndlela, H. B. Friedrich, and M. N. Cele, "Effects of Modifying Acidity and Reducibility on the Activity of NaY Zeolite in the Oxidative Dehydrogenation of n-Octane," *Catalysts*, vol. 10, no. 4, Art. no. 4, Apr. 2020, doi: 10.3390/catal10040363.
[53] Y. Li *et al.*, "Activation of a Carbon Support Through a Two-Step Wet Oxidation and Highly Active Ruthenium–Activated Carbon Catalysts for the Hydrogenation of Benzene," *ChemCatChem*, vol. 6, no. 2, pp. 572–579, 2014, doi: https://doi.org/10.1002/cctc.201300873.
[54] E. S. K. Why, H. C. Ong, H. V. Lee, Y. Y. Gan, W.-H. Chen, and C. T. Chong, "Renewable aviation fuel by advanced hydroprocessing of biomass: Challenges and perspective," *Energy Convers. Manag.*, vol. 199, p. 112015, Nov. 2019, doi: 10.1016/j.enconman.2019.112015.
[55] J. M. Fernández-Morales, E. Castillejos, E. Asedegbega-Nieto, A. B. Dongil, I. Rodríguez-Ramos, and A. Guerrero-Ruiz, "Comparative Study of Different Acidic Surface Structures

in Solid Catalysts Applied for the Isobutene Dimerization Reaction," *Nanomaterials*, vol. 10, no. 6, p. 1235, Jun. 2020, doi: 10.3390/nano10061235.
[56] Z. D. Yigezu and K. Muthukumar, "Catalytic cracking of vegetable oil with metal oxides for biofuel production," *Energy Convers. Manag.*, vol. 84, pp. 326–333, Aug. 2014, doi: 10.1016/j.enconman.2014.03.084.
[57] M. Alherbawi, G. McKay, H. R. Mackey, and T. Al-Ansari, "A novel integrated pathway for Jet Biofuel production from whole energy crops: A Jatropha curcas case study," *Energy Convers. Manag.*, vol. 229, p. 113662, Feb. 2021, doi: 10.1016/j.enconman.2020.113662.
[58] I. Kazemnejad, A. Feizbakhsh, A. Niazi, and A. Tavasoli, "Highly dispersed cobalt Fischer–Tropsch synthesis catalysts supported on γ-Al2O3, CNTs, and graphene nanosheet using chemical vapor deposition," *Int. J. Ind. Chem.*, vol. 10, no. 4, pp. 321–333, Dec. 2019, doi: 10.1007/s40090-019-00195-9.
[59] A. Y. Faid, A. O. Barnett, F. Seland, and S. Sunde, "Optimized Nickel-Cobalt and Nickel-Iron Oxide Catalysts for the Hydrogen Evolution Reaction in Alkaline Water Electrolysis," *J. Electrochem. Soc.*, vol. 166, no. 8, p. F519, May 2019, doi: 10.1149/2.0821908jes.
[60] L. A. De Faria, M. Prestat, J.-F. Koenig, P. Chartier, and S. Trasatti, "Surface properties of Ni+Co mixed oxides: a study by X-rays, XPS, BET and PZC1Presented at the joint ECS-ISE Meeting, 31 August–5 September 1997, Paris, France.1," *Electrochimica Acta*, vol. 44, no. 8, pp. 1481–1489, Dec. 1998, doi: 10.1016/S0013-4686(98)00271-0.
[61] K. A. Cychosz, R. Guillet-Nicolas, J. García-Martínez, and M. Thommes, "Recent advances in the textural characterization of hierarchically structured nanoporous materials," *Chem. Soc. Rev.*, vol. 46, no. 2, pp. 389–414, Jan. 2017, doi: 10.1039/C6CS00391E.
[62] G. Prieto, A. Martínez, P. Concepción, and R. Moreno-Tost, "Cobalt particle size effects in Fischer–Tropsch synthesis: structural and in situ spectroscopic characterisation on reverse micelle-synthesised Co/ITQ-2 model catalysts," *J. Catal.*, vol. 266, no. 1, pp. 129–144, Aug. 2009, doi: 10.1016/j.jcat.2009.06.001.
[63] Q. Cheng *et al.*, "Confined small-sized cobalt catalysts stimulate carbon-chain growth reversely by modifying ASF law of Fischer–Tropsch synthesis," *Nat. Commun.*, vol. 9, no. 1, p. 3250, Dec. 2018, doi: 10.1038/s41467-018-05755-8.
[64] O. Tóth, A. Holló, and J. Hancsók, "Co-processing a waste fatty acid mixture and unrefined gas oil to produce renewable diesel fuel-blending components," *Energy Convers. Manag.*, vol. 185, pp. 304–312, Apr. 2019, doi: 10.1016/j.enconman.2019.02.023.
[65] M. L. Toebes, J. H. Bitter, A. J. van Dillen, and K. P. de Jong, "Impact of the structure and reactivity of nickel particles on the catalytic growth of carbon nanofibers," *Catal. Today*, vol. 76, no. 1, pp. 33–42, Nov. 2002, doi: 10.1016/S0920-5861(02)00209-2.
[66] A. H. Al-Muhtaseb *et al.*, "Efficient utilization of waste date pits for the synthesis of green diesel and jet fuel fractions," *Energy Convers. Manag.*, vol. 127, pp. 226–232, Nov. 2016, doi: 10.1016/j.enconman.2016.09.004.
[67] F. Cheng and X. Li, "Preparation and Application of Biochar-Based Catalysts for Biofuel Production," *Catalysts*, vol. 8, no. 9, Art. no. 9, Sep. 2018, doi: 10.3390/catal8090346.
[68] E. Thompson, A. E. Danks, L. Bourgeois, and Z. Schnepp, "Iron-catalyzed graphitization of biomass," *Green Chem.*, vol. 17, no. 1, pp. 551–556, Dec. 2014, doi: 10.1039/C4GC01673D.
[69] G. Xue *et al.*, "Robust and Low-Cost Flame-Treated Wood for High-Performance Solar Steam Generation," *ACS Appl. Mater. Interfaces*, vol. 9, no. 17, pp. 15052–15057, May 2017, doi: 10.1021/acsami.7b01992.

[70] A. Kotoulas *et al.*, "Carbon-encapsulated cobalt nanoparticles: synthesis, properties, and magnetic particle hyperthermia efficiency," *J. Nanoparticle Res.*, vol. 19, no. 12, p. 399, Dec. 2017, doi: 10.1007/s11051-017-4099-9.
[71] R. Jahromi, M. Rezaei, S. Hashem Samadi, and H. Jahromi, "Biomass gasification in a downdraft fixed-bed gasifier: Optimization of operating conditions," *Chem. Eng. Sci.*, vol. 231, p. 116249, Feb. 2021, doi: 10.1016/j.ces.2020.116249.
[72] B. Donnis, R. G. Egeberg, P. Blom, and K. G. Knudsen, "Hydroprocessing of Bio-Oils and Oxygenates to Hydrocarbons. Understanding the Reaction Routes," *Top. Catal.*, vol. 52, no. 3, pp. 229–240, Apr. 2009, doi: 10.1007/s11244-008-9159-z.
[73] N. Shalaby, S. Harahap, M. Elmelawy, and H. A. El-Syed, "Hydrocracking of Waste Cooking Oil as Renewable Fuel on NiW/SiO2-Al2O3 Catalyst," *J. Adv. Catal. Sci. Technol.*, vol. 2, pp. 27–37, Mar. 2015, doi: 10.15379/2408-9834.2015.02.01.3.
[74] H. Wang, G. Li, K. Rogers, H. Lin, Y. Zheng, and S. Ng, "Hydrotreating of waste cooking oil over supported CoMoS catalyst – Catalyst deactivation mechanism study," *Mol. Catal.*, vol. 443, pp. 228–240, Dec. 2017, doi: 10.1016/j.mcat.2017.10.016.

CHAPTER

4 UNDERSTANDING THE EFFECTS OF FEEDSTOCK BLENDING AND CATALYST SUPPORT ON HYDROTREATMENT OF ALGAE HTL BIOCRUDE WITH NON-EDIBLE VEGETABLE OIL

Abstract

The performance of cobalt-molybdenum (CoMo) on hydrotreating of algae HTL biocrude and carinata oil was investigated. Commercial $CoMo/Al_2O_3$ (CoMo/Al) and synthesized CoMo supported on Douglas fir biochar (CoMo/DF), sulfided or unsulfided catalysts, were compared for hydrodeoxygenation (HDO), hydrodenitrogenation (HDN), hydrodesulfurization (HDS) and hydrodemetallization (HDM) reactions. Results showed that there lies a synergistic effect when HTL algae biocrude and carinata oil blends are hydrotreated. The yield of the upgraded blend (UB) oils retrieved over alumina catalyst was higher than the individual hydrotreated parent oils. For example, a 9% and 5% increase in yield was noted compared to the average of individual hydrotreated parent oils. The higher heating value (syngas) of the UBs were higher irrespective of the support type. The UB produced from sulfided CoMo/Al exhibited superior HDO activity primarily by decarbonylation. This was apparent in increased heating value, carbon addition, higher octane number, and lower total acid number than the oils obtained from the biochar-supported catalysts. Sulfided CoMo/DF catalyzed cracking reactions which lowered the viscosity, followed by high HDN and HDS activity compared to the commercial catalyst. The two supports showed different sorption behaviors. Interestingly, CoMo/DF had an effective sorption mechanism that helped in higher metal removal from the oil. Additionally, presulfiding and DF support exhibited positive results in term of less coke formation. In brief, biochar supports have higher

acidic sites, inorganic mineral oxides, ion exchange capacity, high surface area, pore structure and connectivity. All of these make a substantial contribution to its unique catalytic behavior.

Keywords: *Biochar; Hydrotreatment; Alumina; Hydrodenitrogenation; Hydrodesulfurization; Hydrodemetallization.*

**This work has been published in Energy Conversion and Management, vol, 268, 15 September 2022,115998.*

4.1 Introduction

In the next decade, aviation and marine transportation will still depend on liquid fuels even if ground transportation veers majorly towards the battery. In 2021, the total U.S renewable energy contribution was 9 QBtu (out of a total 72.40 QBtu), approximately 2 QBtu (total 101QBtu) less than pre-covid era (2019). Among different renewable resources, biomass scored the highest energy production by source- 3.6 QBtu in 2021 compared to 5.1 QBtu in 2019 [1]. This could be due to the easy incorporation of stationary bioenergy sources with existing technology and transportation infrastructure. Although biomass is renewable, abundant, and inexpensive, its transformation to renewable fuel face few challenges due to its diverse feedstock, handling issues, conversion strategies, and upgrading processes, and all of these contribute to higher final fuel cost than fossil fuel and is slowing down commercialization [2]–[5]. Apart from biomass, edible and non-edible vegetable oil can be transformed into green diesel and bio-jet fuel.

Carinata oil (*Brassica* carinata), non-edible vegetable oil, also known as Ethiopian Mustard, was chosen as one of the feedstocks in this study. Several studies and decades-long research have established carinata oil for its potential as biodiesel [6], [7], and green diesel [6]–[8] via a catalytic hydro-thermolysis process. Carinata oil is even successfully tested as an aviation drop-in-fuel [9]. Like all developing bio-based fuels, transitioning from a lab- or small-scale to

large-scale production of carinata as a green diesel or bio-jet fuel has faced challenges such as economic feasibility and feedstock availability [10]–[12]. According to renewable identification credit, the cost for bio-jet fuel from carinata lies between $0.85/L to $1.28/L, which is costlier than fossil-based jet fuel ($0.50/L; based on 2021 data) [9]. Another drawback is feedstock availability. However, according to the latest study [13], carinata could be grown as a winter cover crop in the southeastern U.S. and Europe. Nevertheless, cover crops have inherent issues because the crop needs to be harvested before reaching its full maturity. Although carinata seed offers an opportunity to produce renewable drop-in fuel for ground transportation and aviation sectors, uncertainty exists regarding the land-use change, carbon savings, conversion technology yields, cost, co-product allocation, environmental impact, and policies.

Similarly, renewable fuel and biochemical production from microalgae have garnered attention from researchers worldwide because it does not need a large amount of land to grow. Furthermore, it can grow in wastewater, reducing the demand for freshwater and nutrients [14]. Additionally, the biocrude yield from certain strains is 60 times higher than soybeans, and the growth cycle is extremely short [14]. However, commercial algal biocrude production still faces challenges due to the high cost and low efficiency of photobioreactors [15].

Hydrothermal liquefaction (HTL) is a thermochemical conversion pathway with a high conversion and energy efficiency rate to produce biocrude from algae compared to other conversion processes such as pyrolysis [16], [17]. HTL algae biocrude consists of highly reactive oxygenated compounds in the form of carbonyls, phenols, fatty acids and alcohols. It also contains high amounts of N-heterocyclic (~ 4-7 wt.%) compounds and aromatic organometallic complexes. Removal of these compounds requires high temperature and H_2 pressure [18]. During the past decade, algae biocrude stabilization has been carried out by various research groups [19]–[21] in

two-stage sequential hydrotreatment processes and non-isothermal approaches. The catalysts used for hydrotreating undergo deactivation due to coke formation arising from incorrect temperature, residence time, pressure drop, and presence of heavy metals that causes catalyst fouling. Metals such as Al, Ca, Fe, K, Mg, Na (4.0-160 mg/L) and trace elements of Cu, Mn, Ni, and Zn (0.5-2.0 mg/L) are also present in algal biocrude [14]. Hence, demetallization is also necessary since it will cause scaling and corrosion of reactors, deactivation of catalysts, and degradation of the end product. The metal content should be less than 1000ppm in the final product [22], [23].

Heteroatoms, organometallics, and reactive functional groups of HTL algae biocrude present significant challenges during hydrotreatments, such as undesired polymerization reactions that lead to rapid catalyst deactivation and lower liquid yield. Therefore, this study aims to reduce the algae HTL biocrude reactivity by blending it with non-edible vegetable oil (carinata) to improve physicochemical properties. Additionally, blending the two oils may help address the issues of feedstock sustainability, process scale-up, and the cost in HEFA (Hydroprocessed Ester Fatty Acids) refineries.

Researchers have explored vegetable oil, particularly edible oil such as rapeseed, for upgrading liquid intermediates. According to Han et al. [24], vegetable oil acts as a hydrogen donor solvent during the upgrading of pyrolysis bio-oil. Further, Han et al. [25] carried out co-hydrotreatment of rapeseed oil and tire pyrolysis oil over $CoMo/Al_2O_3$ to produce green diesel rich in naphthenic and aromatic compounds since the hydrotreated vegetable oil contains a lower amount of aromatics.

The majority of the literature regarding the blending of algae is either with different petroleum fractions for co-processing in conventional refineries or with vegetable oil to produce biodiesel [26]. There is limited information regarding the co-processing of HTL algae biocrude

with inedible vegetable oil. Wang et al.[27] studied co-hydroprocessing of 10 wt.% of HTL algae and heavy vacuum gas oil (HVGO). A slight decrease in conversion, increased catalyst coking, and a lower percentage of gasoline were observed compared to when the HVGO was used alone. In contrast, complete heteroatom removal was seen in blended feedstock [27], [28]. In another study [19], algae were co-processed with HVGO under FCC (fluid catalytic cracking) conditions where the conversion decreased. This could be due to N-containing molecules in the oil, which are detrimental to the catalyst. Therefore, a mild hydrotreating step was encouraged before the FCC unit. A synergistic effect was observed in a different study when co-upgrading of used engine oil and algae was performed using Pt/C catalyst [29]. The authors reported complete heteroatom removal, higher liquid yield, higher calorific value, and a higher fraction of light aliphatic and aromatic hydrocarbons in the upgraded blend. Similar findings were reported when different distillate fractions of algal biocrude were co-hydrotreated with used engine oil over Pt/C [30].

Catalysts are fundamental for catalytic reactions, but the supports having different morphology, composition, and orientation impact the hydrotreatment process [7], [27], [31], [32]. Metal dispersion and the bonding between active metal and support are affected by the catalyst support, which in turn determines hydrodeoxygenation (HDO), decarboxylation (DCO_2) /decarbonylation (DCO) reaction pathways [31]. catay [33], [34]. Conventional bi-metallic sulfided CoMo/Al and NiMo/Al are used for the commercial hydrotreatment process, where Mo serves as an active element while Co and Ni are promoters [35]. Gamma alumina (γ-Al_2O_3) imparts high surface area, robust mechanical and textural properties, and superior packing density[36], [37]. However, it becomes unstable during HDO reactions of highly oxygenated bio-oils due to the presence of water, which converts into boehmite [36], [38]. Carbon-supported catalysts have a high surface area, are more water resistant, and are more stable than alumina [39], [40]. However,

microporosity can block pores or active sites, making them inaccessible during the deposition of metals while synthesizing catalysts. The previous study [41] motivated us to use carbon-supported catalysts for this study. In our previous study, biochar supported Co and Ni catalysts successfully hydrotreated carinata oil to produce biofuel. Activation is necessary during the catalyst preparation method to reduce the inactive metal oxide phases to their respective active metallic states or sulfide states via the sulfidation process [36]. Sulfided transition metal catalysts are thermally stable and prevent rapid coking and are widely used in refineries for HDS (hydrodesulfurization) and HDN (hydrodenitrogenation) [33], [42]. These catalysts are also used for HDO reactions due to the presence of coordinated unsaturated sites located on the Co/Ni edges of their MoS_2 phase [43].

Cobalt supported on biochar support was able to successfully hydrotreat carinata oil in our previous study [41]. This further motivated us to utilize the same biochar support in the present study and introduce a bimetallic (cobalt and molybdenum) component instead of monometallic (cobalt) component on the support and hydrotreat a mixture of oils (HTL algae and carinata) instead of only carinata. Therefore, in the present study sulfided and unsulfided bimetallic (CoMo) catalysts on two supports (Douglas fir biochar support (DF) and alumina support (Al)) were used to hydrotreat a blend of HTL algae biocrude and carinata oil. Four types of catalysts were used: 1) alumina-supported CoMo (denoted as CoMo/Al), 2) sulfided alumina-supported CoMo (denoted as S-CoMo/Al), 3) Douglas fir biochar (DF)-supported CoMo (denoted as CoMo/DF), and 4) sulfided DF-supported CoMo (denoted S-CoMo/DF). The main objective of this study is to understand the synergistic effect of the blending and the order of reactivity for different supports in terms of HDO, HDN, HDS and HDM.

4.2 Material and Methods

4.2.1 Materials

H_2S gas (100 ppm and balance N_2) and H_2 gas (99.999 mol.%) were purchased from Airgas Inc. (Opelika, AL, USA). DF biomass was hammer milled (passed 1.68 mm) and was obtained from ForestConcepts, LLC (Auburn, Washington, USA). Cobalt (II, III) oxide (~3.4 – 4.5% CoO, ~11.5 - 14.5% MoO; 2.5mm trilobe extrudate) on alumina was purchased from Sigma–Aldrich (St. Louis, MO, USA). The as-received extrudates were ground (ranging between 106 µm and 38 µm) and used as alumina-supported catalysts. Cobalt nitrate hexahydrate (99 wt.% crystalline) and ammonium heptamolybdate, tetrahydrate (99 wt.% crystalline) were purchased from Sigma Aldrich (St. Louis, MO, USA) and were used as received for DF biochar supported catalyst. *Tetraselmis* algae purchased from Reed Mariculture (Campbell, CA, USA) had the following fatty acids profile: 14.5 wt.% palmitic acid methyl ester (C16:0), 15 wt.% linoleic acid methyl ester (C18:3) and the rest mainly consisted of linoleic acid (C18:2). Detailed nutritional analysis of this *Tetraselmis* algae strain could be found elsewhere [44]. Carinata oil was obtained from Applied Research Associates, Inc. (provided by Agrisoma Biosciences, Inc, Gatineau, Quebec, Canada). Detailed physical properties of the carinata oil could be found in our previous study [6], [41].

4.2.2 Catalyst preparation

Hammer milled Douglas Fir (DF) biomass (20 g) was mixed with 350 ml deionized water. To this slurry, calculated amount of metal salts (ammonium heptamolybdate and cobalt nitrate) was added to give a 11.5 wt.% Mo and 3.5 wt.% Co metal loadings on the final catalyst, respectively. The metallic salts mixed with DF biomass slurry was stirred at 80°C for 4 h to obtain a thick mixture. The mixture was then dried at 105°C overnight to obtain catalyst precursors. The

precursors were then activated by reduction using 10% H_2 and 90% N_2 at 400℃ (appendix Figure B1) with a residence time of 5h at 5°C/min with a flow rate of 0.2 l/min. The obtained catalyst was denoted as CoMo/DF. Ground as-received commercial cobalt molybdenum supported on alumina was reduced at (400℃) for 5h to obtain the catalyst represented as CoMo/Al [36], [45]. For sulfidation process, both the DF supported samples and alumina supported samples were prepared as described above under H_2 gas and once the temperature reached 400℃ the sulfidation was initiated by switching on the H_2S gas (0.2 l/min), for a total of 5h to obtain S-CoMo/DF and S-CoMo/Al catalysts, respectively. Finally, all the samples were cooled down to room temperature by passing N_2 gas and strored for further use.

4.2.3 Catalyst characterization

Detailed procedure for TG-TPR, Inductively Coupled Plasma-Optical Emission Spectrometry (ICP-OES), Brunauer–Emmett–Teller (BET)surface area, and X-ray diffraction (XRD) of the catalysts can be found in our previous study [40], [41], [46].

The average size was calculated according to the Scherrer's equation using the full width at half-maximum intensity.

Scherrer equation: $D=K\lambda\beta cos\theta$ (1)

Where D (nm) is the crystallites size, K is the Scherrer constant (0.9), λ (0.15406 nm) is the wavelength of the x-ray source, β is the FWHJ, and θ is the peak position.

4.2.4 HTL experiment

The HTL experiments were performed at a reaction temperature of 275°C and a residence time of 60 min to obtain HTL algae biocrude. For each HTL experiment, 600 g as-received

Tetraselmis algae was used, and the experiment was carried under N_2 atmosphere (appendix Figure B2). Details about the HTL Parr reactor and procedure are given in our previous study [47].

4.2.5 Co-hydroprocessing experiments

The co-hydrotreatment tests were carried out in a 100 mL Parr 4598 bench top reactor. HTL algae biocrude (10gm), carinata oil (10gm), and a 50:50 (wt.) mixture (20 gm in total) of these two oils were performed at 400°C for 5h with 1000 psi of H_2 using feed-to-catalyst mass ratio of 70:1 (10 gm oil and 0.143 gm of catalyst). Identical parameters were used from our previous publications [6], [41] and this study tried to understand the role of biochar as a support for hydrotreating a blend of two oils and when two metals are impregnated on it. Since the motivation of the current study was to understand the effect of catalysts on product yield distribution and properties, the study was not focused to determine the role of process parameters such as temperature, time, H_2 gas pressure, blend ratio and catalyst to oil ratio. All the hydroprocessing experiments were conducted in duplicates.

4.2.6 Analysis of products

For mass-balance purpose, the liquid and solid reaction products were weighed. The liquid products along with the solid products were centrifuged. Details about hydrogen consumption, liquid yield, and solid yield calculations were explained elsewhere [41]. Similarly, detailed procedure and instrument specifications for viscosity, GC-MS, total acid number (TAN), elemental analysis (CHNS-O), higher heating value (HHV), and simulated distillation (SimDis) can be found in previous studies [6], [40], [41], [46]. Boehm titration method could be found elsewhere [48].

Detailed hydrocarbon analysis (DHA) was performed by using Perkin Elmer Clarus 680 GC with FID detector using the PIANO method. PIANO describes the method for determining the amount of paraffins and iso-paraffins (P), aromatics (A), naphthene (N), and olefins (O) within a sample. The PIANO method is mainly used for gasoline-type samples, which is why it is limited to compounds with carbon numbers less than 14. Any C_{15} compounds or heavier were reported as unknown compounds. This method is based on ASTM test method D6730-01 which is specific for the analysis of hydrocarbon components. A small amount (0.2 g) of each sample was weighed to the nearest 0.1 mg and diluted to 10.00 ml with carbon disulfide. A 1.00 µl of the diluted sample was injected into a100 m x 0.25 mm ID capillary column coated with 0.5 µm of 100% dimethyl polysiloxane stationary phase. The initial temperature of the GC injector was set at 200°C and held at this temperature for 43.15 min. The sample injector of the GC was heated to 450°C at 100°C/min and held at this temperature throughout the end of the test. The injected sample was carried through the column by using hydrogen with a flow rate of 100 mL/min. The initial oven temperature was held at 35°C for 5 min, heated to 50°C at 10°C/min and held for 21.5 min. Then the oven temperature was ramped to 340°C with a heating rate of 3.0°C /min and kept at 340°C for 30 min. The FID detector temperature was 250°C with a hydrogen flow rate of 42 mL/min and an air flow rate of 450 mL/min. Each eluting component was identified by comparing its retention time to that established by analyzing reference standards under identical conditions.

The higher heating value (HHV) of the gas were calculated based on the equation below [49].

$$HHV_{gas} = Y_{co} * HHV_{co} + Y_{CH4} * HHV_{CH4} \quad (2)$$

where Y= mole fraction of the gas such as CO (carbon monoxide) and CH_4 (methane), HHV_{co} = **12.68 MJ/m^3, HHV_{CH4} = 39.78 MJ/m^3**

4.3 Results and discussion

4.3.1 Catalyst Characterization

The textural properties of the catalysts such as surface area, pore size, pore volume and pore size distribution are shown in Table 4.1. Biochar supported catalyst achieved a higher BET surface area compared to alumina support. The DF supported catalysts had a lower average pore size (< 2 nm) and lower pore volume compared to alumina. The highest surface area of 391 m^2/g was observed for CoMo/DF, followed by S-CoMo/DF (296 m^2/g), while a decrease of 35% and 14% were noted for CoMo/Al and S-CoMo/Al, respectively.

Table 4.1 BET surface area and pore analysis of catalysts.

	BET surface area	Average Pore size	Total Pore Volume
	m^2/g	nm	cc/g
S-CoMo/DF	296±30	1.69±0.2	0.16±0.02
S-CoMo/Al	252±11	3.82±0.7	0.63±0.01
CoMo/Al	254±14	4.6±0.3	0.63±0.01
CoMo/DF	391±15	1.71±0.2	0.23±0.01

Sulfidation had a prominent effect on the DF supported catalyst compared to alumina support as seen by the decrease in the specific surface area from 391 m^2/g to 296 m^2/g, and total pore volume. This could be due to the deposition of sulfur within the pores in the case of S-CoMo/DF. While alumina catalysts, when sulfided, exhibited a small difference in their textural properties in comparison to their unsulfided counterpart. Therefore, sulfidation mechanism differs based on the type of support. Type I and type II sulfidation mechanism are generally seen in alumina and carbon support, respectively, and it is explained in detail in Section 3.4. In brief, type I support resists complete sulfidation, therefore it could be the reason for the minor difference in the BET surface

area for the alumina catalysts. According to literature, the transition metal sulfided heterogeneous catalysts are made of Mo slabs promoted at the edge by Co and dispersed over a polycrystalline oxide support. Strong ambiguity lies on the role of the oxide support on the sulfide active phases and how it changes its size, texture, surface area and sulfidation degree. Small differences such as alumina polymorphism can be a significant factor [50]. Lower surface area for alumina could be due to higher agglomeration when CoMo is encapsulated by silica [51].

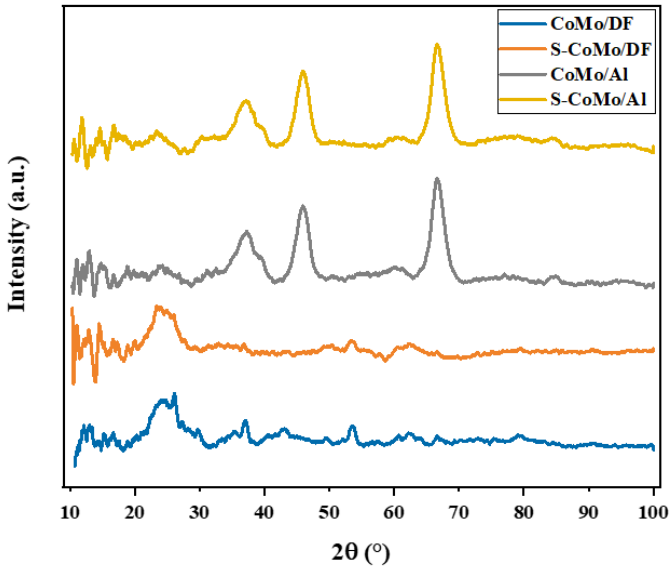

Figure 4.1 XRD patterns of different catalysts.

Both the sulfided and unsulfided alumina catalysts samples showed typical diffraction peaks at 2θ ≈ 45° and 2θ ≈ 65° that confirmed the presence of cubic alumina oxides [52]–[54]. Peaks in the range of 2θ ≈ 30°–35 are due to $CoMoO_4$ crystallites [55]. The peaks are not well defined and it could be due to a promoting effect of cobalt on the support which is well dispersed at a nanoscale [53]–[55]. The weak peak at 2θ ≈ 26° on biochar support could be due to $CoMoO_4$ phase [56]. Literature also suggests that board diffraction peak around 24.9° could be due to amorphous structure of carbon [56]. The other characteristic diffraction peaks were observed at 2θ of about 37° and 54° which are visible in the case of CoMo/DF and this could correspond to MoO2 phase.

The weak interaction of the biochar support with Mo enhances the mobility and cluster of Mo species and the formation of the CoMoO4 phase as we have already seen at 2 θ=26° [56]. There could be more than one highly dispersed Co phase such as CoO but probably the crystallites were too small to provide an adequate XRD signal or the particles were well dispersed on the support [57].

Based on the XRD pattern and Scherrer equation, the $CoMoO_4$ crystal size on alumina support is smaller than biochar support (~ 18nm and ~ 26nm, respectively). Turnover frequency (TOF) or surface specific activity depends on the surficial metal area which are computed using experimentally measure average particle size obtained from XRD [58]. Literature reports are scattered where several research groups have reported that TOF is independent of cobalt particle size while others have reported a decrease in TOF with Co particle sizes smaller than 10 mm [59]–[61]. Another study of hydrogenation of 1,3-butadiene was studied on a series of Pd/Al_2O_3 and the author reported that TOF is independent on PD particle size (> = 4nm) and incomplete (111) terraces are the active sites (using this as rate of normalization) with the help of scanning tunneling microscopy [62]. But, if the rate of normalization is done taking into account the total number of Pd surface atoms then TOF is dependent on particle size [62]. In general, hydrotreatment is thought to not dependent on structure, but some studies suggest that very small particles below a critical threshold of 8-10 nm are less likely to be an effective catalyst. Extremely small particle size could be less effecive due to insufficient edge defects for catalysis to occur, they could slow reaction rates by binding the reactants strongly, and they could prevent reduction or promote oxidation due to high surface area [58]–[62]. Many literature suggests that particle size above approximately 10nm above which TOF are unchanged [58]. Support plays an important role because it imparts a significant effect on the reducibility, activity, and selectivity of the products. A balance between

reducibility and dispersion of the metal precursors determines hydrotreatment performance [60]. Among all the supports, carbon supports are considered to be more inert compared to conventional oxide supports. In our study, we can notice that the crystal size of alumina support is smaller than the biochar support and it exhibited superior HDO activity primarily by decarbonylation. On the other hand, biochar support, catalyzed cracking reactions followed by high HDN and HDS activity compared to the alumina supported catalyst. Therefore, from our study we can suggest hydrotreatment is size independent. However, individually HDO activity was favorable for catalysts having smaller particle size while HDS and HDN activity were size independent. We would also like to add that particle size varies depending on the method used. For example, Ghampson et.al., [58] found that, particles were 20-70% larger when chemisorption (reduction) was used compared to XRD (oxidation), which could be due to sintering of particles during reduction. Additionally, particle size and diameters vary dramatically when incomplete reduction of particles are taken into consideration.

ICP-OES was used to analyze multiple trace metals in catalyst, crude oil and upgraded oil (appendix Table.B2). S-CoMo/DF showed higher S content compared to unsulfided catalyst. This correlates well with the BET surface area (Table.1.1), where the S-CoMo/DF have lower surface area and total pore volume than unsulfided DF catalyst. However, S-CoMo/Al and CoMo/Al have less difference in their S content. Also, there is no substantial difference in their BET surface areas. Therefore, again it could be confirmed that effect of sulfidation was more pronounced in DF supported catalysts than alumina. However, this could be due to the ICP-OES process, where reduced forms of sulfur can be very amenable to volatizing as H_2S or if other elements such as barium are part of the samples matrix, during dissolution pahse barium will precipitate as acid insoluble barium sulfate, resulting in a low bias.

Numerous studies have shown that chemical interactions occur between the alumina support and the transition metal oxides that in turn produces stable species that resist complete sulfidation [63]. No leaching of heavy metal ions from the catalyst were observed for any of the upgraded oils (algae, carinata and blend) irrespective of the catalyst source or sulfidation. The CoMo/Al and S-CoMo/Al had Co loading of 1.8 wt.%, 1.9 wt.%, and Mo metal loading of 7.5 wt.%, 7.7 wt.%, respectively. This loading is lower than the anticipated 3.5 wt.% and 11.5 wt% of Co and Mo (reported by the manufacturer), but it could be due to various reasons such as acid digestion, sampling issues while analyzing the metals or could be due to partial reduction. The synthesized sulfided and unsulfided DF supported catalysts prepared by wetness impregnation method showed 1.7 wt.% content of Co. Approximately, 10 wt.% and 9.8 wt.% of Mo content was seen for CoMo/DF and S-CoMo/DF, respectively. The anticipated weight percent should have been 3.5 wt.% and 11.5 wt.% for Co and Mo, respectively.

4.3.2 Product yield distribution and gas analysis

Figure 4.2 illustrates that the hydrotreated liquid was the most abundant product fraction from the catalytic upgraded blend (UB), upgraded algae (UA), and upgraded carinata (UC) oils. Non-catalytic UB had the lowest liquid yield (60%) and highest wax yield (29.4%). This could be due to absence of catalyst in which the blend underwent rapid saturation of C=C bonds to form large amount of wax. Wax in this study is defined as the portion of the liquid having higher density than the upgraded liquid that settled at the bottom of the centrifuge tube after centrifugation. Addition of catalyst irrespective of the support was beneficial in terms of higher liquid yield, lower wax yield as seen in Figure 4.2. Maximum liquid product yield for the UB was 85% under S-CoMo/Al catalyst and minimum yield was 67% under S-CoMo/DF.

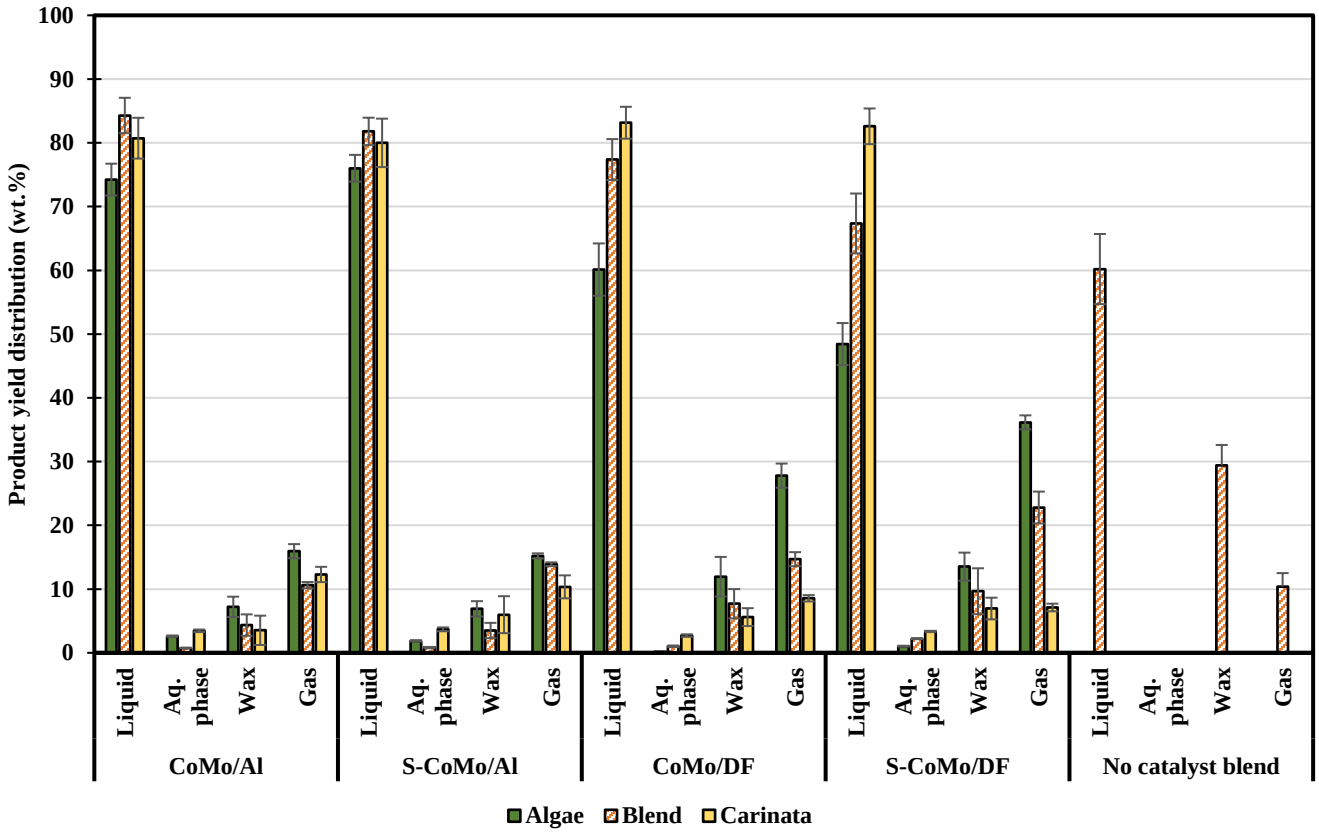

Figure 4.2 Product yield distribution after hydrotreatment of algae and carinata and co-hydrotreatment of their upgraded blend over different supports and sulfidation state.

Irrespective of the sulfided status of the UBs, the DF supported catalyst had the lower liquid yield and higher wax yield compared to alumina support. According to literature [64] this could be due to high dispersion percentage and presence of Bronsted and Lewis acid sites that facilitate both hydrogenation and hydrogenolysis reactions for alumina support. Additionally, biochar support matrix was not inert, as we have seen in our previous study [41]. It has inherent acidic sites, which undergoes cracking and mild hydrogenation [41]. The biochar matrix could have soaked a large proportion of oil and thus a decrease in the liquid yield and an increase in the wax/solid yield was observed. This UC yields under biochar support are comparable to our previous study [41], where DF support was successful to hydrotreat carinata oil.

The gas products mainly consisted of CO, CO_2, CH_4 and C_2-C_5 gases. CO was the most abundant gas, followed by CO_2 and CH_4 gas as seen in Table 2. In our previous study [41], monometallic Co was impregnated on DF biochar support to hydrotreat carinata oil, and our results showed that DCO was absent. However, in this study, DCO was present when bimetallic CoMo was used over the same DF support. Therefore, Mo component might the responsible for DCO pathway. This conclusion is supported by Wang et. al where the authors [65] used Mo_2C supported on activated carbon for hydrotreatment of fatty acids into green diesel. It is interesting to note that, CH_4 gas was not present in the UB irrespective of the support. However, CH_4 was present in the highest quantity in the UC. Therefore, blending of the carinata and HTL algae probably caused a synergistic effect that suppressed methanation reaction. Therefore, DCO and DCO_2 could be the probable reaction pathways to remove oxygen for the blended feedstock along with HDO.

UB produced from DF support resulted in lower amount CO_2 (5 % and 13.7%) and CO gas (56% and 52%) in comparison to alumina support. Table 4.2 further demonstrates that DCO was predominate for UA while UC exhibited lower DCO, higher methanation and DCO_2 compared to UA and UB irrespective of the catalyst support. A study by Buri et.al. [66] reported DCO and DCO_2 were the main reaction pathway for sulfided NiMo species for HDO of palm oil.

Irrespective of the support type and sulfidation status, all the UB gas showed higher heating value (syngas) compared to UA and UC gases as seen in Table 4.2. A synergistic effect could be seen by blending the algae and the carinata oil. Blended oil retrieved over alumina supported catalysts had a lower hydrogen consumption per kg of oxygen removal compared to its upgraded parent feedstock and DF supported catalyst. Additionally, in the case of alumina support, carinata oil could have been acting as hydrogen donor solvent to the hydrogen deficient algae biocrude[25], [28]. On the other hand, higher hydrogen consumption per kg oxygen removal for UB (DF

supported catalyst) could be due to hydrogen spillover effect where the biochar support acts as a hydrogen reservoir [67]. This spillover mechanism is usually seen for carbon supports which have higher oxygen functional groups. Under different types of catalyst support and sulfidation state, UA showed that it is easier to remove O_2 from the oil compared to UC under similar conditions.

Table 4.2 Gas composition and HHV of upgraded oils over different supports.

Catalyst	Hydrotreated oils											
	S-CoMo/Al			CoMo/Al			S-CoMo/DF			CoMo/DF		
	UA	UB	UC	UA	UB	UC	UA	UB	UC	UA	UB	UC
H_2 /kg of O*	47.8	38.2	48.2	47.7	41.8	53.9	58.5	64.1	63.6	55.3	58.8	65.7
ΔP (psi)	-348	-318	-518	-494	-413	-756	-397	-705	-439	-340	-432	-624
CH_4	0.26	ND**	4.92	0.44	ND	5.48	0.03	ND	5.12	0.08	ND	3.14
CO_2	0.72	20.38	11.75	0.63	18.05	12.50	0.18	5.06	8.79	0.19	13.77	10.96
CO	36.57	57.83	9.50	33.32	58.29	10.85	14.54	56.81	16.58	23.15	52.39	19.89
HHVsyngas***	2.46	3.90	2.30	2.34	3.93	1.88	0.98	3.83	2.20	1.57	3.53	2.00

* Mole of hydrogen consumed per kg of oxygen in crude oil, **ND= not detected, *** H_2 free basis.

Overall, less hydrogen consumption occurred in the alumina-based catalysts for the upgraded oils and water was present as one of the reaction products. Therefore, dehydration rection was one of the pathways in the HDO reaction scheme.

It could be seen that in terms of the UB and UC, the UB had lower pressure drop compared to UA and UC for alumina support. Effect on sulfidation is prominent on the pressure drop results for UA and UB (S-CoMo/Al), as it seems to cause less hydrogen consumption, while the opposite is true for UC compared to their unsulfided counterparts. A high pressure drop (high hydrogen consumption) could be due to highest methane gas formation in the case of UC for S-CoMo/Al. On the other hand, for the DF supported catalysts, the sulfidation caused a higher hydrogen consumption for UA and UB and less for UC compared to their unsulfided counterparts. Similarly, high hydrogen consumption on UB could be due formation of aqueous phase after hydrotreatment.

Additionally, higher hydrogen consumption for DF supported catalysts could be due to hydrogen spillover effect where the biochar support acts as a hydrogen reservoir. The significant differences in the reaction pathway between sulfided alumina and sulfided biochar supported catalysts require further studies to explain them. However, it could be due to differences in electronic properties of CoS and MoS_2, that could lead to different adsorption of the blend that consisted of complex molecules on the surface of different sulfides and remove heteroatoms either as HDO or DCO_X **pathway** [68]. However, there is tradeoff between hydrogen consumption and gas generation.

4.3.3 Effect of hydrotreatment on individual feedstock (upgraded algae and upgraded carinata)

For easy comparison, the values for the bulk properties can be found in Table 4.3 and 4.4 Additionally, each bulk property are graphically illustrated. The HTL algae biocrude was a highly viscous oil with a relatively high nitrogen (~4 wt.%), oxygen content (~39 wt.%) and TAN (31 mgKOH/g) and low HHV of 26 MJ/kg. It was not possible to measure the viscosity of the HTL biocrude because it was highly viscous. The oxygen content is considerably high (38.58 wt.%) compared to the literature. Studies by different researchers [61], [62] reported carbon and oxygen content of ~ 70% and ~13% respectively. Methanol was used to extract the HTL biocrude in this study. A ~ 53% increase in carbon and ~ 66% decrease in oxygen content were noted by simply replacing methanol by DCM. The elemental compositions of the biocrude extracted by DCM and methanol are reported in the appendix (Table B1). The carbon and oxygen are well within the literature expected range. Most of the researchers worldwide report this number and term this as biocrude/bio-oil and doesn't do further research or processing such as hydrotreatment of this DCM extracted biocrude to produce fuels or chemicals. Our team in one of our previous studies tried to hydrotreat the DCM extracted biocrude to produce biofuel. But our team ran into multiple issues

such as high reactor pressure, equipment corrosion, catalyst deactivation and polymerization (appendix Figure B3). The DCM polarity, chemical structure, hydrogen bonding, and dipole–dipole interactions with biocrude are likely to make DCM the strongest solvent that could extract most of the HTL organic products, but we were unsuccessful in hydrotreating the DCM extracted biocrude. Chloride content test showed that only DCM-extracted biocrude had a high chloride content and HCL gas was also formed during hydrotreatment. Chlorine-containing molecules were probably formed during rotary evaporation. Also, it is suspected that DCM was trapped within molecular cages of biocrude complex compounds and did not evaporate under vacuum evaporation conditions. Therefore, this study also confirmed our previously published article [34], that the elemental content of HTL biocrude depends on the type of the solvent used during the extraction. In this study methanol compared to DCM extracted less HTL organic products and thus it had 39 wt.% oxygen. Type of solvent along with rotary evaporation time, speed, pressure and biocrude type and amount equally play a huge role in the quality of the extracted HTL biocrude. For details regarding the effect of solvent-extracted biocrude from hydrothermal liquefaction of municipal sewage sludge for hydrotreatment please refer to our previous study [34].

Carinata oil had 0.7 wt.% N, ~18 wt.% O, HHV of ~ 39 MJ/kg and kinematic viscosity of ~ 50 m^2/s as seen in Table 3 and 4. A 23% reduction in N content took place for UA using S-CoMo/DF compared to algal biocrude. Duan and Savage's group [69]–[71] conducted catalytic hydrotreatment of HTL algae (*Nannochlorpsis*) with Pt/C at 400℃ for 240 min at 500psi (initial pressure) and the upgraded oil had nitrogen content of 3.68%. However, they stated that increasing the amount of catalyst increased the denitrogenation. Our study used similar temperature and residence time; however, our study achieved a lower nitrogen content (2.37 wt.%), and this could be due to high H_2 pressure (~1000 psi) which favors HDN reaction over HDO. Another study [70]

by the same group reported a low nitrogen content (1.5 wt.%) was achieved at 530℃ for 360 min with 10% Pt/C catalyst. This conclusion is supported by Haider et.al where the authors found out that HDN needs severe operating conditions compared to HDO [19]. S-CoMo/Al was found to have the highest degree of deoxygenation for both UA (88% decrease) and UC (83% decrease) compared to their crude parent oil. A vast amount of literature [72]–[74] supports that non-sulfided catalysts becomes deactivated sooner than sulfided catalysts due to excessive coke formation. This could have an effect on the HDO activity of the catalyst as well. Similarly, S-CoMo/Al had a positive effect on increasing the C amount in the UA and UC. Almost 99% reduction in TAN (UA) by both DF supports were achieved compared to HTL algae biocrude as seen in Table 3. This indicates DF support catalyzed the reduction of carboxyl groups that reduced the TAN. Similar results were reported by Wang et. al. [75], where the authors described that activated carbon support was successful in hydrogenation of heavy compounds found in algae. After upgrading, the KV_{40} (UC) decreased by 94% compared to carinata oil using S-CoMo/Al. This is due to cracking of large and complicate structures to small and simpler ones. The highest HHV of UC (S-CoMo/Al) was 43.7 MJ/kg a 11% increase from carinata oil, which is in good agreement with the lowest oxygen content among the UC oil.

4.3.4 Effects of sulfidation and catalyst support on upgraded blend oil properties

The synergistic effects (%) were calculated by taking the average between the UA and UC and computing the difference with the UB. Positive sign (+) indicates a favorable change and a negative sign (-) indicates an unfavorable change**.** Detailed calculations of synergistic effect are shown in appendix (Table B3).

The kinematic viscosity (KV) of UA and UC were between 2 to 3 mm^2/s at 40℃ as seen in Table 3 and 4. The KV_{40} (UB) by S-CoMo/DF was the lowest at 1.4 mm^2/s, followed by CoMo/DF (3.3),

CoMo/Al (4.0), and S-CoMo/Al (5.4), respectively. The KV_{40} of diesel is in the range of 1.5-4.5 mm^2/s and our study achieved a lowest KV_{40} of 1.4 mm^2/s. For the S-CoMo/Al support, the KV40 had negative synergistic effect, while the S-CoMo/DF support exhibited a 77.5% decrease (positive synergistic effect). Lower values of KV40 (1.45 m2/s and 3.30 m2/s) could be due to enhanced cracking by the DF support which reduced the complex higher molecular weight compounds into lower-MW and simpler ones.

The UB (CoMo/Al) had the lowest TAN (1.8 mgKOH/g) while S-CoMo/DF showed the highest (6.1 mgKOH/g), this phenomenon is opposite to the KV40 values. UB from sulfided and unsulfided the alumina catalysts exhibited a negative and positive synergistic effect respectively. However, in the case of DF supports, the TAN values from UA were considerably lower compared to UB. This seems to indicate the near complete removal of fatty acids, organic acids, and phenols. In contrast, UB demonstrated a significant increase in the TAN number. DF supports were unfavorable to remove the carboxylic or other oxygenated groups in the oil when both the crude HTL algae and carinata were blended together. It is suspected that oxygenated complexes might have formed which drastically increased the acid number. All of the UBs had HHVs ranging from 44 MJ/kg to 46 MJ/kg. The highest HHV of 46.31 MJ/kg was obtained by the UB produced from S-CoMo/Al, which is comparable to commercially available diesel fuel (46.5 MJ/kg). Unsulfided CoMo/DF had a lowest HHV of 44.0 MJ/kg which was closely followed by 44.83 MJ/kg (sulfided CoMo/DF). The UB with no catalyst showed the lowest HHV of 40 MJ/kg.

Table 4.3 Physiochemical characterization of feedstock and hydrotreated oils over sulfided and unsulfided alumina support.

	Feedstock			Hydrotreated oils									
	Carinata oil	HTL-algae biocrude	Blend	S-CoMo/Al				CoMo/Al				No catalyst	Gasoline
				Algae	Blend	Carinata	Synergistic change %	Algae	Blend	Carinata	Synergistic change %	Blend	
Oil properties													
Elemental composition (wt.%)													
C	70.4	47.85±0.63	59.12	79.39±0.3	83.16 ±0.9	81.27±0.5	+3.5	77.12±1.1	82.44±0.8	79.29±1	+5.4	72.42+1	85-88
H	11.3	10.28±0.40	10.79	11.63±0.1	13.52±0.4	12.57±0.1	+11.7	11.44±0.5	13.42±0	13.511±0.3	+7.5	11.47±0.6	12.6-13
N	0.7	3.085±0.08	1.89	2.98±0.1	1.7±0.1	0.15±0.1	+29.6	3.15±0.1	1.53±0.2	0.22±0.1	+4.5	3.3±0.4	0
O	17.9	38.58±1.03	28.24	4.59±0.2	1.38±0.8	2.98±0.6	+63.5	6.97±2	2.45±1	5.93±0.3	+61	14.98±1	0.05
HHV (MJ/kg)	39.23 ± 0.6	26	32.61	42.43±1	46.31±0.8	43.7±1	+7.54	41.88±1	45.04±0.1	42.84±0.7	+6.33	40.06±1	47.3
TAN (mgKOH/g)	0.68	31	15.5	2.80±0.3	1.83±0.1	0.41±0.1	-12.5	4.11±1	2.8±0.7	2.15±0.2	+10.5	9.8±0.2	0
Density (g/cm^3)	0.9±0.0	NA	NA	0.82±0.3	0.81±0.1	0.78±0.1	-1.25	0.92±0.0	0.84±0.0	0.81±0.1	+2.9	0.91±0.0	0.77 at 15°C
Kinematic viscosity 40°C (m^2/s)	49.5± 0.1	NA*	NA	1.80±0.3	5.43±0.1	2.74±0.8	-140	3.43±0.1	4.02±0.4	3.53±1.3	-15	30.2±1.3	0.5-0.8 at 20°C

*NA – Not possible to measure

Table 4.4 Physiochemical characterization of feedstock and hydrotreated oils over sulfided and unsulfided DF support.

	Feedstock			Hydrotreated oils									
	Carinata oil	HTL-algae biocrude	Blend	S-CoMo/DF				CoMo/DF				No catalyst	Gasoline
				Algae	Blend	Carinata	Synergistic change %	Algae	Blend	Carinata	Synergistic change %	Blend	
Oil properties													
Elemental composition (wt.%)													
C	70.4	47.85±0.63	59.12	77.23±1	81.84±0.6	79.03±2	+4.7	75.21±1	81.06±1	81.55±1	+3.41	72.42±1	85-88
H	11.3	10.28±0.40	10.79	11.21±0.3	13.21±0.1	13.28±0.1	+7.8	11.03±0.2	13.59±0.2	13.60±0.2	+10.3	11.47±0.7	12.6-13
N	0.7	3.085±0.08	1.89	2.37±0.02	1.08±0.2	0.32±0.1	+53.8	3.01±0.1	1.13±0.1	0.19±0.1	+29.8	3.3±0.5	0
O	17.9	38.58±1.03	28.24	9.63±2	3.73±0.6	7.26±1	+55.8	7.05±2	3.58±1	4.56±1	+38.5	14.98±1	0.05
HHV (MJ/kg)	39.6 ± 0.6	26	32.61	41.01±1.1	44.83±0.1	42.07±1.3	+7.92	40.84±0.3	44.06±0.8	42.4±1	+5.86	40.06±1	47.3
TAN (mgKOH/g)	0.68	31	15.5	0.91±0.2	6.1±0.4	0.09±0.05	>100	0.36±0.4	4.5±0.1	3.75±1.1	>100	9.8±0.3	0
Density (g/cm^3)	0.9± 0.0	NA	NA	0.9±0.0	0.85±0.0	0.87±0.1	-8.9	0.88±0.1	0.88±0.1	0.79±0.0	-6.0	0.91±0.0	0.7 at 15℃
Kinematic viscosity 40℃(m^2/s)	49.5± .1	NA	NA	3.67±0.1	1.45±0.4	9.32±0.1	+77.5	2.82±0.6	3.30±1.1	3.14±0.1	-10	30.2±1.3	0.5-0.8 at 20℃

*NA – Not possible to measure

Although the differences in the HHV between the catalysts are small, sulfided catalysts tend to show a higher HHV than unsulfided irrespective of the support. Overall, for the UB, CoMo supported on alumina performed slightly better than DF biochar support. Presence of oxygen reduces the heating value and stability of the bio-oil. The oxygen content in the UB varied from 1.38 wt.% (S-CoMo/Al) to 3.73 wt.% (S-CoMo/DF) and sulfided catalysts fared slightly better than unsulfided catalysts, while the no catalyst UB had 14.9 wt.% of oxygen. Both the supports irrespective of their sulfidation state displayed positive synergistic effects. Correlating with HHV, UB from S-CoMoAl and CoMo/DF showed lowest and highest oxygen content and highest and lowest HHVs, respectively. These results are in good agreement with the lowest TAN content of the UB produced from S-CoMo/Al. Therefore, sulfided alumina were better at HDO, HHV and TAN compared to other catalysts. These activities could be attributable to sulfur vacancies on the Co edges of MoS_2 slabs and the C-O cleavage activity due to Bronsted acid sites (S-H groups) situated on the sulfur edges [36].

The nitrogen content was between 1.08-1.70 wt.%. DF supported catalyst exhibited a higher positive synergistic effect compared to alumina support. Similar results were observed in a study by Dugulan et. al., where sulfided carbons support showed high HDN performance compared to alumina support.

The acid sites of the DF biochar are calculated by Boehm Titration method (Table B4) and it agrees well with NH_3-TPD test from our previous study [41]. CoMo/DF showed stronger acid sites (phenolic 10.3 mmol/g) compared to S-CoMo/DF. Lactonic acid is not present in CoMo/DF and it agrees with the literature where lactonic acid was absent in corn straw biochar as well [76]. According to literature, reductive treatment such as sulfurization leads to stronger modification of the number and type of acid sites. After sulfurization, the OH acid sites which were present in the

highest concentration were replaced by medium acidic sites (C=O). The total acid site density was reduced and the OH and COOH groups were replaced by lactonic acid groups [77], [78]. HDN and HDS reactions are favored by acidity in the catalysts [23]. For example according to Li et.al., [79] and Zhou et.al [80] sulfurization produces higher amount of lactone acid groups which ultimately leads of better HDS performance. Our results agree with the literature S-CoMo/DF catalysts were able to effectively remove nitrogen and sulfur from the feedstock compared to other catalysts. Additionally, Li et. al [79] stated that the desulfurization is based on Lewis-acid theory where the sulfides present in the feedstock as Lewis base gets easily adsorbed to the Lewis acid center of the catalysts. Therefore S-CoMo/DF had a lower surface area (296 m^2/g), higher pore size (1.71nm), medium acid sites and exhibited lower acidity compared to CoMo/DF and demonstrated excellent heteroatom removal compared to CoMo/DF. Along with porosity, surface area and acidic sites, DF biochar inherently consists of alkali and alkaline earth metals and these act as base sites and take part in the base- driven reaction pathway [81]. Therefore, according to our previous data and literature data (appendix Figure B13), DF supported catalysts might have more acidic sites which means that it might have more active sites with higher affinity to adsorb and remove sulfur and nitrogen compared to alumina support [56].

The C and H content of the UB were between 83 wt.% to 81 wt.% and 13.2 to 13.5 wt.%, respectively. The highest C content (83.16 wt.%) of the UB by S-CoMo/Al correlates to the highest HHV among the blends (46.31 MJ/kg) and lowest O (1.38 wt.%) as well. High H/C ratio suggests that an oil underwent successful hydrogenation reaction. Van-Krevelan diagram (Figure 4.3) shows the ratio between the chemically converted oxygen containing organic compounds to carbon and hydrogen to carbon ratio [82]. By computing the individual values (H/C and O/C) for the HTL algae biocrude and crude carinata the average of the blended crude oil is calculated. The average

ratio of H/C and O/C of both of the crude oils were 2.25 and 0.39, respectively. After hydrotreatment without catalyst, the ratio lowered to 1.9 (H/C) and 0.15 (O/C), respectively. It signifies that even without a catalyst hydrotreatment occurred and it was able to partially remove oxygen and increase carbon and hydrogen in the upgraded oil by using heat. However, introduction of catalyst irrespective of support type or sulfidation state was able to further hydrotreat and lower the H/C and O/C ratio to levels as close to commercial gasoline/diesel/kerosene range by favoring HDO, DCO_2, DCO, and catalytic cracking reactions to take place. The commercial oils have negligible oxygen, and the H/C ratio are between 0.6 to 1.8. This study was able to lower the O/C ratio between 0.02 to 0.03 and H/C ratio between 2 to 1.8 for all upgraded oils.

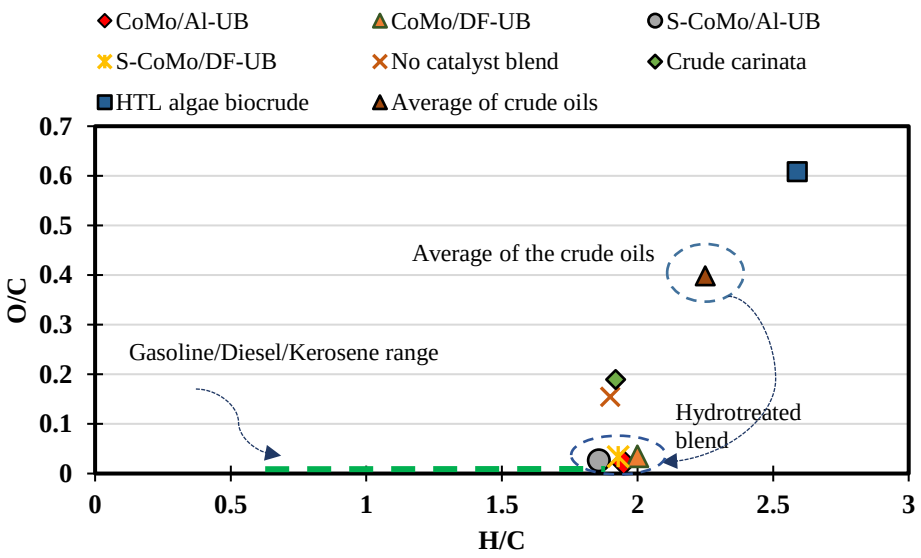

Figure 4.3 Van Krevelen plot (H/C vs. O/C) of commercial fuels, raw carinata, HTL biocrude, and hydrotreated blended feedstock on various catalysts.

From the ICP-OES data (appendix Table. B2) significant amount of Fe, S and K can be seen in the biocrude, and the presence of Fe agrees with previous literature [19]. This is likely due to presence of iron porphyrin structures inherent to algae biocrude that are rich in nitrogen. Compared to HTL algae oil and carinata oil, all the upgraded oil and their blends showed lower

amount of metal content after hydrotreatment. According to Haider et.al [19], where the authors studied hydrodemetallization of *Spirulina* over graded catalyst bed (Mo/Al and NiMo/Al) at different temperatures, reported that demetallization strongly depends on temperature and independent of the nature of hydrotreating catalyst. However, in our study, demetallization was strongly depended on catalyst support. For example, biochar support was able to successfully remove Fe to less than 5 ppm from UA and UB when compared to 95.5 ppm and 20 ppm in UA (S-CoMo/Al and CoMo/Al) and 11.23 ppm and 9.50 ppm in UB (S-CoMo/Al and CoMo/Al), respectively. Approximately 85%, and 74% of S removal could be observed in the case of UA for DF supports compared to CoMo/Al and S-CoMo/Al, respectively. Additionally, lowest amount of S (134 ppm) produced from S-CoMo/DF was observed among all the UB's. Therefore, biochar support was able to reduce appreciable amount of metals in upgraded oil compared to alumina supported catalysts. This could be due to various oxygen containing functional groups, inorganic mineral oxides, ion exchange capacity and high surface area, pore structure and connectivity in a biochar. All of these make a substantial contribution to its unique sorption behavior [83], [84]. Higher HDS activity on sulfided carbon support compared to sulfided alumina is well studied in the literature [56], [63], [85]. A model by Topsoe [36], [86] was based on Co-Mo-S phases in alumina catalyst. In this model, the active phases of CoMo/Al are due to type (I) and type (II). Type (I) consists of MoS_2 monolayer, while type (II) comprises of multilayer slabs of MoS_2 with Co on the edges. Type (I) is less active and incompletely sulfided, due to interaction of the monolayer and alumina support via electronic transfer of Mo-O-Al linkages [36], [87]. While, in type (II) all Mo-O-Al linkages are completely sulfided. High HDS activity in the activated carbon support is due to weak interaction of the support and the active sulfide phase due to the existence of only type (II) Co-Mo-S structures [87]. Therefore, the carbon-supported catalysts are twice as

active for HDS compared to alumina supported catalysts. According to literature, the adsorption properties of carbon and alumina are quite different. For example, NiMo/C showed superior HDN (quinolone) and HDS (dibenzothiophene) activity compared to NiMo/Al, but an unsatisfactory performance was observed in the case of hydrotreatment of heavy gas oil. This is because the polyaromtics compete for adsorption with the HDN/HDS active sites in the carbon support [87]. Therefore, DF supported catalysts, has dual characteristics; as an effective HDS and HDN catalyst and equally effective HDM catalyst due to its effective sorption mechanism [56]. Biochar has high surface area, oxygen functional groups, inorganic mineral oxides, ion exchange capacity, pore structure and connectivity which gives it a unique sorption behavior [40]. After HDM, the metals might have migrated towards the biochar support, but it needs further examination to verify it. Additionally, because of sample size requirement we were unable to perform ICP of the spent catalysts. This would leave the door open for further research and scale up studies to enable us to collect enough spent catalyst samples to verify with ICP.

4.3.5 Chemical composition of hydrotreated oils

Simulated Distillation (SimDis) and DHA analysis of the hydrotreated samples are shown in Figure 4.4 and Figure 4.5, respectively. From 80℃ to 150℃ all the samples have similar distillation traces, which reflects the commonality of paraffin, olefins, cycloalkane (naphthene) and aromatics in each sample [88]. Approximately, 80% of the UB from S-CoMo/DF had boiling point (BP) lower than 250℃, while almost 40% showed similar BP for unsulfided CoMo/DF. This contrast was reflected in the olefin content of the respective UB oils as seen in the DHA analysis (Figure 4.6).

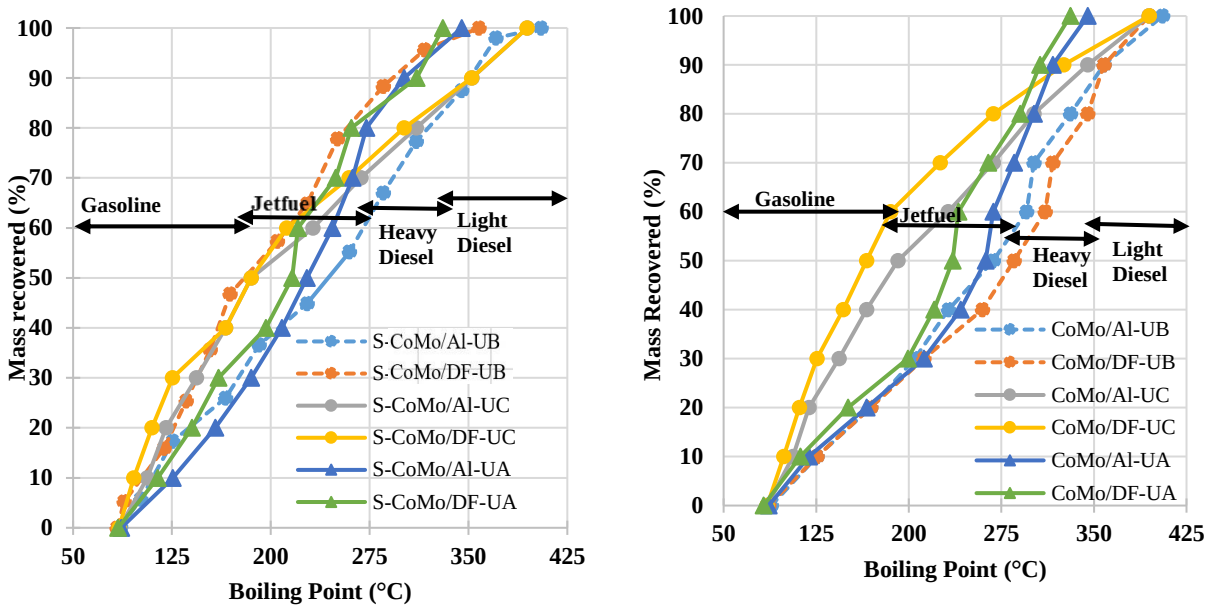

Figure 4.4 Boiling point distribution (simulated distillation, ASTM D2887) for upgraded liquid products produced from different catalyst supports.

For example, a 58% decrease in olefin content, 70% increase in paraffin content was recorded for UB from S-CoMo/DF compared to unsulfided. The distillation traces from UA prepared from alumina-supported catalysts irrespective of sulfidation state are similar. However, a large amount of olefin was found in the case of UA (CoMo/Al). UA produced from DF supported catalysts appeared to shift the distillation curve to lower BP. Similar observation could be seen in the case of UC, where lower distillation cuts were observed for DF- supported catalysts. Overall, DF supported catalyst and sulfided catalysts appeared to have lower BP distribution compared to alumina support and unsulfided catalysts. This could be due to higher cracking propensity of DF support that contributed to the lower fractional cuts. On the other hand, DHA analysis of sulfided catalysts exhibited higher amount of paraffin and lower amount of olefin compared to unsulfided catalyst, while an opposite scenario was observed for DF supported catalyst compared to alumina support.

Since DHA can analyze samples where the hydrocarbons range from C1 to C14, the GC-MS was used to detect volatile hydrocarbons until BP of approximately 350°C. Figure 4.7 and Figure 4.8 shows the GC-MS spectra for S-CoMo/Al and S-CoMo/DF, respectively. HTL algae biocrude is a complex mixture of minor share of n-paraffinic hydrocarbons and majority of heteroatoms (O and N) having high molecular weight. The GC-MS was not able to detect any compounds in algae HTL biocrude before hydrotreatment because of presence of high molecular weight compounds. Comparing the chromatogram, UA (S-CoMo/DF) exhibited higher presence of heteroatoms and unsaturation compared to UA (S-CoMo/Al), these results are in accordance with the CHNO data (Table 4.2 and 4.3). UB does not show any oxygenated or nitrogenated compounds in the GC-MS spectra, but according to the CHNO results appreciable amount of both the heteroatoms are present. For example, HDO must have taken place for oxygenated species (O_X) to O_{X-1}, O_{X-2} etc. but at higher boiling point [19]. This is due to the limitation of GC, since it cannot volatilize higher molecular weight compounds. These heteroatoms could be trapped in higher boiling point fractions or combination of different heteroatoms leading to mass spectral complexity and thus cannot be analyzed by GC [19], [89], [90]. Algae consisted mainly of C_{16}, C_{18} fatty acids and carinata majorly had C_{22} fatty acids. After hydrotreatment, the UB (S-CoMo/DF) displayed higher concentration of C_{17} and C_{21} alkane (i.e., loss of 1 carbon). Therefore, decarboxylation reaction could have taken place. On the other hand, over S-CoMo/Al, C_{16} and C_{20} (i.e., loss of 2 C) were observed. This result is supported by lower BP distillation pattern as seen in Figure 5. Heneicosane ($C_{21}H_{44}$) was the major molecule for UC under both supports. Heptadecane ($C_{17}H_{36}$) and C_{16} cycloalkane were the present in the highest concentration in UA over sulfided alumina and sulfided DF biochar support respectively. No new compounds could be found for the blended feedstock from the GC-MS.

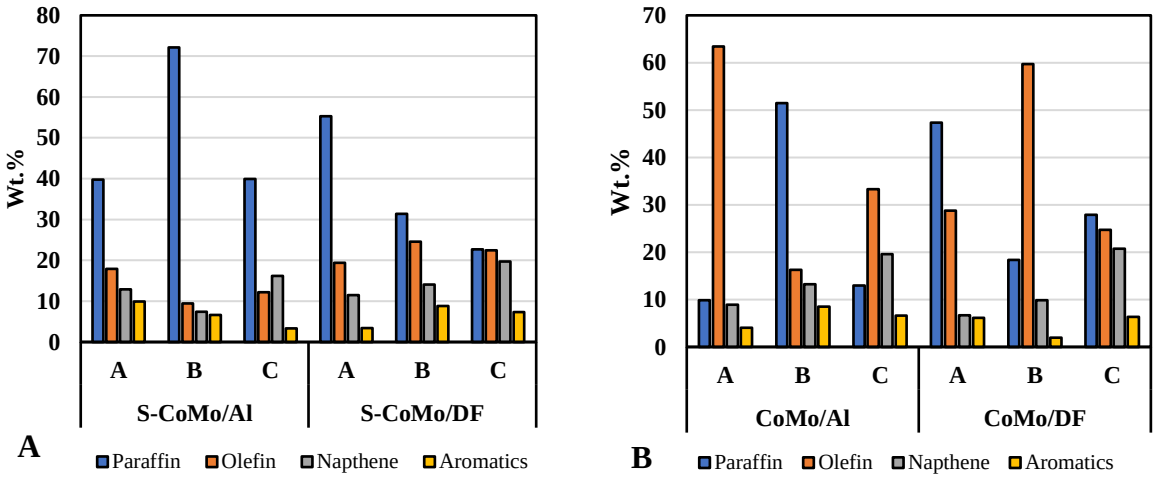

Figure 4.5 Detailed hydrocarbons analysis (P: Paraffin and iso-paraffin, O: Olefin, N: Naphthene, A: Aromatics) of upgraded liquid over different supports and sulfidation state. (A) sulfided catalysts and (B) unsulfided catalysts.

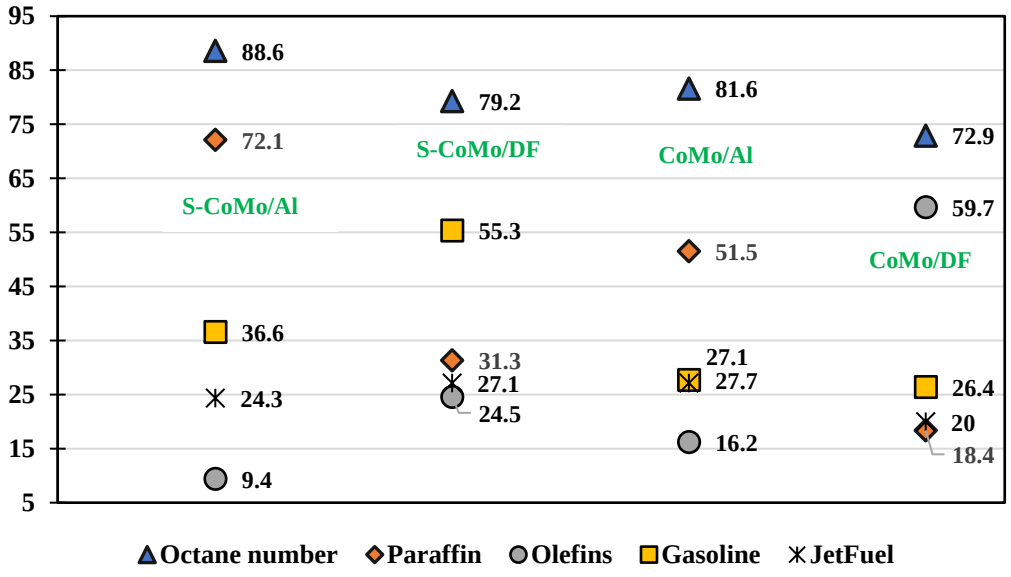

Figure 4.6. Octane number, olefin, paraffin, gasoline, and jet fuel content of UB oils.

Octane number of most commercial gasolines is in the range of 85-95. The octane numbers were determined by the DHA analysis. The octane numbers obtained for the UB are between 88 and 72 (Figure 4.6). The oil having highest octane number had lowest amount olefins (9.41%) while the UB showing 72 as octane number shows highest number of olefins (59.71%) and lowest amount of paraffin and gasoline fraction in the oil. Literature reported that olefins are necessary

for boosting the octane number, but these are not desirable since it causes fouling, smoke, and smog. This study shows a linear relationship between olefin and paraffin content to octane number. The high octane numbers could be due to paraffins that could be present as i-paraffins which gives a higher octane number compared to i-olefins-olefins, cycloalkanes and n-paraffins [91]. Octane numbers of all the upgraded oils could be found in Figure B12 in the appendix.

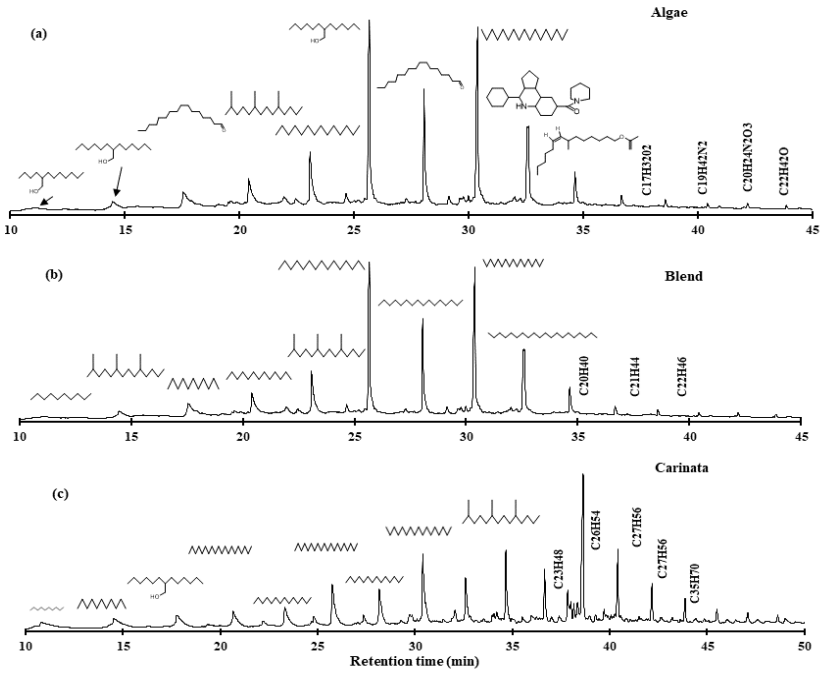

Figure 4.7 GC-MS peaks of upgraded liquid products for (a) Algae (b) Bend (c) Carinata under S-CoMo/Al catalyst.

Oxidative and thermal loss on the fresh and spent catalysts by carrying out TGA experiments under air and nitrogen, respectively. TGA data of fresh and spent catalysts under nitrogen and air are presented in the appendix (Figures B14). Carbon content of the fresh and spent catalysts are exhibited in Table 4.5. Coke formation on catalysts occurs due to adsorption and condensation of alkenes, polar aromatic compounds, and host of other molecules. These compounds have stronger adsorption, cracking and condensation tendencies which tend to form coke.

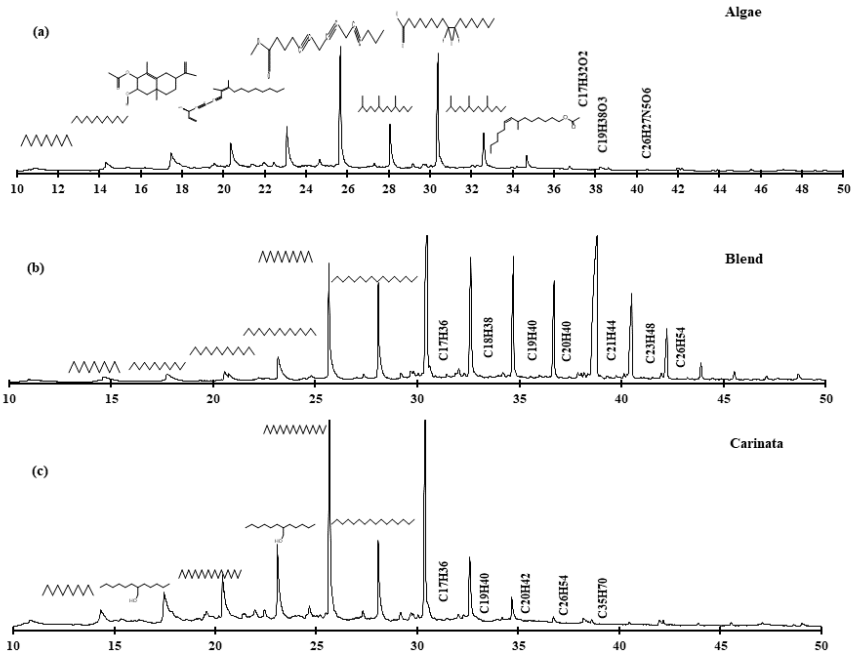

Figure 4.8 GC-MS peaks of upgraded liquid products for (a) Algae (b) Blend (c) Carinata under S-CoMo/DF catalyst.

Table 4.5 shows that fresh alumina supported catalysts have no carbon while fresh DF biochar supported catalysts have approximately 65% carbon. After hydrotreatment, the spent UB catalysts had lesser increase in carbon content compared to UA but higher than UC. This shows that blending the algae and carinata does have a positive synergistic effect with regards to the coke formation. Vegetable oil could have acted as a hydrogen donor and decreased the coke build up in the blended spent catalyst [92]. Comparing the two supports, it is interesting to note that overall DF biochar support revealed lower coke deposition. For instance, a 24% (CoMo/Al) and 20% (S-CoMo/Al) increase in C content for the alumina catalysts compared to 15% (CoMo/DF) and 2% (S-CoMo/DF) in the case of DF supported catalysts for UBs. This is due to fact that carbon supports have the ability to restrict the transformation of coke prone hydrocarbons to coke. The carbons supports are rich in mesopores, and they provide adsorption sites for the free radicals that are produced during the thermal cracking and inhibit them from coupling and polycondensation

[93]. According to literature, alumina supports tend to produce coke because of weak Lewis acid sites [94]. Additionally, Fonseca et.al., reported that dealkylation and condensation of aromatic rings results in coke formation in the case of $CoMo/Al_2O_3$ by solid state 13C NMR [95].

Table 4.5 Carbon content before and after hydrotreatment.

	Fresh	Spent		
		UA	UB	UC
CoMo/Al	0	39.46±4.4	24.6±1.07	15.47±0.1
S-CoMo/Al	0	30.80±0.78	20.13±0.4	17.92±0.6
CoMo/DF	63.47±1.7	75.04±0.5	73.01±0.3	72.6±2
S-CoMo/DF	65.23±1.5	74.55±0.15	66.89±1.0	75.5±3.8

Pre-sulfiding a catalyst with H_2S can suppress coke formation among various other techniques. Presulfidation causes changes in the radical concentration of the reaction system which is correlated with the coking of the catalyst [92]. Table 5 corroborates the results from the literature, and it could be seen that sulfided catalysts compared to its unsulfided counterpart demonstrated lower carbon in the spent catalyst irrespective of the support type.

When comparing the support type, it could be seen that UA (S-CoMo/Al) had a 30% increase in carbon content while UA (S-CoMo/DF) demonstrated almost half the value of it (14.4 % increase). Lower increase in carbon content was noticed from their unsulfided counterparts and for UB and UC as well. This shows that DF biochar's inherent acid sites, higher surface area and surface functional groups might have had major influences on the coking activity. According to literature, catalyst deactivation/coke deposition increases with boiling point of the feedstock fraction and thus removal of metals helps in minimizing coke formation [96]. In our study, DF

support exhibited excellent HDM activity which could have helped in overall lower coke deposition. A higher coke formation for sulfided alumina catalysts compared to sulfided biochar support maybe due to presence of coordination vacancies present on the edges of MoS_2 crystallites. The H_2S can occupy these vacancies and act as Bronsted acid site and promote coke formation [97]. Overall, presulfiding and DF support exhibited positive results in term of less coke formation. Details regarding the type of coke, and weight loss (TGA) could be found in the appendix (Figure B14).

There are few possibilities to take advantage of each of the supports for hydrotreatment of different feedstocks. From this study we have seen that DF biochar supported catalysts are cheap, have high surface area, inherent acidic sites, unique sorption behavior and seem to be a promising support material in hydrotreating reactions of different feedstocks. However, low packing density of carbon support hinders its application in commercial hydrotreatment processes. On the other hand, alumina is stable, but it interacts strongly with transition metals oxides to form species which makes it difficult to reduce or sulfide. Therefore, considering the positive aspects of these two supports, one can create new catalyst for hydrotreatment or use one of support as sacrificial catalyst to make the process more efficient and cost-effective.

Firstly, we can use a dual catalyst bed where the CoMo/DF biochar acts as a fixed guard bed and the feedstock containing impurities such as high metal content flows over it. This guard beds can act as a sacrificial catalyst and remove majority of the inorganics (hydrodemetallization), nitrogen and sulfur in the first stage. Next on the second stage, the main packed bed consisting of CoMo/Al catalyst can hydrodeoxygenate the feed from the first stage and in this way, we can utilize two different supports efficiently to remove metals and heteroatoms.

Secondly, we can prepare a new type of support by mixing the alumina and biochar support in aqueous medium and impregnate it with transition metal oxides, followed by reducing it under hydrogen. This process is similar of what we used in this study to prepare DF biochar support catalyst. Alternatively, via chemical vapor deposition, hybrid biochar coated alumina support could also be prepared as stated in literature [98].

4.4 Conclusion

In this study, sulfided and un-sulfided bimetallic catalyst with two different supports (Douglas fir biochar support and alumina support were used to hydrotreat a blend of HTL algae biocrude and carinata oil. UB produced with the use of sulfided cobalt molybdenum supported on alumina (S-CoMo/Al) revealed high HDO activity mainly by DCO. The lowest oxygen content in the UB retrieved over S-CoMo/Al also showed highest HHV (~46 MJ/kg), highest carbon content (~83 wt.%), octane number (89), jet fuel (27%) and paraffin (72%) fractions and lowest TAN (1.8 mgKOH/g). This study was able to lower the O/C ratio between 0.02 to 0.03 and H/C ratio between 2 to 1.8 for all upgraded oils and are within the range of gasoline/diesel/kerosene. Even though the BET surface area was lower than the DF supported catalyst, CoMo/Al particularly sulfided one performed better than DF supported catalyst. On the other hand, DF supported catalysts catalyzed cracking reactions which reflected on lower viscosity values (1.45 m^2/s) with highest and lowest share of gasoline (55%) and heavy diesel (4.38%), respectively. Interestingly, HDN activity was pronounced in the UB produced from sulfided cobalt molybdenum supported on DF biochar support (S-CoMo/DF) supported catalyst compared to alumina. However, it consumed higher hydrogen gas for hydrotreatment compared to alumina supported catalysts and had the highest amount of oxygen (3.73 wt. %) in the UB. Remarkably, the UB's (DF supported catalysts) helped in removal of heavy metals specially Fe and K and had higher HDM and HDS activity due to its

unique sorption behavior. It also removed appreciable amount of sulfur from all the upgraded oils compared to alumina. In our study, we can notice that the crystal size of alumina support is smaller than the biochar support and it exhibited superior HDO activity primarily by decarbonylation. On the other hand, biochar support, catalyzed cracking reactions followed by high HDN and HDS activity compared to the alumina supported catalyst. Therefore, from our study we can suggest hydrotreatment is size independent. However, individually HDO activity was favorable for catalysts having smaller particle size while HDS and HDN activity were size independent**.** HDN and HDS reactions were favored by higher acidity of the S-CoMo/DF catalysts specially the lactonic acid groups compared to alumina supported catalysts. Hard coke was mostly observed in UA, while UC showed soft coke and UB had a combination of both. Overall, presulfidation and DF support exhibited positive results in term of less coke formation. When DF supported catalysts were used to hydrotreat a blend of HTL algae biocrude and carinata oil it was successful in moderate HDO activity but greater HDN, HDS, HDM activities and enhanced cracking compared to alumina supported catalysts. In summary, biochar supports have higher oxygen containing functional groups (acidic sites), inorganic mineral oxides, ion exchange capacity, high surface area, pore structure and connectivity. All of these make a substantial contribution to its effective sorption and unique catalytic behavior.

4.5 References

[1] "Monthly Energy Review – December 2021," p. 276, 2021.

[2] S. Hansen, A. Mirkouei, and L. A. Diaz, "A comprehensive state-of-technology review for upgrading bio-oil to renewable or blended hydrocarbon fuels," *Renew. Sustain. Energy Rev.*, vol. 118, p. 109548, Feb. 2020, doi: 10.1016/j.rser.2019.109548.

[3] S. Wang, H. Yuan, Y. Wang, and R. Shan, "Transesterification of vegetable oil on low cost and efficient meat and bone meal biochar catalysts," *Energy Convers. Manag.*, vol. 150, pp. 214–221, Oct. 2017, doi: 10.1016/j.enconman.2017.08.020.

[4] B. H. H. Goh *et al.*, "Progress in utilisation of waste cooking oil for sustainable biodiesel and biojet fuel production," *Energy Convers. Manag.*, vol. 223, p. 113296, Nov. 2020, doi: 10.1016/j.enconman.2020.113296.

[5] E. S. K. Why, H. C. Ong, H. V. Lee, Y. Y. Gan, W.-H. Chen, and C. T. Chong, "Renewable aviation fuel by advanced hydroprocessing of biomass: Challenges and perspective," *Energy Convers. Manag.*, vol. 199, p. 112015, Nov. 2019, doi: 10.1016/j.enconman.2019.112015.

[6] H. Jahromi *et al.*, "Production of green transportation fuels from Brassica carinata oil: A comparative study of noble and transition metal catalysts," *Fuel Process. Technol.*, vol. 215, p. 106737, May 2021, doi: 10.1016/j.fuproc.2021.106737.

[7] A. H. Al-Muhtaseb *et al.*, "Efficient utilization of waste date pits for the synthesis of green diesel and jet fuel fractions," *Energy Convers. Manag.*, vol. 127, pp. 226–232, Nov. 2016, doi: 10.1016/j.enconman.2016.09.004.

[8] G. A. Alsultan, N. Asikin-Mijan, H. V. Lee, A. S. Albazzaz, and Y. H. Taufiq-Yap, "Deoxygenation of waste cooking to renewable diesel over walnut shell-derived nanorode activated carbon supported CaO-La2O3 catalyst," *Energy Convers. Manag.*, vol. 151, pp. 311–323, Nov. 2017, doi: 10.1016/j.enconman.2017.09.001.

[9] S. George *et al.*, "A regional inter-disciplinary partnership focusing on the development of a carinata-centered bioeconomy," *GCB Bioenergy*, vol. 13, no. 7, pp. 1018–1029, 2021, doi: 10.1111/gcbb.12828.

[10] A. Bauen, N. Bitossi, L. German, A. Harris, and K. Leow, "Sustainable Aviation Fuels : Status, challenges and prospects of drop-in liquid fuels, hydrogen and electrification in aviation," *Johns. Matthey Technol. Rev.*, vol. 64, no. 3, pp. 263–278, Jul. 2020, doi: 10.1595/205651320X15816756012040.

[11] N. Krobkrong, V. Itthibenchapong, P. Khongpracha, and K. Faungnawakij, "Deoxygenation of oleic acid under an inert atmosphere using molybdenum oxide-based catalysts," *Energy Convers. Manag.*, vol. 167, pp. 1–8, Jul. 2018, doi: 10.1016/j.enconman.2018.04.079.

[12] Z. D. Yigezu and K. Muthukumar, "Catalytic cracking of vegetable oil with metal oxides for biofuel production," *Energy Convers. Manag.*, vol. 84, pp. 326–333, Aug. 2014, doi: 10.1016/j.enconman.2014.03.084.

[13] P. Dwivedi, "Sustainable aviation fuel production from Brassica carinata in the Southern United States," *GCB Bioenergy*, vol. 13, no. 12, pp. 1854–1858, 2021, doi: 10.1111/gcbb.12900.

[14] X. Liu, Y. Guo, A. Dasgupta, H. He, D. Xu, and Q. Guan, “Algal bio-oil refinery: A review of heterogeneously catalyzed denitrogenation and demetallization reactions for renewable process,” *Renew. Energy*, vol. 183, pp. 627–650, Jan. 2022, doi: 10.1016/j.renene.2021.11.020.
[15] M. Ellersdorfer, “Hydrothermal co-liquefaction of chlorella vulgaris with food processing residues, green waste and sewage sludge,” *Biomass Bioenergy*, vol. 142, p. 105796, Nov. 2020, doi: 10.1016/j.biombioe.2020.105796.
[16] L. A. Andrade, F. R. X. Batista, T. S. Lira, M. A. S. Barrozo, and L. G. M. Vieira, “Characterization and product formation during the catalytic and non-catalytic pyrolysis of the green microalgae Chlamydomonas reinhardtii,” *Renew. Energy*, vol. 119, pp. 731–740, Apr. 2018, doi: 10.1016/j.renene.2017.12.056.
[17] C. Yang *et al.*, “Hydrothermal liquefaction and gasification of biomass and model compounds: a review,” *Green Chem.*, vol. 22, no. 23, pp. 8210–8232, Dec. 2020, doi: 10.1039/D0GC02802A.
[18] N. Sharma *et al.*, “Effect of catalyst and temperature on the quality and productivity of HTL bio-oil from microalgae: A review,” *Renew. Energy*, vol. 174, pp. 810–822, Aug. 2021, doi: 10.1016/j.renene.2021.04.147.
[19] M. S. Haider, D. Castello, and L. A. Rosendahl, “The Art of Smooth Continuous Hydroprocessing of Biocrudes Obtained from Hydrothermal Liquefaction: Hydrodemetallization and Propensity for Coke Formation,” *Energy Fuels*, vol. 35, no. 13, pp. 10611–10622, Jul. 2021, doi: 10.1021/acs.energyfuels.1c01228.
[20] D. C. Elliott, H. Wang, R. French, S. Deutch, and K. Iisa, “Hydrocarbon Liquid Production from Biomass via Hot-Vapor-Filtered Fast Pyrolysis and Catalytic Hydroprocessing of the Bio-oil,” *Energy Fuels*, vol. 28, no. 9, pp. 5909–5917, Sep. 2014, doi: 10.1021/ef501536j.
[21] R. h. Venderbosch, A. r. Ardiyanti, J. Wildschut, A. Oasmaa, and H. j. Heeres, “Stabilization of biomass-derived pyrolysis oils,” *J. Chem. Technol. Biotechnol.*, vol. 85, no. 5, pp. 674–686, 2010, doi: 10.1002/jctb.2354.
[22] D. Dong, S. Jeong, and F. E. Massoth, “Effect of nitrogen compounds on deactivation of hydrotreating catalysts by coke,” *Catal. Today*, vol. 37, no. 3, pp. 267–275, Aug. 1997, doi: 10.1016/S0920-5861(97)00022-9.
[23] M. T. H. Siddiqui *et al.*, “Dual-application of novel magnetic carbon nanocomposites as catalytic liquefaction for bio-oil synthesis and multi-heavy metal adsorption,” *Renew. Energy*, vol. 172, pp. 1103–1119, Jul. 2021, doi: 10.1016/j.renene.2021.02.157.
[24] “Alternative Transportation Fuels Production from Cohydrotreatment of Vegetable Oil and Pyrolysis Oils Derived from Biomass and Tires - ProQuest.” https://www.proquest.com/docview/2467153646?pq-origsite=gscholar&fromopenview=true (accessed Jan. 07, 2022).
[25] Y. Han, F. Stankovikj, and M. Garcia-Perez, “Co-hydrotreatment of tire pyrolysis oil and vegetable oil for the production of transportation fuels,” *Fuel Process. Technol.*, vol. 159, pp. 328–339, May 2017, doi: 10.1016/j.fuproc.2017.01.048.
[26] K. Harun, S. Adhikari, and H. Jahromi, “Hydrogen production via thermocatalytic decomposition of methane using carbon-based catalysts,” *RSC Adv.*, vol. 10, no. 67, pp. 40882–40893, 2020, doi: 10.1039/D0RA07440C.
[27] E. Santillan-Jimenez *et al.*, “Co-processing of hydrothermal liquefaction algal bio-oil and petroleum feedstock to fuel-like hydrocarbons via fluid catalytic cracking,” *Fuel Process. Technol.*, vol. 188, pp. 164–171, Jun. 2019, doi: 10.1016/j.fuproc.2019.02.018.

[28] Y. Han, A. P. P. Pires, and M. Garcia-Perez, “Co-hydrotreatment of the Bio-oil Lignin-Rich Fraction and Vegetable Oil,” *Energy Fuels*, vol. 34, no. 1, pp. 516–529, Jan. 2020, doi: 10.1021/acs.energyfuels.9b03344.
[29] B. Wang *et al.*, “Co-hydrotreating of algae and used engine oil for the direct production of gasoline and diesel fuels or blending components,” *Energy*, vol. 136, pp. 151–162, Oct. 2017, doi: 10.1016/j.energy.2016.03.084.
[30] L.-F. Xie, Y.-P. Xu, X.-L. Shi, F. Wang, P.-G. Duan, and S.-C. Li, “Hydrotreating the distillate fraction of algal biocrude with used engine oil over Pt/C for production of liquid fuel,” *Catal. Today*, vol. 355, pp. 65–74, Sep. 2020, doi: 10.1016/j.cattod.2019.03.043.
[31] H. Wang *et al.*, “The Effects of Catalyst Support and Temperature on the Hydrotreating of Waste Cooking Oil (WCO) over CoMo Sulfided Catalysts,” *Catalysts*, vol. 9, no. 8, Art. no. 8, Aug. 2019, doi: 10.3390/catal9080689.
[32] M. Alherbawi, G. McKay, H. R. Mackey, and T. Al-Ansari, “A novel integrated pathway for Jet Biofuel production from whole energy crops: A Jatropha curcas case study,” *Energy Convers. Manag.*, vol. 229, p. 113662, Feb. 2021, doi: 10.1016/j.enconman.2020.113662.
[33] X. Zhao, L. Wei, S. Cheng, and J. Julson, “Review of Heterogeneous Catalysts for Catalytically Upgrading Vegetable Oils into Hydrocarbon Biofuels,” *Catalysts*, vol. 7, no. 3, Art. no. 3, Mar. 2017, doi: 10.3390/catal7030083.
[34] H. Jahromi, T. Rahman, P. Roy, and S. Adhikari, “Hydrotreatment of solvent-extracted biocrude from hydrothermal liquefaction of municipal sewage sludge,” *Energy Convers. Manag.*, vol. 263, p. 115719, Jul. 2022, doi: 10.1016/j.enconman.2022.115719.
[35] Z. He and X. Wang, “Hydrodeoxygenation of model compounds and catalytic systems for pyrolysis bio-oils upgrading,” *Catal. Sustain. Energy*, vol. 1, no. 2013, pp. 28–52, Oct. 2012, doi: 10.2478/cse-2012-0004.
[36] H. Ojagh, “Hydrodeoxygenation (HDO) catalysts Characterization, reaction and deactivation studies,” *undefined*, 2018, Accessed: Feb. 17, 2022. [Online]. Available: https://www.semanticscholar.org/paper/Hydrodeoxygenation-(HDO)-catalysts-reaction-and-Ojagh/1c76ecaa02b38e61557f0cd1992d8a0968fce946
[37] H. Jahromi, S. Adhikari, P. Roy, M. Shelley, E. Hassani, and T.-S. Oh, “Synthesis of Novel Biolubricants from Waste Cooking Oil and Cyclic Oxygenates through an Integrated Catalytic Process,” *ACS Sustain. Chem. Eng.*, Sep. 2021, doi: 10.1021/acssuschemeng.1c03523.
[38] T. M. H. Dabros *et al.*, “Influence of H2O and H2S on the composition, activity, and stability of sulfided Mo, CoMo, and NiMo supported on MgAl2O4 for hydrodeoxygenation of ethylene glycol,” *Appl. Catal. Gen.*, vol. 551, no. C, Dec. 2017, doi: 10.1016/j.apcata.2017.12.008.
[39] R. J.p, “Effect of the support on the structure of Mo-based hydrodesulfurization catalysts : activated carbon versus alumina,” 2003. https://www.semanticscholar.org/paper/Effect-of-the-support-on-the-structure-of-Mo-based-J.P./8c29981c06879766f85f8a7916d192d9e7a8dc40 (accessed Feb. 17, 2022).
[40] P. Wang *et al.*, “Sorption and recovery of phenolic compounds from aqueous phase from sewage sludge hydrothermal liquefaction using bio-char,” *Chemosphere*, p. 131934, Aug. 2021, doi: 10.1016/j.chemosphere.2021.131934.
[41] P. Roy *et al.*, “Performance of biochar assisted catalysts during hydroprocessing of non-edible vegetable oil: Effect of transition metal source on catalytic activity,” *Energy Convers. Manag.*, vol. 252, p. 115131, Jan. 2022, doi: 10.1016/j.enconman.2021.115131.

[42] D. A. Ruddy, J. A. Schaidle, J. R. F. Iii, J. Wang, L. Moens, and J. E. Hensley, "Recent advances in heterogeneous catalysts for bio-oil upgrading via 'ex situ catalytic fast pyrolysis': catalyst development through the study of model compounds," *Green Chem.*, vol. 16, no. 2, pp. 454–490, Jan. 2014, doi: 10.1039/C3GC41354C.
[43] J. A. Tavizón-Pozos, V. A. Suárez-Toriello, P. del Ángel, and J. A. de los Reyes, "Hydrodeoxygenation of Phenol Over Sulfided CoMo Catalysts Supported on a Mixed Al2O3-TiO2 Oxide," *Int. J. Chem. React. Eng.*, vol. 14, no. 6, pp. 1211–1223, Dec. 2016, doi: 10.1515/ijcre-2016-0038.
[44] "Marine Microalgae FAQ," *Reed Mariculture*. https://reedmariculture.com/pages/microalgae-faq (accessed Mar. 07, 2022).
[45] J.-S. Choi *et al.*, "Alumina-supported cobalt–molybdenum sulfide modified by tin via surface organometallic chemistry: application to the simultaneous hydrodesulfurization of thiophenic compounds and the hydrogenation of olefins," *Appl. Catal. Gen.*, vol. 267, no. 1, pp. 203–216, Jul. 2004, doi: 10.1016/j.apcata.2004.03.005.
[46] P. Wang *et al.*, "Enhancement of biogas production from wastewater sludge via anaerobic digestion assisted with biochar amendment," *Bioresour. Technol.*, vol. 309, p. 123368, Aug. 2020, doi: 10.1016/j.biortech.2020.123368.
[47] T. Rahman, H. Jahromi, P. Roy, S. Adhikari, E. Hassani, and T.-S. Oh, "Hydrothermal liquefaction of municipal sewage sludge: Effect of red mud catalyst in ethylene and inert ambiences," *Energy Convers. Manag.*, vol. 245, p. 114615, Oct. 2021, doi: 10.1016/j.enconman.2021.114615.
[48] M. Vifttaria, Nurhayati, and S. Anita, "Surface Acidity of Sulfuric Acid Activated Maredan Clay Catalysts with Boehm Titration Method and Pyridine Adsorption-FTIR," *J. Phys. Conf. Ser.*, vol. 1351, no. 1, p. 012040, Nov. 2019, doi: 10.1088/1742-6596/1351/1/012040.
[49] "Introduction to Biomass Energy Conversions," *Routledge & CRC Press*. https://www.routledge.com/Introduction-to-Biomass-Energy-Conversions/Capareda/p/book/9781466513334 (accessed Apr. 05, 2022).
[50] C. Bara *et al.*, "Surface-dependent sulfidation and orientation of MoS2 slabs on alumina-supported model hydrodesulfurization catalysts," *J. Catal.*, vol. 344, pp. 591–605, Dec. 2016, doi: 10.1016/j.jcat.2016.10.001.
[51] A. M. Hengne, N. S. Biradar, and C. V. Rode, "Surface Species of Supported Ruthenium Catalysts in Selective Hydrogenation of Levulinic Esters for Bio-Refinery Application," *Catal. Lett.*, vol. 142, no. 6, pp. 779–787, Jun. 2012, doi: 10.1007/s10562-012-0822-4.
[52] A. Bakhtyari, M. R. Rahimpour, and S. Raeissi, "Cobalt-molybdenum catalysts for the hydrodeoxygenation of cyclohexanone," *Renew. Energy*, vol. 150, pp. 443–455, May 2020, doi: 10.1016/j.renene.2019.12.119.
[53] A. Afshar Taromi and S. Kaliaguine, "Green diesel production via continuous hydrotreatment of triglycerides over mesostructured γ-alumina supported NiMo/CoMo catalysts," *Fuel Process. Technol.*, vol. 171, pp. 20–30, Mar. 2018, doi: 10.1016/j.fuproc.2017.10.024.
[54] X. Wang *et al.*, "Effect of promoters on the HDS activity of alumina-supported Co–Mo sulfide catalysts," *RSC Adv.*, vol. 5, no. 121, pp. 99706–99711, 2015, doi: 10.1039/C5RA17414G.
[55] A. Bakhtyari, A. Sakhayi, Z. Moravvej, and M. R. Rahimpour, "Converting Cyclohexanone to Liquid Fuel-Grade Products: A Characterization and Comparison Study of Hydrotreating Molybdenum Catalysts," *Catal. Lett.*, vol. 151, no. 11, pp. 3343–3360, Nov. 2021, doi: 10.1007/s10562-021-03575-y.

[56] T. A. Saleh, S. A. AL-Hammadi, I. M. Abdullahi, and M. Mustaqeem, “Synthesis of molybdenum cobalt nanocatalysts supported on carbon for hydrodesulfurization of liquid fuels,” *J. Mol. Liq.*, vol. 272, pp. 715–721, Dec. 2018, doi: 10.1016/j.molliq.2018.09.118.
[57] T. A. Saleh, “Carbon nanotube-incorporated alumina as a support for MoNi catalysts for the efficient hydrodesulfurization of thiophenes,” *Chem. Eng. J.*, vol. 404, p. 126987, Jan. 2021, doi: 10.1016/j.cej.2020.126987.
[58] I. T. Ghampson *et al.*, “Effects of pore diameter on particle size, phase, and turnover frequency in mesoporous silica supported cobalt Fischer–Tropsch catalysts,” *Appl. Catal. Gen.*, vol. 388, no. 1–2, pp. 57–67, Nov. 2010, doi: 10.1016/j.apcata.2010.08.028.
[59] J. L. Eslava, X. Sun, J. Gascon, F. Kapteijn, and I. Rodríguez-Ramos, “Ruthenium particle size and cesium promotion effects in Fischer–Tropsch synthesis over high-surface-area graphite supported catalysts,” *Catal. Sci. Technol.*, vol. 7, no. 5, pp. 1235–1244, Mar. 2017, doi: 10.1039/C6CY02535H.
[60] G. L. Bezemer *et al.*, “Cobalt Particle Size Effects in the Fischer−Tropsch Reaction Studied with Carbon Nanofiber Supported Catalysts,” *J. Am. Chem. Soc.*, vol. 128, no. 12, pp. 3956–3964, Mar. 2006, doi: 10.1021/ja058282w.
[61] N. Semagina and L. Kiwi-Minsker, “Palladium Nanohexagons and Nanospheres in Selective Alkyne Hydrogenation,” *Catal. Lett.*, vol. 127, no. 3, pp. 334–338, Feb. 2009, doi: 10.1007/s10562-008-9684-1.
[62] J. Silvestre-Albero, G. Rupprechter, and H.-J. Freund, “Atmospheric pressure studies of selective 1,3-butadiene hydrogenation on well-defined Pd/Al2O3/NiAl(110) model catalysts: Effect of Pd particle size,” *J. Catal.*, vol. 240, no. 1, pp. 58–65, May 2006, doi: 10.1016/j.jcat.2006.02.024.
[63] H. Farag, D. D. Whitehurst, K. Sakanishi, and I. Mochida, “Carbon versus alumina as a support for Co–Mo catalysts reactivity towards HDS of dibenzothiophenes and diesel fuel,” *Catal. Today*, vol. 50, no. 1, pp. 9–17, Apr. 1999, doi: 10.1016/S0920-5861(98)00476-3.
[64] E. Aryee, J. Essilfie-Dughan, A. K. Dalai, and J. Adjaye, “Comparative Studies of Carbon Nanomaterial and γ-Alumina as Supports for the Ni–Mo Catalyst in Hydrotreating of Gas Oils,” *Energy Fuels*, vol. 35, no. 7, pp. 6153–6166, Apr. 2021, doi: 10.1021/acs.energyfuels.0c02394.
[65] F. Wang *et al.*, “Activated carbon supported molybdenum and tungsten carbides for hydrotreatment of fatty acids into green diesel,” *Fuel*, vol. 228, pp. 103–111, Sep. 2018, doi: 10.1016/j.fuel.2018.04.150.
[66] T. Burimsitthigul, B. Yoosuk, C. Ngamcharussrivichai, and P. Prasassarakich, “Hydrocarbon biofuel from hydrotreating of palm oil over unsupported Ni–Mo sulfide catalysts,” *Renew. Energy*, vol. 163, pp. 1648–1659, Jan. 2021, doi: 10.1016/j.renene.2020.10.044.
[67] “Hydrogen Spillover. Facts and Fiction | Chemical Reviews.” https://pubs.acs.org/doi/pdf/10.1021/cr200346z (accessed Mar. 23, 2022).
[68] D. Kubička and L. Kaluža, “Deoxygenation of vegetable oils over sulfided Ni, Mo and NiMo catalysts,” *Appl. Catal. Gen.*, vol. 372, no. 2, pp. 199–208, Jan. 2010, doi: 10.1016/j.apcata.2009.10.034.
[69] J. Sun, J. Yang, and M. Shi, “Review of Denitrogenation of Algae Biocrude Produced by Hydrothermal Liquefaction,” *Trans. Tianjin Univ.*, vol. 23, no. 4, pp. 301–314, Jul. 2017, doi: 10.1007/s12209-017-0051-4.

[70] P. Duan and P. E. Savage, “Catalytic hydrotreatment of crude algal bio-oil in supercritical water,” *Appl. Catal. B Environ.*, vol. 104, no. 1, pp. 136–143, Apr. 2011, doi: 10.1016/j.apcatb.2011.02.020.
[71] P. Duan and P. E. Savage, “Catalytic treatment of crude algal bio-oil in supercritical water: optimization studies,” *Energy Environ. Sci.*, vol. 4, no. 4, pp. 1447–1456, Mar. 2011, doi: 10.1039/C0EE00343C.
[72] A. Galadima, A. Masudi, and O. Muraza, “Towards sustainable catalysts in hydrodeoxygenation of algae-derived oils: A critical review,” *Mol. Catal.*, p. 112131, Jan. 2022, doi: 10.1016/j.mcat.2022.112131.
[73] T. K. Vo, W.-S. Kim, S.-S. Kim, K. S. Yoo, and J. Kim, “Facile synthesis of Mo/Al2O3–TiO2 catalysts using spray pyrolysis and their catalytic activity for hydrodeoxygenation,” *Energy Convers. Manag.*, vol. 158, pp. 92–102, Feb. 2018, doi: 10.1016/j.enconman.2017.12.049.
[74] A. Popov *et al.*, “Bio-oil hydrodeoxygenation: Adsorption of phenolic compounds on sulfided (Co)Mo catalysts,” *J. Catal.*, vol. 297, pp. 176–186, Jan. 2013, doi: 10.1016/j.jcat.2012.10.005.
[75] Z. Wang, S. Adhikari, P. Valdez, R. Shakya, and C. Laird, “Upgrading of hydrothermal liquefaction biocrude from algae grown in municipal wastewater,” *Fuel Process. Technol.*, vol. 142, pp. 147–156, Feb. 2016, doi: 10.1016/j.fuproc.2015.10.015.
[76] R. He, Z. Peng, H. Lyu, H. Huang, Q. Nan, and J. Tang, “Synthesis and characterization of an iron-impregnated biochar for aqueous arsenic removal,” *Sci. Total Environ.*, vol. 612, pp. 1177–1186, Jan. 2018, doi: 10.1016/j.scitotenv.2017.09.016.
[77] N. Rambabu, S. Badoga, K. K. Soni, A. K. Dalai, and J. Adjaye, “Hydrotreating of light gas oil using a NiMo catalyst supported on activated carbon produced from fluid petroleum coke,” *Front. Chem. Sci. Eng.*, vol. 8, no. 2, pp. 161–170, Jun. 2014, doi: 10.1007/s11705-014-1430-1.
[78] J. Xiong *et al.*, “Quantitative Characterization of the Site Density and the Charged State of Functional Groups on Biochar,” *ACS Sustain. Chem. Eng.*, vol. 9, no. 6, pp. 2600–2608, Feb. 2021, doi: 10.1021/acssuschemeng.0c09051.
[79] J. Li, H. Zhang, X. Tang, and H. Lu, “Adsorptive desulfurization of dibenzothiophene over lignin-derived biochar by one-step modification with potassium hydrogen phthalate,” *RSC Adv.*, vol. 6, no. 102, pp. 100352–100360, 2016, doi: 10.1039/C6RA20220A.
[80] A. Zhou, X. Ma, and C. Song, “Effects of oxidative modification of carbon surface on the adsorption of sulfur compounds in diesel fuel,” *Appl. Catal. B Environ.*, vol. 87, no. 3, pp. 190–199, Apr. 2009, doi: 10.1016/j.apcatb.2008.09.024.
[81] X. Yang *et al.*, “Tin-Functionalized Wood Biochar as a Sustainable Solid Catalyst for Glucose Isomerization in Biorefinery,” *ACS Sustain. Chem. Eng.*, vol. 7, no. 5, pp. 4851–4860, Mar. 2019, doi: 10.1021/acssuschemeng.8b05311.
[82] K. Sharma, D. Castello, M. S. Haider, T. H. Pedersen, and L. A. Rosendahl, “Continuous co-processing of HTL bio-oil with renewable feed for drop-in biofuels production for sustainable refinery processes,” *Fuel*, vol. 306, p. 121579, Dec. 2021, doi: 10.1016/j.fuel.2021.121579.
[83] H. Li *et al.*, “Fabrication and Properties of Carbon-Encapsulated Cobalt Nanoparticles over NaCl by CVD,” *Nanoscale Res. Lett.*, vol. 11, no. 1, p. 432, Sep. 2016, doi: 10.1186/s11671-016-1645-9.
[84] K. Phothong, C. Tangsathitkulchai, and P. Lawtae, “The Analysis of Pore Development and Formation of Surface Functional Groups in Bamboo-Based Activated Carbon during CO2

Activation," *Molecules*, vol. 26, no. 18, p. 5641, Sep. 2021, doi: 10.3390/molecules26185641.
[85] C. K. Groot, V. H. J. De Beer, R. Prins, M. Stolarski, and W. S. Niedzwiedz, "Comparative study of alumina- and carbon-supported catalysts for hydrogenolysis and hydrogenation of model compounds and coal-derived liquids," *Ind. Eng. Chem. Prod. Res. Dev.*, vol. 25, no. 4, pp. 522–530, Dec. 1986, doi: 10.1021/i300024a004.
[86] H. Topsoee, B. S. Clausen, R. Candia, C. Wivel, and S. Moerup, "In situ Moessbauer emission spectroscopy studies of unsupported and supported sulfided Co-Mo hydrodesulfurization catalysts: evidence for and nature of a Co-Mo-S phase," *J Catal U. S.*, vol. 68:2, Apr. 1981, Accessed: Mar. 10, 2022. [Online]. Available: https://www.osti.gov/biblio/6367261-situ-moessbauer-emission-spectroscopy-studies-unsupported-supported-sulfided-co-mo-hydrodesulfurization-catalysts-evidence-nature-co-mo-phase
[87] A. I. Dugulan, J. A. R. van Veen, and E. J. M. Hensen, "On the structure and hydrotreating performance of carbon-supported CoMo- and NiMo-sulfides," *Appl. Catal. B Environ.*, vol. 142–143, pp. 178–186, Oct. 2013, doi: 10.1016/j.apcatb.2013.05.013.
[88] J. M. Jarvis, K. O. Albrecht, J. M. Billing, A. J. Schmidt, R. T. Hallen, and T. M. Schaub, "Assessment of Hydrotreatment for Hydrothermal Liquefaction Biocrudes from Sewage Sludge, Microalgae, and Pine Feedstocks," *Energy Fuels*, vol. 32, no. 8, pp. 8483–8493, Aug. 2018, doi: 10.1021/acs.energyfuels.8b01445.
[89] D. Castello, M. S. Haider, and L. A. Rosendahl, "Catalytic upgrading of hydrothermal liquefaction biocrudes: Different challenges for different feedstocks," *Renew. Energy*, vol. 141, pp. 420–430, Oct. 2019, doi: 10.1016/j.renene.2019.04.003.
[90] M. S. Haider, D. Castello, K. M. Michalski, T. H. Pedersen, and L. A. Rosendahl, "Catalytic Hydrotreatment of Microalgae Biocrude from Continuous Hydrothermal Liquefaction: Heteroatom Removal and Their Distribution in Distillation Cuts," *Energies*, vol. 11, no. 12, Art. no. 12, Dec. 2018, doi: 10.3390/en11123360.
[91] Research Institute of Petroleum Processing, Beijing, China, L. Na, G. Xin, T. Zhiping, and L. Jun, "Composition distribution and characteristic of a typical commercial gasoline in market," *Int. J. Smart Grid Clean Energy*, 2016, doi: 10.12720/sgce.5.3.182-187.
[92] Y. Yan *et al.*, "Coke and radicals formation on a sulfided NiMo/γ-Al2O3 catalyst during hydroprocessing of an atmospheric residue in hydrogen donor media," *Fuel Process. Technol.*, vol. 159, pp. 404–411, May 2017, doi: 10.1016/j.fuproc.2017.02.005.
[93] H. Fukuyama and S. Terai, "An Active Carbon Catalyst Prevents Coke Formation from Asphaltenes during the Hydrocracking of Vacuum Residue," *Pet. Sci. Technol.*, vol. 25, no. 1–2, pp. 231–240, Jan. 2007, doi: 10.1080/10916460601054693.
[94] E. Kordouli *et al.*, "HDO activity of carbon-supported Rh, Ni and Mo-Ni catalysts," *Mol. Catal.*, vol. 441, pp. 209–220, Nov. 2017, doi: 10.1016/j.mcat.2017.08.013.
[95] A. Fonseca, P. Zeuthen, and J. B. Nagy, "13C n.m.r. quantitative analysis of catalyst carbon deposits," *Fuel*, vol. 75, no. 12, pp. 1363–1376, Oct. 1996, doi: 10.1016/0016-2361(96)00106-8.
[96] M. Absi-Halabi, A. Stanislaus, and D. L. Trimm, "Coke formation on catalysts during the hydroprocessing of heavy oils," *Appl. Catal.*, vol. 72, no. 2, pp. 193–215, May 1991, doi: 10.1016/0166-9834(91)85053-X.

[97] T.-R. Viljava, R. S. Komulainen, and A. O. I. Krause, “Effect of H2S on the stability of CoMo/Al2O3 catalysts during hydrodeoxygenation,” *Catal. Today*, vol. 60, no. 1, pp. 83–92, Jul. 2000, doi: 10.1016/S0920-5861(00)00320-5.
[98] L. F. Sharanda *et al.*, “Synthesis and characterisation of hybrid carbon-alumina support,” *Appl. Surf. Sci.*, vol. 252, no. 24, pp. 8549–8556, Oct. 2006, doi: 10.1016/j.apsusc.2005.11.078.

CHAPTER

5 HYDROTREATMENT OF PYROLYSIS BIO-OIL AND TRIGLYCERIDE BLENDS

Abstract

Biofuels have consistently been more expensive than fossil fuels due to heterogeneous nature of the feedstocks and the presence of high amount of oxygen in the feedstocks. In that regard, many commercialization efforts for producing biofuels have focused either the use of vegetable oils or grains. However, the access of oleochemical feedstock is increasingly challenging due to its cost and availability. In order to increase the production of biofuels, one approach is to blend challenging feedstocks such as pyrolysis oil with non-edible triglycerides or animal fats. In this study, an attempt has been made to co-hydroprocess (50:50) pyrolysis oil with carinata oil or poultry fat over two catalyst supports. One of the catalyst supports is biochar, which is a by-product of thermochemical processes such as fast pyrolysis. In the present study, unsulfided bimetallic (CoMo) catalysts on two supports: Douglas fir derived biochar and alumina were used to hydrotreat a blend of Eucalyptus pyrolysis bio-oil with poultry fat and carinata oil. The main objective of the study was to understand the synergistic effect of the blending pyrolysis oil with triglycerides for hydrotreatment under different supports and the impact on the oil quality, hydrodeoxygenation (HDO), catalyst regeneration and coke formation. Biochar supported catalyst exhibited superior HDO compared to alumina support. Higher hydrogen consumption was seen for biochar support as oxygen was removed predominantly via dehydration reaction and higher methane gas formation was also observed. On the other hand, lower amount of coke formation was seen for biochar support. Abundance oxygen containing functional groups, inorganic mineral oxides, high surface area, pore structure and acid sites present in biochar support might have made

it a better HDO catalyst compared to alumina support. Blending the pyrolysis oil with poultry fat yielded better quality of bio-oil over carinata oil and produced higher percentage of jet fuel fraction irrespective of the support type. In summary, pyrolysis oil blended with poultry fat and hydrotreated using biochar support catalysts was more effective in HDO activity and in improving overall bio-oil quality compared to alumina supported catalyst and carinata oil.

Keywords: *Biochar; Hydrotreatment; Alumina; Pyrolysis; Co-hydrotreatment; Hydrodeoxygenation*

5.1 Introduction

Oxygenated (ethanol and butanol) and hydrocarbon fuels (paraffins, olefins, cyclic, and aromatics) can be produced from lignocellulosic biomass. Liquefaction methods such as hydrothermal liquefaction (HTL) and pyrolysis have been extensively used to produce bio-oil from biomass. However, the bio-oil produced from the pyrolysis process is not suitable for "drop-in" transportation fuel because it contains a high amount of oxygen (28-40%) which imparts high acidity, viscosity, lower heating value, and chemical instability [1]–[6]. Pyrolysis bio-oil consists of water (19-30 wt.%), organic compounds (20-30 wt.%), water-soluble (28-36 wt.%) and water-insoluble (15-23 wt.%) high molecular weight compounds (oligomers) [2], [7]–[9]. In other words, bio-oil consists of 4-6 mmol/g of carbonyl groups, 1-4 mmol/g of phenolic groups, 0.5-2.1 mmol/g of carboxylic acids, and 3-5 mmol/g of aliphatic OH groups [2]. The reactive functional group (40 mol% of COOH groups, 50 mol% of C=O groups, and 90 mol% of OH) causes steric challenges upon interaction with catalytic surfaces [2], [3], [7].

Therefore, to produce a fuel-grade hydrocarbon from bio-oil, the removal of oxygen is necessary, and this process can be expensive. Oxygen can be removed either as H_2O with the

addition of hydrogen or in the form of CO_2 and/or CO, which causes a decrease in the final product yield [2]. The upgrading of bio-oil to hydrocarbon fuel with the use of hydrogen is called the hydrotreatment/upgrading technique. Although the production of pyrolysis oil has been proven at the commercial level, the upgrading is at the end of the demonstration level [10]–[12]. A biorefinery concept where the biocrude produced from HTL or pyrolysis followed by deoxygenation and chemical upgrading process represents the most favorable pathway for the production of biofuel and value-added products [13].

In a trailblazer paper published in 1984 concluded that single stage hydrotreatment by $NiMo/Al_2O_3$ and $CoMo/Al_2O_3$ is not sufficient for HDO due to rapid and severe coke formation which leads to catalyst deactivation [14]. Another pioneer research which was patented reported that in presence of suitable catalyst in a two-step hydrotreatment process using mild severity condition in the first stage reduced the formation of coke and improved the final fuel qualities [2], [13], [15], [16]. The first stage (100℃-300℃) helps in transformation of carbonyl and carboxyl functional groups into alcohols by the help of noble metal catalyst such as Ru, Pt, and Pd [13]. Due to exceptional catalytic activity on aldehyde hydrogenation at low temperatures, Ru had been proven to be better than other noble metals catalysts for first stage stabilization [2], [17]. Conventional sulfided catalysts such as $NiMo/Al_2O_3$ and $CoMo/Al_2O_3$ were used for the second stage HDO at elevated temperature (350℃-400℃).

According to literature, upgraded bio-oil yield varies between 17- 92 wt.%, oxygen and coke content of 1-16 wt.% and 4-30 wt.%, respectively, from batch reactor experiments [2], [18]–[21]. Typically, 11-16 wt.% of oxygen is reported in upgraded bio-oils but to get lower than 3wt.%, a hydrogen donor solvent such as tetralin along with hydrogen is required to remove oxygen from

heavier oligomeric fractions [2]. Total hydrodeoxygenation may result in thermal runaway especially in batch reactors since reactions are exothermic in nature [10], [22].

Traditionally, transition sulfided metal catalysts such as NiMo and CoMo supported on alumina was used extensively for the HDO treatment. Additionally, the alumina support is prone to coke formation due to acidic site, and it deactivates faster under the presence of water [23]. Nobel metal catalysts are excellent choice for the HDO, but high price and regeneration make it difficult to use. It has been seen that these catalysts are less susceptible to deactivation under water and maintain stability even without sulfur in the feed. Pt/C, Pd/C and Ru/C have high reactivity to activation of hydrogen gas, and these could hydrogenate reactive compounds to alcohols at low temperatures (100-300℃) [15]. Earlier studies have found that the hydrogenation with sulfided CoMo resulted in polymerization after single step while a two-step treatment using Ru/C resulted in no catalyst fouling until 48h [24]. The first step helps in increasing H/C while O/C remains same due to hydrogenation of carbonyls and sugars [2].

Catalyst support imparts acid and basic sites which are essential for hydrogenation of carbonyls into alcohol, dehydration of alcohols to olefins, and saturation of olefins to alkanes [10]. A synergistic effect occurs between the acidic site of the support and the metal active centers. Deoxygenation and hydrogenation occur in acid and metal sites, respectively. Literature have shown that bifunctional catalysts where both carbonyl and hydroxyl groups get activated by metal sites and acidic supports, respectively were popular choice for HDO of pyrolysis oils [25], [26]. Shape selectivity, pore size and distribution are important for producing and tuning of aromatic hydrocarbons. A study by Fun et.al reported that porous structure of activated carbon was responsible for catalytic activity for hydrogenation of bio-oil rather than the surface functionality. A density functional theory study by Rub et.al., [27] stated that defects of graphene near the Ru

particles were not catalytically active and summarized that carbon supported catalysts are inert compared to acidic supports (alumina and zeolites). On the other hand, noble metal supported on acidic supports weaken the aryl-oxygen bonds by saturation of aromatics and the acidic supports help in removal of oxygen via C-O bond cleavage [2]. For example, during the HDO of m-cresol over Pt/Al_20_3, it was seen that 3-methylcyclohexanol was formed by hydrogenation reactions and the alcohol was converted to toluene over the alumina support [28]. However, alumina supports accelerate the rate of polycondensation which induces coke formation and subsequent catalyst deactivation. Carbon supported catalysts give preference to ring saturation/hydrogenation rather than HDO, but deoxygenation takes place primarily via decarbonylation of C-C bonds [2], [29].

There is an essential need to maintain the development of lignocellulosic biomass to biofuel conversion as this could be the solution for energy security, use of diverse domestic natural resources, advance the biofuel and bioproduct industries and most importantly to reduce greenhouse gas emissions. Even though HDO of fast pyrolysis oil have been studied for more than thirty-five years, it is well known that catalytic HDO does not remove complete oxygen. To mitigate the problem, pyrolysis bio-oils are blended with petroleum fractions for coprocessing [2], [30]–[32], [34]–[40]. Biofuels have been extensively researched and tested for blended fuels production particularly with petroleum [41] and blending pyrolysis oil with petroleum-based oil represents the most economically advantageous pathway for commercialization [42]. Further, co-processing of pyrolysis oil with the low-quality refinery streams such as light cycle oil may better justify since their individual upgrading is not profitable. A study by Athanasios et al. [43] reported that after blending with light cycle oil (LCO), the liquid product had negligible water, oxygen, total acid number, higher gasoline and diesel fraction and reduced hydrogen consumption (9%) compared to standalone LCO hydroprocessing. Hydroprocessing of ester and fatty acids can be

converted into hydrocarbons to be used as diesel and jet fuels [44], [45, p.]. Hydroprocessed ester and fatty acid units (HEFA) fuels are produced worldwide by Neste, UOP, ENI, Galp Energie, Renewable Energy Group [45], [46]. Yellow greases (tallow and waste cooling oil) comprise of 70% of total triglycerides. Between 1.5-35 kg of H_2 is consumed per 100 kg of feedstock to produce 75-85 kg of diesel range hydrocarbons, 1-5 kg of naphtha and 4-5 kg of propane [56]. Therefore, blending vegetable oil or animal waste with pyrolysis oil could be an effective way to reduce HEFA production cost [56], [47]. HDO conditions (300-500℃, 300-1450 psi, NiMo, Pd, ZSM-5) at HEFA are similar to HDO of pyrolysis oil [56], [48], [49]. Our previous study showed that there is a synergistic effect occurred when vegetable oil (Carinata oil) was blended with HTL algal biocrude. Carinata oil acted as a hydrogen donor and the upgraded blended feedstock exhibited lower hydrogen consumption, decreased coke formation and interestingly CH_4 gas was not present in the gas phase. Moreover, Douglas fir biochar supported catalysts (DF) catalyzed cracking reactions, lower viscosity, higher HDN, HDS, HDM activity compared to $CoMo/Al_2O_3$. This further motivated us to explore the alumina and DF supports and Carinata oil as one of the blending feedstocks for hydrotreatment of more complex pyrolysis oil this time. Additionally, there is a little understanding about the behavior of pyrolysis oil and vegetable oil/animal fat when subjected to HDO under different catalyst supports. Hence, the aim of this research was to assess the co-hydrotreatment of fast pyrolysis oil and Carinata oil or poultry fat to identify synergistic effects if any.

Therefore, in the present study unsulfided bimetallic Cobalt molybdenum catalysts on Douglas fir biochar support (DF) and alumina support (Al) were used to hydrotreat a blend of eucalyptus pyrolysis bio-oil with Carinata oil and poultry fat. Two catalysts were used: 1) Cobalt molybdenum supported on alumina. (denoted as CoMo/Al), and 2) Cobalt molybdenum supported

on Douglas Fir biochar. (denoted as CoMo/DF). The main objective of this study was to understand the synergistic effect of the blending pyrolysis oil with triglycerides such as Carinata oil and poultry fat for hydrotreatment under different supports and the impact on the oil quality, HDO, catalyst regeneration and coke formation.

5.2 Material and Methods

5.2.1 Materials

Hydrogen (H_2) gas (99.999 mol.%) were purchased from Airgas Inc. (Opelika, AL, USA). Douglas Fir (DF) biomass was hammer milled (passed 1.68 mm) and was obtained from Forest Concepts, LLC (Auburn, Washington, USA). Cobalt (II, III) oxide (~3.4 – 4.5% CoO, ~11.5 - 14.5% MoO; 2.5mm trilobe extrudate) on alumina was purchased from Sigma–Aldrich (St. Louis, MO, USA). The as-received extrudates were ground (ranging between 106 µm and 38 µm) and used as alumina-supported catalysts. Cobalt nitrate hexahydrate (99 wt.% crystalline) and ammonium heptamolybdate, tetrahydrate (99 wt.% crystalline) were purchased from Sigma Aldrich (St. Louis, MO, USA) and were used as received for DF biochar supported catalyst.

Bio-oil was produced by pyrolyzing eucalyptus biomass in a stainless-steel proprietary auger fed reactor developed at Mississippi State University [50]. The runs employed a reheated nitrogen gas purge. Auger (3 in diameter and 40 in in length) rotating at 12 rpm were used to move the biomass through a heated tube and multiple heated bands along the reactor length were used to supply heat [61]. Solid feed takes about 30 s to traverse the 450 °C pyrolysis zone and a total of ~50 s to move to the char exit point [61]. The majority of the pyrolysis forming the vapor occurs in the first 4−5 s in the pyrolysis zone [61]. Vapors passed into a condenser system to recover several liquid fractions. Bio-oil was collected after the pyrolysis reaction had been continuously

generating bio-oil for 30 min to ensure steady state conditions. Non condensed gases exited the condenser system at ambient temperature. Most of the solid biochar was moved through the reactor by the rotating auger to a char removal pot [61]. The bio-oil was then filtered to separate the char from the organic fraction. The organic fraction was used for hydrotreatment experiments. *Eucalyptus benthamii* (E. benthamii) samples were obtained from ArborGen's plantation in South Florida. It was a 7-years old without bark sample. Poultry fat was obtained from Charles Miller Jr. Poultry Research and Education Center at Auburn University (AL, USA). Carinata oil was obtained from Applied Research Associates, Inc. (provided by Agrisoma Biosciences, Inc, Gatineau, Quebec, Canada). Detailed physical properties of the Carinata oil could be found in our previous study [51], [52].

5.2.2 Catalyst preparation

DF biomass (20 g) was mixed with 350 ml deionized water. To this slurry, calculated amount of metal salts (ammonium heptamolybdate and cobalt nitrate) was added to give a 11.5 wt.% Mo and 3.5 wt.% Co metal loadings on the final catalyst, respectively. The metallic salts mixed with DF biomass slurry was stirred at 80℃ for 4 h to obtain a thick mixture. The mixture was then dried at 105°C overnight to obtain catalyst precursors. The precursors were then activated by reduction using 10% H_2 and 90% N_2 at 400℃ with a residence time of 5h at 5°C/min with a flow rate of 0.2 l/min. The obtained catalyst was denoted as CoMo/DF. Ground as-received commercial cobalt molybdenum supported on alumina was reduced at (400℃) for 5h to obtain the catalyst represented as CoMo/Al [53], [54]. Finally, all the samples were cooled down to room temperature by passing N_2 gas and stored them for further use. Ruthenium, 5% on activated carbon powder was procured on Alfa Aesar (USA).

5.2.3 Catalyst characterization

Detailed procedure and instrument specifications for Thermogravimetric analysis (TGA), simulated distillation (SimDis), Brunauer–Emmett–Teller (BET) surface area and NH_3-TPD of the catalysts can be found in our previous publications. X-ray photoelectron spectroscopy (XPS) was performed using NAP-XPS system operating in UHV mode equipped with an XR 50 MF Al Kα X-ray Source with a μ-FOCUS 600 X-ray monochromator. The Al K_α radiation was used with an X-ray beam energy of 1486.7 eV and power of 100 W. A PHOIBOS NAP *in situ* 1D-DLD hemispherical electron energy analyzer (~0.85 eV energy resolution and 0.3 mm entrance aperture) collected the spectra. The pressure during the entire acquisition was better than $\sim 10^{-8}$ mbar. Pass energy of 100 eV, step size of 1 eV and dwell time of 100 ms was used to acquire survey spectrum while pass energy of 20 eV, step size of 0.1 eV and dwell time of 1 s was utilized. Scofield relative sensitivity factors (RSF) were used in quantification and linear transmission was assumed over the measured range [55]. Spectra were charge referenced to primary char C1s peak at 284.4 eV [56], and, where available, to Al 2p at 74.9 eV [57] Spectral data were processed using CasaXPS v 2.3.23PR1.0 software suite [58].

5.2.4 Catalytic cracking experiment

The experiment was carried out at 400℃ with a residence time of 2h with 500 psi of nitrogen cold pressure with CoMo/Al.

5.2.5 Hydrolysis of fat experiment

The hydrolysis of the poultry skin was carried 400℃ with a residence time of 2h with 500 psi of nitrogen cold pressure with CoMo/Al.

5.2.6 Mild hydrotreatment experiments

Mild hydrotreatment experiments were carried out in a 450 mL Parr bench top reactor for stabilization purpose. Pyrolysis oil and Ru/C catalyst were hydrotreated at 150℃ for 2h with 1000 psi of initial hydrogen gas using feed-to-catalyst mass ratio of 70:1. The mild hydrotreatment results are provided in the supplementary information (Table. S1). After mild hydrotreatment and centrifugation there were two distinct phases of oil (Figure. S1). The phase which had lower water content was selected as an organic phase and was used for further severe hydrotreatment experiments.

5.2.7 Hydrotreatment experiments

The co-hydrotreatment tests were carried out in a 100 mL Parr 4598 bench top reactor. Pyrolysis oil (15 g), Carinata oil (15 g), and a 50:50 (wt.%) mixture (30 g in total) of these two oils were performed at 400℃ for 4h with 1000 psi of H_2 using feed-to-catalyst mass ratio of 70:1 (30 g oil and 0.42 g of catalyst). Hydrotreatment experiments with only pyrolysis oil was performed by using 20 g of oil and 0.31g of catalyst (70:1 ratio). Identical parameters were used from our previous publications [62], [63]. The process parameters such as temperature, time, H_2 gas pressure, blend ratio and catalyst to oil ratio were studied. All the hydroprocessing experiments were conducted in duplicates.

5.2.8 Analysis of products

For mass-balance purpose, the liquid and solid reaction products were weighed. The liquid products (organic and aqueous phase) along with the solid products were centrifuged at relative centrifugal force of 2000 g for 15 min for phase separation. After centrifugation, the organic phase on the top was collected and analyzed. While the aqueous phase and the solid were settled at the

bottom. The solids were filtered and washed with hexane and stored for further analysis. The aqueous phase was also stored. Details about hydrogen consumption, liquid yield, and solid yield calculations were explained elsewhere [62]. Similarly, detailed procedure and instrument specifications for viscosity, GC-MS, total acid number (TAN), elemental analysis (CHNS-O), higher heating value (HHV), and simulated distillation (SimDis) can be found in previous studies [63], [62], [59], [60].

5.3 Results and discussion

5.3.1 Catalyst characterization

NH_3-TPD analysis was carried out to evaluate the distribution of acid sites such as weak (<200℃), moderate (>200℃ and <400℃) and strong (>400℃) (Figure 1). According to Ndlela et.al. [52], the weak acidic sites correspond to desorption of loosely bound ammonia, while ammonia desorption at temperature greater than 400℃ corresponds to strong acidic sites. A medium intensity desorption peak at higher temperature was observed for RDF, and this could be due to the support's acidity containing oxygen functional groups. The acidic material of a carbon supports may depend on the presence of carboxylic, hydroxide, phenol and lactone groups [53. CoMo/DF exhibited a broad sharp desorption peak at 650℃ (strong acid site). This result can be confirmed from our previous study where Co nitrate and hydroxide salts supported on biochar exhibited similar results. On the other hand, a sharp contrast could be seen where CoMo/Al demonstrated lower acid sites ranging from 250 to 450 ℃.

The BET surface area of the biochar supported catalysts are higher compared to alumina supported catalysts (Table 1). This phenomenon is also observed by other authors in the literature.

The average pore is in micropore range for the CoMo/DF compared to CoMo/Al which is in the mesopore range.

XPS survey spectrum of reduced Douglas fir biochar without any metal impregnation is shown in Figure 2. It is comprised from 96 % carbon with small amount of oxygen as inferred via XPS quantification (Table 2). C1s peak at 284.4 eV shown in inset due to the aromatic C-C/C-H bonds [56]. Figure 2 and Figure 3 shows the Co 2p, Mo3d regions before and after hydrotreatment of pyrolysis oil respectively. In as synthesized catalysts, Co $2p_{3/2}$ at 780.5 eV is due to the mixture of Co_3O_4 and $Co(OH)_2$ while Mo $3d_{5/2}$ peak at 232.8 eV is due to MoO_3 [61], [62] Al2p peak at 74.9 eV is due to Al_2O_3 [57]. Quantification of the high resolution XPS regions provides for the surface elemental composition of as synthesized and reacted catalysts.

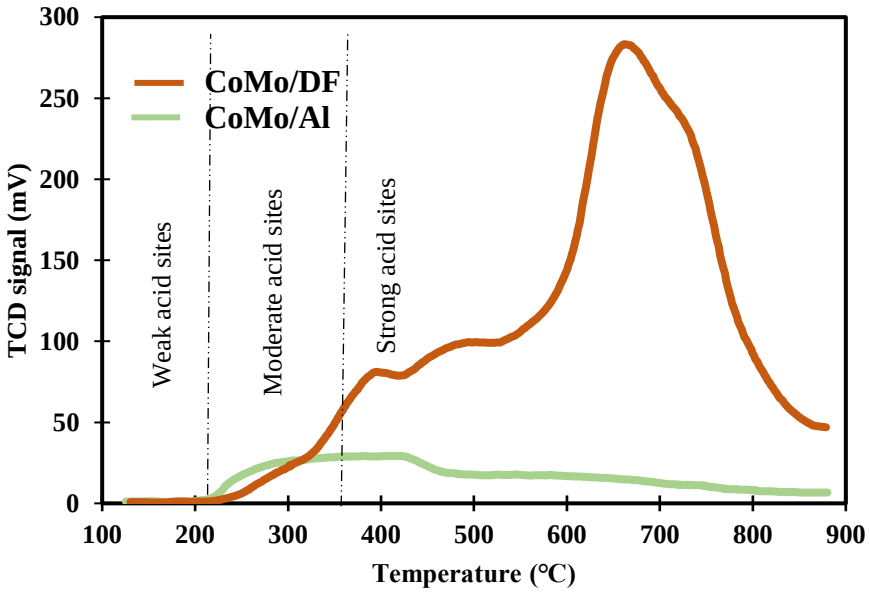

Figure 5.1 TPD of CoMo/DF and CoMo/Al catalysts.

Table 1. Physisorption data of the catalysts.

Catalysts	BET surface area (m2/g)	Average Pore size (nm)	Total Pore Volume (cc/g)
CoMo/Al	240	3.9	0.68
CoMo/DF	391	1.7	0.20

Table 2. XPS high resolution spectra quantification.

Sample	Al 2p, %	C1s, %	Co 2p, %	Mo 3d, %
CoMo/Al	77.5	14.7	3.0	4.8
CoMo/DF	0.0	98.2	0.7	1.1

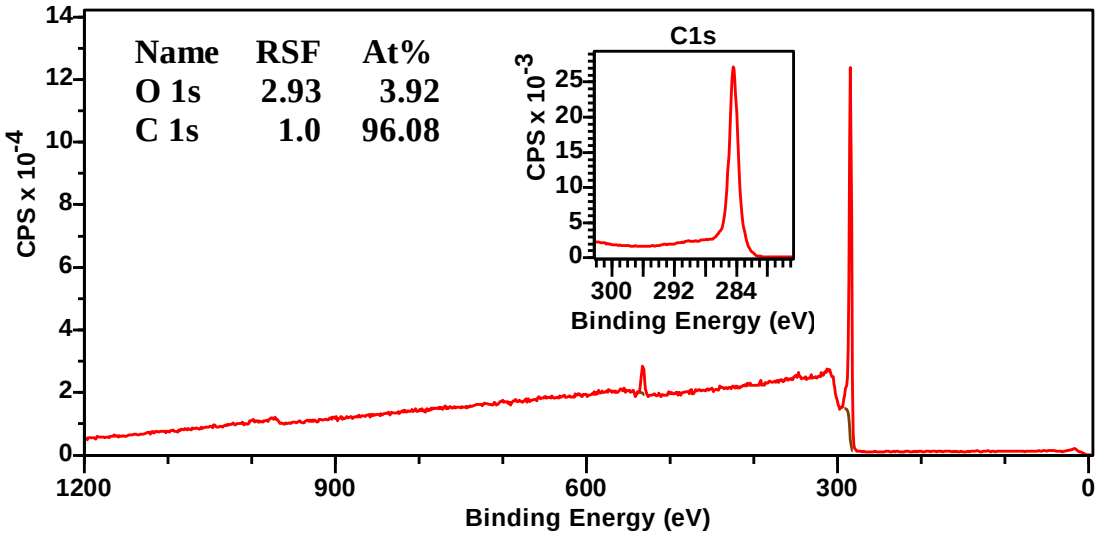

Figure 5.2 XPS data of the DF support.

5.3.2 Product yield distribution and gas analysis

Pyrolysis oil blended with Carinata and poultry fat hydrotreated over CoMo/DF is denoted as BCA/DF and BPF/DF. Similarly, over CoMo/AL it is denoted as BCA/AL and BPF/AL.

Pyrolysis oil hydrotreated over CoMo/Al and CoMo/DF is denoted as PY/AL and PY/DF. Mild hydrotreatment was conducted over Ru/C and it consisted of two phases (dark and a light phase) after centrifugation. The dark phase (organic) had 17.5% of water content and HHV of 23 MJ/kg and was used for further hydrotreatment in this study. While the aqueous phase had a water content 65.66% and HHV of 13.18 MJ/kg was stored for future use.

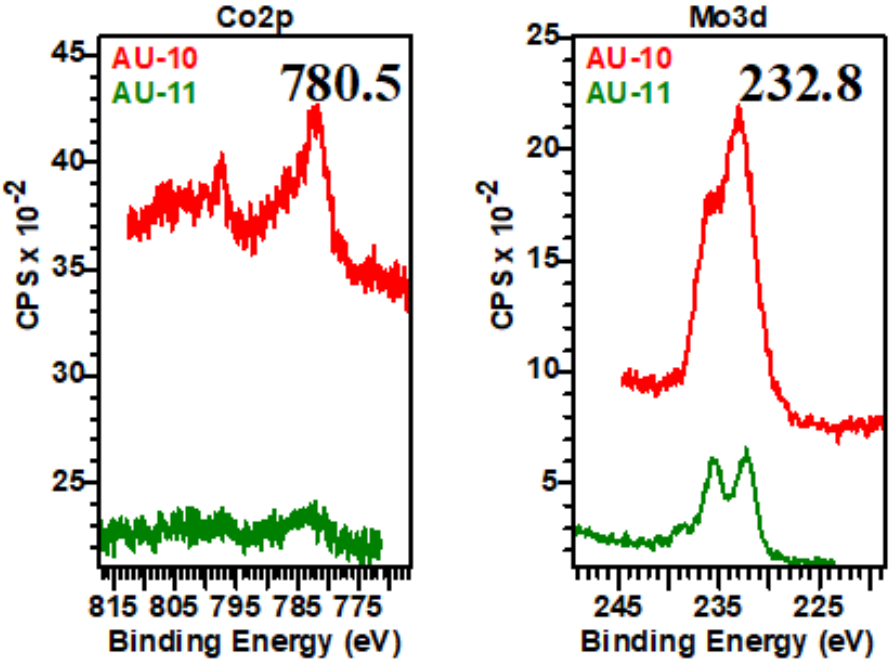

Figure 5.3 XPS data of the CoMo/Al and CoMo/DF catalysts.

Figure 4 illustrates the oil, aqueous phase, gas, and solid yield of the hydrotreated pyrolysis, Carinata, poultry fat and their blends. Overall, alumina supported catalysts produced slightly higher liquid yield, and gas yield compared to biochar supported catalysts for the upgraded blended bio-oils. Maximum oil yield of ~76% was observed for CoMo/Al for both the BCA and BPF upgraded oils. This is closely followed by the CoMo/DF catalysts for BPF (74.63%) and BCA (73.57%), respectively. A positive synergistic effect in terms of liquid yield could be seen in the

case of biochar supported catalysts or BPF and BCA oils. Higher solid and aqueous yield were seen for CoMo/DF. Solid is defined as the portion of the liquid having higher density than the upgraded liquid that settled at the bottom of the centrifuge tube after centrifugation. A higher amount of solid was observed of biochar

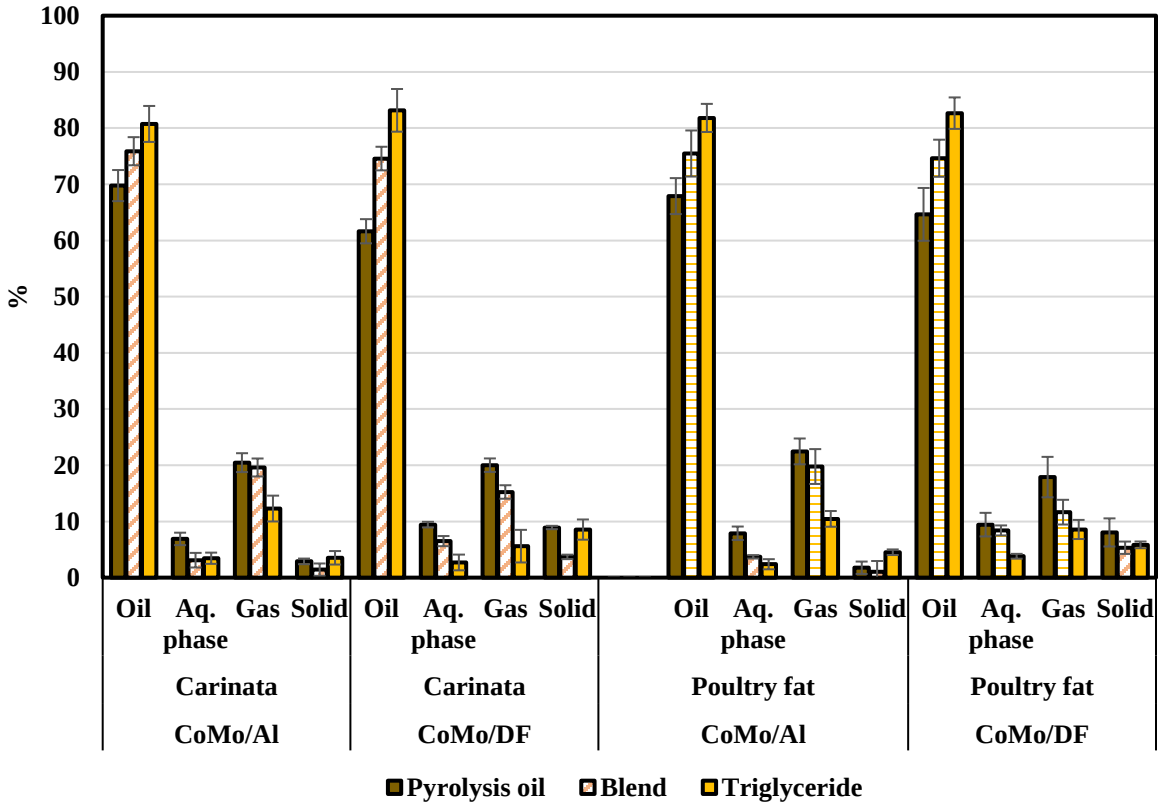

Figure 5.4 Product yield distribution after hydrotreatment of pyrolysis oil, Carinata oil, poultry fat and co-hydrotreatment of their upgraded blend over different supports.

supported catalysts compared to alumina supported catalysts irrespective of whether it is blended or not. This result aligns with our previous studies [35], [62]. This is due to the biochar matrix could have soaked a large proportion of oil and thus a decrease in the liquid yield and an increase in the wax/solid yield was observed. Higher amount of aqueous phase in the upgraded blended oils

(UBO) are due to hydrogenolysis of C-O bond (water as a byproduct) and dehydration reactions in the case of biochar supported catalysts. Without blending the upgraded pyrolysis oils had much lower liquid yield and higher solid yield. Additionally, 69% (Carinata) and 67% (poultry fat) liquid yield was for alumina supported catalysts and 61% (Carinata) and 62% (poultry fat) was observed for biochar supported catalysts. Liquid, gas and solid yield for upgraded Carinata over CoMo/Al and CoMo/DF are in accordance with our previous study [35].

Table 5.1 Gas composition and HHV of upgraded oils over different supports.

	CoMo/Al					CoMo/DF				
	PY	BCA	CA	BPF	PF	PY	BCA	CA	BPF	PF
CH_4	29.60	5.14	80.80	12.05	82.70	38.40	18.0	83.15	14.27	80.80
CO	51.0	39.50	3.45	34.50	2.40	43.83	18.14	2.70	22.0	22.0
CO_2	17.80	23.0	12.30	24.60	10.45	13.10	19.30	5.60	17.40	17.40
H_2 / kg of O*	56.60	31.8	54.0	28.16	51.34	39.80	67.60	65.70	38.50	58.50

*Mole of hydrogen consumed per kg of oxygen in crude oil.

The gas products mainly consisted of CO, CO_2, and CH_4 gas. A higher amount of CH_4 and CO gas formation in the UBO could be noticed in the case of CoMo/DF and CoMo/Al, respectively. Alternatively, a higher amount CH_4 was present for the hydrotreated triglycerides (Carinata and poultry fat) irrespective of the support type. After blending the pyrolysis oil with Carinata or poultry fat, the amount of CH_4 gas formed in the UBO were lower compared to their individual feedstock. Therefore, bending with triglycerides probably caused a synergistic effect that caused this phenomenon. The hydrogen consumption per kg of oxygen for CoMo/DF were higher compared to CoMo/Al. Higher hydrogen consumption per kg oxygen removal could be due to hydrogen spillover effect where the biochar support acts as a hydrogen reservoir [67]. This spillover mechanism is usually seen for carbon supports which have higher oxygen functional

groups. Additionally, high hydrogen consumption on CoMo/DF could be due to the formation of higher amount of aqueous phase after hydrotreatment. However, there is tradeoff between hydrogen consumption and gas generation. A lower hydrogen consumption could be seen for UBO produced from CoMo/Al compared to individually hydrotreated parent oils. Therefore, another possible synergistic effect could be seen. From the gas data, it can be assumed that decarbonylation (DCO) and decarboxylation (DCO_2) pathways were preferred for oxygen removal along with HDO [63], [64] or CoMo/Al. A study by Buri et al. [66] reported DCO and DCO_2 were the main reaction pathways for sulfided NiMo species for HDO of palm oil. For the UBO produced from CoMo/DF the oxygen was removed predominantly via dehydration and methanation reactions as seen from Figure 4 and Table 3. According to a study by Puente et. al. [65], the study reported that acid sites are responsible for dehydration of alcohols to alkenes and finally to paraffins. According to the previous studies [35], [62], biochar has inherent acidic sites, and these sites could play a role in dehydration reactions. Therefore, the triglycerides could be acting as a hydrogen donor solvent to the hydrogen deficient feedstocks [25], [28]. Similar results have been reported in literature where CoMo/DF favor methane formation largely due to presence of alkali and alkaline earth metals or due to [66]. Moreover, production of methane could be due to hydrogenation of coke deposited in the biochar pores [66]–[68].

5.3.3 Effect of hydrotreatment on individual feedstock (upgraded pyrolysis oil, cracked Carinata and cracked poultry fat)

Cracked Carinata oil had 78 wt.% C, ~11 wt.% O, HHV of ~ 40 MJ/kg and kinematic viscosity of ~ 12 m^2/s as seen in Table 4. Results are in accordance with our previous study. Cracked poultry fat showed 76 wt.% C, ~10 wt.% O, HHV of ~ 39MJ/kg and kinematic viscosity of ~ 17 m^2/s. Pyrolysis oil had 42 wt.% C, ~50 wt.% O, HHV of ~ 17 MJ/kg and kinematic

viscosity of ~ 12.6 m^2/s as seen in Table 4. After hydrotreatment ~82% and ~78% decrease in oxygen content and ~ 85% and ~ 76% increase in carbon content was noticed for pyrolysis oil produce from CoMo/DF and CoMo/Al respectively. These results translated well with the HHV where both the supports improved it, but the biochar supported catalysts comparatively increased it more than alumina supported catalysts. Alumina support is hydrophilic nature and under the presence of high-water content and acidic compounds the support loses it stability and could not tolerate HDO of bio-oils. While non-alumina supports such as biochar in this case was seen to achieve good deoxygenation degree. In literature typically, 11-16 wt.% of oxygen is reported for upgraded bio-oils but to get lower than 3wt.% a hydrogen donor solvent such as tetralin along with hydrogen is required to remove oxygen from heavier oligomeric fractions [2]. Comparing the two supports for hydrotreatment of Carinata oil, biochar support performed better in terms of carbon addition, deoxygenation degree, and kinematic viscosity. But TAN values were relatively higher. In contrast, the alumina support performed better at deoxygenation, HHV, and TAN. For both the upgraded triglycerides, the TAN was higher for the biochar support. This indicates that the biochar support could not catalyze the reduction of carboxyl groups. According to a previous study [69], activated carbon shows some acidity which can originate from the surface oxygen functional groups. Similar results were reported by Lee et. al. [70], where the authors described that activated carbon support was successful in hydrogenation of heavy compounds but was unsuccessful in removing TAN. Irrespective of triglycerides or pyrolysis oil the UBO from biochar support demonstrated lower KV_{40} compared to their original feedstock. This is due to cracking of large and complicate structures to small and simpler ones caused by biochar support. It is well documented in literature that biochars are excellent at cracking tar [71], [73]. The water content of all the hydrotreated oil was lower than the determinable range.

Table 5.2 Physiochemical characterization of feedstock and hydrotreated blended oils over alumina and Douglas fir biochar supported catalysts.

Feedstocks				Hydrotreated oils													
				CoMo/Al							CoMo/DF						
Oil properties	Pyrolysis oil	Cracked Carinata oil	Cracked Poultry Fat	Pyrolysis oil	Blend	Carinata	Synergistic change %	Blend	Poultry Fat	Synergistic change %	Pyrolysis oil	Blend	Carinata	Synergistic change %	Blend	Poultry fat	Synergistic change %
C (wt.%)	42.38	78.2	76.32	76	80.16	79.29	+3.00	81.02	80.13	+3.55	78.71	82.88	81.55	+3.43	83.01	80.73	+4.13
H (wt.%)	6.63	11.8	12.03	11.16	11.62	13.50	+5.72	11.05	12.7	+7.39	10.01	13.08	13.6	+10.82	12.84	12.1	+16.14
O (wt.%)	50.77	9.9	11.01	10.85	7.02	6.18	+17.48	6.17	5.18	+23.02	9.73	2.90	4.34	+58.66	2.59	6.11	+67.20
HHV (MJ/kg)	17.10	40.6	39.04	38.0	40.76	42.84	+0.86	41.34	41.04	+4.63	36	42.4	42.4	+8.58	42.1	40.56	+9.98
TAN (mg KOH/g)	72.72	63.12	49.43	11.7	5.81	2.15	+16.10	4.25	3.60	+44.44	9.1	3.97	3.75	+38.21	3.1	4.76	+55.27
Density (g/cm^3)	1.15	0.9	0.9	0.90	0.88	0.81	+2.92	0.89	0.82	+3.49	0.9	0.87	0.79	+2.96	0.88	0.85	+0.57
Kinematic viscosity 40 ^oC (m^2/s)	12.60	49.5	55.12	17.20	8.01	3.53	+22.82	4.66	6.2	+60.17	12.1	5.43	3.14	+28.74	3.3	4.7	+60.71

5.3.4 Effects of catalyst support on upgraded blend oil properties

The synergistic effects (%) were calculated by taking the average between pyrolysis oil and cracked Carinata oil or cracked poultry fat and computing the difference with their respective blends. Positive sign (+) indicates a favorable change.

The deoxygenation degree of the upgraded blends of either Carinata or poultry fat from both the supports showed positive synergistic effect. The oxygen content for the UBO varied between 2.5 to 7 wt.%. CoMo/DF support showed lower oxygen content particularly for BPF (2.5 wt.%) followed by 2.9 wt.% for BCA. While BCA from CoMo/Al had the highest amount of oxygen left in the oil (7 wt.%). There was a negative synergistic effect (-5.7% and -7.3%) for CoMo/Al for hydrogen addition. This could be due lower hydrogen consumption compared to biochar support and most of the hydrogen could have removed via aqueous phase after hydrotreatment. Higher hydrogen content was observed for biochar support compared to alumina support. This result is well aligned with our gas and hydrogen consumption data reported in Table 3 were we reported that biochar support consumed more hydrogen and produced more methane gas. In terms of carbon addition, the synergistic effects were mostly similar except for BPF produced from CoMo/DF where it had the highest carbon addition of 83 wt.% (+4 % synergistic effect). The HHVs varied between 40 to 42 MJ/kg with BCA produced from CoMo/DF demonstrated highest HHV of 42.88 MJ/kg.

The HVV correlates well with high values of carbon and hydrogen, and low values of oxygen in the UBO as discussed earlier. Among the blends, CoMo/DF exhibited lower TAN values and highest synergistic effects compared to CoMo/Al. BPF and BCA from biochar support had TAN values of 3.1 and 3.97 mgKOH/g while BCA and BPF from alumina support had 5.8 and 4.25 mgKOH/g. This indicates that there are still fatty acids, organic acids, and phenols left in the oil.

All the supports achieved a positive synergistic effect and lowest KV_{40} value was achieved by BPF (3.3 m^2/s) from CoMo/DF. The KV_{40} of diesel is in the range of 1.5–4.5 mm^2/s and our study achieved a lowest KV_{40} of 1.4 mm^2/s. Lower values of KV_{40} could be due to enhanced cracking by the biochar support which reduced the complex higher molecular weight compounds into lower-MW and simpler ones. From the bulk characterization, it could be summarized that biochar support imparted better positive synergistic effects compared to alumina support. As already discussed, the alumina support is unstable under aqueous environment which is a primary product of dehydration reactions during HDO and thus does not produce higher HDO degree compared to non-alumina supported catalysts. On the other hand, biochar support is hydrophobic and have high hydrothermal resistance. Mesoporous carbon helps in sweeping of water outside the catalyst particle and thus it is one of the most successful supports for bio-oil HDO [70]. Higher acid sites and surface area might have helped the biochar support for a higher HDO degree than the alumina support. A study by Snare et al. reported that Pd/C and Pt/C achieved higher deoxygenation degree compared to Pd/Al_2O_3 and Pt/ Al_2O_3 [69]. It is attributed to larger specific surface area that reduces sintering of metal particles. They suggested potential promotion of demethylation associated to the oxygen containing functional groups. Another study by Yafei Shen et. al., [71] indicated that biochar support can introduce deoxidation ability into non-noble metal catalysts such as Ni or Co and are successful in conversion of phenolic compounds to cyclohexane [44], [71], [72]. Biochar's activities can be ascribed to the ash content and inorganic elements such as K, P ,Ca, Fe and Mg, which play a pivotal role in tar cracking and deoxygenation at high temperatures [66], [73]. Ca is known for its deoxygenation properties [66], [74] while K suppressed formation of long chain molecules [71], [73]. However higher amount can retard the formation of stable compounds. In particular, high concentration of Si would affect the efficiency of metal impregnation because of

sintering upon melting at high temperature and reduced the degree of metal dispersion [75], [76]. Acid sites accelerate the hydrogenation of C=O in the biomass [72], [77]. A study by Tang et al.[78] reported that hydrogen donor solvents such as ethanol gets adsorbed on the metal sites (acid sites) of biochar supported catalyst and it forms alkoxide salts and helps in hydrogenation. In this study, both the triglycerides could be source of hydrogen which were helpful for dehydrogenation of alcohols and further promoted the migration of hydrogen to unsaturated bonds on metal sites for hydrogenation [72], [79], [80].

5.3.5 Chemical composition of hydrotreated oils

Simulated distillation (SimDis) and GC-MS analysis of the UBOs are shown in Figure 5 and Figure 6 respectively. Crude Carinata oil consisted of erucic acid, a C_{22} fatty acid with one double bond, as the major component with ~ 40 wt.% in the oil [62]. Poultry fat was made up of majorly oleic acid (C18:1) and linoleic acid (C18:2) with approximately 30 wt.% each followed by palmitic acid (C16:0) with 20% wt.%. Poultry fat's fatty acid composition from our study agrees well with the literature [81]. After cracking experiments, cracked poultry fat consisted of majorly C15 (pentadecane) while cracked Carinata consisted majorly of C20 (eicosane) hydrocarbons. While pyrolysis oil consisted of mainly oxygenates such as phenols and acids with higher molecular weight of greater than C25. After hydrotreating the pyrolysis oil over alumina and DF support, both the oils consisted mainly of oxygenates and olefins with majority of compounds higher than C20. However, after blending with triglycerides (Figure 6), it could be seen that the distribution of molecules is majorly within C6 to C21 hydrocarbons. Correlating with SimDis (Figure 5) BCA from CoMo/Al and BCA from CoMo/DF had higher percentage of gasoline fraction compared to other fractions. For BPF from CoMo/Al, it consisted mainly of pentadecane

(C15) and hexadecenoic acid (C16) But it had higher amount of jet fuel fraction that could be due to higher amount of paraffins and naphthene from C8 to C12.

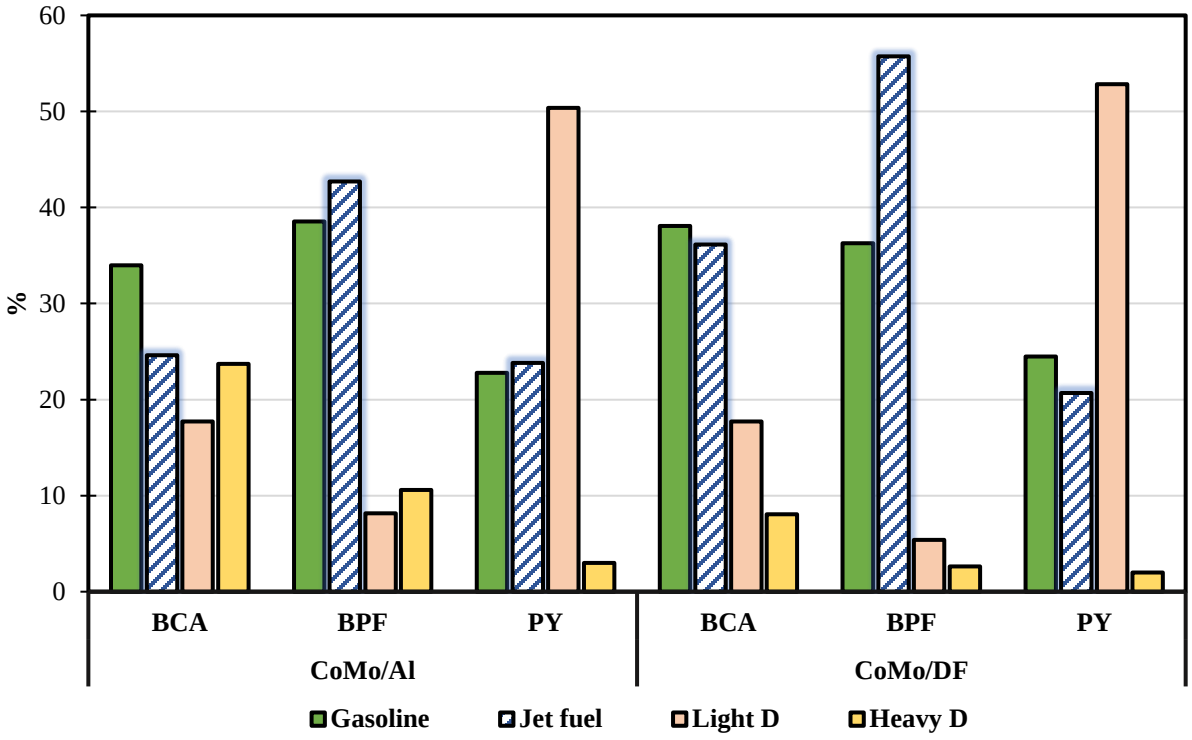

Figure 5.5 Boiling point distribution (simulated distillation, ASTM D2887) for upgraded liquid products produced from different catalyst supports.

Comparing with the alumina supported catalysts, biochar supported catalysts showed a large amount of jet fuel fraction particularly BPF from CoMo/DF, this could be due to presence of higher amount of paraffins, aromatics, naphthene's from C8 to C17. In summary, DF support exhibited higher jet fuel fraction consisting of mainly paraffins, naphthene and aromatics and lowest amount of light and heavy diesel and this is could be due to higher cracking propensity of DF support that contributed to the lower fractional cuts. This is in accordance to our previous study [35], [62].

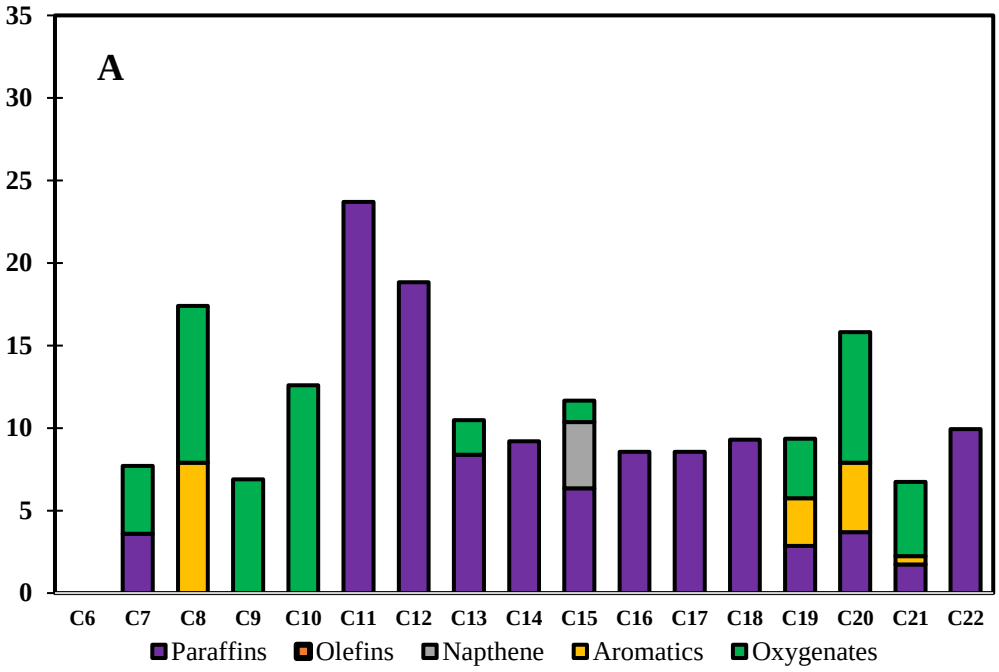
A
35
30
25
20
15
10
5
0
C6 C7 C8 C9 C10 C11 C12 C13 C14 C15 C16 C17 C18 C19 C20 C21 C22
Paraffins
Olefins
Napthene
Aromatics
Oxygenates

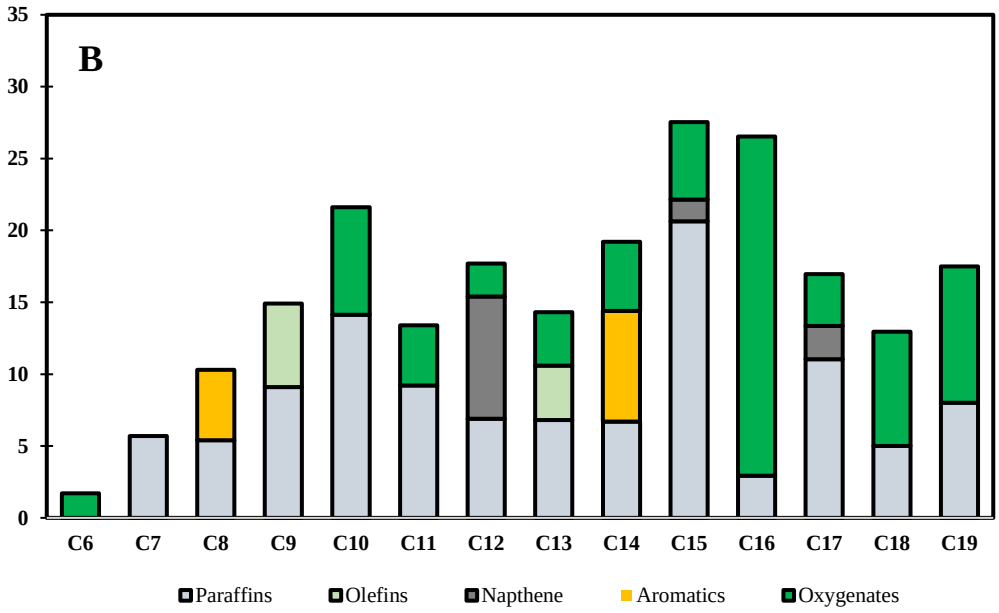
B
35
30
25
20
15
10
5
0
C6 C7 C8 C9 C10 C11 C12 C13 C14 C15 C16 C17 C18 C19
Paraffins
Olefins
Napthene
Aromatics
Oxygenates

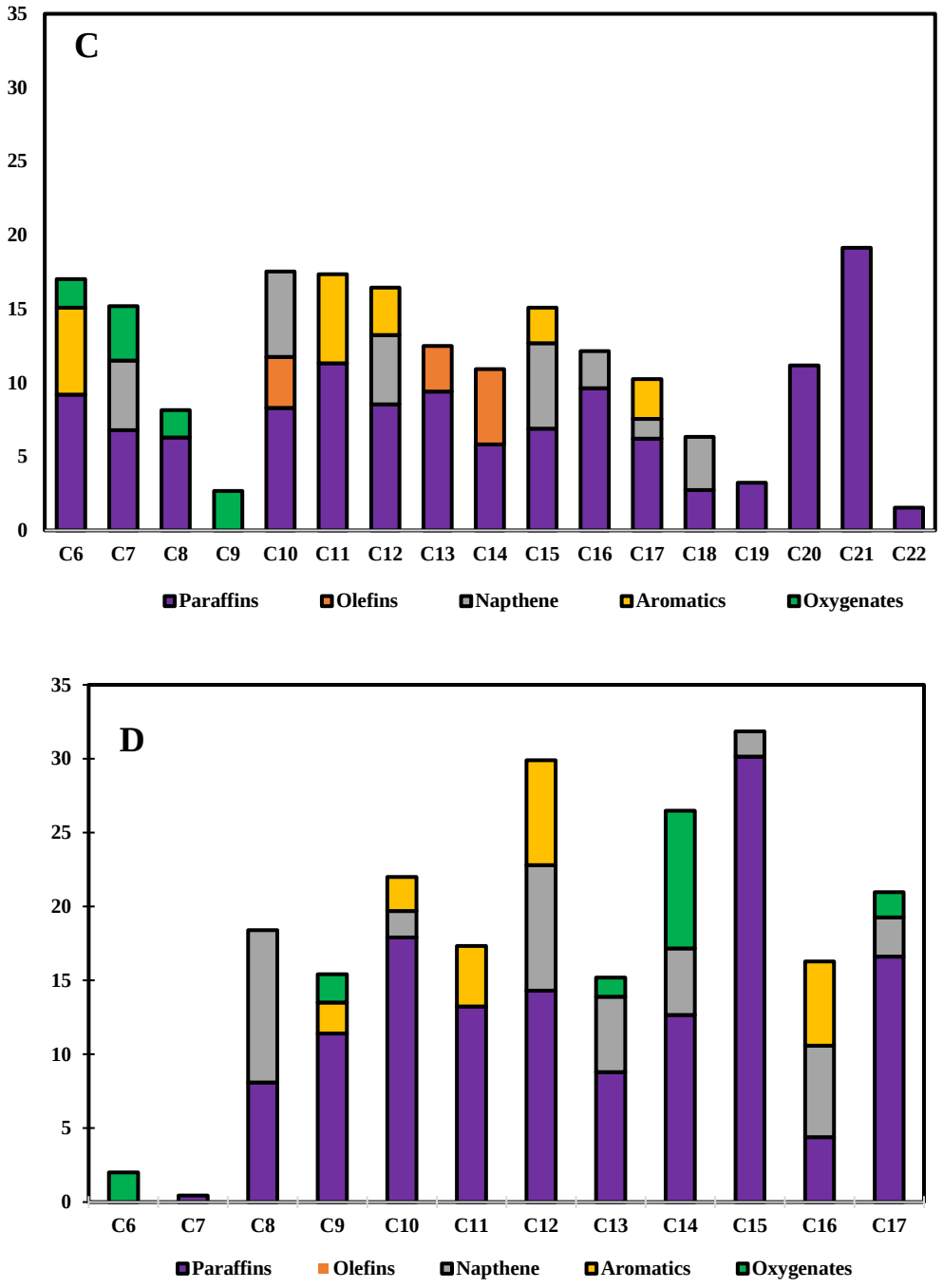

Figure 5.6 Area percent of different compounds classes identified and quantified by the GC-MS; (A)BCA from CoMo/Al, (B) BPF from CoMo/Al, (C)BCA from CoMo/DF and (D) BPF from CoMo/DF.

Overall, poultry fat had majority of hydrocarbons in the C15 range while Carinata had in C17 range which could have contributed to higher jet fuel fraction and heavy diesel fraction respectively. Alumina support had higher amount of oxygenates of higher molecular weight which could have contributed to higher fractional cuts in the SimDis and is in accordance with CHNS data (Table 5).

Table 5.3 Carbon content of the catalysts before and after hydrotreatment.

Fresh		Spent				
(wt.%)		BCA	BPF	PY	CA	PF
CoMo/Al	0	48.6	41.7	65.7	15.4	14.8
CoMo/DF	63.5	76.4	73.7	85.5	72.6	70.1

Table 5.4 BET surface area of the catalysts before and after hydrotreatment.

Samples	BET (m2/g)	Pore radius (nm)	Pore volume (cc/g)
CoMo/Al	240	3.9	0.68
CoMo/DF	391	1.69	0.2
BCA/AL	7	1.7	0.01
BPF/AL	58	1.52	0.07
BCA/DF	6.0	1.91	0.02
BPF/DF	15	1.71	0.05

Table 5.5 XPS analysis of spent catalyst from BPF

Sample	Al 2p, %	C1s, %	Co 2p, %	Mo 3d, %
CoMo/Al	1.7	97.9	0.3	0.1
CoMo/DF	0.0	99.5	0.4	0.01

Carbon content of the fresh and spent catalysts are exhibited in Table 5. Coke formation occurs due to adsorption, condensation and cracking of alkenes, polar aromatics, and other molecules.

Table 6 shows that fresh DF support have approximately 65% carbon and fresh alumina support have no carbon. After hydrotreatment of only pyrolysis oil a 65% and 35% increase in carbon content could be seen for alumina and biochar support. Alumina revealed higher coke deposition than biochar support could be due to alumina's instability during HDO reactions. However, after blending with the triglycerides the alumina support had lower increase in carbon content (48 wt.% and 41 wt.%) which suggests a positive synergistic effect. In the case of biochar support, a 20% (BCA) and 15% (BPF) increase in carbon content was seen. Triglycerides could have acted as a hydrogen donor and decreased the coke build up in the spent catalyst irrespective of the support. Overall, lower coke deposition could be noticed for biochar support and for poultry fat triglyceride. The DF support has the ability to restrict the transformation of coke prone hydrocarbons to coke. These supports have adsorption site for free radicals that are produced during cracking reactions and inhibit them from coupling and polycondensation. Literature reports that alumina supports accelerate the rate of polycondensation which induces coke formation and subsequent catalyst deactivation due to the presence of weak Lewis acid sites [82].

DF supported catalyst achieved a higher BET surface area compared to alumina support (Table 6). The DF supported catalysts had a lower average pore size (less than 2nm) and lower pore volume compared to alumina as discussed earlier. After experiments, it could be seen that both the catalysts had more than 90% decrease in their surface area except for BPF produced from alumina which showed a 75% decrease. Initial high loading of the active Co and Mo catalyst as well as alumina support in fresh catalyst were dramatically decreased, as shown in Table 7. After the reaction, the intensities of Co, Mo and Al support decrease dramatically as biochar carbon accumulates on the catalyst surface. Overall, poultry fat demonstrated lower coke formation compared to Carinata. This is confirmed by the oxidative loss tests carried out by using TGA experiments of the bio-oils

and the spent catalysts under air. Blending with poultry fat increased the stability of the bio-oils compared to hydrotreatment of only pyrolysis oil as seen in Figure 7.

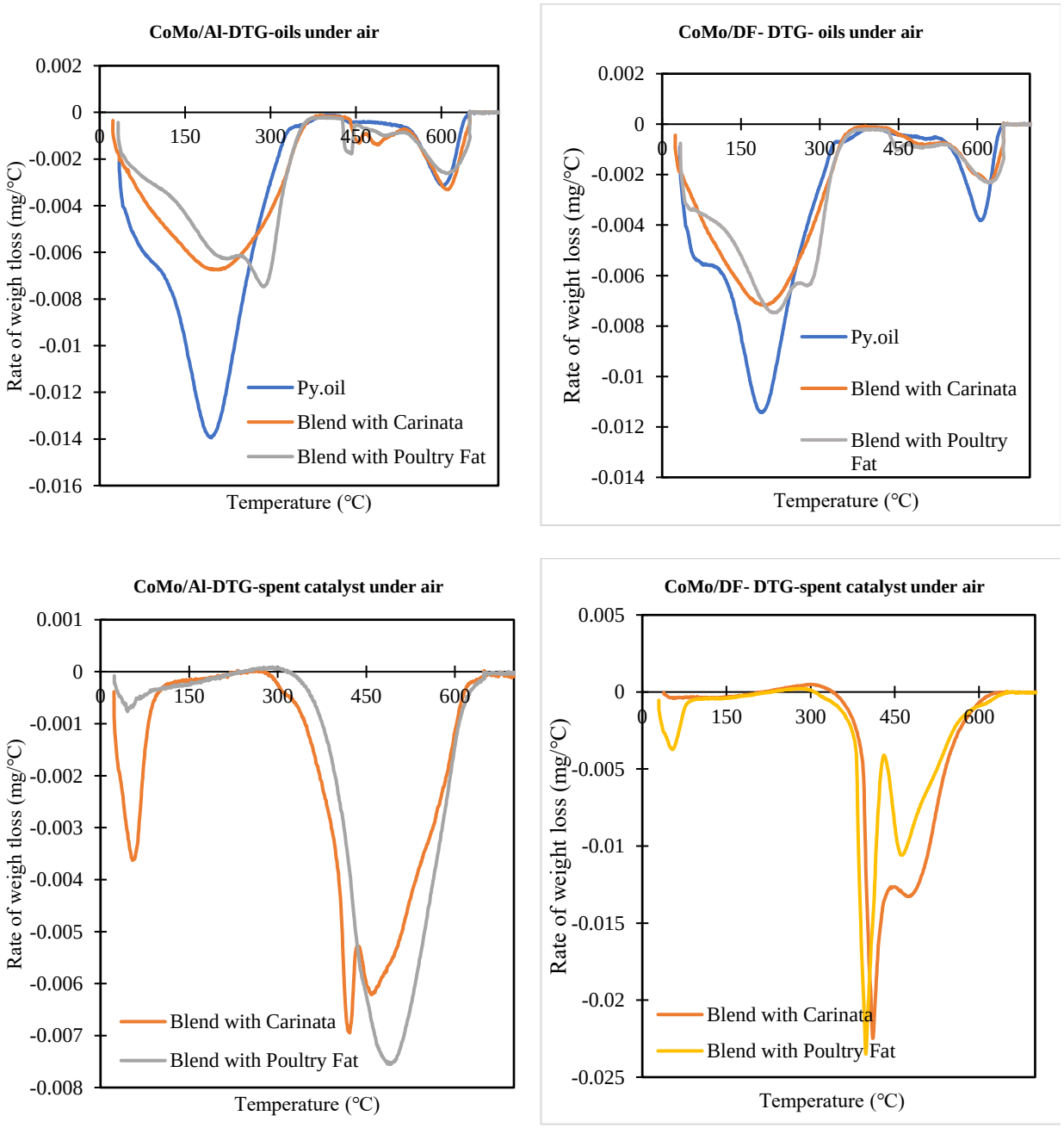

Figure 5.7 Oxidative stability and coke formation of the oils and spent catalysts.

5.4 Conclusion

In the present study unsulfided bimetallic (CoMo) catalysts on two supports (Douglas fir biochar support (DF) and alumina support (Al)) were used to hydrotreat a blend of Eucalyptus pyrolysis bio-oil with Carinata oil and poultry fat. Two types of catalysts were used: 1) Cobalt molybdenum supported on alumina. (denoted as CoMo/Al), and 2) Cobalt molybdenum supported on Douglas Fir biochar. (denoted as CoMo/DF). The main objective of this study was to understand the synergistic effect of the blending two different types of triglycerides (Carinata and poultry fat) with pyrolysis oil to understand the order of reactivity for different supports in terms of yield, HDO and coke formation. Overall, blended hydrotreated oil produced from biochar support showed better positive synergistic effect in terms of carbon and hydrogen addition, oxygen removal, HHV and viscosity. While alumina supported catalyst exhibited a higher liquid yield. Biochar supported catalysts demonstrated higher jet fuel fraction consisting of mainly of paraffins and lowest amount of light and heavy diesel. Oxygen was predominantly removed via dehydration for which the biochar support consumed higher amount of hydrogen. Alumina support removed oxygen predominantly via decarboxylation and decarbonylation reactions. Lower amount of coke formation was seen for biochar support. Abundance oxygen containing functional groups, inorganic mineral oxides, high surface area, pore structure and acid sites makes biochar support a better HDO catalyst compared to alumina support. On the other hand, blending the pyrolysis oil with poultry fat yielded better quality of bio-oil over Carinata oil and produced higher percentage of jet fuel fraction. This could be due to mass transfer limitations owing to presence of C18 fatty acids compared to C22 of Carinata oil. In summary, pyrolysis oil blended with poultry fat and hydrotreated using DF support catalysts was more effective in HDO activity and in improving overall bio-oil quality compared to alumina supported catalyst and Carinata oil.

5.5 References

[1] R. W. Jenkins, A. D. Sutton, and D. J. Robichaud, “Chapter 8 - Pyrolysis of Biomass for Aviation Fuel,” in *Biofuels for Aviation*, C. J. Chuck, Ed. Academic Press, 2016, pp. 191–215. doi: 10.1016/B978-0-12-804568-8.00008-1.

[2] Y. Han *et al.*, “Hydrotreatment of pyrolysis bio-oil: A review,” *Fuel Process. Technol.*, vol. 195, p. 106140, Dec. 2019, doi: 10.1016/j.fuproc.2019.106140.

[3] F. Stankovikj, A. G. McDonald, G. L. Helms, M. V. Olarte, and M. Garcia-Perez, “Characterization of the Water-Soluble Fraction of Woody Biomass Pyrolysis Oils,” *Energy Fuels*, vol. 31, no. 2, pp. 1650–1664, Feb. 2017, doi: 10.1021/acs.energyfuels.6b02950.

[4] N. Koike *et al.*, “Upgrading of pyrolysis bio-oil using nickel phosphide catalysts,” *J. Catal.*, vol. 333, pp. 115–126, Jan. 2016, doi: 10.1016/j.jcat.2015.10.022.

[5] S. Kadarwati *et al.*, “Polymerization and cracking during the hydrotreatment of bio-oil and heavy fractions obtained by fractional condensation using Ru/C and NiMo/Al2O3 catalyst,” *J. Anal. Appl. Pyrolysis*, vol. 118, pp. 136–143, Mar. 2016, doi: 10.1016/j.jaap.2016.01.011.

[6] T. N. Pham, D. Shi, and D. E. Resasco, “Evaluating strategies for catalytic upgrading of pyrolysis oil in liquid phase,” *Appl. Catal. B Environ.*, vol. 145, pp. 10–23, Feb. 2014, doi: 10.1016/j.apcatb.2013.01.002.

[7] F. Stankovikj, A. G. McDonald, G. L. Helms, and M. Garcia-Perez, “Quantification of Bio-Oil Functional Groups and Evidences of the Presence of Pyrolytic Humins,” *Energy Fuels*, vol. 30, no. 8, pp. 6505–6524, Aug. 2016, doi: 10.1021/acs.energyfuels.6b01242.

[8] F. Stankovikj and M. Garcia-Perez, “TG-FTIR Method for the Characterization of Bio-oils in Chemical Families,” *Energy Fuels*, vol. 31, no. 2, pp. 1689–1701, Feb. 2017, doi: 10.1021/acs.energyfuels.6b03132.

[9] F. Stankovikj, C.-C. Tran, S. Kaliaguine, M. V. Olarte, and M. Garcia-Perez, “Evolution of Functional Groups during Pyrolysis Oil Upgrading,” *Energy Fuels*, vol. 31, no. 8, pp. 8300–8316, Aug. 2017, doi: 10.1021/acs.energyfuels.7b01251.

[10] P. Lahijani, M. Mohammadi, A. R. Mohamed, F. Ismail, K. T. Lee, and G. Amini, “Upgrading biomass-derived pyrolysis bio-oil to bio-jet fuel through catalytic cracking and hydrodeoxygenation: A review of recent progress,” *Energy Convers. Manag.*, vol. 268, p. 115956, Sep. 2022, doi: 10.1016/j.enconman.2022.115956.

[11] M. Kousoulidou and L. Lonza, “Biofuels in aviation: Fuel demand and CO2 emissions evolution in Europe toward 2030,” *Transp. Res. Part Transp. Environ.*, vol. 46, pp. 166–181, Jul. 2016, doi: 10.1016/j.trd.2016.03.018.

[12] K. Onarheim, I. Hannula, and Y. Solantausta, “Hydrogen enhanced biofuels for transport via fast pyrolysis of biomass: A conceptual assessment,” *Energy*, vol. 199, p. 117337, May 2020, doi: 10.1016/j.energy.2020.117337.

[13] G. Bagnato, A. Sanna, E. Paone, and E. Catizzone, “Recent Catalytic Advances in Hydrotreatment Processes of Pyrolysis Bio-Oil,” *Catalysts*, vol. 11, no. 2, Art. no. 2, Feb. 2021, doi: 10.3390/catal11020157.

[14] D. C. Elliott and E. G. Baker, “Upgrading biomass liquefaction products through hydrodeoxygenation,” *Biotechnol Bioeng Symp U. S.*, vol. 16:14, Art. no. CONF-840509-, Jan. 1984, Accessed: Sep. 18, 2022. [Online]. Available: https://www.osti.gov/biblio/6457778

[15] D. C. Elliott and E. G. Baker, “Process for upgrading biomass pyrolyzates,” US4795841A, Jan. 03, 1989 Accessed: Sep. 18, 2022. [Online]. Available: https://patents.google.com/patent/US4795841A/en
[16] E. G. Baker and D. C. Elliott, “Catalytic Hydrotreating of Biomass-Derived Oils,” in *Pyrolysis Oils from Biomass*, vol. 376, 0 vols., American Chemical Society, 1988, pp. 228–240. doi: 10.1021/bk-1988-0376.ch021.
[17] J. Gagnon and S. Kaliaguine, “Catalytic hydrotreatment of vacuum pyrolysis oils from wood,” *Ind. Eng. Chem. Res.*, vol. 27, no. 10, pp. 1783–1788, Oct. 1988, doi: 10.1021/ie00082a008.
[18] H. Jahromi and F. A. Agblevor, “Upgrading of pinyon-juniper catalytic pyrolysis oil via hydrodeoxygenation,” *Energy*, vol. 141, pp. 2186–2195, Dec. 2017, doi: 10.1016/j.energy.2017.11.149.
[19] Y. Elkasabi, C. A. Mullen, A. L. M. T. Pighinelli, and A. A. Boateng, “Hydrodeoxygenation of fast-pyrolysis bio-oils from various feedstocks using carbon-supported catalysts,” *Fuel Process. Technol.*, vol. 123, pp. 11–18, Jul. 2014, doi: 10.1016/j.fuproc.2014.01.039.
[20] H. Pucher *et al.*, “Biofuels from liquid phase pyrolysis oil: a two-step hydrodeoxygenation (HDO) process,” *Green Chem.*, vol. 17, no. 2, pp. 1291–1298, Feb. 2015, doi: 10.1039/C4GC01741B.
[21] X. Zhang *et al.*, “Catalytic Upgrading of Bio-oil over Ni-Based Catalysts Supported on Mixed Oxides,” *Energy Fuels*, vol. 28, no. 4, pp. 2562–2570, Apr. 2014, doi: 10.1021/ef402421j.
[22] V. K. Venkatakrishnan, J. C. Degenstein, A. D. Smeltz, W. N. Delgass, R. Agrawal, and F. H. Ribeiro, “High-pressure fast-pyrolysis, fast-hydropyrolysis and catalytic hydrodeoxygenation of cellulose: production of liquid fuel from biomass,” *Green Chem.*, vol. 16, no. 2, pp. 792–802, Jan. 2014, doi: 10.1039/C3GC41558A.
[23] P. Roy *et al.*, “Understanding the effects of feedstock blending and catalyst support on hydrotreatment of algae HTL biocrude with non-edible vegetable oil,” *Energy Convers. Manag.*, vol. 268, p. 115998, Sep. 2022, doi: 10.1016/j.enconman.2022.115998.
[24] D. C. Elliott, H. Wang, R. French, S. Deutch, and K. Iisa, “Hydrocarbon Liquid Production from Biomass via Hot-Vapor-Filtered Fast Pyrolysis and Catalytic Hydroprocessing of the Bio-oil,” *Energy Fuels*, vol. 28, no. 9, pp. 5909–5917, Sep. 2014, doi: 10.1021/ef501536j.
[25] I. Yeboah, Y. Li, K. Rajendran, K. R. Rout, and D. Chen, “Tandem Hydrodeoxygenation Catalyst System for Hydrocarbons Production from Simulated Bio-oil: Effect of C–C Coupling Catalysts,” *Ind. Eng. Chem. Res.*, vol. 60, no. 5, pp. 2136–2143, Feb. 2021, doi: 10.1021/acs.iecr.1c00113.
[26] A. N. Kay Lup, F. Abnisa, W. M. A. W. Daud, and M. K. Aroua, “Synergistic interaction of metal–acid sites for phenol hydrodeoxygenation over bifunctional Ag/TiO2 nanocatalyst,” *Chin. J. Chem. Eng.*, vol. 27, no. 2, pp. 349–361, Feb. 2019, doi: 10.1016/j.cjche.2018.08.028.
[27] M. Rubeš, J. He, P. Nachtigall, and O. Bludský, “Direct hydrodeoxygenation of phenol over carbon-supported Ru catalysts: A computational study,” *J. Mol. Catal. Chem.*, vol. 423, pp. 300–307, Nov. 2016, doi: 10.1016/j.molcata.2016.07.007.
[28] P. T. M. Do, A. J. Foster, J. Chen, and R. F. Lobo, “Bimetallic effects in the hydrodeoxygenation of meta-cresol on γ-Al2O3 supported Pt–Ni and Pt–Co catalysts,” *Green Chem.*, vol. 14, no. 5, pp. 1388–1397, May 2012, doi: 10.1039/C2GC16544A.

[29] D. M. Alonso, J. Q. Bond, and J. A. Dumesic, “Catalytic conversion of biomass to biofuels,” *Green Chem.*, vol. 12, no. 9, pp. 1493–1513, Sep. 2010, doi: 10.1039/C004654J.
[30] M. Benés, R. Bilbao, J. M. Santos, J. Alves Melo, A. Wisniewski, and I. Fonts, “Hydrodeoxygenation of Lignocellulosic Fast Pyrolysis Bio-Oil: Characterization of the Products and Effect of the Catalyst Loading Ratio,” *Energy Fuels*, vol. 33, no. 5, pp. 4272–4286, May 2019, doi: 10.1021/acs.energyfuels.9b00265.
[31] R. L. Ware *et al.*, “Tracking Elemental Composition through Hydrotreatment of an Upgraded Pyrolysis Oil Blended with a Light Gas Oil,” *Energy Fuels*, vol. 34, no. 12, pp. 16181–16186, Dec. 2020, doi: 10.1021/acs.energyfuels.0c02437.
[32] A. H. Zacher, M. V. Olarte, D. M. Santosa, D. C. Elliott, and S. B. Jones, “A review and perspective of recent bio-oil hydrotreating research,” *Green Chem.*, vol. 16, no. 2, pp. 491–515, 2014, doi: 10.1039/C3GC41382A.
[33] W. Jin, L. Pastor-Pérez, D. Shen, A. Sepúlveda-Escribano, S. Gu, and T. Ramirez Reina, “Catalytic Upgrading of Biomass Model Compounds: Novel Approaches and Lessons Learnt from Traditional Hydrodeoxygenation – a Review,” *ChemCatChem*, vol. 11, no. 3, pp. 924–960, 2019, doi: 10.1002/cctc.201801722.
[34] D. C. Elliott *et al.*, “Catalytic Hydroprocessing of Fast Pyrolysis Bio-oil from Pine Sawdust,” *Energy Fuels*, vol. 26, no. 6, pp. 3891–3896, Jun. 2012, doi: 10.1021/ef3004587.
[35] D. C. Elliott and T. R. Hart, “Catalytic Hydroprocessing of Chemical Models for Bio-oil,” *Energy Fuels*, vol. 23, no. 2, pp. 631–637, Feb. 2009, doi: 10.1021/ef8007773.
[36] D. C. Elliott, “Historical Developments in Hydroprocessing Bio-oils,” *Energy Fuels*, vol. 21, no. 3, pp. 1792–1815, May 2007, doi: 10.1021/ef070044u.
[37] D. C. Elliott, “Biofuel from fast pyrolysis and catalytic hydrodeoxygenation,” *Curr. Opin. Chem. Eng.*, vol. 9, pp. 59–65, Aug. 2015, doi: 10.1016/j.coche.2015.08.008.
[38] D. C. Elliott, D. Beckman, A. V. Bridgwater, J. P. Diebold, S. B. Gevert, and Y. Solantausta, “Developments in direct thermochemical liquefaction of biomass: 1983-1990,” *Energy Fuels*, vol. 5, no. 3, pp. 399–410, May 1991, doi: 10.1021/ef00027a008.
[39] D. C. Elliott and E. G. Baker, “Biomass liquefaction product analysis and upgrading,” Pacific Northwest Lab., Richland, WA (USA), PNL-SA-11807; CONF-8309194-1, Sep. 1983. Accessed: Sep. 18, 2022. [Online]. Available: https://www.osti.gov/biblio/5427343
[40] D. C. Elliott, S.-J. Lee, and T. R. Hart, “Stabilization of Fast Pyrolysis Oil: Post Processing Final Report,” Pacific Northwest National Lab. (PNNL), Richland, WA (United States), PNNL-21549, Mar. 2012. doi: 10.2172/1047417.
[41] X. Han, H. Wang, Y. Zeng, and J. Liu, “Advancing the application of bio-oils by co-processing with petroleum intermediates: A review,” *Energy Convers. Manag. X*, vol. 10, p. 100069, Jun. 2021, doi: 10.1016/j.ecmx.2020.100069.
[42] S. Hansen, A. Mirkouei, and L. A. Diaz, “A comprehensive state-of-technology review for upgrading bio-oil to renewable or blended hydrocarbon fuels,” *Renew. Sustain. Energy Rev.*, vol. 118, p. 109548, Feb. 2020, doi: 10.1016/j.rser.2019.109548.
[43] A. Dimitriadis *et al.*, “Evaluation of a Hydrotreated Vegetable Oil (HVO) and Effects on Emissions of a Passenger Car Diesel Engine,” *Front. Mech. Eng.*, vol. 4, p. 7, 2018, doi: 10.3389/fmech.2018.00007.
[44] M. Pearlson, C. Wollersheim, and J. Hileman, “A techno-economic review of hydroprocessed renewable esters and fatty acids for jet fuel production,” *Biofuels Bioprod. Biorefining*, vol. 7, no. 1, pp. 89–96, 2013, doi: 10.1002/bbb.1378.

[45] Y. Han, A. P. P. Pires, and M. Garcia-Perez, "Co-hydrotreatment of the Bio-oil Lignin-Rich Fraction and Vegetable Oil," *Energy Fuels*, vol. 34, no. 1, pp. 516–529, Jan. 2020, doi: 10.1021/acs.energyfuels.9b03344.
[46] G. Seber, R. Malina, M. N. Pearlson, H. Olcay, J. I. Hileman, and S. R. H. Barrett, "Environmental and economic assessment of producing hydroprocessed jet and diesel fuel from waste oils and tallow," *Biomass Bioenergy*, vol. 67, pp. 108–118, Aug. 2014, doi: 10.1016/j.biombioe.2014.04.024.
[47] Y. Han, F. Stankovikj, and M. Garcia-Perez, "Co-hydrotreatment of tire pyrolysis oil and vegetable oil for the production of transportation fuels," *Fuel Process. Technol.*, vol. 159, pp. 328–339, May 2017, doi: 10.1016/j.fuproc.2017.01.048.
[48] X. Zhao, L. Wei, J. Julson, Q. Qiao, A. Dubey, and G. Anderson, "Catalytic cracking of non-edible sunflower oil over ZSM-5 for hydrocarbon bio-jet fuel," *New Biotechnol.*, vol. 32, no. 2, pp. 300–312, Mar. 2015, doi: 10.1016/j.nbt.2015.01.004.
[49] I. Kubičková, M. Snåre, K. Eränen, P. Mäki-Arvela, and D. Yu. Murzin, "Hydrocarbons for diesel fuel via decarboxylation of vegetable oils," *Catal. Today*, vol. 106, no. 1, pp. 197–200, Oct. 2005, doi: 10.1016/j.cattod.2005.07.188.
[50] J. Charles U. Pittman *et al.*, "Characterization of Bio-oils Produced from Fast Pyrolysis of Corn Stalks in an Auger Reactor," *ACS Publications*, May 14, 2012. https://pubs.acs.org/doi/pdf/10.1021/ef3003922 (accessed Oct. 09, 2022).
[51] P. Roy *et al.*, "Performance of biochar assisted catalysts during hydroprocessing of non-edible vegetable oil: Effect of transition metal source on catalytic activity," *Energy Convers. Manag.*, vol. 252, p. 115131, Jan. 2022, doi: 10.1016/j.enconman.2021.115131.
[52] H. Jahromi *et al.*, "Production of green transportation fuels from Brassica carinata oil: A comparative study of noble and transition metal catalysts," *Fuel Process. Technol.*, vol. 215, p. 106737, May 2021, doi: 10.1016/j.fuproc.2021.106737.
[53] H. Ojagh, "Hydrodeoxygenation (HDO) catalysts Characterization, reaction and deactivation studies," *undefined*, 2018, Accessed: Feb. 17, 2022. [Online]. Available: https://www.semanticscholar.org/paper/Hydrodeoxygenation-(HDO)-catalysts-reaction-and-Ojagh/1c76ecaa02b38e61557f0cd1992d8a0968fce946
[54] J.-S. Choi *et al.*, "Alumina-supported cobalt–molybdenum sulfide modified by tin via surface organometallic chemistry: application to the simultaneous hydrodesulfurization of thiophenic compounds and the hydrogenation of olefins," *Appl. Catal. Gen.*, vol. 267, no. 1, pp. 203–216, Jul. 2004, doi: 10.1016/j.apcata.2004.03.005.
[55] J. H. Scofield, "Hartree-Slater subshell photoionization cross-sections at 1254 and 1487 eV," *J. Electron Spectrosc. Relat. Phenom.*, vol. 8, no. 2, pp. 129–137, Jan. 1976, doi: 10.1016/0368-2048(76)80015-1.
[56] M. Smith, L. Scudiero, J. Espinal, J.-S. McEwen, and M. Garcia-Perez, "Improving the deconvolution and interpretation of XPS spectra from chars by ab initio calculations," *Carbon*, vol. 110, pp. 155–171, Dec. 2016, doi: 10.1016/j.carbon.2016.09.012.
[57] L. Sharma, X. Jiang, Z. Wu, J. Baltrus, S. Rangarajan, and J. Baltrusaitis, "Elucidating the origin of selective dehydrogenation of propane on γ-alumina under H2S treatment and co-feed," *J. Catal.*, vol. 394, pp. 142–156, Feb. 2021, doi: 10.1016/j.jcat.2020.12.018.
[58] N. Fairley *et al.*, "Systematic and collaborative approach to problem solving using X-ray photoelectron spectroscopy," *Appl. Surf. Sci. Adv.*, vol. 5, p. 100112, Sep. 2021, doi: 10.1016/j.apsadv.2021.100112.

[59] P. Wang *et al.*, “Sorption and recovery of phenolic compounds from aqueous phase from sewage sludge hydrothermal liquefaction using bio-char,” *Chemosphere*, p. 131934, Aug. 2021, doi: 10.1016/j.chemosphere.2021.131934.
[60] P. Wang *et al.*, “Enhancement of biogas production from wastewater sludge via anaerobic digestion assisted with biochar amendment,” *Bioresour. Technol.*, vol. 309, p. 123368, Aug. 2020, doi: 10.1016/j.biortech.2020.123368.
[61] M. C. Biesinger, B. P. Payne, A. P. Grosvenor, L. W. M. Lau, A. R. Gerson, and R. St. C. Smart, “Resolving surface chemical states in XPS analysis of first row transition metals, oxides and hydroxides: Cr, Mn, Fe, Co and Ni,” *Appl. Surf. Sci.*, vol. 257, no. 7, pp. 2717–2730, Jan. 2011, doi: 10.1016/j.apsusc.2010.10.051.
[62] J. Baltrusaitis *et al.*, “Generalized molybdenum oxide surface chemical state XPS determination via informed amorphous sample model,” *Appl. Surf. Sci.*, vol. 326, pp. 151–161, Jan. 2015, doi: 10.1016/j.apsusc.2014.11.077.
[63] T. Cordero-Lanzac, J. Rodríguez-Mirasol, T. Cordero, and J. Bilbao, “Advances and Challenges in the Valorization of Bio-Oil: Hydrodeoxygenation Using Carbon-Supported Catalysts,” *Energy Fuels*, vol. 35, no. 21, pp. 17008–17031, Nov. 2021, doi: 10.1021/acs.energyfuels.1c01700.
[64] M. Snåre, I. Kubičková, P. Mäki-Arvela, K. Eränen, and D. Yu. Murzin, “Heterogeneous Catalytic Deoxygenation of Stearic Acid for Production of Biodiesel,” *Ind. Eng. Chem. Res.*, vol. 45, no. 16, pp. 5708–5715, Aug. 2006, doi: 10.1021/ie060334i.
[65] G. de la Puente, A. Gil, J. J. Pis, and P. Grange, “Effects of Support Surface Chemistry in Hydrodeoxygenation Reactions over CoMo/Activated Carbon Sulfided Catalysts,” *Langmuir*, vol. 15, no. 18, pp. 5800–5806, Aug. 1999, doi: 10.1021/la981225e.
[66] M. Ouadi, M. A. Bashir, L. G. Speranza, H. Jahangiri, and A. Hornung, “Food and Market Waste–A Pathway to Sustainable Fuels and Waste Valorization,” *Energy Fuels*, vol. 33, no. 10, pp. 9843–9850, Oct. 2019, doi: 10.1021/acs.energyfuels.9b01650.
[67] M. Hervy *et al.*, “Reactivity and deactivation mechanisms of pyrolysis chars from bio-waste during catalytic cracking of tar,” *Appl. Energy*, vol. 237, pp. 487–499, Mar. 2019, doi: 10.1016/j.apenergy.2019.01.021.
[68] N. Wang, D. Chen, U. Arena, and P. He, “Hot char-catalytic reforming of volatiles from MSW pyrolysis,” *Appl. Energy*, vol. 191, pp. 111–124, Apr. 2017, doi: 10.1016/j.apenergy.2017.01.051.
[69] M. J. Polovina, B. M. Babić, B. Kaluđerović, and A. Dekanski, “Surface characterization of oxidized activated carbon cloth,” *Carbon*, vol. 35, no. 8, pp. 1047–1052, 1997, doi: 10.1016/S0008-6223(97)00057-2.
[70] J. Lee, K.-H. Kim, and E. E. Kwon, “Biochar as a Catalyst,” *Renew. Sustain. Energy Rev.*, vol. 77, pp. 70–79, Sep. 2017, doi: 10.1016/j.rser.2017.04.002.
[71] Y. Shen and K. Yoshikawa, “Tar Conversion and Vapor Upgrading via in Situ Catalysis Using Silica-Based Nickel Nanoparticles Embedded in Rice Husk Char for Biomass Pyrolysis/Gasification,” *Ind. Eng. Chem. Res.*, vol. 53, no. 27, pp. 10929–10942, Jul. 2014, doi: 10.1021/ie501843y.
[72] S. Wang, H. Li, and M. Wu, “Advances in metal/ biochar catalysts for biomass hydro-upgrading: A review,” *J. Clean. Prod.*, vol. 303, p. 126825, Jun. 2021, doi: 10.1016/j.jclepro.2021.126825.

[73] M. Hervy *et al.*, “Catalytic cracking of ethylbenzene as tar surrogate using pyrolysis chars from wastes,” *Biomass Bioenergy*, vol. 117, pp. 86–95, Oct. 2018, doi: 10.1016/j.biombioe.2018.07.020.
[74] Y. Lin, C. Zhang, M. Zhang, and J. Zhang, “Deoxygenation of Bio-oil during Pyrolysis of Biomass in the Presence of CaO in a Fluidized-Bed Reactor,” *Energy Fuels*, vol. 24, no. 10, pp. 5686–5695, Oct. 2010, doi: 10.1021/ef1009605.
[75] D. Yao *et al.*, “Hydrogen production from biomass gasification using biochar as a catalyst/support,” *Bioresour. Technol.*, vol. 216, pp. 159–164, Sep. 2016, doi: 10.1016/j.biortech.2016.05.011.
[76] X. Xiong, I. K. M. Yu, L. Cao, D. C. W. Tsang, S. Zhang, and Y. S. Ok, “A review of biochar-based catalysts for chemical synthesis, biofuel production, and pollution control,” *Bioresour. Technol.*, vol. 246, pp. 254–270, Dec. 2017, doi: 10.1016/j.biortech.2017.06.163.
[77] Z. Gao, L. Yang, G. Fan, and F. Li, “Promotional Role of Surface Defects on Carbon-Supported Ruthenium-Based Catalysts in the Transfer Hydrogenation of Furfural,” *ChemCatChem*, vol. 8, no. 24, pp. 3769–3779, 2016, doi: 10.1002/cctc.201601070.
[78] Z. Tang *et al.*, “Co-pyrolysis of microalgae with low-density polyethylene (LDPE) for deoxygenation and denitrification,” *Bioresour. Technol.*, vol. 311, p. 123502, Sep. 2020, doi: 10.1016/j.biortech.2020.123502.
[79] X. Tang, L. Hu, Y. Sun, G. Zhao, W. Hao, and L. Lin, “Conversion of biomass-derived ethyl levulinate into γ-valerolactone via hydrogen transfer from supercritical ethanol over a ZrO2 catalyst,” *RSC Adv.*, vol. 3, no. 26, pp. 10277–10284, Jun. 2013, doi: 10.1039/C3RA41288A.
[80] B. Cai, X.-C. Zhou, Y.-C. Miao, J.-Y. Luo, H. Pan, and Y.-B. Huang, “Enhanced Catalytic Transfer Hydrogenation of Ethyl Levulinate to γ-Valerolactone over a Robust Cu–Ni Bimetallic Catalyst,” *ACS Sustain. Chem. Eng.*, vol. 5, no. 2, pp. 1322–1331, Feb. 2017, doi: 10.1021/acssuschemeng.6b01677.
[81] F. Toldrá-Reig, L. Mora, and F. Toldrá, “Trends in Biodiesel Production from Animal Fat Waste,” *Appl. Sci.*, vol. 10, no. 10, Art. no. 10, Jan. 2020, doi: 10.3390/app10103644.
[82] E. Kordouli *et al.*, “HDO activity of carbon-supported Rh, Ni and Mo-Ni catalysts,” *Mol. Catal.*, vol. 441, pp. 209–220, Nov. 2017, doi: 10.1016/j.mcat.2017.08.013.

CHAPTER

6 HYDROCARBON BIOLUBRICANTS FROM HYDROTREATED RENEWABLE AND WASTE DERIVED LIQUID INTERMEDIATES

Abstract

There is a need to support the biofuel sector not only by utilizing waste materials for its production but also by finding uses of co-products through an integrated approach. Due to bio-oil's diverse composition, other applications of it are emerging such as foams, resins and most importantly as biolubricants, a product with an increasing global demand. In this study, four hydrocarbon biolubricants (HBL) were produced via a hydrotreatment process. Two samples were produced using hydrothermal liquefaction (HTL) of algae (HAL) and sewage sludge (HSS) whereas the other two samples were from nonedible oil (carinata; HCA) and animal fat (poultry fat; HPF) were evaluated for their tribological properties and compared with mineral base oil (MBO). These potential biolubricants samples had viscosity indices (VI) ranging from 197 to 254, pour points (PP) from -10℃ to -20℃, Noack volatilities between 16% to 23%. The coefficient of frictions (COF) for HAL and HSS were lower than MBO, HPF, HCA but the wear was higher. Large amounts of oxygenates and olefins imparted higher VI and PP to HPF. Even though both HSS and HAL demonstrated higher amounts of paraffin it exhibited lower thermo-oxidative stability, poor pour point, higher volatility compared to other samples. In the case of HAL and HSS, the aromatics could have comparatively played a bigger role in determining the lubricating properties than the paraffin alone. HPF had the lowest wear, highest VI and PP but higher COF. While volatility and COF were predominantly dependent on the cyclic structures, unsaturation, and heteroatoms. The results indicated that the hydrotreated bio-oil produced from HTL biocrude and waste precursors can be considered as eco-friendly hydrocarbon biolubricants blend stock.

Keywords: *Biolubricants; Bio oil; Hydrocarbon biolubricants; Hydrotreatment; Tribology; Friction.*

6.1 Introduction

As the world becomes ever-more wary of the impacts of climate change, the onus is on us, as an ingenious and adaptive species, to find solutions and strategies to bring the global carbon dioxide (CO_2) emissions (energy related) to net zero by 2050 and limit the global temperature rise to 1.5℃ [1], [2]. One of the approaches for carbon neutrality is a biorefinery concept that allows efficient production of renewable fuels along with value-added bioproducts. Even after 20 years of development, the biofuel cost is higher than fossil fuel which has slowed down commercialization [3]. This is due to challenges such as diverse feedstock, handling issues, conversion strategies, and upgrading processes among others [4]. Therefore, there is a need to permanently support the biofuel sector not only by utilizing waste materials and but also by utilization of co-products which can be obtained in an integrated approach [5], [6]. Due to its diverse composition, other applications of bio-oil are emerging such as foams, resins and most importantly as biolubricants. The latter application highlights the ability of bio-oil as a source of value-added bioproducts [6]–[8].

Lubricants are either liquid, semi-solid (e.g. grease) or solid (e.g. polytetrafluoroethylene) substances used to reduce friction between contacting surfaces and decrease wear [9]. The main functions of lubricants are (a) controlling friction and wear, (b) cleaning contact, and (c) cooling the contact [10]. Different lubricants have different physiochemical properties that influence performance for a wide range of applications such as metal working and transmission fluids, engine, motors. Most common physicochemical properties are as follows (a) general properties: viscosity index (VI), total acid number (TAN); (b) cold flow properties (CFP): cloud point (CP)

and pour point (PP); (c) high temperature properties: flash point and volatility; (d) stability: thermo-oxidative and hydrolytic stability; (e) performance properties: anti-wear, lubricity, foam and rust prevention; and (f) environmental metrics: biodegradability and eco-toxicity [9].

Lubricants are made of 90% base oil and 10% additives. Conventional lubricant's base oils are composed of esters, hydrogenated, polyolefins, silicones, and fluorocarbons [10], [11]. Esters, and mixture of natural and synthetic esters have gained commercial success as base oils for biolubricants. There are several pathways to produce biolubricants from vegetable oil that are either esters or a hydrocarbon-based lubricant (HBL). There are currently two main routes to produce hydrocarbon based biolubricants; 1) hydrotreatment (HYD) and 2) electrochemical decarboxylation via Kolbe electrolysis but it is not technologically developed. On the other hand, HYD process is a hydrogen intensive process, requires high temperatures and waste feedstocks that make the catalyst more prone to poisoning. Ester groups are more prone to hydrolytic attack and highly polar ester groups cannot be used in certain seals, additives and non-polar base oils [9], [12], [13]. Fatty acid methyl esters (FAME) are commercially more successful than HBL but they cannot be used in various applications due to poor OS and CFP [14], [15]. Therefore, HYD is necessary to improve the OS, CFP, hydrolytic stability but it is not as commonly used in the market as synthetic esters and FAMEs. This could be due to fact that HYD is mostly used in petroleum refineries to produce fuel, and the overall process is expensive due to the use of hydrogen at high temperatures and pressure.

Among potential co-products of the biofuel industry, biolubricants have an increasing demand and provide substantial value. Therefore, this paper will focus on hydrocarbon based biolubricants (HBL) produced by HYD process. Details of synthetic esters and fatty acids for biolubricants applications can be found elsewhere [9]. The most common method to produce HBL

is by HYD, the conventional process which is used in petroleum refineries. HYD comprises of hydrodeoxygenation, decarbonylation and decarboxylation processes with sulfided Ni-Mo and Co-Mo catalysts at high pressure (50 bar) and temperatures (450℃) with CO_2, CO, propane, and water as byproducts. Complete or partial hydrogenation/hydrotreatment processes are used to produce HBL and it is done mainly to improve the OS of the oil. This lubricant is used in engine and hydraulic oils, greases, metal working and transmission fluids [9]. HBL requires low temperatures compared to traditional hydrotreatment process since high temperatures tend to create trans isomers from hydrogenation of fatty acids which increase the melting points and impart reduced cold flow properties [9].

Apart from the process, the chemical structure of the lubricant dictates its physical properties. It is well reviewed in the literature [9], [16]–[19]. The most important ones are the molecular weight, degree of unsaturation, branching, linearity structure and functional groups. Branching reduces PP without affecting the molecular weight. Increasing molecular weight increases VI, and flash point but decreases CFP. Unsaturation causes lower OS, thus HYD is necessary to convert polyunsaturated moieties to monounsaturated ones, but excessive saturation can decrease the CFP. But Ho et al., [9] reported that commercial isoalkane BL achieved PP of -81℃ in spite of being fully saturated.

Approximately 80-90% of conventional lubricants are fossil fuel based mineral oil and it raises concern due to global warming associated to extraction, spills, biodegradability and ecotoxicity [16], [20]. Biolubricants are better alternatives to mineral oils, and it generally exhibits superior lubricity, VI, and CFP. Owing to the long chain fatty acids and polar groups from vegetable oils, excellent tribological properties can be obtained from biolubricants [21]–[26]. However , vegetable oils have poor hydrolytic stability and thermal stability compared to mineral

oils [10], [11] owing to unsaturation and the presence of β-CH groups in its glycerol backbone which is reactive to oxygen and ultimately leads to the conversion of C=C bonds to oxidation products such as carboxylic and epoxide.[5], [27]–[30].

Apart from hydrolytic stability, the large-scale production of biolubricants from vegetable oils may bring global imbalance to the food supply and demand market [31]. Nearly 66% of fuel energy is lost to the surroundings because of the thermal, frictional, and transmission loss. Therefore, there is a need to design sustainable BL to enhance fuel efficiency. More than 1% savings in GDP can be attained by applying better lubricants in transportation, manufacturing, and power generation sectors. Waste-based bioproducts such as biofuel and biolubricants could be a key driver for the energy transition. Lubricant production from municipal sludge, animal waste, and quick growing marine algae could be a game changer for energy transition. In 2019, 4.75 million metric ton of municipal sewage sludge were generated in the USA and only 51% was applied as a manure and the rest was disposed via landfilling (22%), incineration (16%) and other management practices (10%) [32]. Another most common waste is the chicken fat/skin which is generated from poultry sector which accounts for more than 80% of all livestock production in the world [33]. These are not removed during chicken meat processing and is not used in the food industry. Presently, rendering is the major waste valorization pathway for poultry processing byproducts such as meat, feather, blood meal and skin fats [34]. Apart from land pollution, waterways cause terrible algal blooms that are damaging the commercial fisheries, tourism, recreation and most importantly the marine life and water supply. It is estimated that more than $1B and $6.5B annual costs are incurred by harmful algal blooms for the marine and freshwater systems respectively. Studies have shown that biocrude can be produced by utilizing sewage sludge, chicken fat and algae and subsequent upgradation by hydrotreatment must be used to

produce biofuel and other value-added products such as biolubricants from biocrude [4], [32], [35]–[38]. Apart from the waste resources as discussed above we have also used non-edible vegetable oil feedstock (Carinata) for one of our BL feedstocks. Several studies and decades-long research have established carinata oil for its potential as biodiesel, green diesel, chemicals even recently as an aviation drop-in-fuel [3], [39]–[41].

There are numerous thermochemical pathways to produce biocrude, but HTL is the most promising way since it eliminates the need to dry the feedstock as the water at supercritical conditions acts as a non-polar solvent for organics [42]. Bio crude produced from HTL is highly viscous and is not suitable for direct usage as BL base oil owing to high oxygen content, high moisture content, high acidity and viscosity which usually arises from the nitrogenated and oxygenated monomeric, dimeric, and oligomeric compounds [23], [26], [43]. Therefore, upgrading of biocrude via catalytic hydrogenation and cracking, esterification and emulsification are usually carried out to remove undesirable compounds from bio-oil and tune its properties towards base oils [32], [44], [45]. Only a handful of publications have reported using bio-oil as a bio-lubricant. A study by [46] reported that partial hydrogenation of palm oil using Pd/γ-Al_2O_3 as catalyst produces wax. If however, they were able to increase the oxidative stability of the oil from 13.8h to 22.8 h without producing wax by using optimal reaction conditions. The study by [47] has evaluated bio-oil produced from different strains of HTL algae followed by catalytic esterification. The authors reported excellent tribological behaviors of the esterified oils and were good replacement for vegetable oil BLs. Previous study by [26] reported that bio-oils produced using poultry litter, pine, and algae from fast pyrolysis, HTL and tar from gasification processes exhibited impressive COF and wear and tear properties when used as BLs. However, the produced

BLs had high oxygen, moisture, acid number and low viscosity which limits its intended use, and it requires further hydrotreatment.

The key challenges involved is the lack of understanding of physicochemical, thermophysical, and tribological properties of BL if they are produced by utilizing waste and renewable resources such as municipal sewage sludge, poultry waste, algae, and non-edible oil. An integrated bio-refinery system is economically more feasible than just waste/biomass resources to fuels. Therefore, in this study biocrude produced from HTL from various waste resources such as sewage sludge, poultry fat, algae, and non-edible vegetable oil were hydrotreated. These hydrotreated oils are then compared with commercial mineral base oil. The aim of this work was twofold: (1) evaluate the feasibility of waste derived hydrotreated bio-oils as hydrocarbon based biolubricants, and (2) investigate the tribological behaviors of the upgraded bio-oils. The obtained results can provide a useful insight into application of hydrotreated bio-oils as HBLs and hope this study can help to fill the research gap in the exploration of hydrotreated bio-oils as biolubricants blend stock.

6.2 Material and Methods

6.2.1 Materials

Cobalt (II, III) oxide (~3.4 – 4.5% CoO, ~11.5 - 14.5% MoO; 2.5mm trilobe extrudate) on alumina was purchased from Sigma–Aldrich (St. Louis, Missouri, USA). The as-received extrudates were ground (ranging between 106 µm and 38 µm) and used as alumina-supported catalysts. H_2 gas (99.99 mol.%) was purchased from Airgas Inc. (Opelika, Alabama, USA). Steel disks (1018) having 2.75-inch diameter, 0.260-inch thickness with 0.5 µm average roughness were purchased from Davis Machine Works (Opelika, Alabama, USA). High carbon chrome steel balls of 10 mm diameter (49AE77) were obtained from McMasterCarr (Illinois, USA). *Tetraselmis*

algae was purchased from Reed Mariculture (Campbell, California, USA) whereas carinata oil was obtained through Applied Research Associates, Inc. (Albuquerque, New Mexico, US , provided by Agrisoma Biosciences, Inc, Gatineau, Quebec, Canada), respectively. Detailed fatty acid profile and physical properties of algae and carinata can be found in our previous studies [3], [4]. Municipal sewage sludge was collected, after the belt-filter press, from a local wastewater treatment facility (H.C. Morgan Water Pollution Control Facility, Auburn, Alabama, USA) and detailed information is provided elsewhere [32]. Poultry fat was obtained from Poultry Science Department (Auburn University, AL, USA). Lastly, mineral base oil was obtained from Petro-Canada Lubricants Inc. (Ontario, Canada).

6.2.2 Catalyst Preparation

Ground as-received commercial cobalt molybdenum supported on alumina was reduced at 400℃ for 4h under 10% H_2 and 90% N_2 gas and the samples were cooled down to room temperature by passing N_2 gas and stored for further use. This catalyst was denoted as CoMo/Al.

6.2.3 HTL Experiments

The HTL experiments were performed at a reaction temperature of 275 °C and a residence time of 60 min to obtain HTL algae and sewage sludge biocrude. For each HTL experiment, 600 g as-received *Tetraselmis* algae and sewage sludge was used, and the experiment was carried under nitrogen atmosphere. Details about the HTL reactor and procedure are given in our previous study [32].

6.2.4 Hydrotreatment Experiments

Hydrotreatment (HYD) tests were carried out in a 100 mL Parr 4598 bench top reactor. Carinata oil, poultry fat, HTL biocrudes such as algae and sewage sludge were hydrotreated at 400℃ for 5 h with 1000 psi of hydrogen (cold pressure/starting pressure) using a feed-to-catalyst

mass ratio of 70:1 (35 g oil and 0.5 g of catalyst). These reaction parameters were identical to our previous studies [3], [4], [48]. Since the motivation of the current study was to understand the tribological properties of hydrotreated oils, the study was not focused on determining the role of process parameters such as temperature, time, hydrogen gas pressure, and catalyst to oil ratio. All the hydroprocessing experiments were conducted in duplicates. The hydrotreated oils produced from HTL algae biocrude, HTL sewage sludge biocrude, carinata oil and poultry fat are denoted as HAL, HSS, HCA and HPF, respectively.

6.2.5 Analysis of Products

For mass-balance purpose, the liquid and solid reaction products were weighed. The liquid products along with the solid products were centrifuged. Details about hydrogen consumption, liquid yield, and solid yield calculations are explained elsewhere [3], [48]. Detailed procedure and instrument specifications for GC–MS, total acid number (TAN), and elemental analysis (CHNS-O) can be found in our previous studies [3], [48], [49]. The kinematic viscosities at 40°C and 100 °C (KV40 and KV100), and the viscosity index (VI) of the samples were measured using a viscometer (SVM 3001, Anton Paar, Austria). The VI was determined according to ASTM D2270, while KV40 and KV100 were determined according to ASTM D445 [49]. The thermal and oxidative stability of the produced BL and MBO were e evaluated using a Shimadzu TGA50 (Shimadzu, Japan) under nitrogen and air atmosphere with a heating rate of 10°C/min from room temperature up to 700°C. Noack volatility studies of synthesized biolubricants was carried out according to ASTM D6375 using a thermogravimetric method on the same Shimadzu TGA-50 (Shimadzu, Japan) [49]. At first, approximately, 45±3 mg of oil was heated at 235°C at a rate of 50°C/min (no hold time). Next, it was heated to 250°C (5°C/min) with a hold time of 60 min [49].

The evaporative loss (%) was determined by calculating the weight difference at the beginning to the amount of oil left after holding it for 60 min at 250℃.

DSC experiments were performed using DSC instrument (model Q200-1014) for pour point analysis. A sample of approximately 7-10 mg was placed in an aluminum pan beside an empty pan (reference pan) in the DSC module. The procedure involved rapidly heating the sample to 50℃ from room temperature and holding it at an isothermal condition for 10 min to help in homogenizing and dissolve any waxy material present in the oil. Then the sample was cooled to -30℃ at a rate of 5℃/min (1 min hold time). Furthermore, the same sample was heated from -30℃ to 50℃ at a steady rate of 5℃/min [50]. DSC is capable of providing direct measurement of variation in enthalpy for the oil undergoing physical and chemical change during heating and cooling period [50]–[53]. During the cooling cycle, the DCS thermograms showed a single broad exothermic peak. This peak was associated with the change in phase from liquid to solid phase. This phase change signified that the sample underwent crystallization and released more amount of heat energy. DSC offers a quick and easy way to determine PP and it requires less amount of oil compared to the conventional method [50], [54].

6.2.6 Tribological Tests

Firstly, the hydrotreated oils were filtered using a 0.2 μm filter to remove char particles prior to conducting the tribological tests. To evaluate the coefficient of friction (COF), a ball on a disk tribometer (Bruker/CETR UMT-3) was employed. 1018 steel disks (2.75-inch diameter, 0.260-inch thickness) having 0.5 μm average roughness were used for the tests. 52100 high carbon steel balls (10 mm) were used as a counterface [26]. Approximately 2ml of hydrotreated oil was spread on the surface of the rotating disk (63.7 rev/min), while a load of 50 N was applied on it for 30 min [26]. The COF value was obtained directly from the machine and each test was

conducted three times. The wear grooves formed on the steel disks after the COF tests, were analyzed for their cross-sectional areas by using profilometer (Veeco Dektak 150 stylus) [26]. A 12.5 μm stylus tip was passed perpendicularly over the wear grooves with a 3.00 mg force, and a 4000.0 μm radial measurement [26]. The height of the surface was calculated by fitting a line over the remaining data. The cross-sectional area of the groove was then found by removing the worn profiles from the flat surface line.

6.3 Results and discussion

Hydrotreated bio-oils are composed of many complex chemical compounds and functional groups. All of which require additional processes and detailed understanding for complete separation according to their main composition. However, the scope of this study is to specifically realize the lubrication properties of HYD bio-oils produced from HTL treatment, non-edible oil and poultry fat.

6.3.1 Chemical Characterization

GC-MS chromatograms showed more than hundreds of peaks on average. For this study, we selected compounds which had peak area percentage exceeding 0.2% of the total ion chromatogram area. Detailed information on the semi-quantification of the compounds is provided in the appendix (Table. D1-A to H). Overall, the majority of GC-MS detected compounds were classified into long chain paraffins and iso-paraffins, olefins, naphthene and aromatics and acids/oxygenates (Figure 6.1). MBO exhibited only paraffins in the range of C_{22}-C_{29}, while other fractions were not detected. According to the previous literature, crude carinata, crude algae and poultry fat consisted majorly of C_{22} [48], C_{16} [55], and C_{18} [56] fatty acids. Our previous study reported that after hydrotreatment over CoMo/Al, the hydrotreated oil mainly consisted of heneicosane ($C_{21}H_{44}$) for carinata and pentadecane ($C_{15}H_{32}$) for algae and our new GC-MS results

conforms it again, i.e., loss of 1 carbon (decarboxylation) could have taken place during hydrotreatment. Previous literature [56] stated that poultry fat consists mainly of linoleic (C18:2) and linolenic acids (C18:3) fatty acids, therefore after hydrotreatment the GC-MS results showed higher fraction of heptadecane ($C_{17}H_{36}$) and octadecane ($C_{18}H_{38}$). On the other hand, HSS consisted mainly of tridecane ($C_{13}H_{28}$), and pentadecane ($C_{15}H_{32}$). All hydrotreated oils showed paraffin yields as the highest followed by naphthene and aromatics, then olefins and lastly by oxygenates.

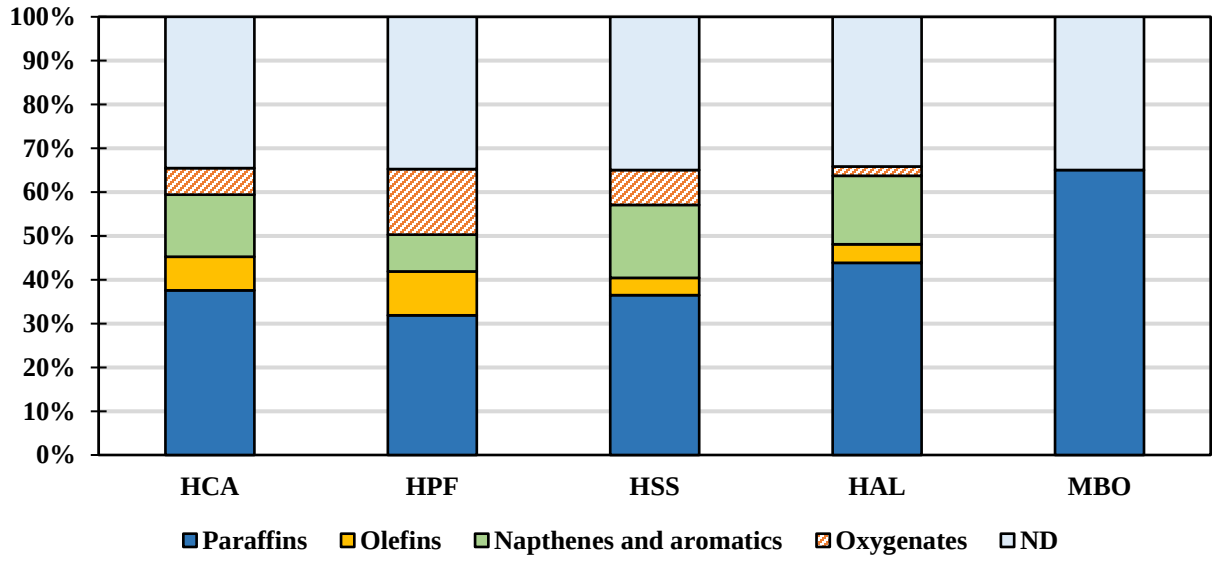

Figure 6.1 GC-MS analysis of the hydrotreated oils and mineral base oils. ND = not determined (35%).

HAL had the highest share of paraffins (44%), while HPF had the lowest (32%). The highest paraffin content could be due to rapid hydrogenation compared to cracking [48]. HPF showed the highest amount of olefins (10%) and the lowest amount of naphthene, and aromatics (8%) and it could be a product of cracking rather than hydrogenation of C=C bonds. Thermal and oxidative stability of biolubricants is attributed to their unsaturation degree. However, saturation of too many double bonds significantly affects their freezing point but it can be molecularly

modified by branching [57], [58]. Apart from saturation, polarity also influences lubricant properties. Oxygenate fraction in the GC-MS consists of acids, ketones, aldehydes, hydroxyl, and carbonyl groups. Polar groups foster adsorption on the metal surface, creates a monolayer which results in reduced wear and friction by removing free radicals [59]. According to the literature [5], [29], [60], addition of hydroxyl groups in polyunsaturated fatty acids increases the VI and lubricity property. Moreover, this study did not quantify all the compounds; it could be the case that the remaining unquantified compounds were largely consisted of aromatics or other unsaturated compounds of higher molecular weight. Furthermore, chemical composition can be tuned during HYD process for example, saturated hydrocarbons can be increased by increasing hydrogen pressure. For example, a 40 bar of hydrogen pressure resulted up to 90% selectivity for paraffins in the case of cashew nutshell oil [61]. Similar results were reported where the oxidative stability of the vegetable oil was increased due to the conversion of unsaturated fatty acids to saturated ones but increasing to high pressure (2bar) resulted in wax formation at 1h of reaction time [46]. Additionally, olefins and aromatics can be formed from fragmentation and electron impact ionization during GC-MS analysis which signifies the need for other chemical characterization processes [4].

TAN measures the number of acid constituents in BL, and it indicates the potential of corrosion to the machine parts and hydrolytic stability, therefore the TAN value should be nearly zero [62]. MBO had nearly negligible TAN value (0.06 mgKOH/g), this was followed by HCA (0.64 mgKOH/g) as seen in Table 6.1. TAN values for HSS, and HAL were 1.96 mgKOH/g and 1.55 mgKOH/g. High oxygen content for HSS (6.0 wt.%) and HPF (5.5 wt.%) co-relates well with their high TAN values (1.96 mgKOH/g and 3.8 mgKOH/g) and highest percentage of oxygenates (15% and 8%) in the GC-MS. This could be due to the presence of carboxylic acids, phenolics,

and organic acids in the oil that did not get converted into hydrocarbons during hydrotreatment. Nitrogen content of 2.86 wt.% and 2.98 wt.% were observed for HSS and HAL, which is in accordance with the literature [36], [63]. Heteroatom have shown great potential as additives. For example, Kontham et al., reported that additives based on substituted phenyl rings, sulfur and nitrogen produced from 10-undecenoic acids and aldehydes enhanced the tribological properties of BLs [62].

Pour point is the lowest temperature below which the lubricant loses its flowability and becomes semi-solid [10]. A high degree of unsaturation lowers the PP [64]. Vegetable oils having higher saturated fatty acids, along with a higher combination of polyunsaturated fatty acids compared to monounsaturated fatty acids and are crucial for lower PP [65]. It is due to bent in the molecular arrangement that prevents close packing under cold temperatures [54], [64]. From Table 6.1 it could be seen that HPF exhibited highest PP (-20℃), followed by HCA (-14℃), HSS (-12.5℃), and HAL (-10℃). MBO had a PP of -61℃ [66]. DSC thermograms of all the samples are in appendix (Figure D1). Paraffins (65%) with long chains ranging from C_{27} to C_{44} were observed for MBO which imparted exceptional CFP. On the other hand, HPF had the highest amount of olefins (10%) among all the hydrotreated oils which conforms with most literature data that high unsaturation helps in lowering PP [24], [67].

This trend is also seen in the case of HCA which had a PP of -14℃ and an olefin content of 7.7% and paraffin content of 38%. Even though HAL had the highest paraffin content after MBO it did not reflect in higher PP values. Instead, both HSS and HAL which had similar lower amount of olefins (4% and 4.2%), and higher amount of naphthene and aromatics content (16.6% and 15.1%) exhibited poor PP values (-10℃ and -12.5℃). Even though the PP reported here for the hydrotreated oils such as HSS, HAL, HCA and HPF are not compatible with cold climates,

these can be used as lubricants in applications such as chainsaw and dust suppression fluids for countries where the temperatures are warm [68]. Alternatively, biodegradable PP depressants along with diluents such as polyalphaolefin can be added to improve the PP for usage in cold climate by hindering crystallization and disrupting the stacking mechanism [69], [70].

Table 6.1 Physiochemical properties of the hydrotreated oils and mineral base oil.

Hydrotreated oils	Viscosity Index (VI)	Viscosity (mm^2/s)	Pour Point (PP) °C	Noack Volatility (@250°C ,1h wt.%)	TAN (mgKOH/g)	C (wt.%)	H (wt.%)	N (wt.%)	O (wt.%)
Carinata oil (HCA)	197.8	3.36	-14	16.12	0.64	83.97	12.97	0.13	2.83
Poultry Fat (HPF)	254	4.01	-20	18.11	3.80	81.61	12.01	0.14	5.55
HTL-Algae (HAL)	243.4	2.14	-12.5	20.52	1.96	79.39	11.631	2.98	4.59
HTL-Sewage Sludge (HSS)	231.3	3.10	-10	23.71	1.55	78.24	10.69	2.86	6.01
Mineral base oil (MBO)	132	33.04	-61	1.45	0.06	85.75	11.19	0	2.98

Viscosity depends on the molecular weight and increases with lowered molecular flexibility. By increasing branching and ring structures the flexibility of the molecule could be reduced [71]. It also increases according to the chain length of the hydrocarbon amount of the fatty acids [10]. Increasing the OH groups and branching in polyunsaturated fatty acids have shown to increase VI and lubricity of biolubricants [29], [30], [60]. VI is high for flexible structures such as one with long linear aliphatic chains and decreases under the presence of branching and ring (inflexible) [71]. According to a study by Shomchoam et al., [46] VI of partially hydrotreated palm -oil over Pd/γ-Al_2O_3 was reported to be 192, which is similar to our study for HCA (197). While

a review by Ho et al., [9], reported that the VI of hydrocarbon-based bio-lubricant is between 107 to 172 and ester-base lubricants are between 46 to 278 depending on their molecular structure (mono ester, diester etc.). In our study, most of the hydrotreated oils other than the vegetable oil (HCA) had a high VI of 243 (HAL), 231 (HSS), 254 (HPF), respectively. This correlates well with the PP as discussed. Higher amount of inflexibility (naphthene and aromatics) for both HSS and HAL could be the reason for slightly lower VI compared to HPF. It is generally desirable for a base fluid to have a high VI and low pour point. In our study HPF demonstrated both, this could be due to presence of higher amount of unsaturation, oxygenates and lowest amount of rigidity (ring structures).

Thermo-gravimetric analysis (TGA) was used to determine the thermal and oxidative stability of the oil under nitrogen and oxygen atmospheres, respectively. TG and DTG curves of hydrotreated oils and mineral base under air atmosphere is shown in Figure 6.2. All the DTG curves showed a major single continuous step for thermal decomposition. This suggested decomposition of higher molecular weight hydrocarbons to lower molecular ones along with emission of gases such as CO_2, and CO [50] and corresponds to the decomposition of saturated and unsaturated fatty acids. According to literature, unsaturation or double bond in an alkenyl chain under exposure to oxygen makes the bond prone to free radical's attack and lead to the formation of peroxide, polymerization and thermal and oxidative degradation [20], [46]. During oxidation process initial decomposition takes place due to free radical abstraction of a hydrogen atom in the hydrocarbon structure. The rate of this abstraction depends on the stability of the free radical formed. The order of stability are as follows CH_3>ArH=-CH_2->-CHR->-CH_2-CHCH-> -CH_2-Ar->-CHCH-CH_2-CHC where Ar = benzene ring [71].

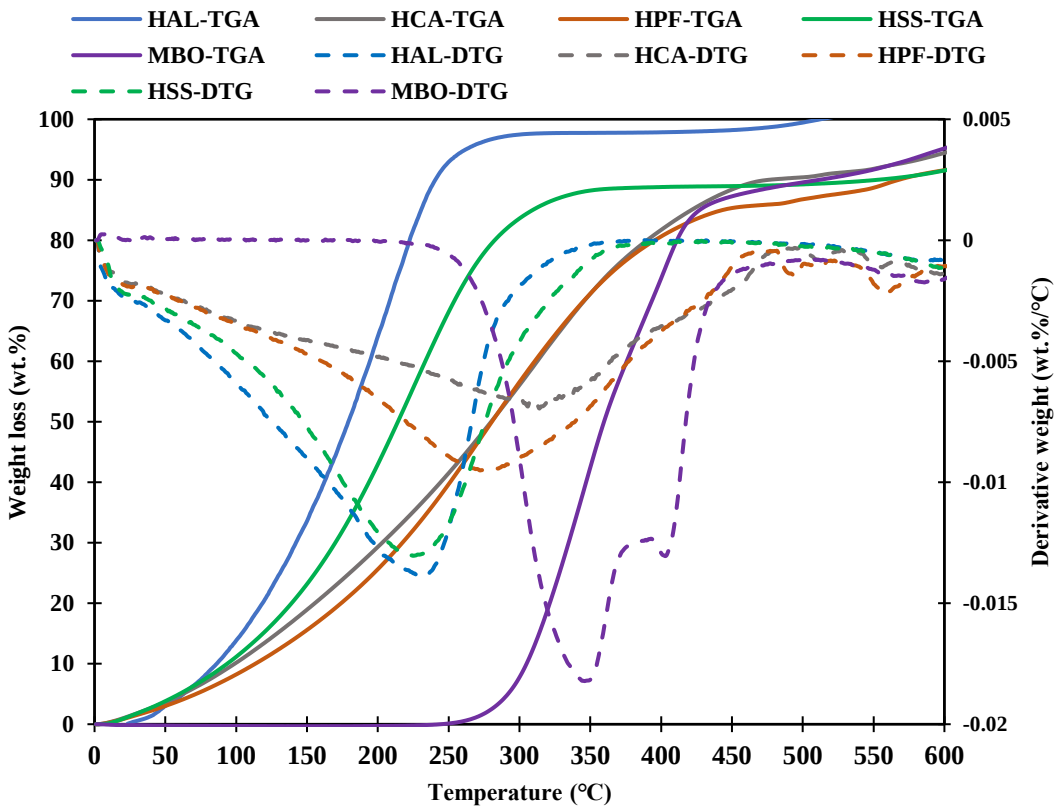

Figure 6.2 Thermogravimetric analyses of the hydrotreated bio-oil samples and mineral base oil.

MBO had the highest thermal stability at 350°C. From our earlier discussions regarding the chemical composition from GC-MS, it was noticed that MBO contained saturated hydrocarbons (paraffins). Literature reports that vegetable oil samples with higher saturated levels give higher percentages of weight loss in the beginning. Among the hydrotreated oils both HSS and HAL had a decomposition peak at 230°C. On the other hand, the HCA exhibited the highest oxidative stability at 315°C and HPF at 281°C. HAL consisted of highest amount of saturated hydrocarbons in the GC-MS, therefore it was expected to show highest thermal stability, however the TGA thermograms contradicts the earlier findings. Lower decomposition temperatures for HSS and HAL could be due to the higher degree of unsaturation in the aromatics compared to the olefins. This behavior is supported by the higher percentage of aromatics (17% and 16%) for both the oils

compared to the other oils. In the case of HCA, the highest oxidative stability could be attributed to the significant presence of saturated hydrocarbons (C_{21}). Therefore, we can report that in the case of hydrotreated oils oxidative stability was strongly dependent on the carbon number of the saturated hydrocarbons and on the aromatic content of the oils. Moreover, the oxidative stability of BL could be significantly improved by using antioxidant additives or synthetic antioxidants [50]. The decomposition temperature of the bio-oils could be higher if the lower molecular weight compounds could be removed via a distillation process. Under inert atmosphere (appendix, Figure D2), MBO, HCA and HPF were thermally stable up to temperature 400℃, 300℃ and 245℃, respectively. Both HSS and HAL were thermally stable up to 220℃.

Noack volatility decreases with increasing molecular weight but increases with branching and cyclic (flexibility) structures because it inhibits close packing and lowers the strength of intermolecular forces at high temperature [71]–[73]. Minimum acceptable volatility specifications for commercial SAE 5W-30, SAE 10W-30, and 15W-30 engine oils allow maximum evaporative weight losses of 25, 20, and 15%, respectively, by the Noack method [49]. MBO had the lowest Noack volatility (1.45%) compared to other hydrotreated oils. This is because the hydrotreated oils contained a mixture of varied structures which increased the volatility compared to MBO which mainly consists of handful of components having same average molecular weight. Therefore, MBO maintained the initial viscosity until the oxidative degradation temperature was dominant. Noack volatility was highest for HAL (23.7%) followed by HSS (20.5%), HPF (18.11%) and lastly by HCA (16.12%). Volatility loss of greater than 20% for HSS and HAL is expected due to a high amount of cyclics and aromatics (17% and 16%) as seen in Figure 6.3 and could be due to the predominant presence of paraffins of lower molecular weights such as tridecane, pentadecane and

heptadecane. While the lowest volatility for HCA could be due to presence of lower amount of napthene and aromatics, higher amounts of olefin and oxygenates compared to HAL and HSS.

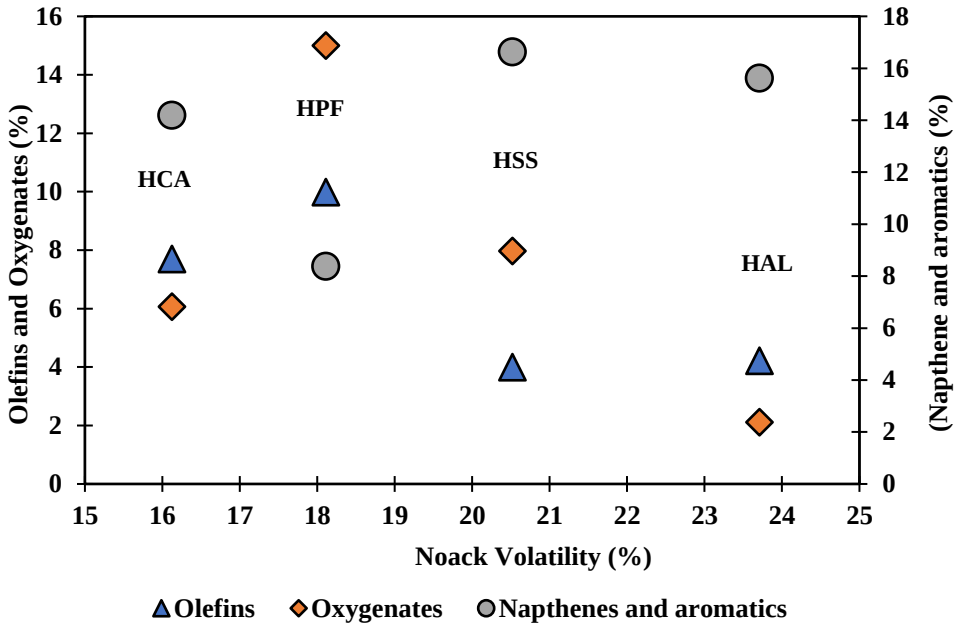

Figure 6.3 Noack volatility, olefin, oxygenates, naphthene and aromatics content of bio-oils.

3.2 Tribological Properties of HBO.

Coefficient of friction and wear profile

Lubrication tests for the hydrotreated oils were conducted within the boundary lubrication regime of the Stribeck curve which corresponds to low velocity, high pressure resulting in surface asperities being in contact with each other. In this regime, extreme pressure, anti-wear additives and surface characteristics play an important role. Boundary lubrication is usually seen in piston rings at top and bottom dead centers in modern diesel engine, fuel injection systems among others [74]–[76]. The boundary lubrication regime is selected for this study since it depends mostly on the lubricity, friction and wear properties of the fluid while other regimes depends mostly on the viscosity. The tribological properties of the hydrotreated oils were compared with the mineral base oil (MBO).

COF is the measure of the amount of friction present between two surfaces and it is defined as the ratio between friction force resisting the motion between two surfaces to the normal force pressing the two surfaces together [26]. A lower COF is desired for lubricants. The tests were within the boundary lubrication regime, where there is asperity contact between the surfaces. The hydrotreated bio-oil creates a film layer with the contacting surface. The contacting surface revolves at 63.7 rev/s and a load (50N) was applied which causes the film layer to be pushed away and both the surfaces come in contact [26]. The load is then carried by the solid contacts and the key contribution to the frictional force is the amount of energy required mostly for the shearing of the contacting asperities [71]. Therefore, boundary lubrication coefficients show little reliance on the viscosity of the lubricant. If the film is thick and strong it will reduce the wear by reducing the metal-metal contact. Lubricants containing higher polar groups such as esters form adsorbed layers compared to less polar lubricants (mineral oils or synthetic hydrocarbons) and thus impart low boundary COF [71]. In our study, MBO had a COF of 0.085. HPF exhibited the highest COF (0.087), while HAL showed the lowest (0.05). HSS and HAL had the higher amount of paraffins, nitrogenates, cyclic and lower amounts of polar groups compared to HPF and HCA, and exhibited the lowest COF (Figure 6.4). HAL and HSS bio-oil must have formed a layer that improved the metal-to-metal separation [77].

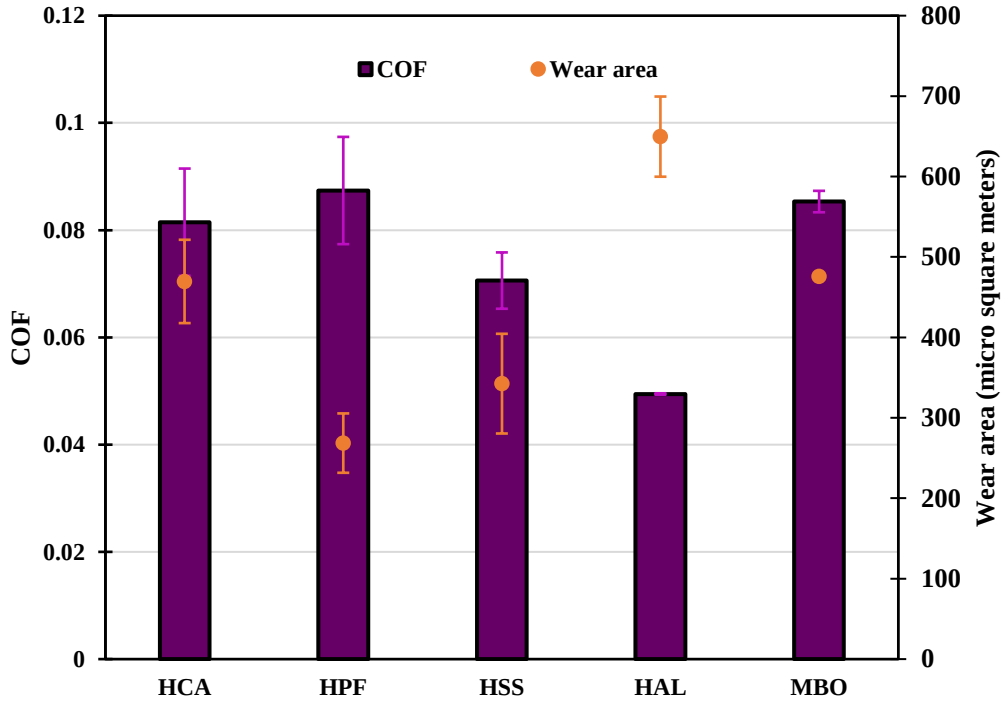

Figure 6.4 COF and wear profile of the hydrotreated oils and mineral base oil.

According to the literature, nitrogenated compounds, amides, and acids can act as friction modifying additives and enhance tribological properties [62]. The bio-oil from HPF had a higher amount of oxygenated groups as seen from GC-MS, elemental composition, and elevated TAN. According to literature, the polar groups promote adsorption on the metal surface, providing high strength lubricant films [78]. This result is also supported by a study from [26] where the authors had similar findings and the lower COF was due to polar organic compounds produced from pyrolysis oil. Another study reported that the inclusion of oxygen functional groups in the order of COOH > CHO > OH > $COOCH_3$ > C=O > C-O-C can greatly affect the fuel's lubricity. Oxygenated groups result in dipole-dipole interactions and these forces are stronger and localized than the dispersion forces that act between the aliphatic hydrocarbons [71], [79]. HCA exhibited COF of 0.081 which could be due to combination of straight chain and alkenes-based hydrocarbons could have helped to form a film layer via adsorption on the metal surface [23], [26]. Therefore,

from our study hydrotreated oils having higher amount of nitrogenated compounds, paraffins and aromatics exhibited lower COF compared to bio-oils having higher amount of unsaturation and oxygenated groups.

A profilometer was used to obtain the wear profiles of the samples. The worn cross-sectional area of the groove was analyzed numerically as seen in the Figure 6.4. Though HCA, HAL and HSS had the lower COF than HPF, the wear scar area was larger compared to HPF. This finding is consistent with other literature [78]. A metallic soap film is formed due to the reaction between the metallic surface and the lubricant, and the wear increases due to the continuous removal of the film. By further chemical reactions especially the nitrogenated compounds in the case of HAL and HSS the metallic film might have reformed and since the metallic film has a low shear strength the COF were low [78]. Another theory could be that polarity promotes adsorption which results in lower friction by forming a thin layer which induces metal-metal separation. Therefore, if nanoparticles cannot permeate the contact area, their deposition on the metal surface will not be efficient and this will increase the wear area [77]. Therefore, a lower COF does not guarantee a lower wear and the wear scar depends on the corrosion and or oxidative wear that occurs due to chemical reaction between the lubricant and the medium. It was already discussed that crude poultry fat had higher amount of oleic acid (mono and poly unsaturated) and it might have undergone more cracking versus hydrodeoxygenation compared to other samples. Therefore, there might be a possibility that oleic acid could be still present in the HPF. Literature suggests that presence of oleic acid plays a vital role in lowering the wear scar in the case of vegetable oils and in natural esters compared to standard mineral base oil [23]. High degrees of unsaturation in the oleic acid could have resulted in lower wear, good oxidative **stability**, and CFP for HPF.

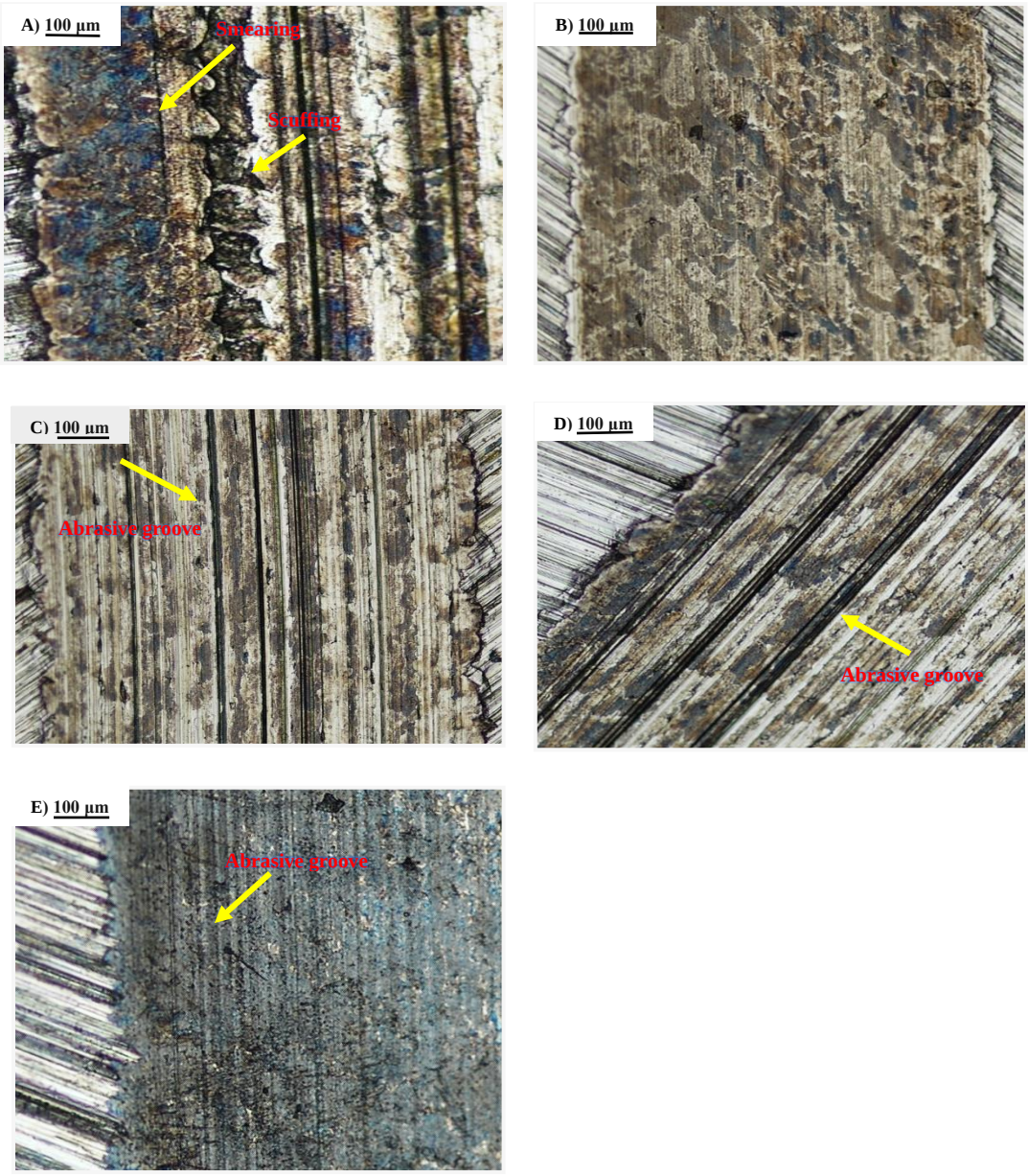

Figure 6.5 Wear surfaces of disk samples: (a) HCA, (b)HPF, (c) HSS, (d) HAL and (e) MBO.

Figure 6. 5 illustrates the microscopic images of the wear grooves of the samples. Particularly, HAL demonstrated well-defined wear grooves with higher depth compared to the other samples. Shallow grooves on HCA could be due to scuffing. It could be seen that the wear mechanism for HPF was different compared to other bio-oil samples. Abrasive type grooves were not seen for

HPF. According to previous study by [23] the HPF could have undergone micro plowing, to form a protective triboflim to stop abrasion.

6.4 Conclusions

The purpose of this study was based on the fact that success of the biofuel industry will be achieved not only by the utilizing of the waste and low-cost renewable feedstock but also by the value aggregation of bioproducts that may be obtained in a combined way through a biorefinery approach. In this study four types of hydrotreated oil such as inedible vegetable oil (HCA), poultry fat skin (HPF), hydrothermal liquefied biocrude from algae (HAL) and sewage sludge (HSS) were tested for their tribological properties without additives to be used as HBL and compared with mineral base oil (MBO). HBL are simple in their composition and can be directly used in complex formulations and can be a direct replacement of petroleum-based lubricant base oil. Hydrotreated poultry fat exhibited a slightly higher coefficient of friction (COF), lowest wear scar area, highest PP and VI, moderate oxidative stability (OS) compared to other samples. The chemical analysis reveals that HPF had the highest amounts of oxygenates, and unsaturation that could have contributed to impressive CFP and moderate OS. On the other hand, hydrotreated algae bio-oil (HAL) and hydrotreated sewage sludge bio-oil (HSS) samples exhibited higher nitrogenates and aromatics and cyclic compounds that demonstrated the lowest COF, higher VI, lower PP and but also the highest volatility and wear cross-sectional area. In the case of HAL and HSS, the aromatics could have comparatively played a bigger role in determining the lubricating properties than the paraffin alone. Higher carbon content increased the pour points and decreased the viscosity index. A high volatility of HBLs were dependent on higher amounts of cyclic structures and lower amounts of olefins and oxygenates. While the COF was lower for bio-oils that demonstrated higher cyclic structures, lower unsaturation, and polar groups. The evaporative loss

(Noack volatility) of HCA was below 17% which was within the acceptable range of most commercial engine oils. All HBL exhibited higher acid number, lower flash point and higher PP than conventional biolubricants base oil, which suggests additive, must be employed for better biolubricants properties. Among all the samples, HPF could be used as a biolubricants blend stock but the extensive hydrodeoxygenation is required for complete TAN removal. Distillation of hydrotreated bio-oil into different fractional cuts might give higher thermal decomposition temperature as similar to MBO. The present study can support the establishment of hydrocarbon biolubricants produced from hydrothermal liquefaction of waste feedstocks and encourage research on using renewable hydrocarbon based biolubricants as alternatives to current fossil-based lubricants and ester based biolubricants.

6.5 References

[1] S. Wydra, B. Hüsing, J. Köhler, A. Schwarz, E. Schirrmeister, and A. Voglhuber-Slavinsky, "Transition to the bioeconomy – Analysis and scenarios for selected niches," *J. Clean. Prod.*, vol. 294, p. 126092, Apr. 2021, doi: 10.1016/j.jclepro.2021.126092.

[2] G. Rapp *et al.*, "Indian mustard bioproducts dry-purification with natural adsorbents - A biorefinery for a green circular economy," *J. Clean. Prod.*, vol. 286, p. 125411, Mar. 2021, doi: 10.1016/j.jclepro.2020.125411.

[3] P. Roy *et al.*, "Performance of biochar assisted catalysts during hydroprocessing of non-edible vegetable oil: Effect of transition metal source on catalytic activity," *Energy Convers. Manag.*, vol. 252, p. 115131, Jan. 2022, doi: 10.1016/j.enconman.2021.115131.

[4] P. Roy *et al.*, "Understanding the effects of feedstock blending and catalyst support on hydrotreatment of algae HTL biocrude with non-edible vegetable oil," *Energy Convers. Manag.*, vol. 268, p. 115998, Sep. 2022, doi: 10.1016/j.enconman.2022.115998.

[5] E. J. Parente *et al.*, "Production of biolubricants from soybean oil: Studies for an integrated process with the current biodiesel industry," *Chem. Eng. Res. Des.*, vol. 165, pp. 456–466, Jan. 2021, doi: 10.1016/j.cherd.2020.11.012.

[6] H. Machado, A. F. Cristino, S. Orišková, and R. Galhano dos Santos, "Bio-Oil: The Next-Generation Source of Chemicals," *Reactions*, vol. 3, no. 1, Art. no. 1, Mar. 2022, doi: 10.3390/reactions3010009.

[7] P. Wang *et al.*, "Enhancement of biogas production from wastewater sludge via anaerobic digestion assisted with biochar amendment," *Bioresour. Technol.*, vol. 309, p. 123368, Aug. 2020, doi: 10.1016/j.biortech.2020.123368.

[8] P. Wang *et al.*, “Sorption and recovery of phenolic compounds from aqueous phase from sewage sludge hydrothermal liquefaction using bio-char,” *Chemosphere*, p. 131934, Aug. 2021, doi: 10.1016/j.chemosphere.2021.131934.
[9] C. K. Ho, K. B. McAuley, and B. A. Peppley, “Biolubricants through renewable hydrocarbons: A perspective for new opportunities,” *Renew. Sustain. Energy Rev.*, vol. 113, p. 109261, Oct. 2019, doi: 10.1016/j.rser.2019.109261.
[10] R. Narayana Sarma and R. Vinu, “Current Status and Future Prospects of Biolubricants: Properties and Applications,” *Lubricants*, vol. 10, no. 4, Art. no. 4, Apr. 2022, doi: 10.3390/lubricants10040070.
[11] P. V. Joseph, D. Saxena, and D. K. Sharma, “Study of some non-edible vegetable oils of Indian origin for lubricant application,” *J. Synth. Lubr.*, vol. 24, no. 4, pp. 181–197, 2007, doi: 10.1002/jsl.39.
[12] S. Boyde, “Hydrolytic stability of synthetic ester lubricants,” *J. Synth. Lubr.*, vol. 16, no. 4, pp. 297–312, 2000, doi: 10.1002/jsl.3000160403.
[13] M. R. Greaves and E. Zaugg Hoozemans, “Improving ester hydrolytic stability using triblock polyalkylene glycols,” *Ind. Lubr. Tribol.*, vol. 70, no. 2, pp. 418–422, Jan. 2018, doi: 10.1108/ILT-09-2017-0272.
[14] A. Anwar and A. Garforth, “Challenges and opportunities of enhancing cold flow properties of biodiesel via heterogeneous catalysis,” *Fuel*, vol. 173, pp. 189–208, Jun. 2016, doi: 10.1016/j.fuel.2016.01.050.
[15] A. N. Afifah, S. Syahrullail, N. I. Wan Azlee, and A. M. Rohah, “Synthesis and tribological studies of epoxidized palm stearin methyl ester as a green lubricant,” *J. Clean. Prod.*, vol. 280, p. 124320, Jan. 2021, doi: 10.1016/j.jclepro.2020.124320.
[16] J. C. J. Bart, E. Gucciardi, and S. Cavallaro, *Biolubricants: Science and Technology*. Elsevier, 2012.
[17] M. P. Schneider, “Plant-oil-based lubricants and hydraulic fluids,” *J. Sci. Food Agric.*, vol. 86, no. 12, pp. 1769–1780, 2006, doi: 10.1002/jsfa.2559.
[18] C. J. Reeves, A. Siddaiah, and P. L. Menezes, “A Review on the Science and Technology of Natural and Synthetic Biolubricants,” *J. Bio- Tribo-Corros.*, vol. 3, no. 1, p. 11, Jan. 2017, doi: 10.1007/s40735-016-0069-5.
[19] C.-H. Chan, S. W. Tang, N. K. Mohd, W. H. Lim, S. K. Yeong, and Z. Idris, “Tribological behavior of biolubricant base stocks and additives,” *Renew. Sustain. Energy Rev.*, vol. 93, pp. 145–157, Oct. 2018, doi: 10.1016/j.rser.2018.05.024.
[20] S. Almasi, B. Ghobadian, G. Najafi, and M. D. Soufi, “A review on bio-lubricant production from non-edible oil-bearing biomass resources in Iran: Recent progress and perspectives,” *J. Clean. Prod.*, vol. 290, p. 125830, Mar. 2021, doi: 10.1016/j.jclepro.2021.125830.
[21] S. Asadauskas, J. M. Perez, and J. L. Duda, “Oxidative stability and antiwear properties of high oleic vegetable oils©,” *Tribol. Lubr. Technol.*, vol. 52, pp. 877–882, Dec. 1996, Accessed: Sep. 04, 2022. [Online]. Available: http://www.scopus.com/inward/record.url?scp=0030431722&partnerID=8YFLogxK
[22] A. E. Atabani *et al.*, “Non-edible vegetable oils: A critical evaluation of oil extraction, fatty acid compositions, biodiesel production, characteristics, engine performance and emissions production,” *Renew. Sustain. Energy Rev.*, vol. 18, pp. 211–245, Feb. 2013, doi: 10.1016/j.rser.2012.10.013.
[23] S. K C, S. Adhikari, and R. L. Jackson, “AN INVESTIGATION OF THE FRICTION AND WEAR PROPERTIES OF HIGH OLEIC VEGETABLE-BASED AND MINERAL OILS,”

Int. J. Agric. Environ. Bioresearch, vol. 06, no. 06, pp. 01–20, 2021, doi: 10.35410/IJAEB.2021.5679.

[24] H. M. Mobarak *et al.*, "The prospects of biolubricants as alternatives in automotive applications," *Renew. Sustain. Energy Rev.*, vol. 33, pp. 34–43, May 2014, doi: 10.1016/j.rser.2014.01.062.

[25] P. Nagendramma and S. Kaul, "Development of ecofriendly/biodegradable lubricants: An overview," *Renew. Sustain. Energy Rev.*, vol. 16, no. 1, pp. 764–774, Jan. 2012, doi: 10.1016/j.rser.2011.09.002.

[26] K. C. Sanjeev, S. Adhikari, R. L. Jackson, and N. Jain, "Friction and wear properties of biomass-derived oils via thermochemical conversion processes," *Biomass Bioenergy*, vol. 155, p. 106269, Dec. 2021, doi: 10.1016/j.biombioe.2021.106269.

[27] F. M. T. Luna *et al.*, "Oxidative Stability of Acylated and Hydrogenated Ricinoleates Using Synthetic and Natural Antioxidants," *J. Chem.*, vol. 2019, p. e3973657, May 2019, doi: 10.1155/2019/3973657.

[28] V. B. Borugadda and V. V. Goud, "Improved thermo-oxidative stability of structurally modified waste cooking oil methyl esters for bio-lubricant application," *J. Clean. Prod.*, vol. 112, pp. 4515–4524, Jan. 2016, doi: 10.1016/j.jclepro.2015.06.046.

[29] N. Salih, J. Salimon, B. M. Abdullah, and E. Yousif, "Thermo-oxidation, friction-reducing and physicochemical properties of ricinoleic acid based-diester biolubricants," *Arab. J. Chem.*, vol. 10, pp. S2273–S2280, May 2017, doi: 10.1016/j.arabjc.2013.08.002.

[30] J. Salimon, N. Salih, and B. M. Abdullah, "Diesters Biolubricant Base Oil: Synthesis, Optimization, Characterization, and Physicochemical Characteristics," *Int. J. Chem. Eng.*, vol. 2012, p. e896598, Feb. 2012, doi: 10.1155/2012/896598.

[31] M. M. Gui, K. T. Lee, and S. Bhatia, "Feasibility of edible oil vs. non-edible oil vs. waste edible oil as biodiesel feedstock," *Energy*, vol. 33, no. 11, pp. 1646–1653, Nov. 2008, doi: 10.1016/j.energy.2008.06.002.

[32] T. Rahman, H. Jahromi, P. Roy, S. Adhikari, E. Hassani, and T.-S. Oh, "Hydrothermal liquefaction of municipal sewage sludge: Effect of red mud catalyst in ethylene and inert ambiences," *Energy Convers. Manag.*, vol. 245, p. 114615, Oct. 2021, doi: 10.1016/j.enconman.2021.114615.

[33] H. Chowdhury *et al.*, "Synthesis of biodiesel from chicken skin waste: an economic and environmental biofuel feedstock in Bangladesh," *Environ. Sci. Pollut. Res.*, vol. 28, no. 28, pp. 37679–37688, Jul. 2021, doi: 10.1007/s11356-021-13424-5.

[34] O. Zinina, S. Merenkova, and M. Rebezov, "Analysis of modern approaches to the processing of poultry waste and by-products: prospects for use in industrial sectors," *Food Sci Technol*, p. 10, 2022.

[35] M. Perera, J. Yan, L. Xu, M. Yang, and Y. Yan, "Bioprocess development for biolubricant production using non-edible oils, agro-industrial byproducts and wastes," *J. Clean. Prod.*, vol. 357, p. 131956, Jul. 2022, doi: 10.1016/j.jclepro.2022.131956.

[36] J. Sun, J. Yang, and M. Shi, "Review of Denitrogenation of Algae Biocrude Produced by Hydrothermal Liquefaction," *Trans. Tianjin Univ.*, vol. 23, no. 4, pp. 301–314, Jul. 2017, doi: 10.1007/s12209-017-0051-4.

[37] M. Xie, H. Tan, and G. Zhao, "A clean and sustainable strategy to produce bio-lubricant with high-bearing and good anti-oxidation ability from Lanzhou lily," *J. Clean. Prod.*, vol. 371, p. 133333, Oct. 2022, doi: 10.1016/j.jclepro.2022.133333.

[38] N. A. Abdul Razak, N.-A. Mijan, Y. H. Taufiq-Yap, and D. Derawi, "Production of green diesel via hydrogen-free and solventless deoxygenation reaction of waste cooking oil," *J. Clean. Prod.*, vol. 366, p. 132971, Sep. 2022, doi: 10.1016/j.jclepro.2022.132971.
[39] A. Alam and P. Dwivedi, "Modeling site suitability and production potential of carinata-based sustainable jet fuel in the southeastern United States," *J. Clean. Prod.*, vol. 239, p. 117817, Dec. 2019, doi: 10.1016/j.jclepro.2019.117817.
[40] L. D'Avino, R. Dainelli, L. Lazzeri, and P. Spugnoli, "The role of co-products in biorefinery sustainability: energy allocation versus substitution method in rapeseed and carinata biodiesel chains," *J. Clean. Prod.*, vol. 94, pp. 108–115, May 2015, doi: 10.1016/j.jclepro.2015.01.088.
[41] G. Fiorentino, M. Ripa, S. Mellino, S. Fahd, and S. Ulgiati, "Life cycle assessment of Brassica carinata biomass conversion to bioenergy and platform chemicals," *J. Clean. Prod.*, vol. 66, pp. 174–187, Mar. 2014, doi: 10.1016/j.jclepro.2013.11.043.
[42] V. I. Anikeev, "Chapter 1 - Synthesis of Biodiesel Fuel in Supercritical Lower Alcohols with and without Heterogeneous Catalysts (Thermodynamics, Phase and Chemical Equilibriums, Experimental Studies)," in *Supercritical Fluid Technology for Energy and Environmental Applications*, V. Anikeev and M. Fan, Eds. Boston: Elsevier, 2014, pp. 1–29. doi: 10.1016/B978-0-444-62696-7.00001-0.
[43] Y. L. Cheryl-Low, P. S. Kong, and H. V. Lee, "Environmentally adapted bio-oil compounds-derived polyolesters synthesis: Optimization and properties of base fluids," *J. Hazard. Mater.*, vol. 407, p. 124365, Apr. 2021, doi: 10.1016/j.jhazmat.2020.124365.
[44] X. Chen, X. Ma, L. Chen, X. Lu, and Y. Tian, "Hydrothermal liquefaction of Chlorella pyrenoidosa and effect of emulsification on upgrading the bio-oil," *Bioresour. Technol.*, vol. 316, p. 123914, Nov. 2020, doi: 10.1016/j.biortech.2020.123914.
[45] H. Jahromi, T. Rahman, P. Roy, and S. Adhikari, "Hydrotreatment of solvent-extracted biocrude from hydrothermal liquefaction of municipal sewage sludge," *Energy Convers. Manag.*, vol. 263, p. 115719, Jul. 2022, doi: 10.1016/j.enconman.2022.115719.
[46] B. Shomchoam and B. Yoosuk, "Eco-friendly lubricant by partial hydrogenation of palm oil over Pd/γ-Al2O3 catalyst," *Ind. Crops Prod.*, vol. 62, pp. 395–399, Dec. 2014, doi: 10.1016/j.indcrop.2014.09.022.
[47] Y. Xu, X. Zheng, X. Hu, K. D. Dearn, and H. Xu, "Effect of catalytic esterification on the friction and wear performance of bio-oil," *Wear*, vol. 311, no. 1, pp. 93–100, Mar. 2014, doi: 10.1016/j.wear.2013.12.029.
[48] H. Jahromi *et al.*, "Production of green transportation fuels from Brassica carinata oil: A comparative study of noble and transition metal catalysts," *Fuel Process. Technol.*, vol. 215, p. 106737, May 2021, doi: 10.1016/j.fuproc.2021.106737.
[49] H. Jahromi, S. Adhikari, P. Roy, M. Shelley, E. Hassani, and T.-S. Oh, "Synthesis of Novel Biolubricants from Waste Cooking Oil and Cyclic Oxygenates through an Integrated Catalytic Process," *ACS Sustain. Chem. Eng.*, Sep. 2021, doi: 10.1021/acssuschemeng.1c03523.
[50] V. Babu Borugadda and V. V. Goud, "Comparative studies of thermal, oxidative and low temperature properties of waste cooking oil and castor oil," *J. Renew. Sustain. Energy*, vol. 5, no. 6, p. 063104, Nov. 2013, doi: 10.1063/1.4830257.
[51] M. Garcia-Perez, T. T. Adams, J. W. Goodrum, K. C. Das, and D. P. Geller, "DSC studies to evaluate the impact of bio-oil on cold flow properties and oxidation stability of bio-diesel," *Bioresour. Technol.*, vol. 101, no. 15, pp. 6219–6224, Aug. 2010, doi: 10.1016/j.biortech.2010.03.002.

[52] A. Adhvaryu, S. Z. Erhan, and J. M. Perez, “Wax appearance temperatures of vegetable oils determined by differential scanning calorimetry: effect of triacylglycerol structure and its modification,” *Thermochim. Acta*, vol. 395, no. 1, pp. 191–200, Jan. 2002, doi: 10.1016/S0040-6031(02)00180-6.
[53] P. Claudy, J.-M. Létoffé, B. Neff, and B. Damin, “Diesel fuels: determination of onset crystallization temperature, pour point and filter plugging point by differential scanning calorimetry. Correlation with standard test methods,” *Fuel*, vol. 65, no. 6, pp. 861–864, Jun. 1986, doi: 10.1016/0016-2361(86)90082-7.
[54] N. H. Jayadas and K. P. Nair, “Coconut oil as base oil for industrial lubricants—evaluation and modification of thermal, oxidative and low temperature properties,” *Tribol. Int.*, vol. 39, no. 9, pp. 873–878, Sep. 2006, doi: 10.1016/j.triboint.2005.06.006.
[55] “Marine Microalgae FAQ,” *Reed Mariculture*. https://reedmariculture.com/pages/microalgae-faq (accessed Mar. 07, 2022).
[56] F. Toldrá-Reig, L. Mora, and F. Toldrá, “Trends in Biodiesel Production from Animal Fat Waste,” *Appl. Sci.*, vol. 10, no. 10, Art. no. 10, Jan. 2020, doi: 10.3390/app10103644.
[57] S. J. Reaume and N. Ellis, “Use of Isomerization and Hydroisomerization Reactions to Improve the Cold Flow Properties of Vegetable Oil Based Biodiesel,” *Energies*, vol. 6, no. 2, Art. no. 2, Feb. 2013, doi: 10.3390/en6020619.
[58] Y. X. Xu, M. A. Hanna, and S. J. Josiah, “Hybrid hazelnut oil characteristics and its potential oleochemical application,” *Ind. Crops Prod.*, vol. 26, no. 1, pp. 69–76, Jun. 2007, doi: 10.1016/j.indcrop.2007.01.009.
[59] B. J. Pafford, P. E. Godici, R. H. Schlosberg, H. S. Aldrich, M. A. Krevalis, and J. T. Kim, “Polyol ester compositions with unconverted hydroxyl groups for use as lubricant base stocks,” EP0938536A1, Sep. 01, 1999 Accessed: Sep. 04, 2022. [Online]. Available: https://patents.google.com/patent/EP0938536A1/en
[60] J. Oh, S. Yang, C. Kim, I. Choi, J. H. Kim, and H. Lee, “Synthesis of biolubricants using sulfated zirconia catalysts,” *Appl. Catal. Gen.*, vol. 455, pp. 164–171, Mar. 2013, doi: 10.1016/j.apcata.2013.01.032.
[61] C. A. Scaldaferri and V. M. D. Pasa, “Green diesel production from upgrading of cashew nut shell liquid,” *Renew. Sustain. Energy Rev.*, vol. 111, pp. 303–313, Sep. 2019, doi: 10.1016/j.rser.2019.04.057.
[62] G. Appiah, S. K. Tulashie, E. E. A. Akpari, E. R. Rene, and D. Dodoo, “Biolubricant production via esterification and transesterification processes: Current updates and perspectives,” *Int. J. Energy Res.*, vol. 46, no. 4, pp. 3860–3890, 2022, doi: 10.1002/er.7453.
[63] P. Duan and P. E. Savage, “Catalytic hydrotreatment of crude algal bio-oil in supercritical water,” *Appl. Catal. B Environ.*, vol. 104, no. 1, pp. 136–143, Apr. 2011, doi: 10.1016/j.apcatb.2011.02.020.
[64] L. I. Farfan-Cabrera, M. Franco-Morgado, A. González-Sánchez, J. Pérez-González, and B. M. Marín-Santibáñez, “Microalgae Biomass as a New Potential Source of Sustainable Green Lubricants,” *Molecules*, vol. 27, no. 4, Art. no. 4, Jan. 2022, doi: 10.3390/molecules27041205.
[65] B. Sharma, U. Rashid, F. Anwar, and S. Erhan, “Lubricant properties of Moringa oil using thermal and tribological techniques,” *J. Therm. Anal. Calorim.*, vol. 96, no. 3, pp. 999–1008, Jun. 2009, doi: 10.1007/s10973-009-0066-8.
[66] “Specialty Base Oils | Our Products | Petro-Canada Lubricants.” http://lubricants.petro-canada.com/en-ca/category/base-oils (accessed Sep. 11, 2022).

[67] J. A. Cecilia, D. Ballesteros Plata, R. M. Alves Saboya, F. M. Tavares de Luna, C. L. Cavalcante, and E. Rodríguez-Castellón, "An Overview of the Biolubricant Production Process: Challenges and Future Perspectives," *Processes*, vol. 8, no. 3, Art. no. 3, Mar. 2020, doi: 10.3390/pr8030257.
[68] K. V. Fernandes, A. Papadaki, J. A. C. da Silva, R. Fernandez-Lafuente, A. A. Koutinas, and D. M. G. Freire, "Enzymatic esterification of palm fatty-acid distillate for the production of polyol esters with biolubricant properties," *Ind. Crops Prod.*, vol. 116, pp. 90–96, Jun. 2018, doi: 10.1016/j.indcrop.2018.02.058.
[69] R. K. Singh, A. Kukrety, and A. K. Singh, "Study of Novel Ecofriendly Multifunctional Lube Additives Based on Pentaerythritol Phenolic Ester," *ACS Sustain. Chem. Eng.*, vol. 2, no. 8, pp. 1959–1967, Aug. 2014, doi: 10.1021/sc500389f.
[70] B. K. Sharma, A. Adhvaryu, Z. Liu, and S. Z. Erhan, "Chemical modification of vegetable oils for lubricant applications," *J. Am. Oil Chem. Soc.*, vol. 83, no. 2, pp. 129–136, Feb. 2006, doi: 10.1007/s11746-006-1185-z.
[71] L. R. Rudnick, *Synthetics, Mineral Oils, and Bio-Based Lubricants: Chemistry and Technology*. CRC Press, 2020.
[72] C. M. Murphy and W. A. Zisman, "Structural Guides for Synthetic Lubricant Development," *Ind. Eng. Chem.*, vol. 42, no. 12, pp. 2415–2420, Dec. 1950, doi: 10.1021/ie50492a016.
[73] E. L. Niedzielski, "Neopentyl Polyol Ester Lubricants-Bulk Property Optimization," *Prod. RD*, vol. 15, no. 1, pp. 54–58, Mar. 1976, doi: 10.1021/i360057a010.
[74] N. W. M. Zulkifli, M. A. Kalam, H. H. Masjuki, M. Shahabuddin, and R. Yunus, "Wear prevention characteristics of a palm oil-based TMP (trimethylolpropane) ester as an engine lubricant," *Energy*, vol. 54, pp. 167–173, Jun. 2013, doi: 10.1016/j.energy.2013.01.038.
[75] S. M. Hsu and R. S. Gates, "Boundary lubricating films: formation and lubrication mechanism," *Tribol. Int.*, vol. 38, no. 3, pp. 305–312, Mar. 2005, doi: 10.1016/j.triboint.2004.08.021.
[76] B. J. Hamrock, S. R. Schmid, and B. O. Jacobson, *Fundamentals of Fluid Film Lubrication*, 2nd ed. Boca Raton: CRC Press, 2004. doi: 10.1201/9780203021187.
[77] M. F. Trajano, E. I. F. Moura, K. S. B. Ribeiro, and S. M. Alves, "Study of oxide nanoparticles as additives for vegetable lubricants," *Mater. Res.*, vol. 17, pp. 1124–1128, Oct. 2014, doi: 10.1590/1516-1439.228213.
[78] N. H. Jayadas, K. Prabhakaran Nair, and A. G, "Tribological evaluation of coconut oil as an environment-friendly lubricant," *Tribol. Int.*, vol. 40, no. 2, pp. 350–354, Feb. 2007, doi: 10.1016/j.triboint.2005.09.021.
[79] P. J. Sniegoski, "Selectivity of the Oxidative Attack on a Model Ester Lubricant," *E Trans.*, vol. 20, no. 4, pp. 282–286, Jan. 1977, doi: 10.1080/05698197708982844.

CHAPTER

7 CONCLUSIONS AND FUTURE RECOMMENDATIONS

7.1 Summary

Production of biofuels and biolubricants via hydrotreatment process has been demonstrated in this study. Feedstocks in this study ranged from triglycerides such as carinata oil and poultry waste to hydrothermal liquefied biocrude produced from waste and biomass precursors such as sewage sludge, and algae and finally pyrolysis oil from eucalyptus biomass. This research was conducted to examine the influence of biochar and alumina supported catalysts during hydrotreatment of the above-mentioned feedstocks to biofuels and biolubricants. This study evaluated the influence of different metal salts impregnated on biochar supported catalyst for hydrotreatment of triglycerides (carinata oil) to transportation fuels. This research further investigated the effect of bimetals impregnated on biochar and alumina supports for upgrading a blend of triglyceride and algae biocrude to fuel range hydrocarbons. This study also analyzed the effect of different hydrothermal liquefaction of heterogeneous catalyst supports for a blend comprising of two triglycerides (carinata oil and poultry fat) with pyrolysis bio-oil. Finally, this research examined he feasibility of hydrotreatment process for different types of waste precursors and HLT biocrude as biolubricants. Each of these objectives were fulfilled, and the major findings and conclusions are summarized below:

Objective 1: In this objective, two catalyst preparation methods were applied to the two-transition metal (Ni and Co) salts (OH and NO3) assisted with biochar for hydrotreating carinata oil. Synchroton method showed that by aqueous deposition synthesis method, OH-sourced metals

occupied the surface, while NO_3-sourced metals were dispersed mostly inside the pores. It was seen that saturation, and cracking of triglycerides, decarboxylation, and partial hydrogenation were surface phenomena. Methanation, dehydrogenation of free fatty acids and aromatization reactions were pore phenomena. The nature of the metal, catalyst BET specific surface area, and catalyst preparation method played major role in carinata upgrading. Catalytic cracking followed by hydrotreatment delivered better results than sing stage cracking or hydrotreatment. Finally, a reaction network was proposed based on chemical analysis of the upgraded carinata oil and erucic acid model compound. Cobalt nitrate ($CoNO_3$) supported on biochar fared better compared to $NiNO_3$, NiOH and CoOH. In conclusion, biochar support was able to successfully hydrotreated carinata oil and this research can provide knowledge that can help to have a better control on the final product properties. For example, the nitrate-to-hydroxide ratio can be varied during catalyst preparation to achieve desired reaction products.

Objective 2: In the previous objective mono metal supported on biochar catalyst was successful in hydrotreating carinata oil. Therefore, in this objective bimetallic biochar support and commercial alumina support were selected for hydrotreatment of a blend of carinata oil and hydrothermal liquefaction algae biocrude. The catalysts were activated by sulfidation and the sulfided catalysts irrespective of the support type was successful in removing more oxygen, sulfur, nitrogen and adding carbon, hydrogen, and increasing higher heating value and removing total acid number. Overall, biochar supported catalysts were highly successful in removing metal and catalyzed cracking reactions. It had lowest viscosity (1.45 m2/s), highest and lowest share of gasoline (55%) and heavy diesel (4.38%) and less ess coke formation. Overall, alumina supported catalysts had highest HHV (46 MJ/kg), carbon addition (83 wt.%), octane number (89), jet fuel (27%) and paraffin (72%) fractions and lowest TAN (1.8 mgKOH/g). In summary, advantage of these two

supports can be taken by using one of support as sacrificial catalyst (guard bed and packed bed) or create new support. In summary, biochar supports have higher oxygen containing functional groups (acidic sites), inorganic mineral oxides, ion exchange capacity, high surface area, pore structure and connectivity. All of these make a substantial contribution to its effective sorption and unique catalytic behavior.

Objective 3: In the previous objective the biochar and alumina supported catalysts were successful in hydrotreating a blend of carinata oil and HTL algae biocrude. Therefore, in this objective the same catalysts were used for hydrotreating a blend of more complex oil; pyrolysis bio-oil and carinata oil or poultry fat. The blended hydrotreated oil produced from biochar supported catalysts showed better positive synergistic effect in terms of carbon and hydrogen addition, oxygen removal, HHV and viscosity. While alumina supported catalyst exhibited a higher liquid yield. Biochar support demonstrated higher jet fuel fraction consisting of mainly of paraffins and lowest amount of light and heavy diesel and produced lower coke. Abundant oxygen containing functional groups, inorganic mineral oxides, high surface area, pore structure and acid sites makes biochar support a better HDO catalyst compared to alumina support. On the other hand, blending the pyrolysis oil with poultry fat yielded better quality of bio-oil over carinata oil. In summary, pyrolysis oil blended with poultry fat and hydrotreated using biochar support catalysts was more successful in HDO activity and in improving overall bio-oil quality compared to alumina supported catalyst and carinata oil.

Objective 4: Even after 20 years of development, the biofuel cost is higher than fossil fuel which has slowed down commercialization. The key challenges involved is the lack of understanding of physicochemical, thermophysical, and tribological properties of biolubricants if they are produced by utilizing waste and renewable resources. Hydrocarbon chain number and cold flow properties

in hydrotreated bio-oil have the potential to be used as bio-lubricants. The main objective of this study was to evaluate the feasibility of waste derived hydrotreated bio-oils as hydrocarbon based biolubricants, and (2) investigate the tribological behaviors of the upgraded bio-oils. In this study four types of hydrotreated oil such as inedible vegetable oil (HCA), poultry fat skin (HPF), hydrothermal liquefied biocrude from algae (HAL) and sewage sludge (HSS) were tested for their tribological properties without additives to be used as HBL and compared with mineral base oil (MBO). Hydrotreated poultry fat exhibited a slightly higher coefficient of friction (COF), lowest wear scar area, highest PP and VI, moderate oxidative stability (OS) compared to other samples. The chemical analysis reveals that HPF had the highest amounts of oxygenates, and unsaturation that could have contributed to impressive CFP and moderate OS. On the other hand, hydrotreated algae bio-oil (HAL) and hydrotreated sewage sludge bio-oil (HSS) samples exhibited higher nitrogenates and aromatics and cyclic compounds that demonstrated the lowest COF, higher VI, lower PP and but also the highest volatility and wear cross-sectional area. All HBL exhibited higher acid number, lower flash point and higher PP than conventional biolubricants base oil, which suggests additive, must be employed for better biolubricants properties. Among all the samples, HPF could be used as a biolubricants blend stock but the extensive hydrodeoxygenation is required for complete TAN removal. The present study can support the establishment of hydrocarbon biolubricants produced from hydrothermal liquefaction of waste feedstocks and encourage research on using renewable hydrocarbon based biolubricants as alternatives to current fossil-based lubricants and ester based biolubricants.

7.2 Recommendations

In this study HTL biocrudes and pyrolysis oil underwent successful hydrodeoxygenation, denitrogenation, desulfurization and demetallization of various feedstocks to fuel range hydrocarbons and biolubricants. The overall cost of the process will be affected by the deoxygenation degree and catalyst deactivation. Presence of oxygen does not necessarily mean that the product is not suitable for use. Oxygenates such as ethanol is added in gasoline for improved combustion properties [1]. However, the presence of certain types of oxygenated compounds such as phenols, cresol is detrimental for the fuel [1]. The extent of deoxygenation needs to be improved and any incomplete deoxygenation affects the final quality of the fuel which ultimately impacts the economic consequences of a biorefinery.

Modification of biochar support: This study shows that biochar supported catalysts were successful in hydrotreatment of hydrothermal liquified biocrude and pyrolysis oil. Biomass has high content of oxygen, therefore reasonable carbonization and activation are necessary to optimize the dispersion of active metals on the surface. Construction of surface defects i.e., oxygen vacancies can alter the absorption of reactant molecules and hence overall catalytic activity. Therefore, the future study will should try to modify the -OH-, C=O and C=OOH groups on the surface that provides nucleation sites for the metal nanoparticle. This in turn can provide better dispersion, higher surface area with well-developed micro and mesopores, pore volume and stability of the metal active sites. Common activators which are used in literature are steam, carbon dioxide, potassium hydroxide, potassium carbonate, phosphoric acid, sulfonation, nitration so on [2], [3]. The BET surface area of a hardwood-biochar increased from 0.13 to 207 $m^2 g^{-1}$ after pre-treatment with KOH. Therefore, altering the surface of biochar surface can vastly improve the catalytic activity [3], [4].

Biomass type: Biomass consists of varying amounts of hemicellulose, cellulose, lignin, and ash content therefore different biomass will yield different types of biochars with distinctive physiochemical properties under same temperature. Therefore, composition dictates the temperature under which the biomass should be reduced in order to obtain desirable porous structure. Additionally, inorganic elements are the active sites for methane decomposition and hydrogen production. Therefore, future study should focus on studying different biomass feedstocks and study the effects of it during hydrotreatment. For example, pine biochar demonstrated a 50% higher surface area than peanut hull biochar under same pyrolytic conditions [3].

Biochar type: Biochar produced from pyrolysis, hydrothermal liquefaction or gasification will impart different catalytic activity. Additionally, biochar from non-biomass sources such as sewage sludge, algae, poultry fat might give better results upon activation. For example, the surface area and pore volume of rice straw biochar increased from 140 to 772 m^2/g and from 0.09 to 0.42 cm^3/g while the sewage sludge surface area and pore volume increased from 18 to 793 m^2/g and from 0.02 to 0.61 cm^3/g after activating it with KOH respectively [3], [5]. Therefore, biochar production from different sources needs to be tested.

Parametric study: Although bio-oil hydrotreatment is a complex reaction mechanism parametric study can help to comprehend it a little better. In this study, co-hydroprocessing of two feedstocks were carried out at 50:50 ratio, with a hydrogen pressure of 1000 psi, temperature of 400C and oil to catalyst ratio of 70:1. Varying the process parameters will change the final product distribution, hence it needs to be investigated.

Distillation: Hydrotreatment removes heteroatoms via hydrogenation, dehydration, hydrodeoxygenation, decarbonylation, decarboxylation, hydrocracking, hydrodenitrogenation,

hydrodesulfurization to produce a blend of hydrocarbons ranging from C_6 to C_{25} (average). This blend is difficult to use as "drop-in" transportation fuel or building in refineries. Hence, fractional distillation is necessary to fractionate the hydrotreated bio-oil into gasoline, jet fuel, diesel and vacuum gas oil fractions based on relative volatility. Distillation improves the quality of the biofuel and make it suitable for final use. Distillation should be performed for the hydrotreated bio-oils produced and further characterization of different fractions should be carried out.

Regeneration of catalysts: Regeneration of catalysts using in-situ methods such as oxygen, air, inert gas, at different temperature have been used to remove coke deposits [6]. Washing with NaOH, and ammonia have also been used to remove carbonaceous deposits. This study used as a reducing agent (H2 90% and N2 10%) to regenerate catalyst so that the transition metal remains in its highest metallic state. Other regeneration methods and re-using the regenerated catalysts for multiple cycles needs is recommended for future study,

7.3 References

[1] M. V. Olarte et al., "Characterization of upgraded fast pyrolysis oak oil distillate fractions from sulfided and non-sulfided catalytic hydrotreating," Fuel, vol. 202, pp. 620–630, Aug. 2017, doi: 10.1016/j.fuel.2017.03.051.

[2] S. Wang, H. Li, and M. Wu, "Advances in metal/ biochar catalysts for biomass hydro-upgrading: A review," J. Clean. Prod., vol. 303, p. 126825, Jun. 2021, doi: 10.1016/j.jclepro.2021.126825.

[3] J. Lee, K.-H. Kim, and E. E. Kwon, "Biochar as a Catalyst," Renew. Sustain. Energy Rev., vol. 77, pp. 70–79, Sep. 2017, doi: 10.1016/j.rser.2017.04.002.

[4] A. M. Dehkhoda, A. H. West, and N. Ellis, "Biochar based solid acid catalyst for biodiesel production," Appl. Catal. Gen., vol. 382, no. 2, pp. 197–204, Jul. 2010, doi: 10.1016/j.apcata.2010.04.051.

[5] J. S. Cha et al., "The low-temperature SCR of NO over rice straw and sewage sludge derived char," Chem. Eng. J., vol. 156, no. 2, pp. 321–327, Jan. 2010, doi: 10.1016/j.cej.2009.10.027.

[6] M. Martin-Martinez, J. J. Rodriguez, R. T. Baker, and L. M. Gómez-Sainero, "Deactivation and regeneration of activated carbon-supported Rh and Ru catalysts in the hydrodechlorination of

chloromethanes into light olefins," Chem. Eng. J., vol. 397, p. 125479, Oct. 2020, doi: 10.1016/j.cej.2020.125479.

8 APPENDIX A

8.1 Supplementary information for Chapter 3.

Performance of biochar assisted catalysts during hydroprocessing of non-edible vegetable oil: Effect of transition metal source on catalytic activity

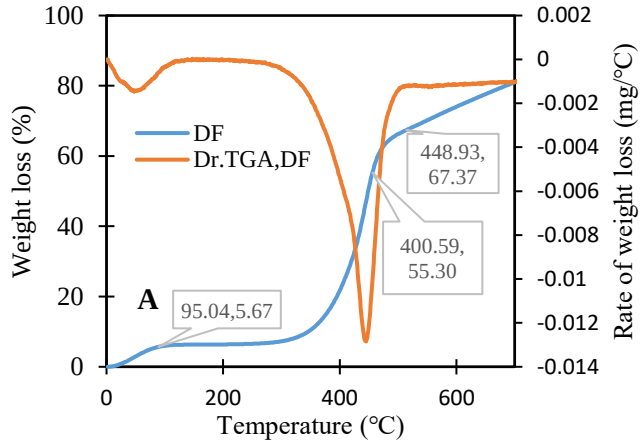

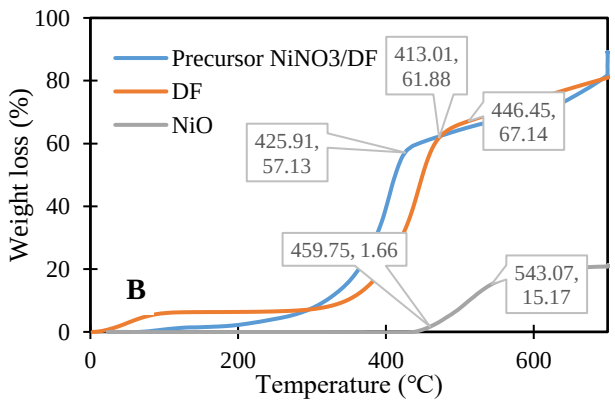

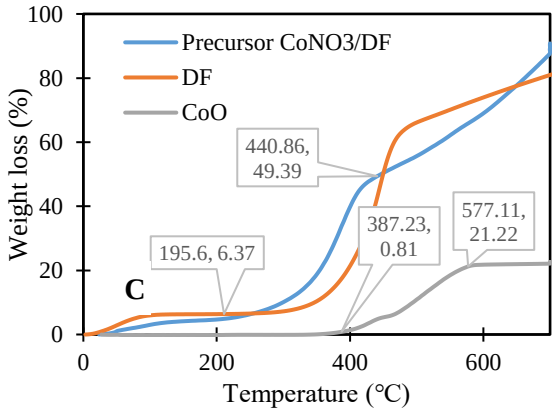

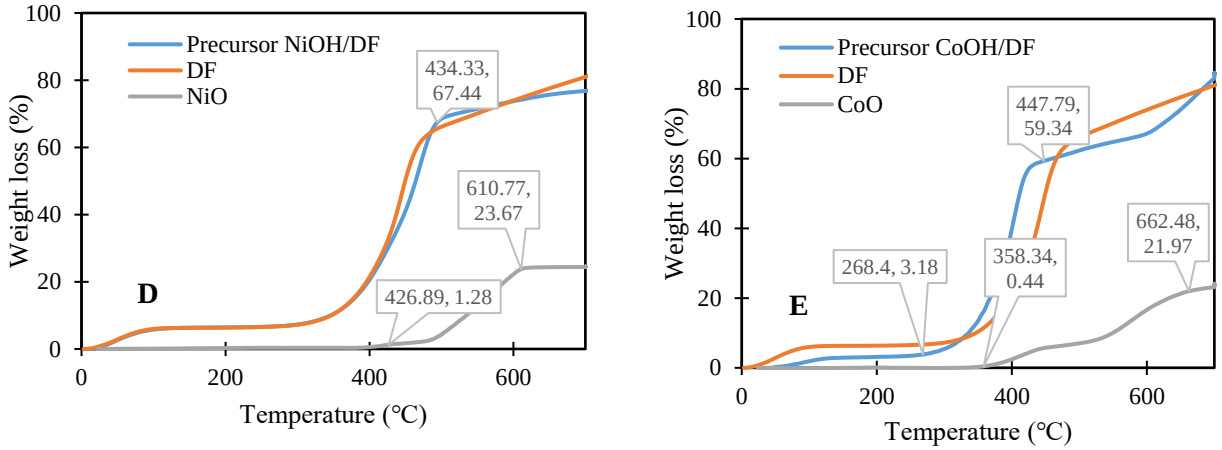

Figure A 1. TG-TPR thermograms in 10%H_2 (balance N_2) atmosphere: (A) DF biomass. (B) Precursor $NiNO_3$/DF, DF and calcined nickel nitrate hexahydrate. (C) Precursor $CoNO_3$/DF, DF and calcined cobalt nitrate hexahydrate. (D) Precursor NiOH/DF, DF, and calcined nickel hydroxide. (E) Precursor CoOH/DF, DF and calcined cobalt hydroxide.

At temperatures lower than about 100 °C, a small weight change of the samples is attributed to moisture evaporation. Figure A1, showed a weight loss of approximately 6.0 % to 60 % in the temperature range of 100℃ to 408℃. The decomposition peaked at 450℃ with 65% weight loss for DF biomass, and then followed by approximately 88% at 700℃. From the DTG curve, a sharp decomposition peak could be noticed at 445℃. Figure A1, shows the weight loss curves for DF, precursor $NiNO_3$/DF, and calcined $NiNO_3.6H_2O$. Approximately 60% of weight loss occurred at 413℃ for the DF, while the precursor showed the weight loss of 57% at 425℃. Approximately 86 % weight loss occurred at 700℃ for the precursor. The NiO (or calcined $NiNO_3.6H_2O$) reduction peak started at 460℃, peaked at 543℃ with 1.6% and 15% weight loss respectively. In the case of Figure A1, a weight loss of approximately 6% to 50% occurred between 195℃ and 440℃ respectively. Approximately 88 % weight loss occurred at 700℃ for the precursor. The CoO (or calcined $CoNO_3.6H_2O$) reduction peak started at 387℃, peaked at 577℃ with a weight loss of 0.81% and 21.22% respectively. In the case of the hydroxides, the percent mass loss of NiOH/DF

precursor was quite similar to the DF biomass, 67% weight loss was seen at 434℃. Approximately 76 % weight loss occurred at 700℃ occurred for the precursor. The NiO (or calcined $Ni(OH)_2$) reduction peak started at 426℃, peaked at 610℃ with 1.28% and 23.67% of weight loss respectively. The precursor CoOH/DF showed a mass loss of approximately 3% to 60% between 268℃ and 447℃.The CoO (or calcined $Co(OH)_2$) reduction peak started at 358℃, peaked at 662℃ and approximately 81 % weight loss occurred at 700℃ for the precursor.

TGA analyses of fresh and spent catalysts under air and nitrogen are presented in Figure A2; A-I. Initial weight loss under nitrogen and air flow up to 200℃ was essentially due to the removal of water and volatile materials. According to the figure, the weight loss under inert atmosphere occurs mainly in two different stages: drying and thermal decomposition. Additionally, for the air atmosphere decomposition/oxidation of coke compounds/char takes place as well. For the fresh support (RDF), the weight loss was 54% under N_2 compared to 86% under air at 700℃ (Figures A2-B and A2-A, respectively). For the spent RDF, few decomposition peaks could be noticed at 360℃, 440℃ and 670℃ under air (Fig. A2-A) which are absent in the inert atmosphere (Fig. A2-B). These could be mainly attributed to the decomposition of carbonaceous residue which are retained in the pores and cavities of the spent catalyst. Similarly, for the fresh $NiNO_3$/DF the weight loss under air (Fig. A2-C) was 17% less compared to under N_2 (Fig. A2-D). The coke deposition within the pores, did not let the catalyst undergo complete oxidation. The sharp peaks under N_2 are replaced by blunt and broad peaks, this again could be attributed to the carbon deposition on the catalysts. For the spent catalyst under CC-HYD treatment, a coke decomposition peak at 634℃ could be noticed. Similarly, for fresh $CoNO_3$/DF under N_2 (Fig. A2-F), it showed peaks at 394℃ and 688℃, these could be assigned to biochar support structure decomposition. The CC-HYD process, did not seem to influence coke decomposition peaks, a small blunt peak was observed at

630℃, which could be again due to support decomposition. However, under air (Fig. A2-E), both of the fresh and spent catalyst showed large decomposition peak at 326℃ and 513℃ respectively. This highlights the fact that support combustion and coke decomposition took place under air. Similar observation could be seen for NiOH/DF catalysts (Fig. A2-G and A2-H). For the CoOH/DF under air (Fig. A2-I), metal oxidation peak could be noticed, at 435℃, which was expected.

Under air	Under N_2

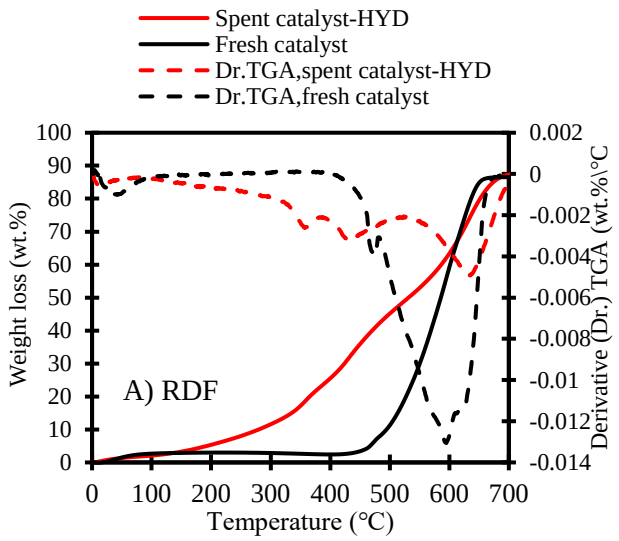

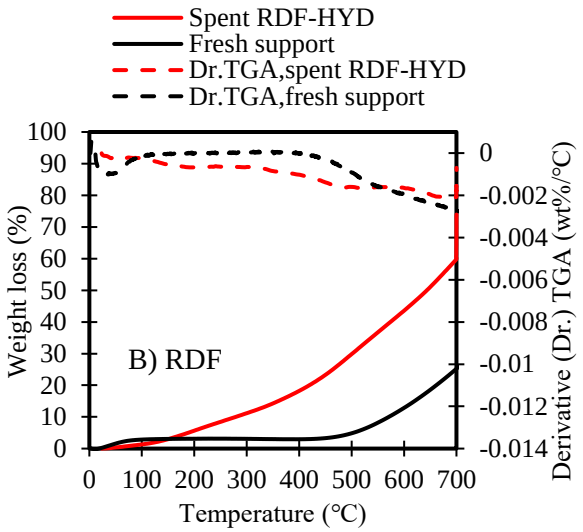

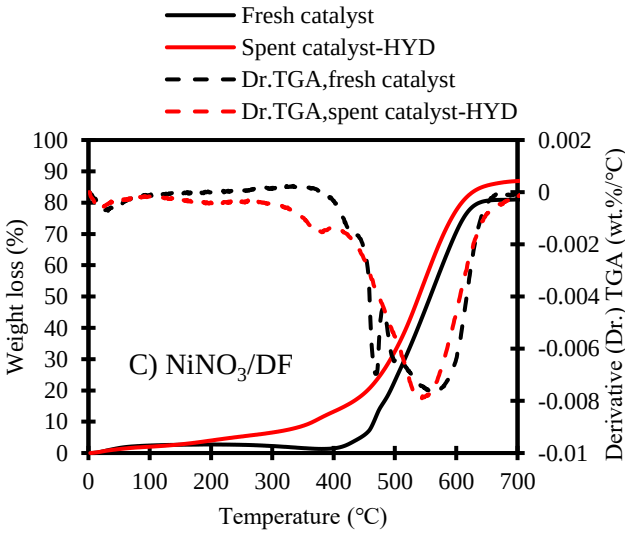

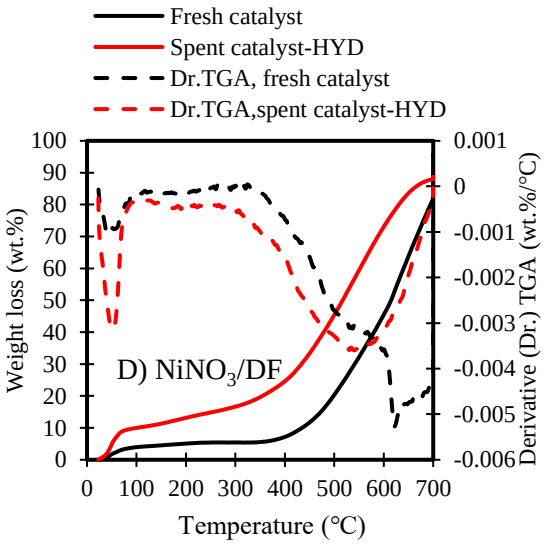

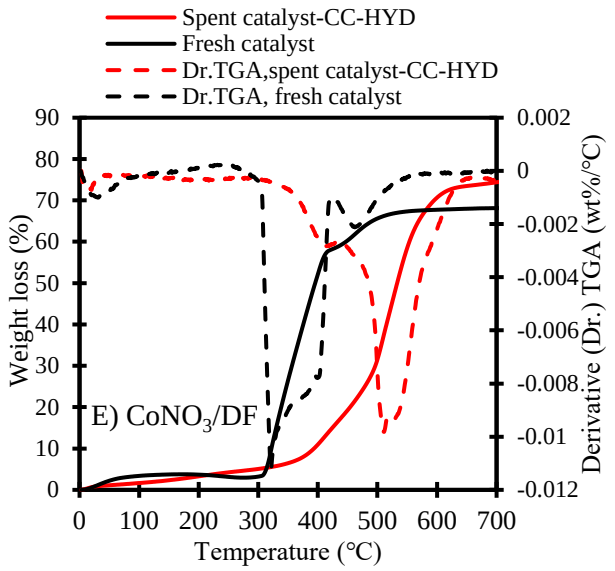
Spent catalyst-CC-HYD
Fresh catalyst
Dr.TGA,spent catalyst-CC-HYD
Dr.TGA, fresh catalyst
E) CoNO3/DF
Weight loss (%)
Derivative (Dr.) TGA (wt%/°C)
Temperature (°C)

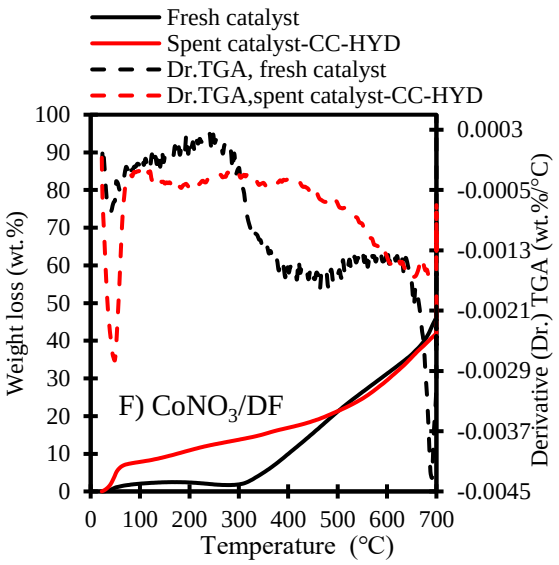
Fresh catalyst
Spent catalyst-CC-HYD
Dr.TGA, fresh catalyst
Dr.TGA,spent catalyst-CC-HYD
F) CoNO3/DF
Weight loss (wt.%)
Derivative (Dr.) TGA (wt.%/°C)
Temperature (°C)

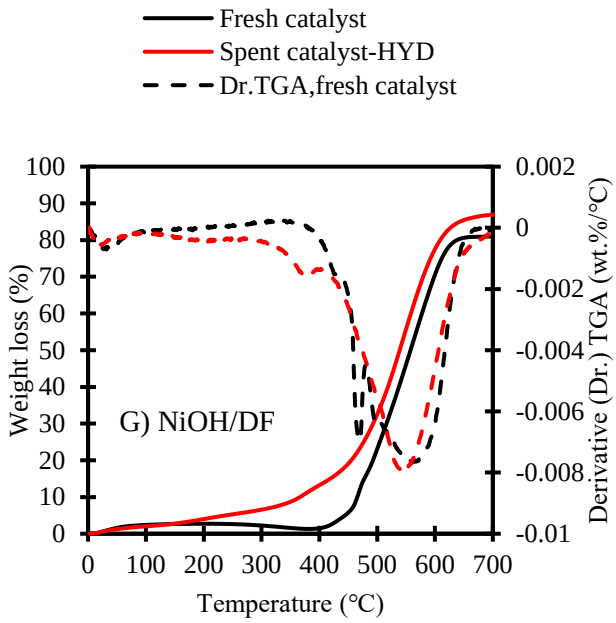
Fresh catalyst
Spent catalyst-HYD
Dr.TGA,fresh catalyst
G) NiOH/DF
Weight loss (%)
Derivative (Dr.) TGA (wt.%/°C)
Temperature (°C)

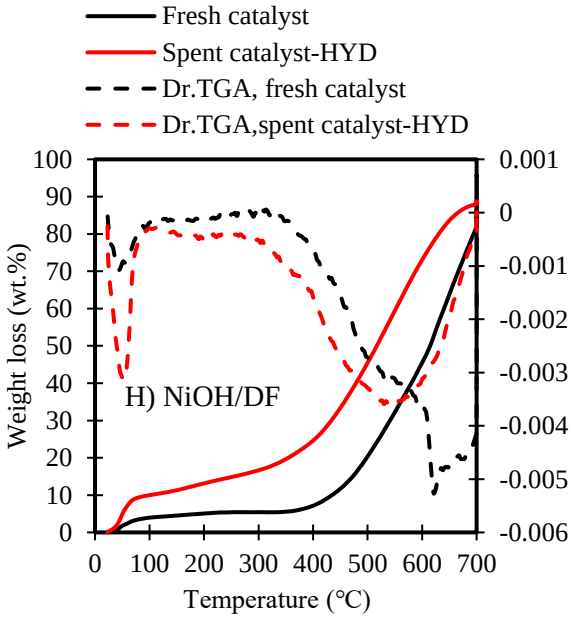
Fresh catalyst
Spent catalyst-HYD
Dr.TGA, fresh catalyst
Dr.TGA,spent catalyst-HYD
H) NiOH/DF
Weight loss (wt.%)
Temperature (°C)

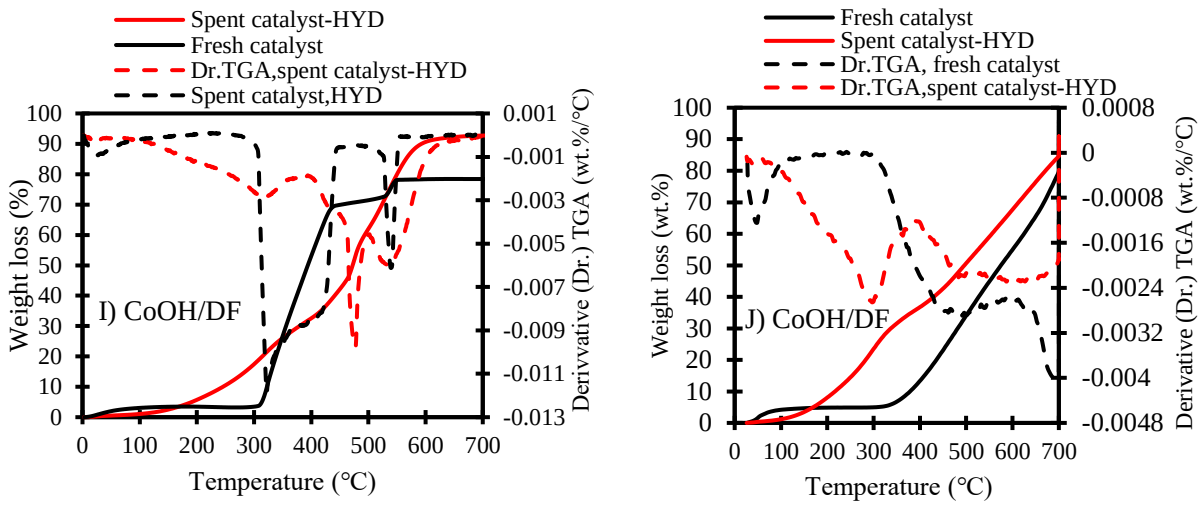

Figure A 2. TGA analyses of fresh and spent catalysts under air and nitrogen.

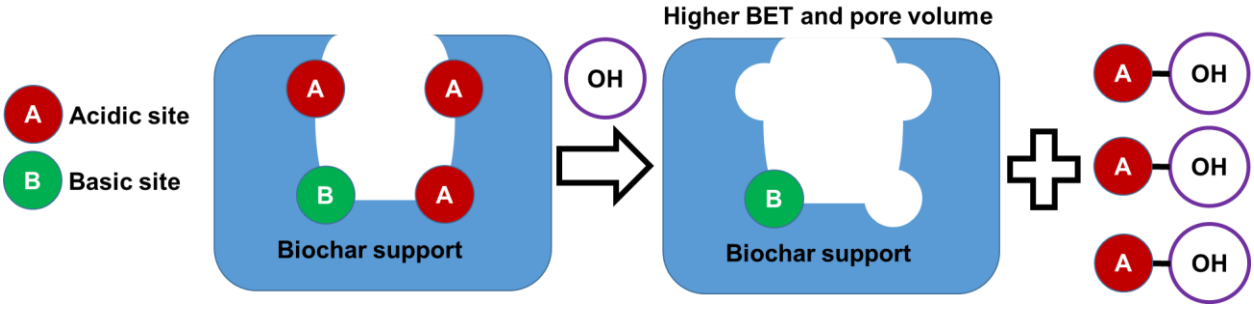

Figure A 3A: Influence of metal source (OH) on BET specific surface area and pore volume.

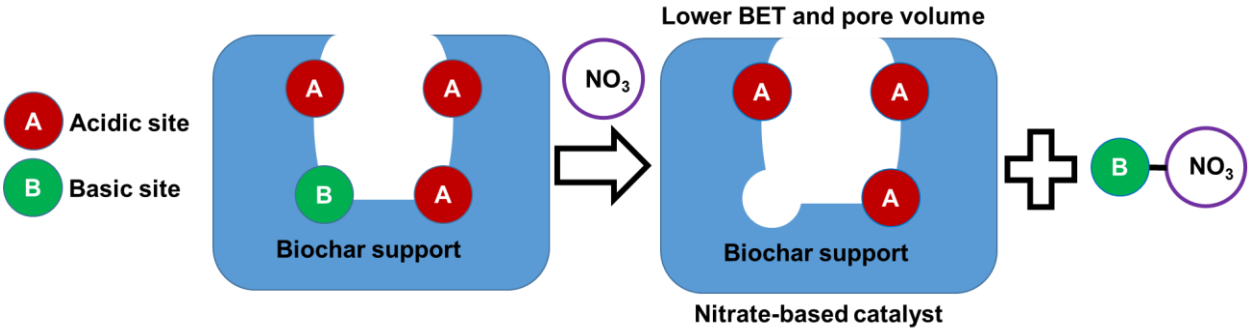

Figure A 4 B: Influence of metal source (NO_3) on BET specific surface area and pore volume.

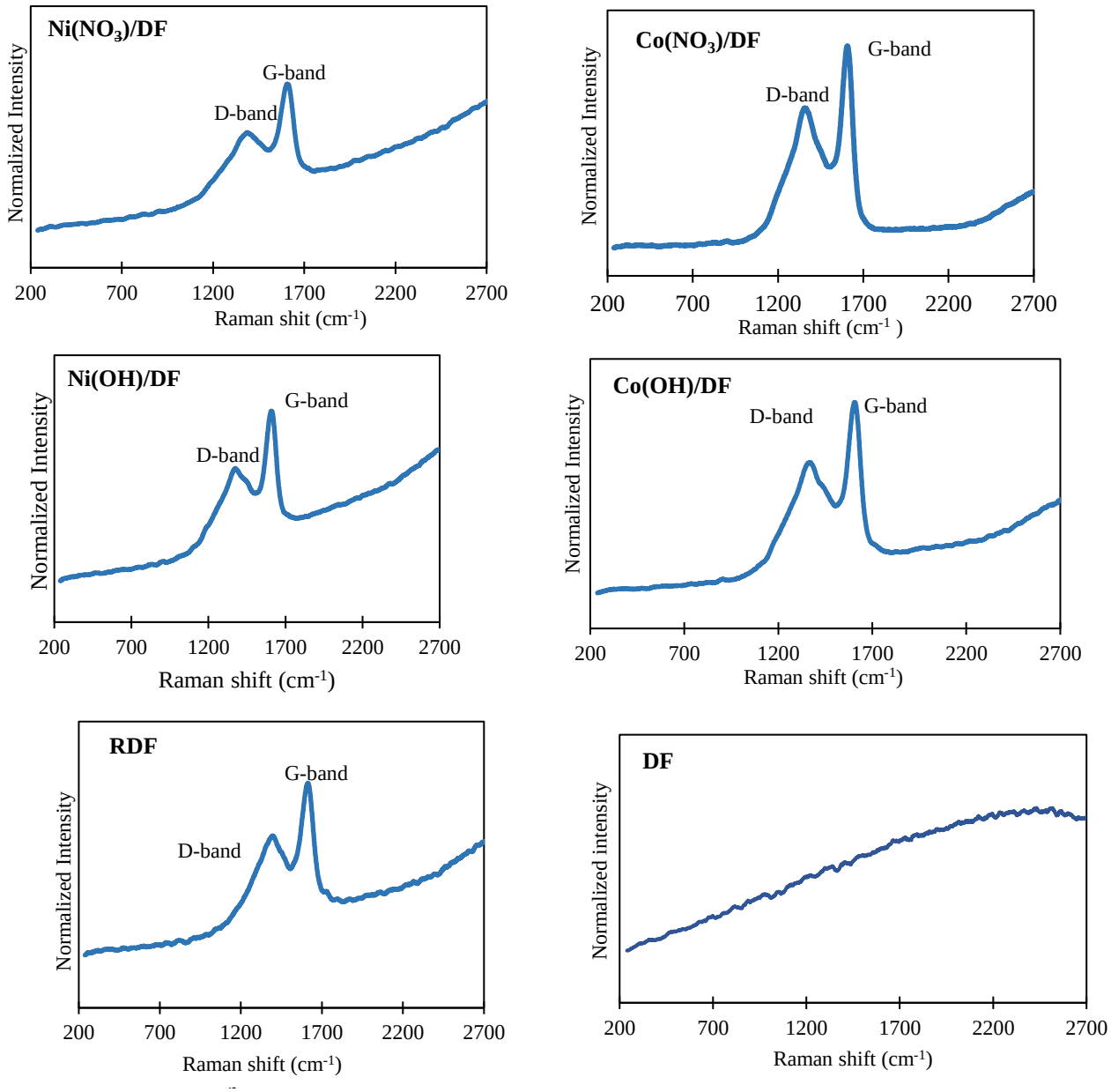

Figure A 5. Raman spectra of the catalysts, support, and the biomass.

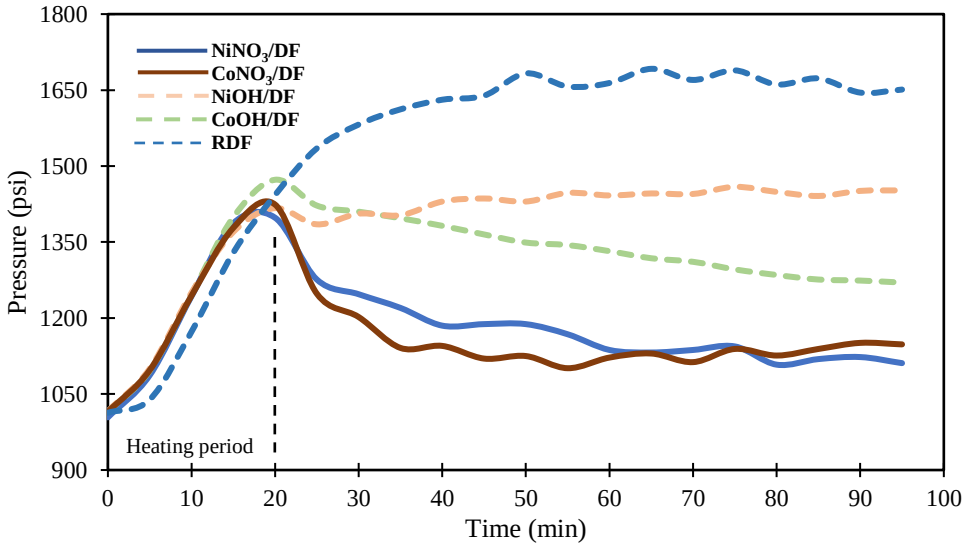

Figure A 6 A. Reactor pressure profile during the HYD experiments.

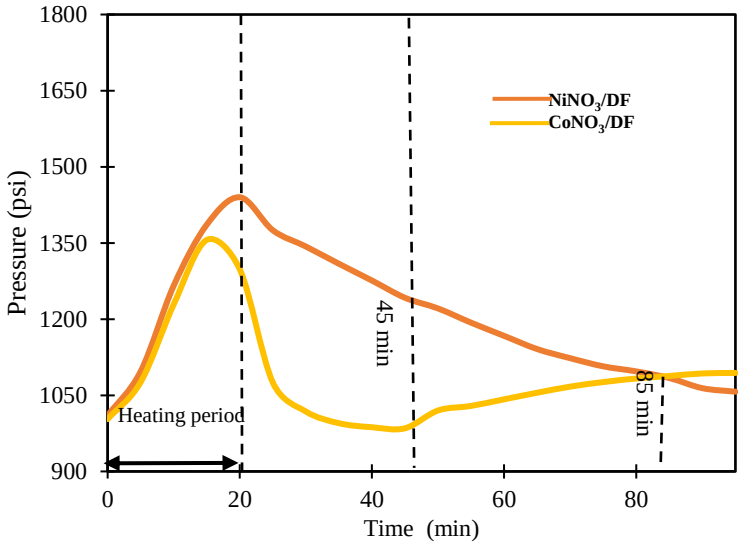

Figure A 6 B. Reactor pressure during CC-HYD experiments using different catalysts.

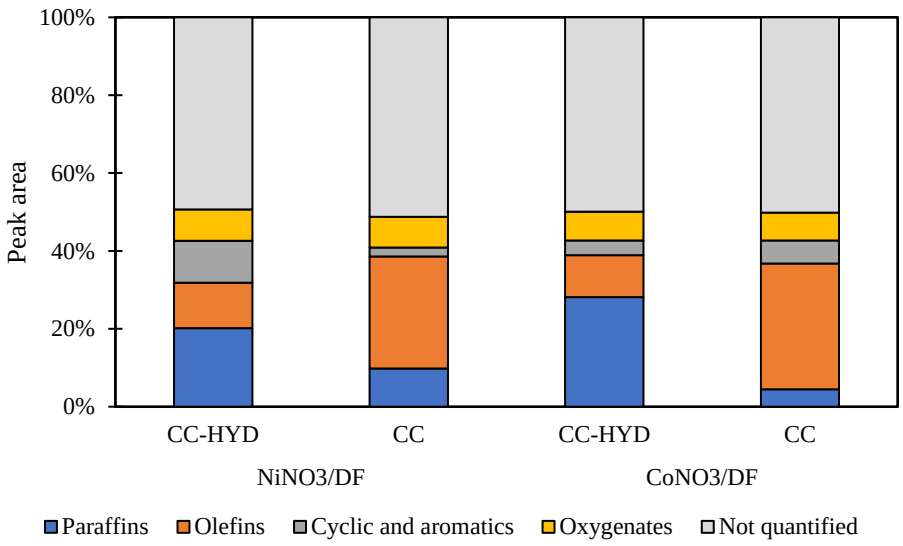

Figure A 7. Semi quantification and classification of upgraded carinata oil products by CC-HYD method of top seventy- fifty GC-MS peaks.

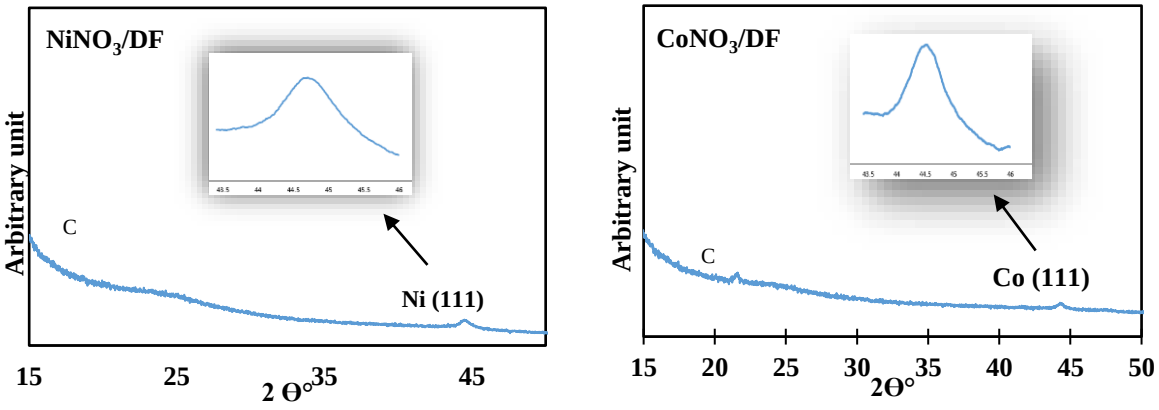

Figure A 8. XRD of nitrate catalysts.

Table A 1. pH of the metallic salt slurries.

	Metallic salt + DF biomass + H_2O	Metallic salt + H_2O
$NiNO_3$	3.30	6.1
$CoNO_3$	4.01	5.8
NiOH	5.86	8.7
CoOH	6.97	8.3
DF biomass	4.7 (no metal)	NA*

*Not applicable

Table A 2 A. ICP analysis of crude oil, biomass, catalyst support and catalysts.

	Catalyst support, biomass, and crude oil (wt.%)					
	DF	RDF	$NiNO_3$/DF	$CoNO_3$/DF	NiOH/DF	CoOH/DF
Al	0.0024	0.3151	0.2690	0.7420	0.3134	0.6400
B	0.0007	0.0013	NA	NA	NA	NA
Ca	0.0347	0.1712	0.1770	0.2760	0.1200	0.2900
Cd	<0.0002	<0.0002	<0.0005	<0.0005	<0.0005	<0.0005
Co	0.0001	0.0066	0.0280	10.8000	0.0140	8.6000
Cr	<0.0002	0.0025	0.0260	0.0140	0.0450	0.0200
Cu	<0.001	0.0022	0.0040	<0.0025	0.0080	0.0070
Fe	0.0055	1.0559	0.7870	3.6100	0.5300	0.8900
K	0.0428	0.1342	0.1870	0.1260	0.2100	0.0.26
Mg	0.0061	0.0190	0.0260	0.0330	0.0700	0.0400
Mn	0.0036	0.0113	0.0133	0.0134	0.0210	0.0140
Mo	<0.0002	<0.0002	<0.001	<0.001	<0.001	<0.001
Na	<0.01	0.1966	0.1350	0.2900	0.3500	0.0570
Ni	<0.0002	0.0190	10.9000	0.2080	8.2000	<0.01
P	0.0062	0.0169	0.0110	0.0140	0.0130	0.0180
Pb	<0.0005	<0.0005	<0.005	<0.005	<0.005	<0.005
S	<0.002	0.0048	NA	NA	NA	NA
Si	<0.01	0.0722	NA	NA	NA	NA
Zn	<0.001	0.0014	0.0420	0.0039	0.0100	0.0070

Table A 2 B: ICP analysis of upgraded oils.

	Upgraded oils (wt.%)						
	Carinata oil	$NiNO_3$-HYD	$CoNO_3$-HYD	NiOH-HYD	CoOH-HYD	$NiNO_3$-CC-HYD	$CoNO_3$-CC-HYD
Al	<0.002	0.0014	<0.002	0.0023	<0.002	0.0070	0.0130
B	<0.002	0.0005	0.0003	0.0007	0.0003	<0.0005	<0.005
Ca	<0.01	0.0123	<0.01	0.0175	<0.01	0.0350	0.0340
Cd	<0.0002	<0.0002	<0.0002	<0.0002	<0.0002	<0.0005	<0.0005
Co	<0.00005	0.0005	0.0157	0.0005	0.0068	<0.005	0.0150
Cr	<0.002	0.0260	0.0051	0.0173	0.0051	0.0290	0.0370
Cu	<0.001	<0.001	<0.001	<0.001	<0.001	<0.0025	<0.0025
Fe	<0.002	0.0821	0.0348	0.0821	0.0265	0.0362	0.5520
K	<0.01	<0.011	<0.012	<0.011	<0.012	<0.005	0.0090
Mg	<0.002	0.0041	0.0055	0.0028	<0.002	0.0210	0.0030
Mn	<0.001	0.0012	0.0018	0.0012	<0.001	0.0065	0.0157
Mo	<0.002	0.0003	0.0007	0.0008	0.0008	0.0030	0.0120
Na	<0.01	<0.01	<0.01	<0.01	<0.01	0.0120	0.0390
Ni	<0.002	0.0500	0.0011	0.0266	0.0015	0.0460	0.0200
P	<0.002	0.0004	0.0003	0.0007	0.0006	0.0220	<0.005
Pb	<0.0005	<0.0005	<0.0005	<0.0005	<0.0005	<0.005	<0.005
S	<0.002	<0.002	<0.002	<0.002	<0.002	<0.05	<0.05
Si	<0.01	<0.01	<0.01	<0.01	<0.01	<0.005	0.0060
Zn	<0.001	<0.001	<0.001	<0.001	<0.001	0.0060	<0.0005

Some metals, such as Ca, K in the upgraded oil is assumed to be due to the suspended catalyst that was not separated after centrifugation because. Ultra-filtration might be needed for complete separation of the catalyst from the oil. In the case of catalysts, the increase in metal contents (i.e. Ca and K) as compared with DF, are because of the reduction process. During reduction there is a loss of oxygenated functional groups and volatile compounds, what is left behind are carbon, other metals and compounds which are not volatile. Therefore, the concentration of the carbon and other metals increases after reduction. This higher concentration after reduction is reflected in the ICP

analysis. Additionally, the origin of some metals such as Fe in upgraded oil and the catalysts was neither from the DF biomass (0.0055%) nor from Carinata oil (<0.002%). Most likely Fe was physically mixed with the catalyst during the reduction process because of aging/rusting of the reduction tube.

Table A 3: Physiochemical characterizations of upgraded oil by HYD treatment for 75 min and 300 min (5 hours).

	Reaction time (min)					
	75			300		
Catalyst	RDF	$CoNO_3$/DF	CoOH/DF	RDF	$CoNO_3$/DF	CoOH/DF
H_2 consumption (mol/kg oil)	2.09	2.79	2.41	2.07	3.19	3.02
Oxygen content (wt.%)	5.9±2.4	8.06±1.1	7.4±0.8	5.5±1.3	2.5±1.2	1.8±0.5
Dynamic viscosity at 40 °C (cP)	38.3±3.2	18.2±2.1	16±0.5	33.5±3.1	8.2±1.7	10.3±0.7

Table A 4. Semi-quantification of top fifty GC/MS-detectable compounds after CC-HYD treatment of carinata oil over $NiNO_3$/DF catalyst.

Paraffins	**Area %**
Octadecane	1.6968
Heptadecane	1.6532
Dodecane	1.192
2-Methylpropane	0.8402
Nonadecane	0.8158
Butane	0.7339
Docosane	0.5941
Tetradecane	0.5811
Tricosane	0.5457
Undecane	0.4602
2,3,5-Trimethylhexane	0.4412
Heptane	0.4291
Total	**9.9833**
Olefins	**Area %**
1-Nonadecene	6.9864
1-Docosene	4.7108
1-Octadecene	3.6005
1-Pentadecene	2.4547
1-Hexadecene	2.3897
1-Tetradecene	1.9363

1-Nonyne	1.8013
1-Dodecene	1.6598
Nonadecene	0.9461
1-Tricosene	0.4712
1-Heptadecene	0.4299
Total	**27.3867**
Cyclic and aromatics	**Area %**
Tetradecahydroanthracene	0.5806
Cyclotriacontane	0.48
Cyclopentane, (2-methylpropyl)-	0.4722
Cyclopentane	0.44
Cyclotetradecane	0.3644
Total	**2.3372**
Oxygenates	Area %
Oxalic acid, cyclobutyl heptadecyl ester	3.2211
arachidic acid	0.9628
Stearate	0.9317
E-15-Heptadecenal	0.8104
E-14-Hexadecenal	0.7769
Butanoate	0.9614
E-8-Methyl-9-tetradecen-1-ol acetate	0.3767
Total	**8.041**

Table A 5. Semi-quantification of top fifty GC/MS-detectable compounds after CC-HYD treatment of carinata oil over $CoNO_3$/DF catalyst.

Paraffins	**Area %**
Nonadecane	6.8143
Hexadecane	6.4891
Undecane	5.6796
Octadecan	2.2392
Tricosane	0.7395
Dodecane	0.1627
Octadecane	0.0902
Total	**22.2146**
Olefins	**Area %**
1-Hexadecene	2.9005
1-Pentadecene	2.8073
(1-nonyne)	2.6831
1-Nonadecene	2.0681
10-Heneicosene (c,t)	1.5922
17-Pentatriacontene	1.3296
1-Docosene	1.3208
1-Hexacosene	0.82
7-Tetradecene	0.4197
1-Tridecene	0.3907

9-Tricosene, (Z)-	0.2745
Z-1,6-Tridecadiene	0.0771
Total	**16.6836**
Cyclic and aromatics	**Area %**
Cyclohexadecane	1.1532
Cyclohexyl benzoate	0.7321
Cyclohexane, 1,2-dimethyl-3-pentyl-4-propyl-	0.5615
Cyclohexane, 1-(1,5-dimethylhexyl)-4-(4-methylpentyl)-	0.5277
Cyclotetracosane	0.3943
Cyclopentane, 1-pentyl-2-propyl-	0.1916
Cyclopropane, 1-methyl-1-(2-methylpropyl)-2-nonyl-	0.1289
Cyclotetradecane	0.0797
Total	**3.769**
Oxygenates	Area %
E-15-Heptadecenal	1.909
1-Heneicosyl formate	0.9221
Tetradecanal	0.7902
Oxalic acid, cyclobutyl pentadecyl ester	0.9192
Oxirane, 2-decyl-3-(5-methylhexyl)-, cis-(.+/-.)	0.7472
Oxalic acid, isobutyl tetradecyl ester	0.5574
22-Tricosenoic acid	0.4215
E-14-Hexadecenal	0.414
Cycloeicosane	0.2867
10-Heptadecenoate	0.2243
9-Pentadecenoic acid	0.1013
E-2-Methyl-3-tetradecen-1-ol acetate	0.0872
Xanthumin	0.0458
Total	**7.4259**

Table A 6. Semi-quantification of top fifty GC/MS-detectable compounds after HYD treatment of carinata oil over $NiNO_3$/DF catalyst.

Paraffins	**Area %**
Heptadecane	4.5701
Tricosane	0.8204
Ethane;pentane	0.6503
2-Methylenebornane	0.4841
2-Methylenebornane	0.4805
Octadecane, 1-(ethenyloxy)-	0.4054
Ethane	0.3529
Octadecane	0.2861
Total	**8.0498**

Olefins	**Area %**
3-Heptadecene, (Z)-	1.9022
9-Eicosene, (E)-	1.8621
1-nonyne	1.6163
1-Hexacosene	1.5718
1-Nonadecene	2.2596
1-Docosene	0.9698
4-Butylphenylacetylene	0.92
Perhydrophenalene	1.8536
octadecene	0.7184
1-Heneicosene	0.7112
9-Octadecene, (E)-	0.6337
1,2-Diphenyl-1-propenyl	0.6301
1-Dodecyne	1.669
(Bicycloheptane)	0.4421
1-Heptadecene	0.4572
9-Tricosene, (Z)-	0.657
1-Undecyne	0.3536
1-Hexadecene	0.3631
1-Pentadecene	0.5998
1-tetradecene	0.6612
Total	22.9147
Oxygenates	**Area %**
Propan-1-ol;propan-2-ol;hydrate	4.0456
E-14-Hexadecenal	1.8391
Dicyclohexyl ketone	1.1237
oleate	0.9126
Oxirane, tetradecyl-	0.7979
E-15-Heptadecenal	0.5615
Oxalic acid, cyclobutyl heptadecyl ester	1.2471
Oxirane, 2-decyl-3-(5-methylhexyl)-, cis-	0.5267
Acetic acid, trifluoro-, hexadecyl ester	1.1012
13-Tetradecen-1-ol acetate	0.3584
Hexahydropyridine, 1-methyl-4-[4,5-dihydroxyphenyl]-	0.3858
E-8-Methyl-9-tetradecen-1-ol acetate	0.3564
1-Eicosanol	0.6978
5,6,6-Trimethyl-5-(3-oxobut-1-enyl)-1-oxaspiro[2.5]octan-4-one	0.2995
2-Methyl-Z,Z-3,13-octadecadienol	0.2994
Total	**15.5393**
Cyclic and aromatics	**Area %**
1,2-Bis(trimethylsilyl)benzene	2.8926
1,3-Diphenylpropane	1.8679
Cyclotriacontane	1.2294
Cyclotetradecane	1.0431

1-Dodecyne	0.6654
hexylcyclohexane	0.6405
pentylcyclohexane	0.6307
hexylbenzene	0.5578
Cyclohexylidenecyclohexane	0.3858
Benzo[h]quinoline, 2,4-dimethyl-	0.368
2-Methyl-7-phenylindole	0.3476
1-Cyclopentylcyclododecene	0.2896
Total	15.5393

Table A 7. Semi-quantification of top fifty GC/MS-detectable compounds after HYD treatment of carinata oil over $CoNO_3$/DF catalyst.

Paraffins	**Area %**
Tridecane	0.3279
Nonane	0.3265
Octadecane	0.303
Undecane	0.2675
Dodecane	0.2524
Hexadecane	0.2296
Isopentane	1.75
Total	3.41
Olefins	**Area %**
1-Nonadecene	3.0337
1-Dodecyne	1.9604
9-Tricosene, (Z)-	1.5243
1-Pentadecene	1.0968
Tetradecahydroanthracene	0.9952
1-Docosene	0.8479
3-Eicosene, (E)-	0.8169
1-tetradecene	0.722
1-Octadecene	0.717
1-Undecene	0.5294
Hexylbenzene	0.501
10-Heneicosene (c,t)	0.4838
Hexylbenzene	0.4524
1-Heptadecene	0.4523
17-Pentatriacontene	0.2277
Total	14.3608
Cyclic & aromatics	**Area %**
1,2-Diphenyl-1-propenyl	10.2447
(Bicycloheptane)	3.2889
methylcyclopentane	0.8981

1,3-Diphenylpropane		0.8473
2-Methylpropane;propylbenzene		0.7924
1,3-Diphenylpropene		0.6565
Cyclohexadecane		0.6321
Cyclohexylidenecyclohexane		0.6219
Cyclotetracosane		0.613
pentylcyclohexane		0.5901
(2-methylbutane		0.4866
Cyclododecyne		0.4864
Cyclopropylacetylene		0.4026
Cyclopentadecane		0.3789
(2-methylbutane;toluene)		0.3711
Butylbenzene		0.3555
2-Methylpropane		0.3502
(Diphenylmethane)		0.3028
Hexylcyclohexane		0.2974
(Perhydrophenalene)		0.2619
(1-Cyclopentylcyclododecene)		0.2582
Cyclotetradecane		0.2313
Total		
	23.3679	
Oxygenates		
	Area %	
Propan-1-ol;propan-2-ol;hydrate		7.6088
Dicyclohexyl ketone		2.9832
Oxalic acid, cyclobutyl pentadecyl ester		2.249
13-Tetradecen-1-ol acetate		1.9654
tert-Hexadecanethiol		1.3516
2- Chloropropionic acid, hexadecyl ester		0.9904
2-(Acetoxymethyl)-3-(methoxycarbonyl)biphenylene		0.9356
E-14-Hexadecenal		0.8614
2-Methyl-Z,Z-3,13-octadecadienol		0.7924
1,2-Diphenyl-1-propenyl		0.617
E-8-Methyl-9-tetradecen-1-ol acetate		0.511
Dodecanoate		0.4803
13-Octadecenal, (Z)-		0.3271
2-Heptadecenal		0.3069
Octadecanal		0.3024
E-2-Methyl-3-tetradecen-1-ol acetate		0.288
E-2-Methyl-3-tetradecen-1-ol acetate		0.288
Heptadecanoic acid, heptadecyl ester		0.2872
Total	23.2457	

Table A 8. Semi-quantification of top fifty GC/MS-detectable compounds after CC treatment of carinata oil over $NiNO_3$/DF catalyst.

Paraffins	**Area %**
Undecane	2.8681
Tricosane	2.5273
Pentane	2.3236
Tetratriacontane	1.2111
Ethane	0.8709
Total	**9.801**
Olefins	**Area %**
1-nonyne	3.9728
1-Tetradecene	3.5199
1-Nonadecene	2.3535
Butylnaphthalene	1.4416
1-Docosene	1.3988
1-Dodecene	1.1006
1-Octadecene	0.9985
1,8,15-Hexadecatriyne	0.916
1-Dodecyne	0.8102
10-Heneicosene	0.8072
1,8,15-Hexadecatriyne	0.7865
2,6-Diisopropylnaphthalene	0.6993
9-Tricosene, (Z)-	0.5987
4-octenyl	0.5919
Total	**19.9955**
Cyclic and aromatics	**Area %**
Cyclopentadecane	3.4474
Hexylcyclohexane	2.1778
Cyclotriacontane	1.0644
Naphthalene, diheptyl-2-methyl-	1.0114
1,3-Diphenylpropane	1.4213
Cycloundecane	0.7442
Octylbenzene	1.2068
Total	**11.0733**
Oxygenates	**Area %**
13-Tetradecen-1-ol acetate	2.9487
Oxalic acid, isobutyl hexadecyl ester	1.598
E-14-Hexadecenal	1.2753
4-Hexyloxyphenol	1.1622
1-Heneicosyl formate	0.7801
1-Tricosanol	0.5725
Total	**8.3368**

Table A 9. Semi-quantification of top fifty GC/MS-detectable compounds after CC treatment of carinata oil over $CoNO_3$/DF catalyst.

Paraffins	**Area %**
2-methylpropane	3.2913
Tricosane	1.1842
Total	**4.4755**
Olefins	**Area %**
10-Heneicosene (c,t)	7.6715
1-Nonadecene	6.5458
1-Dodecene	5.8294
(1-Tetradecene)	4.7006
1-Tridecyne	4.5919
(1-Undecyne)	1.5651
5-Eicosene, (E)-	1.428
Total	**32.3323**
Cyclic and aromatics	**Area %**
Cyclododecanol, 1-ethenyl-	2.1888
2-(Acetoxymethyl)-3-(methoxycarbonyl)biphenylene	1.4736
(Diphenylmethane)	1.1769
Cyclohexadecane	1.047
Total	**5.8863**
Oxygenates	**Area %**
1-Heneicosanol	3.0696
E-14-Hexadecenal	2.8452
Methyl 3-(acetyloxymethyl)biphenylene-2-carboxylate	1.21
Total	**7.1248**

Table A 10. Semi-quantification of top fifty GC/MS-detectable compounds after HYD treatment of carinata oil over NiOH/DF catalyst.

Paraffins	**Area %**
Tricosane	1.3851
Undecane	1.0212
Octacosane	1.007
Propane	0.988
hexadecane	0.402
Octadecane	0.3348
Total	5.1381
Olefins	**Area %**
1-Tridecyne	3.7787
(1-Dodecyne)	2.1618
1-Heptadecene	2.6893
1-Nonadecene	2.6151
1-Hexacosene	3.8492

1-Undecyne	2.1404
9-Eicosene, (E)-	1.6162
1-Docosene	1.2686
(1,2-Diphenyl-1-propenyl)	1.0679
13-Methyl-Z-14-nonacosene	0.9161
octadecene	0.8784
1-Hexadecene	0.6539
hexamethylbenzene	0.4646
3-Octadecene, (E)-	0.4476
cis-1-Chloro-9-octadecene	0.4263
1-Pentadecene	0.411
10-Heneicosene (c,t)	0.3099
2-Tetradecene, (E)-	0.3024
1-Octadecene	0.2989
Total	27.4251
Cyclic and aromatics	**Area %**
1,2-Diphenyl-1-propenyl	4.3683
1,3-Diphenylpropene	3.4167
hexamethylbenzene	2.5207
Cyclopentylbicyclohexyl	1.7735
Phenanthrene	1.0754
Cyclohexane, 1-(1,5-dimethylhexyl)-4-(4-methylpentyl)-	0.8886
Cyclopentane, 1,1'-[3-(2-cyclopentylethyl)-1,5-pentanediyl]bis-	0.8338
Nonadecylbenzene	0.7645
Bicycloheptane	0.7013
Octahydrophenanthrene	0.5441
Cyclopentylbicyclohexyl	0.4003
Hexamethylbenzene	0.3844
Total	20.016
Oxygenates	**Area %**
E-14-Hexadecenal	1.948
Oxirane, tetradecyl-	1.0478
Oxalic acid, pentadecyl propyl ester	0.6732
1,30-Triacontanediol	0.4922
E-15-Heptadecenal	0.487
13-Tetradecen-1-ol acetate	3.5658
E-8-Methyl-9-tetradecen-1-ol acetate	0.3697
2-Heptadecenal	0.3612
E-11(13,13-Dimethyl)tetradecen-1-ol acetate	0.3468

2-Octadecyl-propane-1,3-diol	0.3292
Tetradecanal	0.3032
1-Hexacosene	0.2943
Total	10.2184

Table A 11. Semi-quantification of top fifty GC/MS-detectable compounds after HYD treatment of carinata oil over CoOH/DF catalyst.

Paraffins	**Area %**
Dodecane	2.6489
Olefins	**Area %**
1-Hexadecene	13.1018
1-Tetradecene	9.7605
1-Pentadecene	3.5438
1-Octadecene	2.5317
17-Pentatriacontene	2.2417
1-Nonadecene	2.2316
Total	**33.4111**
Olefins	**Area %**
1-Hexadecene	13.1018
1-Tetradecene	9.7605
1-Pentadecene	3.5438
1-Octadecene	2.5317
17-Pentatriacontene	2.2417
1-Nonadecene	2.2316
Total	**33.4111**
Cyclic and aromatics	**Area %**
Cyclotetradecane	8.4071
Cyclopentadecane	2.2137
Total	**10.6208**
Oxygenates	**Area %**
Vinyl lauryl ether	3.504
E-14-Hexadecenal	2.7534
11,13-Dimethyl-12-tetradecen-1-ol acetate	2.2139
Total	**8.4713**

Table A 12 .Semi-quantification of top fifty GC/MS-detectable compounds after HYD treatment of carinata oil over RDF catalyst.

Paraffins	**Area %**
Heptadecane	8.1607
Nonadecane	7.2697
Octadecane	3.2372
Tricosane	1.9446

Total	20.6122
Olefins	**Area %**
1-Heptadecene	5.3079
1-Nonadecene	3.1286
3-Eicosene	2.1604
1-Pentadecene	3.8399
10-Heneicosene	1.565
1-Dodecene	1.4831
Total	17.4849
Cyclic and aromatics	**Area %**
Hexylcyclohexane	7.5474
Cyclotridecane	2.2475
Cyclopropylacetylene	1.3678
Cyclohexane	1.0614
1,3-Diphenylpropane	1.0177
Total	13.2418
Oxygenates	**Area %**
Propanol	1.9569
Cyclohexyl benzoate	1.6787
13-Tetradecen-1-ol acetate	1.5639
1-Hexacosanol	1.1522
C26H54O	1.116
2-(Acetoxymethyl)-3-(methoxycarbonyl)biphenylene	1.1115
Total	8.5792

Table A 13. Yield distribution of the upgraded oil by HYD treatment.

	Yield distribution (wt. %)									
Catalyst	**RDF**	**std.**	**$NiNO_3$/DF**	**std.**	**$CoNO_3$/DF**	**std.**	**NiOH/DF**	**std.**	**CoOH/DF**	**std.**
Liquid	63.5	2.7	79.6	3.3	83.7	1.1	70.0	2.3	68.3	2.0
Wax	13.1	0.7	7.2	1.4	5.6	0.6	9.7	0.8	11.0	0.3
Gas	23.3	2.5	13.2	2.0	10.7	0.7	20.3	1.5	20.7	2.4

Table A 14. Yield distribution of the upgraded oil by CC-HYD treatment.

	Yield distribution (wt. %)							
Catalyst	**NiNO3/DF**				**CoNO3/DF**			
Treatment	**CC**	**Std.**	**CC-HYD**	**Std.**	**CC**	**Std.**	**CC-HYD**	**Std.**

Liquid	79.9	1.71	86.7	1.30	70.0	3.78	89.3	1.84
Wax	7.1	0.75	5.6	0.57	10.1	2.25	5.0	0.69
Gas	13.0	2.31	7.7	1.87	19.9	6.03	5.7	1.15

Table A 15. Physical properties of Douglas fir biomass.

Physical Property	**Measured value**
Bulk density	0.0943 g/cm^3
Particle density	1.5611 g/cm^3
Moisture content	8.65%
Average particle size	1046 µm
Heating value	19.865 MJ/kg
Volatile matter	82.85%
Ash content	0.29%
Fixed carbon	16.86%
Extractives	3.44%
Lignin	35.79%
C	54.20%
H	5.575
N	0.05%
S	0.03
O	38.08%

Appendix B

8.2 Supporting Information for Chapter 4

Understanding the effects of feedstock blending and catalyst support on hydrotreatment of algae HTL biocrude with non-edible vegetable oil

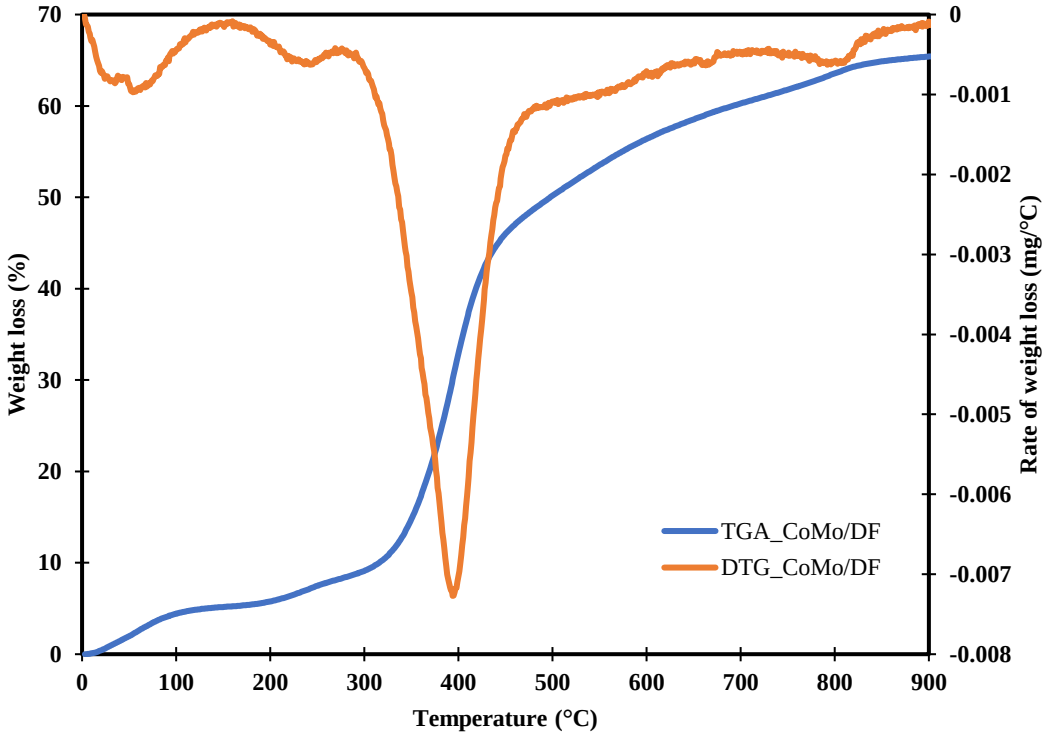

Figure B 1. TG-TPR thermograms in 10% H_2 (balance N_2) atmosphere of CoMo supported on DF support.

Figure B 2. As received Tetraselmis algae and HTL biocrude after solvent extraction.

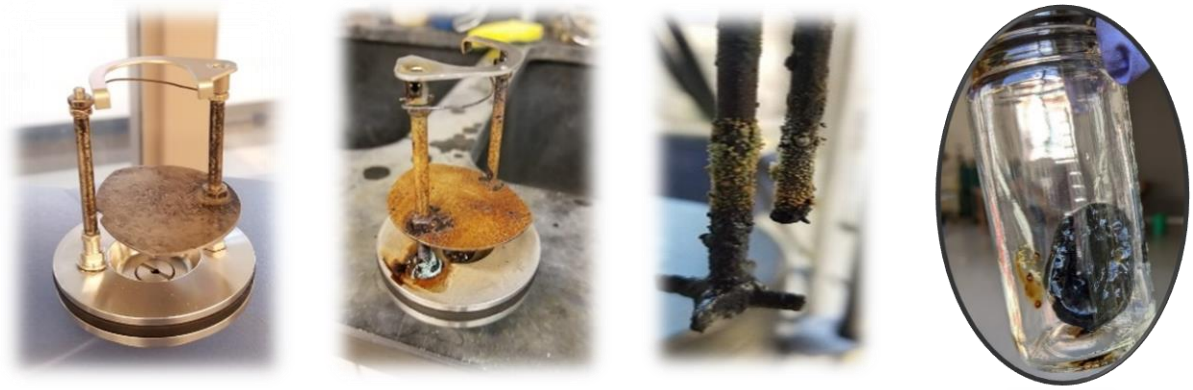

Figure B 3. Corrosion of equipment after hydrotreatment of DCM extracted HTL biocrude.

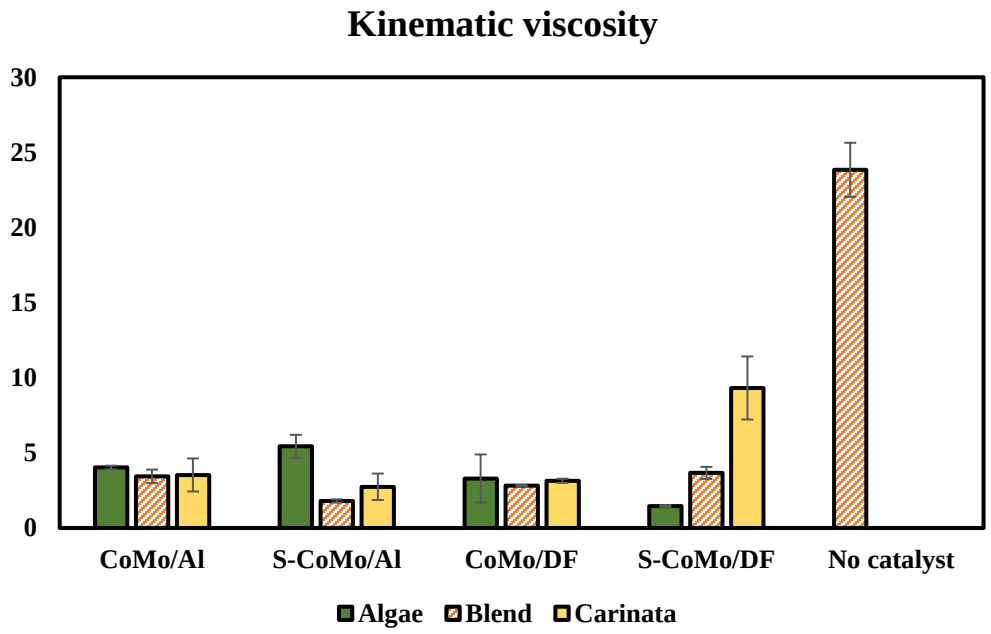

Figure B 4. Kinematic viscosity of UA, UB, and UC oils over different catalyst supports and sulfidation states.

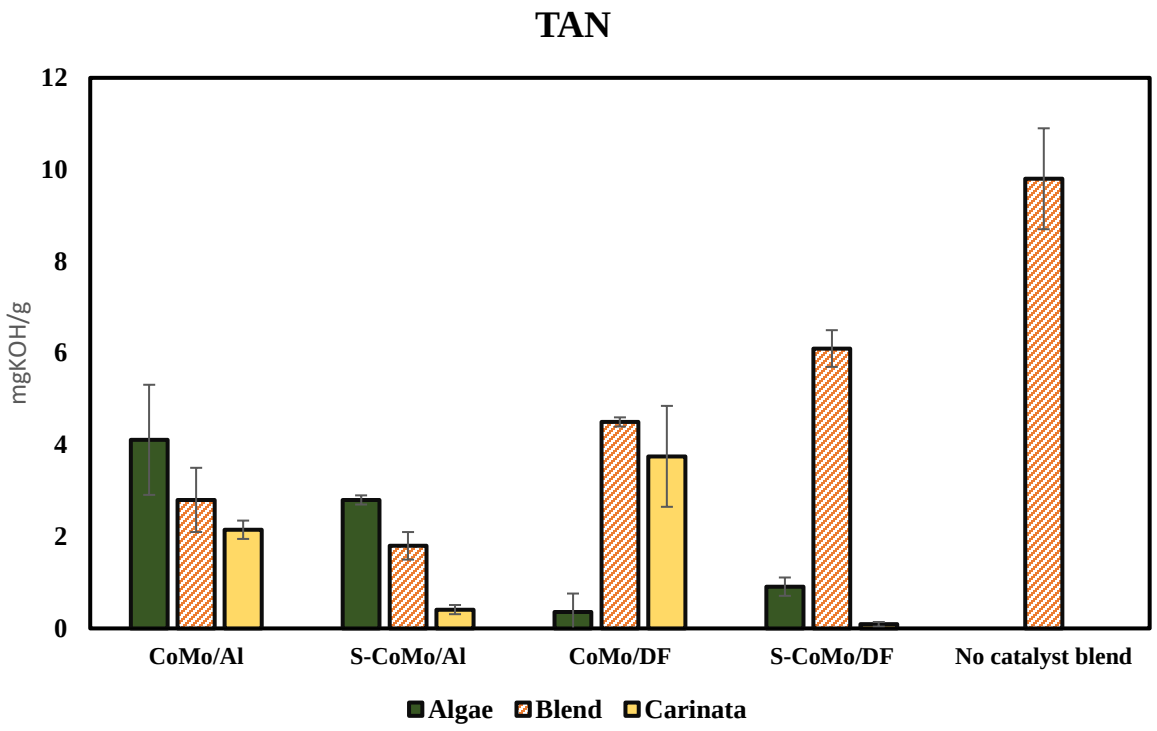

Figure B 5. TAN of UA, UB, and UC oils over different catalyst supports and sulfidation states.

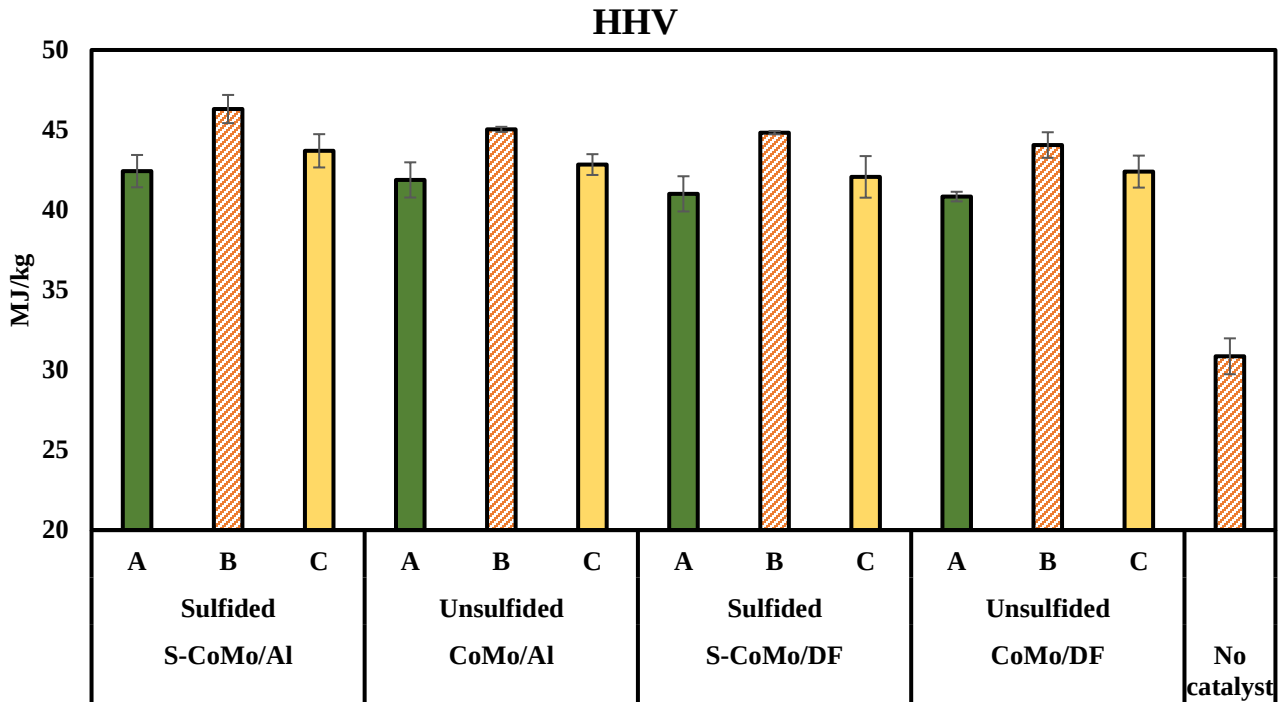

Figure B 6. HHV of UA, UB, and UC oils over different catalyst supports and sulfidation states.

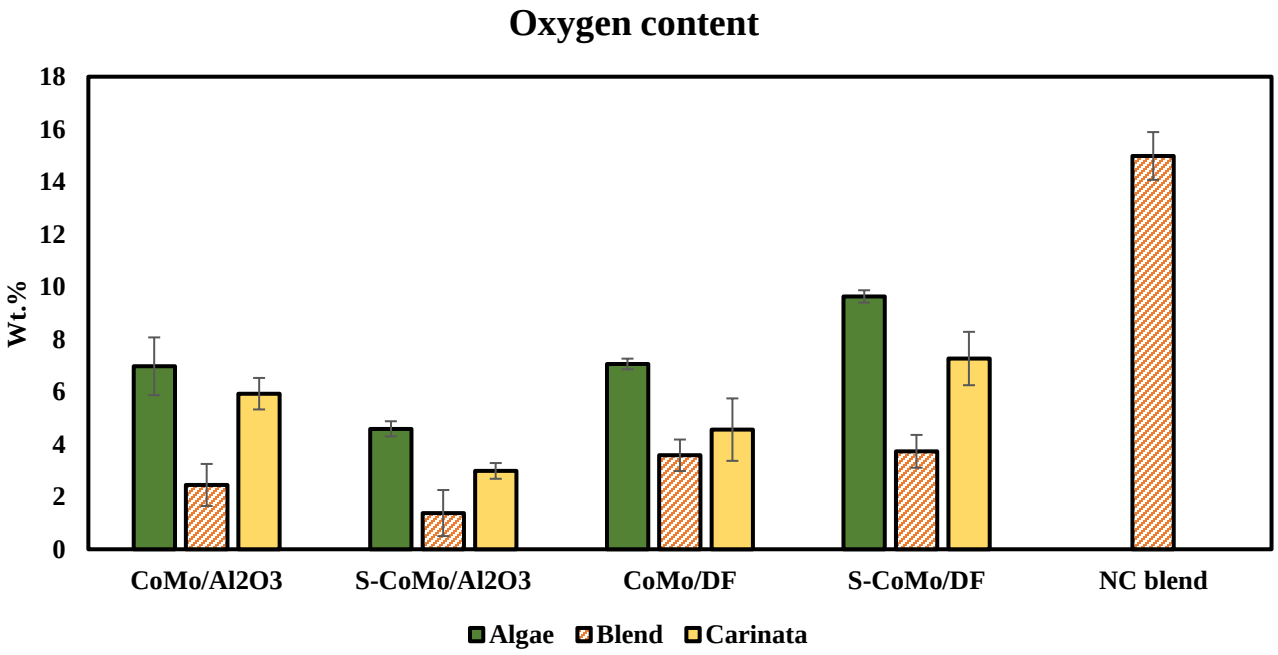

Figure B 7. Oxygen content of UA, UB, and UC oils over different catalyst supports and sulfidation states.

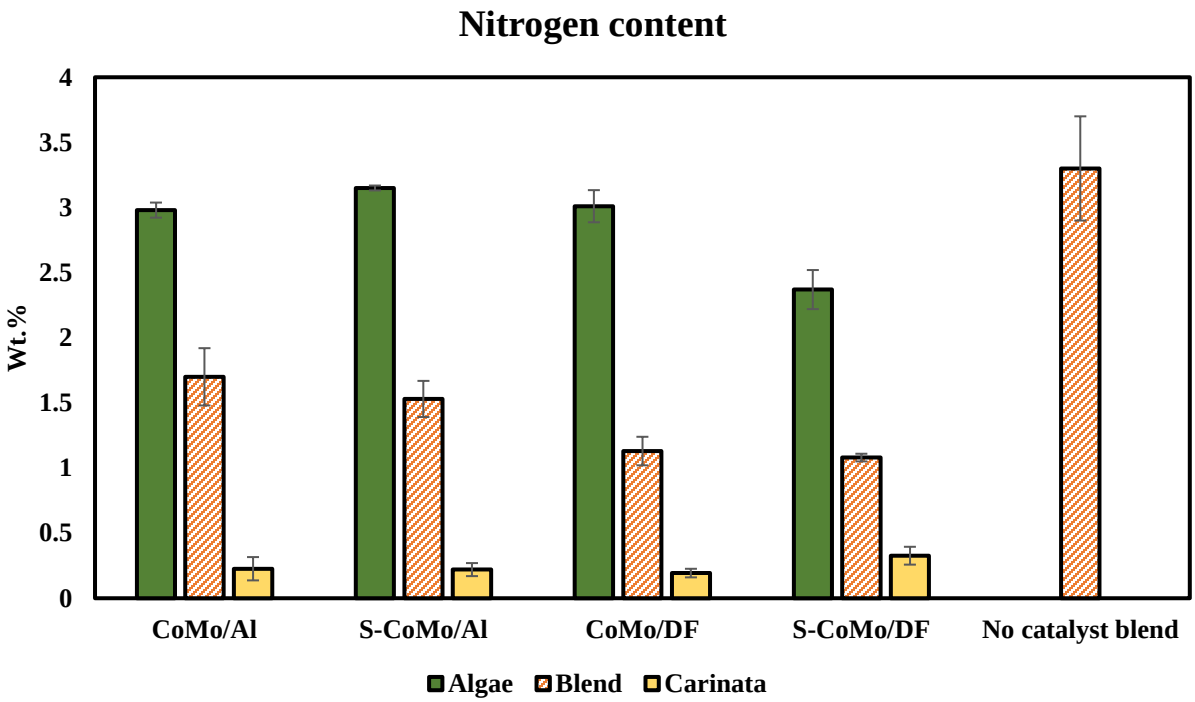

Figure B 8. Nitrogen content of UA, UB, and UC oils over different catalyst supports and sulfidation state.

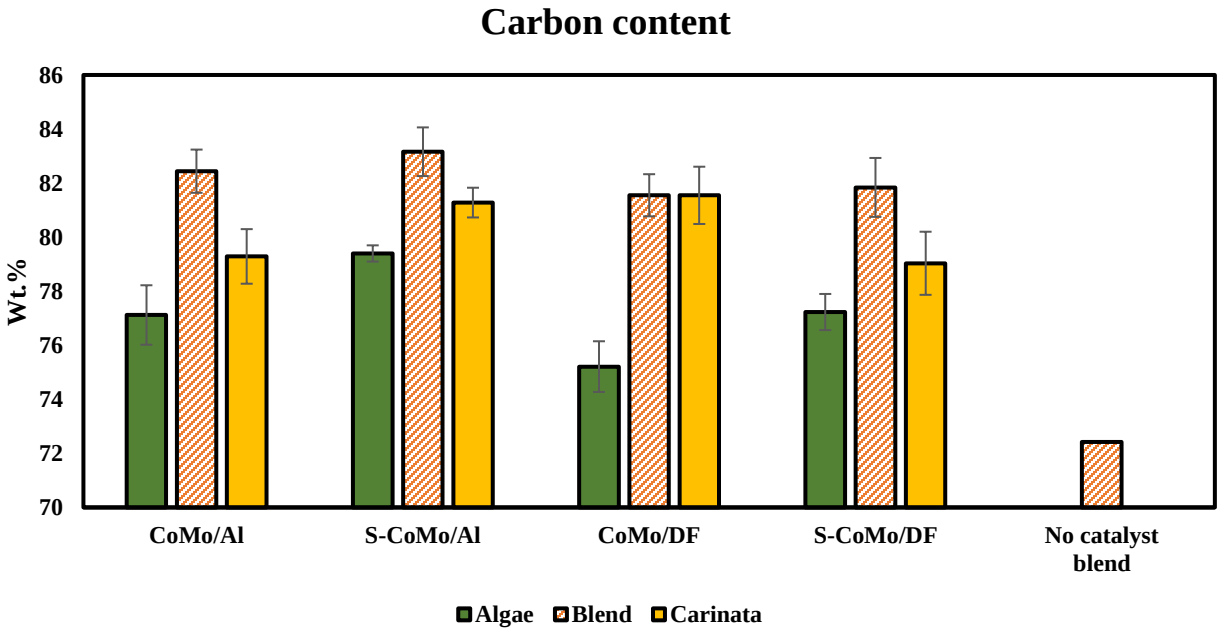

Figure B 9.Carbon content of UA, UB, and UC oils over different catalyst supports and sulfidation states.

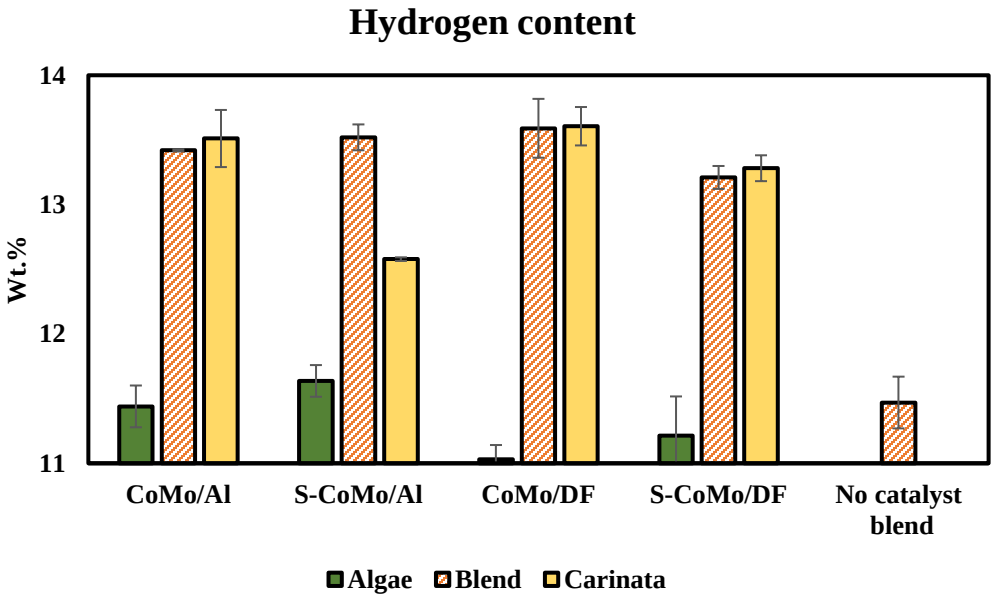

Figure B 10. Hydrogen content of UA, UB, and UC oils over different catalyst supports and sulfidation states.

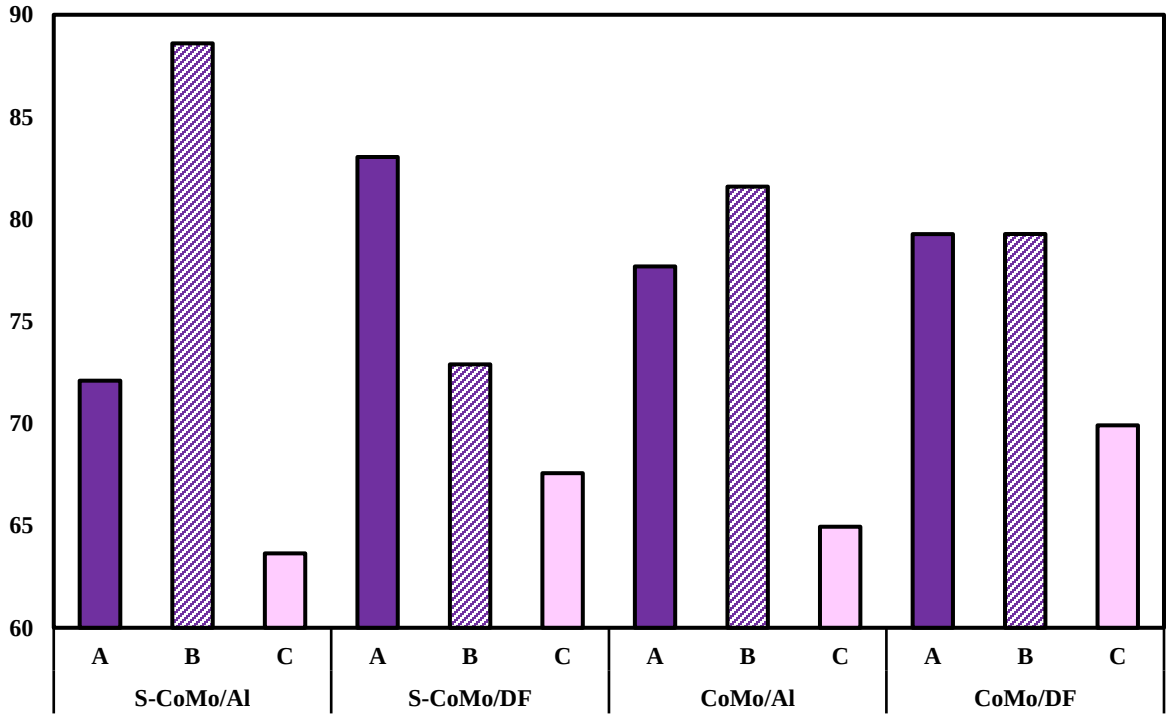

Figure B 11. Octane number of UA, UB, and UC oils over different catalyst supports and sulfidation states.

Table B 1. Elemental analysis of solvent extracted HTL biocrude.

Present study (*Tetraselmis sp.*)					
	C [%]	H [%]	N [%]	S [%]	O [%]
Methanol extracted HTL algae biocrude (as reported in the present study)	47.85±0.6	10.28±0.4	3.08±0.0	0.21±0.0	38.58±1.0
DCM extracted HTL algae biocrude (as reported here)	73.09±1.2	9.22±0.2	3.72±0.1	0.36±0.2	13.60±1.1
Literature data (*Tetraselmis sp.*)					
DCM extracted HTL algae biocrude [1]	71	9.5	5	0.6	14.0
DCM extracted HTL algae biocrude [2]	72.4	8.7	6.7	n.r	12.2

Table B 2. ICP characterization of the catalysts and oils.

	Al aluminum	**B** boron	**Ca** calcium	**Cd** cadmium	**Cr** chromium	**Co** Cobalt	**Cu** copper	**Fe** iron	**K** potassium
					(ppm)				
HTL algae biocrude	25.105	11.544	<25.0	<0.50	1.335	37.91	13.061	1075.02	1982.9
Upgraded oils									
CoMo/Al-UA	54.068	4.149	<25.0	<0.50	0.733	22.21	<2.50	20.983	855.27
S-CoMo/Al-UA	270.322	3.685	<25.0	<0.50	0.83	88.17	2.577	95.537	354.771
CoMo/DF-UA	11.181	2.347	<25.0	<0.50	<0.50	8.33	<2.50	<5.00	76.25
S-CoMo/DF-UA	9.23	1.12	<25.0	<0.50	<0.50	6.16	<2.50	<5.00	55.25
CoMo/Al-UC	80.528	2.281	<25.0	<0.50	0.561	10.19	<2.50	<5.00	<25.0
S-CoMo/Al-UC	26.759	0.507	<25.0	<0.50	<0.50	3.84	<2.50	<5.00	<25.0
CoMo/DF-UC	<5.00	2.064	<25.0	<0.50	0.794	2.66	<2.50	41.04	<25.0
S-CoMo/DF-UC	<4.93	4.90	29.5	<0.49	<0.49	3.22	<2.47	18.27	<24.7
No catalyst-UB	<5.00	6.204	<25.0	<0.50	7.358	34.27	<2.50	21.392	645.858
CoMo/Al-UB	<5.00	1.269	<25.0	<0.50	<0.50	64.9	<2.50	11.232	165.052
S-CoMo/Al-UB	<5.00	1.459	<25.0	<0.50	0.601	55.58	2.771	9.505	569.397
CoMo/DF-UB	27.792	2.803	<25.0	<0.50	1.794	3.78	<2.50	<5.00	710.708
S-CoMo/DF-UB	<2.48	4.69	14.6	<0.25	0.50	2.99	2.73	4.86	445
Fresh Catalysts									
CoMo/Al	387565	<0.50	1005.53	3.074	<0.50	18981.7	10.841	406.435	<25.0
CoMo/DF	33698.5	<0.50	1137.28	<0.50	6.173	17878.35	17.616	5905.59	811.012
S-CoMo/Al	405249	2.387	1013.1	3.156	2.387	19989.11	11.933	703.848	119.332
S-CoMo/DF	1043.2	<1.07	924.1	<1.07	35.16	17197	22.36	4104.28	982

	Mg magnesium	**Mn** manganese	**Mo** molybdenum	**Na** sodium	**Ni** nickel	**P** phosphorus	**Pb** lead	**S** sulfur	**Si** silicon	**Zn** zinc
					(ppm)					
HTL algae crude	29.633	<2.50	<1.00	13118.5	280.496	37.52	<0.50	4469.32	<25.0	13.49
				Upgraded oils						
CoMo/Al-UA	9.276	<2.50	19.112	5909.14	9.695	28.836	<0.50	1299.65	37.477	<2.50
S-CoMo/Al-UA	<5.00	<2.50	162.908	2117.38	50.703	18.183	<0.50	762.347	60.907	<2.50
CoMo/DF-UA	5.417	<2.50	<1.00	<25.0	2.858	2.519	<0.50	193.552	42.906	2.536
S-CoMo/DF-UA	3.38	<2.50	<1.00	<25.0	1.34	2.02	<0.50	110.41	31.83	1.21
CoMo/Al-UC	<5.00	<2.50	21.558	<25.0	6.133	3.697	<0.50	74.539	43.367	<2.50
S-CoMo/Al-UC	<5.00	<2.50	7.473	<25.0	1.608	2.085	<0.50	52.014	36.048	<2.50
CoMo/DF-UC	<5.00	<2.50	8.705	<25.0	3.16	1.253	<0.50	61.528	27.355	<2.50
S-CoMo/DF-UC	7.70	<2.47	63.47	<24.7	1.27	3.68	<0.19	33.5	<24.7	<2.47
No catalyst -UB	33.48	2.744	<1.00	4257.48	9.815	4.643	<0.50	445.383	154.949	<2.50
CoMo/Al-UB	<5.00	<2.50	<1.00	<25.0	6.529	1.545	<0.50	207.538	67.436	<2.50
S-CoMo/Al-UB	<5.00	<2.50	<1.00	49.224	8.213	2.105	<0.50	198.297	32.769	<2.50
CoMo/DF-UB	6.377	<2.50	<1.00	812.317	5.334	3.828	<0.50	190.381	92.752	<2.50
S-CoMo/DF-UB	3.79	<1.24	6.52	949.6	1.05	4.20	<0.10	134.9	161.8	1.42
				Fresh Catalysts						
CoMo/AL	317.19	<2.50	75193.5	302.413	142.638	9815.95	2.469	1483	990.944	71.155
CoMo/DF	187.942	67.304	101697	1140.7	192.999	877.869	<0.05	620	1523.95	18.018
S-CoMo/Al	346.751	<2.50	77317	317.7	258.7	10329	2.41	1716	997.2	74.91
S-CoMo/DF	173.91	92.89	98260	528.3	98.71	136.19	<0.41	4373	953.3	15.68

Table B 3. Synergistic effect calculation.

Catalyst type	Type of characterization	Algae	Carinata	Average	Blend	Calculation	Synergistic change
S-CoMo/Al	Carbon (wt.%)	79.39	81.27	(79.39+81.27)/2 = 80.33	83.16	• (83.16-80.33) = 2.83 • 2.83/80.33 = 0.035 • 0.035/100 = 3.5	+3.5%
CoMo/DF	Viscosity 40°C(m^2/s)	2.82	3.14	(2.82+3.14)/2 = 2.98	3.30	• (2.98-3.30) = -0.32 • -0.32/2.98 = -0.107 • -0.107/100 = 10.7	-10.7%

Table B 4. Acid sites of DF biochar support determined by Boehm Titration method.

Catalysts	Surface functional groups (mmol/g)				
	Phenolic	Lactonic	Carboxyl	Total acid sites	Basic sites
CoMo/DF	10.3	-10.6	11.5	11.2	6.4
S-CoMo/DF	-0.5	8.9	2.1	10.5	5.7

NH_3-TPD analysis was carried out to evaluate the distribution of acid sites such as weak (<200°C), moderate (>200°C and <400°C) and strong (>400°C). The weak acidic sites correspond to desorption of loosely bound ammonia, while ammonia desorption at temperature greater than 400°C corresponds to strong acidic sites. A medium intensity desorption peak at higher temperature was observed for DF, and this could be due to the support's acidity containing oxygen functional groups. From our previous study we have seen that introduction of metals such as $CoNO_3$, CoOH, $NiNO_3$, and NiOH on biochar support introduced medium to strong acidic sites

on the DF biochar support (Figure 5). If the same trend holds true, then we might expect similar medium to strong acidic sites for bimetallic CoMo impregnated on DF support as well.

Figure B13-A is from our previous study where we used the same DF biochar support to hydrotreat carinata oil. On the other hand, alumina support demonstrated a high intensity peak lower temperature TPD curve compared to DF support (B13-B). This again supports our conclusion that DF support have high inherent oxygen functional groups that impart strong acid sites and take part in hydrogenation reactions. The NH_3-TPD profile of the bimetallic CoMo supported on carbon is demonstrated in Figure B13-C. The NH_3 uptake is seen at high temperature of approximately 660℃ and 730℃. This signifies a strong oxidized support consisting mainly of carboxylic and lactone acid groups. Alternatively, CoMo/alumina support as seen in Figure B13-D, shows low temperature (250℃) NH_3 desorption peaks i.e., weak acid sites compared to CoMo supported on carbon. Acidity favors HDN and HDS by changing the electronic properties of the active sites. Therefore, according to our previous data and literature data, DF supported catalysts might have more acidic sites which means that it might have more active sites with higher affinity to adsorb and remove sulfur and nitrogen compared to alumina support [3].

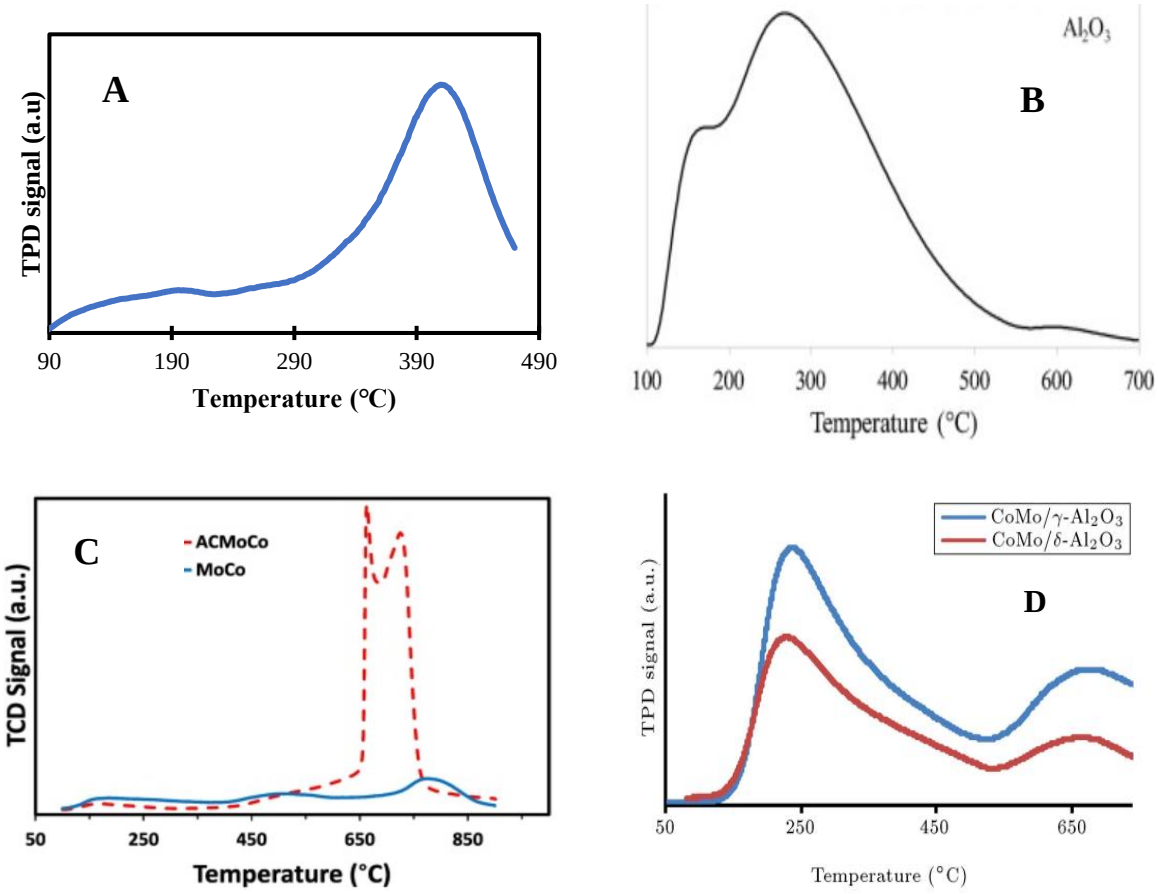

Figure B 12. NH3-TPD curves for (A) DF biochar support from our previous study [4], (B) Al2O3 support [5] (C) CoMo impregnated on activated carbon [3] (D) CoMo/alumina support [6].

TGA Under Nitrogen **TGA Under air**

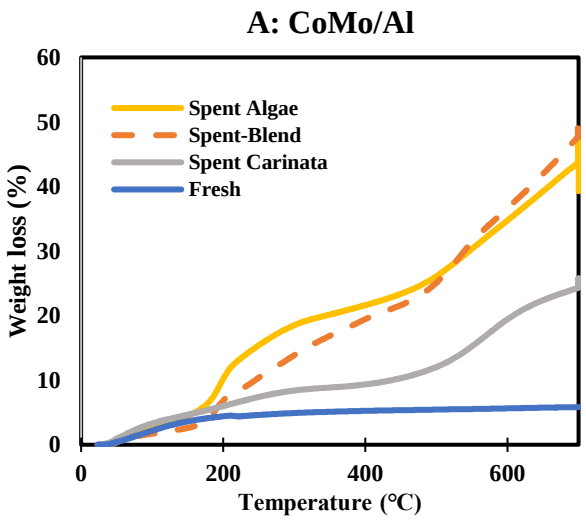

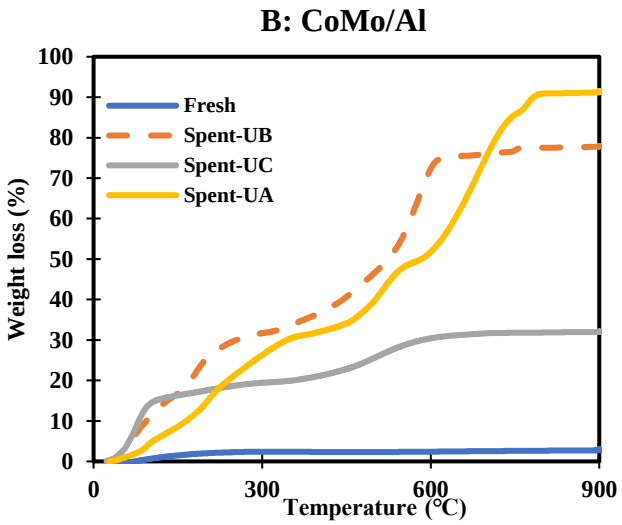

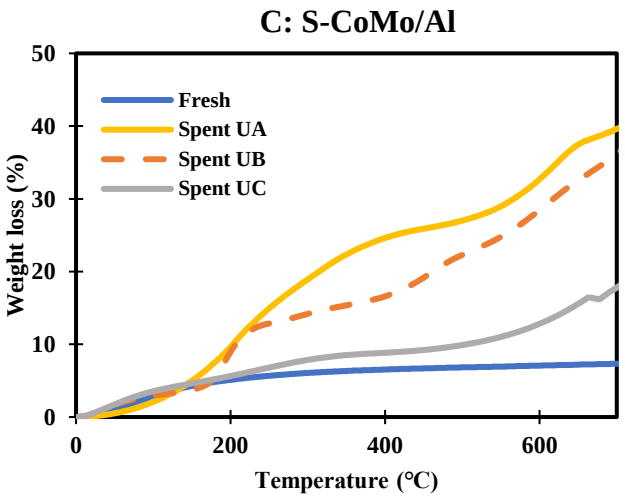

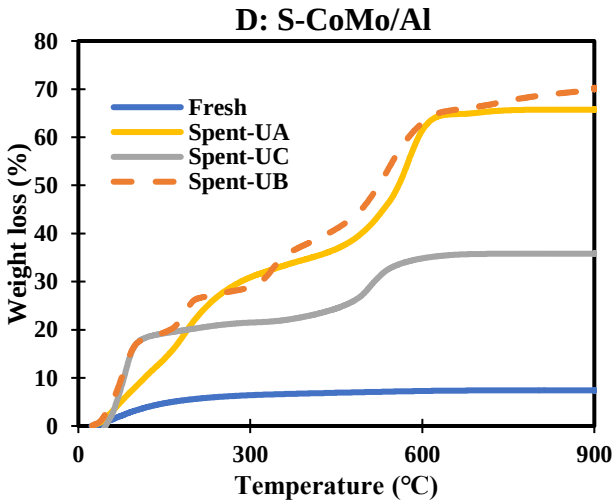

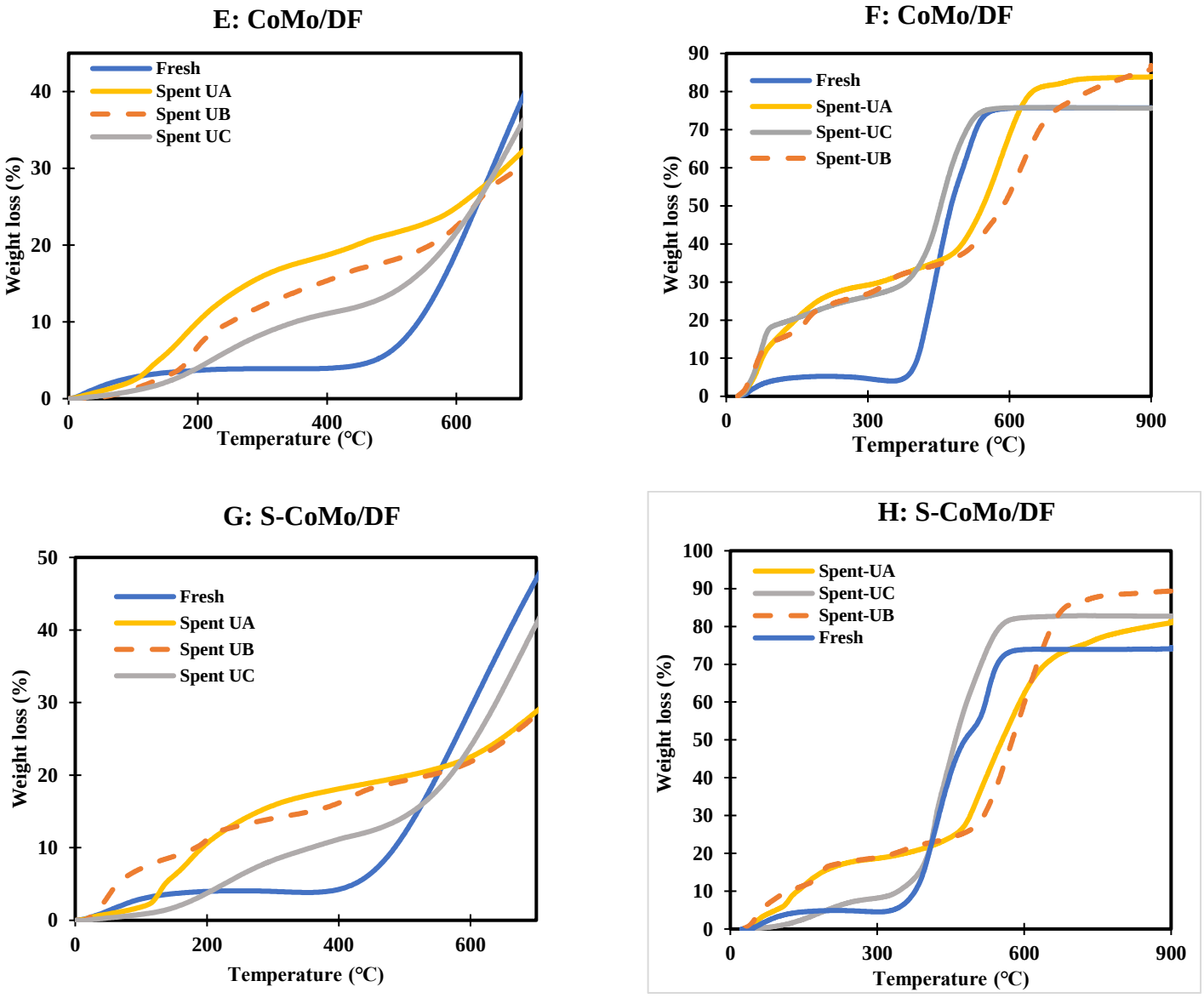

Figure B 13. TGA analyses of fresh and spent catalysts under air and nitrogen.

DTG Under Nitrogen **DTG Under air**

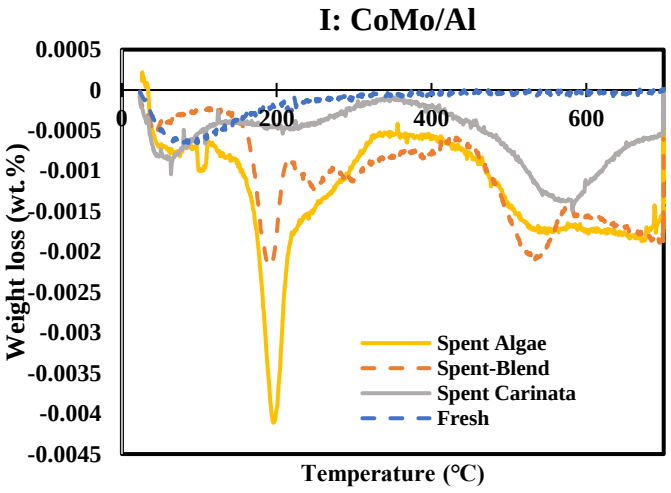

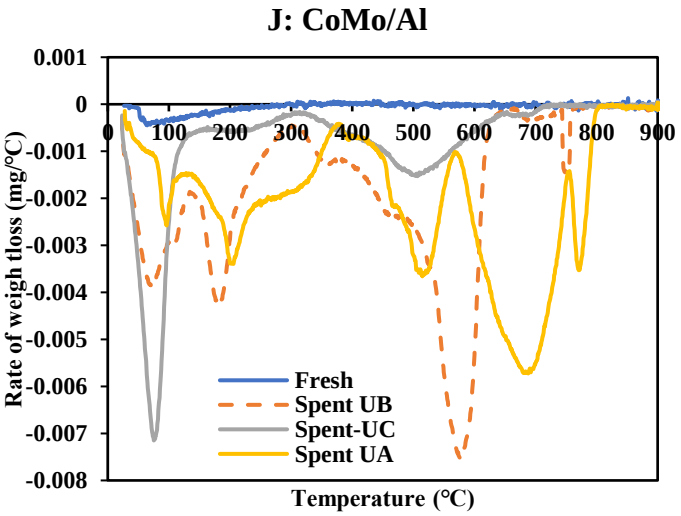

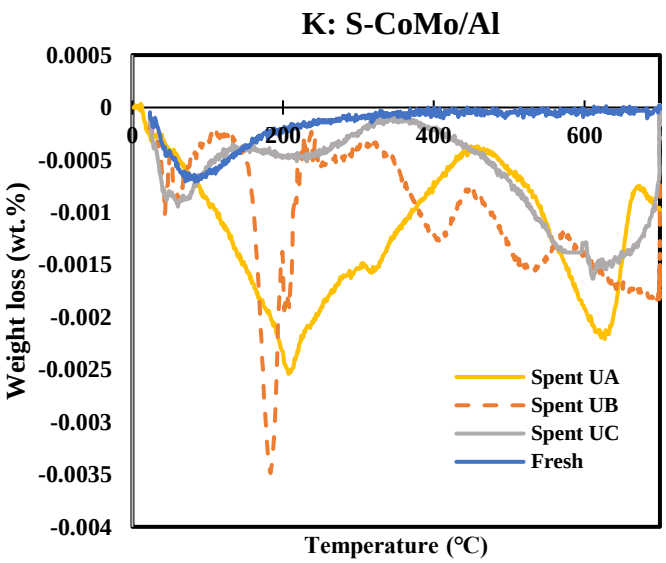

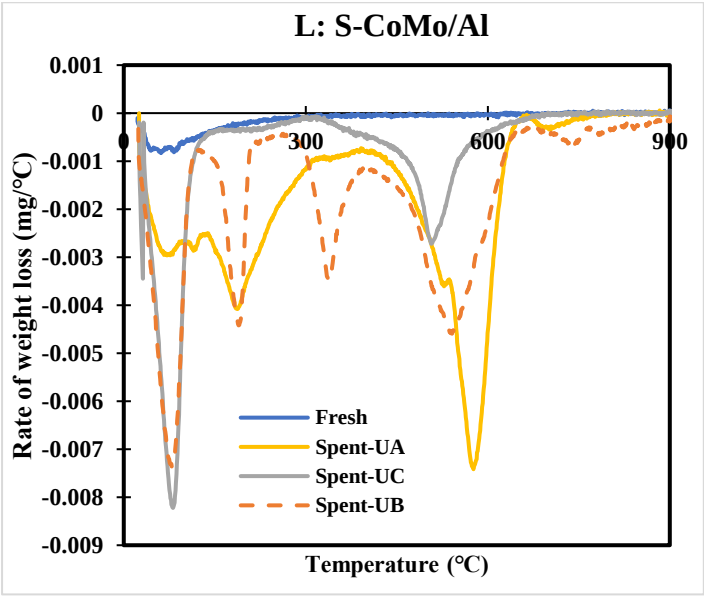

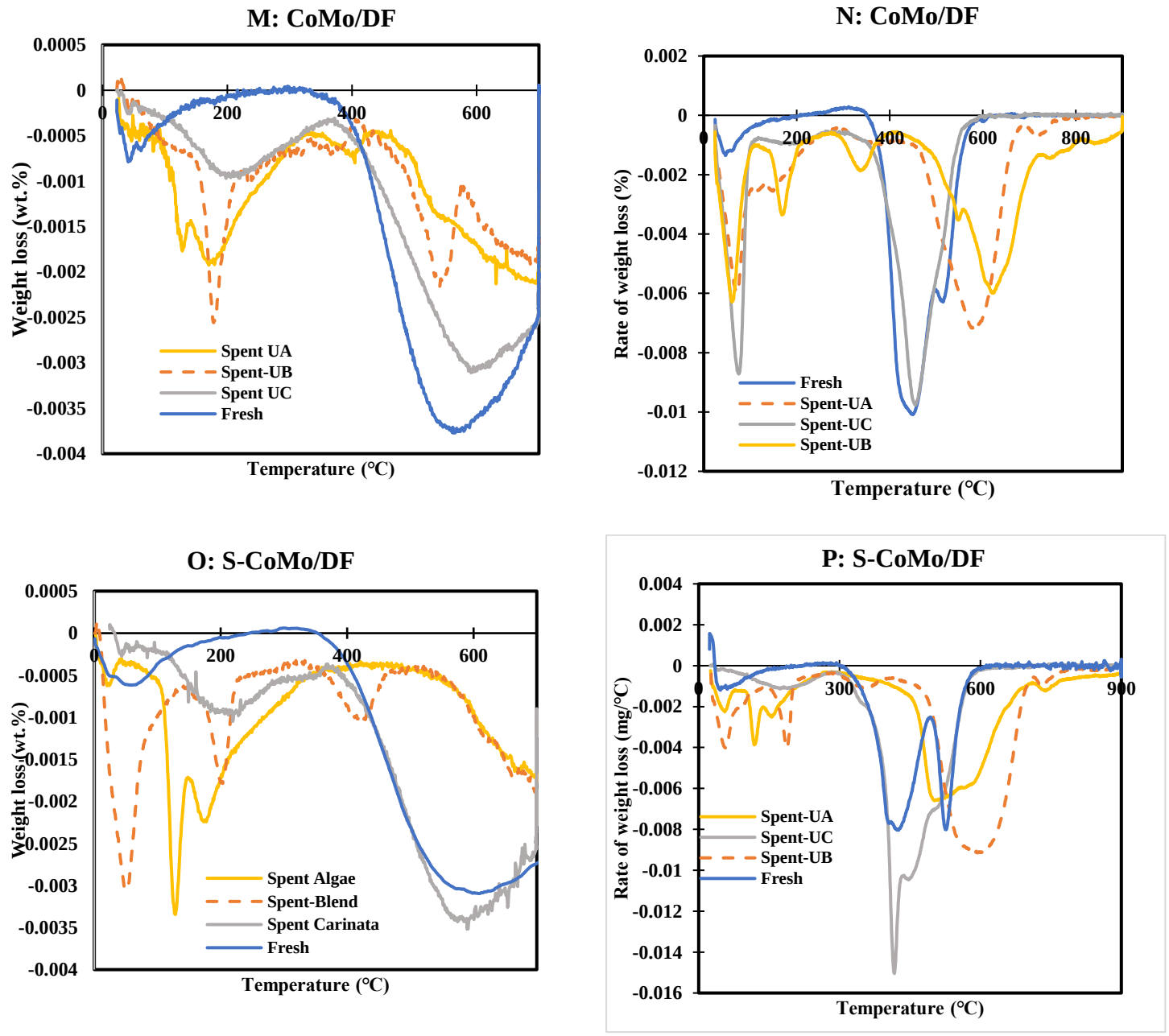

Figure B 14. DTG analyses of fresh and spent catalysts under air and nitrogen

Researchers have categorized coke in two types based on techniques such as TPO, TGA, 13C NMR [7] etc. In our study we have used TGA under air and N_2 to analyze the weight loss and type of coke formed for the spent catalysts. Figure 14 shows the TGA thermograms for a heating rate

of 10°C/min and flow rate 20 mL/min of air or nitrogen. The actual and derivative weight losses from 23°C to 900°C were recorded and presented in the figure. Initial weight loss under nitrogen and air flow up to 200°C was essentially due to the removal of water and volatile materials. According to the figure 14, the weight loss under inert atmosphere occurs mainly in two different stages: drying and thermal decomposition. Additionally, for the air atmosphere decomposition/oxidation of coke compounds/char takes place as well. According to Yan et. al., [7] soft coke mainly comprises of aromatics which get reversibly adsorbed on the catalyst sites and can be remove by oxidation at temperatures around 300°C. Hard/refractory coke gets adsorbed deeply on the support and can removed under air at temperatures above 400°C. Coke could be deposited on the external surface, on the metallic sites and inside the micropores of the catalyst.

Alumina support irrespective of sulfidation status, and TGA atmosphere the fresh catalyst and spent catalysts from UCs demonstrated lower weight loss compared to UB and UA. For UC a weight loss of 18% (Figure 14A; CoMo/Al, N_2),20% (Figure 14C; S-CoMo/Al.N_2), 30%(Figure 14B; CoMo/Al, air) and 34% (Figure 14D; S-CoMo/Al air) were recorded. In terms of the DTG curve, a small decomposition peak below 200°C (Figure 14-I and 14-K under N_2) was replaced by a sharp peak (Figure 14J and 14L under air). A broad decomposition peak from 580°C to 600°C could be due to alumina support decomposition which could be seen in all DTG graphs irrespective of sulfided or non-sulfided catalysts [8].

Once again, for the alumina supported catalysts, the weight loss curve for UA and UB followed a consistent trend, and the weight loss percentage were approximately similar except for CoMo/Al (Figure 14B; under air). For example, under N_2 atmosphere, UA and UB demonstrated a 51% (Figure 14A: CoMo/Al),39% (Figure 14A: CoMo/Al), 40% (Figure 14C:S-CoMo/Al) and 36% (Figure 14C: S-CoMo/Al) weight loss respectively. As expected, the weight loss was higher under

air was higher and it could be mainly attributed to the decomposition of carbonaceous residue which are retained in the pores and cavities of the spent catalyst.

Overall, UB had lower weight loss compared to UA under nitrogen and air atmosphere. DTG curves (Figure 14J) under air shows that after 200℃, UB had a sharp decomposition peak at 573℃, while UA had three decomposition peaks at 512℃, 689℃, and 775℃ (Figure 14J). On the other hand, under N_2 atmosphere, UA, UB, and UC exhibited broad decomposition peaks but with overlapping temperature ranges ranging from 535℃ to 590℃. Therefore, multiple, sharp decomposition peaks of UA under air signify oxidation of coke deposits. From DTG curves, it looks like hard coke could have probably formed during hydrotreatment of algae and by blending the DTG temperature peaks shifted towards lower temperature regions.

Similarly, for the sulfided catalysts on alumina (Figure B14K-S) sharp decomposition peaks for UC (518℃), UB (535℃), and UA (574℃) could be seen. It is to be noted that a synergistic effect for the blended feedstock is apparent for the alumina support irrespective of the sulfidation source. For instance, the UB had lower decomposition peaks compared to UA alone but higher than UC. This phenomenon could be due to the fact that carinata oil could have been acting as a hydrogen donor and decreased the coke build up in the UB [7].

The fresh and UC spent catalysts followed a comparable trend for DF biochar supported catalysts. Approximately, 64% (Figure 14E; CoMo/DF) and 72% (Figure 14G; S-CoMo/DF) weight loss for fresh catalysts occurred under inert atmosphere. With introduction of air, a 13% weight loss occurred for fresh catalyst (Figure 14F; CoMo/DF), while a minor decrease 1.8% was seen for sulfided S-CoMo/DF. In terms of DTG curves under air (Figure 14N and Figure 14P), sharp decomposition peaks at approximately 450℃ for fresh and UC could be assigned to biochar

support structure decomposition. After sulfidation, these biochar decomposition peaks have been shifted to lower temperatures 420℃ (fresh) and 418℃ (UC).

UA (Figure 14N; 625℃, CoMo/DF; Figure 14P; 517℃, S-CoMo/DF), UB (Figure 14N 581℃, CoMo/DF; Figure 14P; 605 ℃, S-CoMo/DF) under air are blunt and broad peaks which are in sharp contrast with the N_2 atmosphere, this again could be attributed to the carbon deposition on the catalysts and the coke deposition within the pores, did not let the catalyst undergo complete oxidation. With sulfidation the UA and UB had their decomposition peaks shifted to higher temperatures under air (Figure 14P). Similarly, fresh catalyst's decomposition peaks showed at higher temperatures at 491℃ (S-CoMo/DF) and 567℃ (CoMo/DF). This highlights the fact that support combustion and coke decomposition took place under air. In terms of coke type, the DF supported catalysts produced hard coke as all the decomposition peaks were higher than 400℃.

[1] B. E. Eboibi, D. M. Lewis, P. J. Ashman, and S. Chinnasamy, "Effect of operating conditions on yield and quality of biocrude during hydrothermal liquefaction of halophytic microalga Tetraselmis sp," *Bioresour. Technol.*, vol. 170, pp. 20–29, Oct. 2014, doi: 10.1016/j.biortech.2014.07.083.

[2] D. López Barreiro *et al.*, "Influence of strain-specific parameters on hydrothermal liquefaction of microalgae," *Bioresour. Technol.*, vol. 146, pp. 463–471, Oct. 2013, doi: 10.1016/j.biortech.2013.07.123.

[3] T. A. Saleh, S. A. AL-Hammadi, I. M. Abdullahi, and M. Mustaqeem, "Synthesis of molybdenum cobalt nanocatalysts supported on carbon for hydrodesulfurization of liquid fuels," *J. Mol. Liq.*, vol. 272, pp. 715–721, Dec. 2018, doi: 10.1016/j.molliq.2018.09.118.

[4] P. Roy *et al.*, "Performance of biochar assisted catalysts during hydroprocessing of non-edible vegetable oil: Effect of transition metal source on catalytic activity," *Energy Convers. Manag.*, vol. 252, p. 115131, Jan. 2022, doi: 10.1016/j.enconman.2021.115131.

[5] A. P. Glotov, A. V. Vutolkina, N. A. Vinogradov, A. A. Pimerzin, V. A. Vinokurov, and Al. A. Pimerzin, "Enhanced HDS and HYD activity of sulfide Co-PMo catalyst supported on alumina and structured mesoporous silica composite," *Catal. Today*, vol. 377, pp. 82–91, Oct. 2021, doi: 10.1016/j.cattod.2020.10.010.

[6] M. Zarezadeh-Mehrizi, A. Afshar Ebrahimi, and A. Rahimi, "Comparison of γ and δ-Al2O3 supported CoMo catalysts in the hydrodesulfurization of straight-run gas oil," *Sci. Iran.*, vol. 0, no. 0, pp. 0–0, Feb. 2019, doi: 10.24200/sci.2019.50969.1948.

[7] Y. Yan *et al.*, "Coke and radicals formation on a sulfided NiMo/γ-Al2O3 catalyst during hydroprocessing of an atmospheric residue in hydrogen donor media," *Fuel Process. Technol.*, vol. 159, pp. 404–411, May 2017, doi: 10.1016/j.fuproc.2017.02.005.

[8] D. Redaoui, F. Sahnoune, M. Heraiz, and A. Raghdi, "Mechanism and Kinetic Parameters of the Thermal Decomposition of Gibbsite Al(OH)3 by Thermogravimetric Analysis," 2017, doi: 10.12693/APHYSPOLA.131.562.

APPENDIX C

8.3 Supplementary Information for Chapter 5

Hydrotreatment of Pyrolysis Bio-oil and Triglyceride Blends

Table C1. Physiochemical characterization of mildly hydrotreated pyrolysis oil.

Oil Properties	Mild hydrotreated pyrolysis oil (150°C, 2h)
C (wt.%)	54.68
H (wt.%)	5.94
O (wt.%)	38.32
HHV (MJ/kg)	23
TAN (mg KOH/g)	58
Density (g/cm3)	1.23
Kinematic Viscosity (m2/s)	42.6

Figure C1. Different phases of mildly hydrotreated oil.

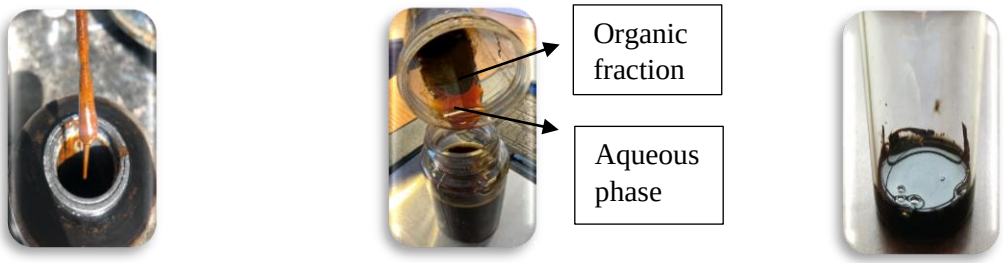

Step1: Mild hydrotreated bio-oil

Step2: Mild hydrotreated bio-oil after centrifugation

Step3: Organic fraction of the centrifuged oil used for severe hydrotreatment (water content 17%)

APPENDIX D

8.4 Supplementary Information for Chapter 6

Hydrocarbon biolubricants from hydrotreated renewable and waste derived liquid intermediates

Table D 1. Chemical composition of HAL bio-oil.

	Paraffin	**Area%**	**Olefin**	**Area%**
Hydrotreated HTL Algae Bio-oil	Pentadecane	9.8942	Tridecane	1.0955
	Heptadecane	8.4257	Naphthalene	1.0928
	Tetradecane	5.366	1-Heptadecene	0.8738
	Hexadecane	4.4013	Diphenylethyne	0.594
	"Hexadecane,	3.2935	5-Methyl-1-phenylhexa-1,3,4-triene	0.5559
	2,6,10,14-tetramethyl-"	2.8161		
	Tridecane	3.1294		
	Dodecane	1.9907		
	Nonadecane	0.8782		
	Tridecane	0.8655		
	Dodecane	0.8416		
	Undecane	0.7874		
	Dodecane	0.7528		
	Eicosane	1.0114		

	Decane	1.0114		
	Tetradecane	0.5193		
	1,9-Dichlorononane	0.3456		
Total		***44.97***		***4.21***

Table D1B: Chemical composition of HAL bio-oil.

	Napthene and Aromatics	**Area%**	**Oxygenates**	**Area%**
Hydrotreated HTL Algae Bio-oil	Cyclohexane, (1-methylpropyl)-	0.9604	Phenol, 3-(1-methylethyl)-	0.2912
	Cyclohexane, 1,1'-(1,3-propanediyl)bis-	0.9488	Phenol, 2,2'-methylenebis[6-(1,1-dimethylethyl)-4-ethyl-	0.3334
	Diphenylmethane	0.9807	Pyridine, 4-ethyl-, 1-oxide	0.3837
	1H-Pyrrolo[2,3-b]pyridine, 2-ethyl-	1.3986	Phenol, 3-(1-methylethyl)-	0.4782
	1H-Indene, 2,3-dihydro-4,7-dimethyl-	1.1388	Phenol, 3-(2-aminoethyl)-	0.3951
	1,4-Methanonaphthalene, 1,4-dihydro-	1.8698	n-Butanoic acid,methyl(tetramethylene)silyl ester	0.5233
	1H-Indene, 2,3-dihydro-5-methyl-	0.8614	Phenol, 3-(1-methylethyl)-	0.2912
	Benzene, 1,3,5-trimethyl-2-(1-methylethenyl)-	0.7954		
	Naphthalene, 1-methyl-	0.6979		
	1H-Indene, 2,3-dihydro-1,3-dimethyl-	0.5878		
	1,4-Methanonaphthalene, 1,4-dihydro-	0.5809		
	Naphthalene, 2,3-dimethyl-	0.54		
	1,4-Ethanoisoquinoline, 1,2,3,4-tetrahydro-2-methyl-	0.5348		
	Phthalazine, 1-methyl-	0.5299		
	3,3'-Dimethylbiphenyl	0.5136		
	1H-Indole, 2-methyl-	0.4771		
	1H-Indole, 1,2,3-trimethyl-	0.471		
	Naphthalene, 2-methyl-	0.4528		
	Naphthalene, 1,3-dimethyl-	0.4357		
	Naphthalene, 2-(1-methylethyl)-	0.4234		
	9H-Fluorene, 2,3-dimethyl-	0.4176		
	Total	***15.61***		***2.11***

Table D1C: Chemical composition of HCA bio-oil.

	Paraffin	**Area%**	**Olefin**	**Area%**
	Heneicosane	4.2675	10-Heneicosene (c,t)	0.8451
	Pentadecane	3.0839	1-Nonadecene	0.6992
	Heptadecane	2.6892	1-Nonadecene	0.6581
	Nonadecane	2.386	17-Pentatriacontene	0.5733
	Hexadecane	2.2346	1-Hexadecene	0.5214

Hydrotreated Carinata Bio-oil	Octadecane	1.9103	3-Eicosene, (E)-	0.4332
	Tridecane	1.908	9-Tricosene, (Z)-	0.4317
	Undecane	1.6485	1-Docosene	0.4309
	Tetradecane	1.6426	17-Pentatriacontene	0.4006
	Eicosane	1.532	9-Tricosene, (Z)-	0.4002
	Dodecane	1.3287	9-Tricosene, (Z)-	0.3722
	Docosane	1.3038	1-Nonadecene	0.3506
	Octadecane	1.259	1-Docosene	0.3469
	Heptadecane	1.1061	1-Hexacosene	0.3269
	Pentadecane	0.929	Pentadec-7-ene, 7-bromomethyl-	0.3226
	Pentacosane	0.8442	1-Heptadecene	0.2933
	Tetracosane	0.8317	1-Heptadecene	0.287
	Heptacosane	0.6975	4-Chlorobenzenesulfonamide, N-methyl-	0.2754
	Octacosane	0.6721		
	Hexacosane	0.5756		
	Decane, 1-iodo-	0.5711		
	Octacosane	0.457		
	Nonacosane	0.5102		
	Tridecane, 6-propyl-	0.5388		
	Decane, 1-iodo-	0.5711		
	Octadecane, 1-chloro-	0.515		
	Tetracosane	0.441		
	Tetracontane, 3,5,24-trimethyl-	0.4244		
	Octacosane	0.3501		
	1-Chloroeicosane	0.3348		
	Tricosane	0.2722		
	Total	***37.56***		***7.69***

Table D1D: Chemical composition of HCA bio-oil.

	Napthene and Aromatics	**Area%**	**Oxygenates**	**Area%**
Hydrotreated	"Dodecane, 1-cyclopentyl-4-(3-cyclopentylpropyl)-"	0.883 0.8242	13-Tetradecen-1-ol acetate Phenol, 2,2'-methylenebis[6-(1,1-dimethylethyl)-4-ethyl-	0.5428 0.9401
	Cyclooctadecane, ethyl-	0.7899	1-Docosanethiol	0.5388
	Cyclohexane, octyl-	0.7516	13-Tetradecen-1-ol acetate	0.5428
	Cyclohexane, 1,2-dimethyl-3-pentyl-4-propyl-	0.7359	Oxirane, tetradecyl-	0.4521
	Undecane, 2-cyclohexyl-	0.7342	Octadecanal	0.4076
	Heptylcyclohexane	0.7199	1-Docosanethiol	0.3843
	Cyclohexane, 1,1'-(1,4-butanediyl)bis-	0.6095	Oxalic acid, cyclohexylmethyl octyl ester	0.3749
	Heptylcyclohexane	0.4534	7-Oxabicyclo[4.1.0]heptane, 1,5-dimethyl-	0.3434

Carinata Bio-oil	Cyclohexane, 1-(1,5-dimethylhexyl)-4-(4-methylpentyl)-	0.4734	p-Menth-8(10)-en-9-ol, cis-	0.335
	Cyclopentane, 1,1'-[4-(3-cyclopentylpropyl)-1,7-heptanediyl]bis-	0.4597	E-14-Hexadecenal	0.3166
	Cyclohexane, 1-(1,5-dimethylhexyl)-4-(4-methylpentyl)-	0.5289	1,2-Benzisothiazole, 3-(hexahydro-1H-azepin-1-yl)-, 1,1-dioxide	0.3145
	Cyclotetradecane	0.4353	Oxirane, 2-decyl-3-(5-methylhexyl)-, cis-(.+/-.)-	0.2857
	Cyclohexane, 1-(1,5-dimethylhexyl)-4-(4-methylpentyl)-	0.4239	Oxalic acid, isobutyl octadecyl ester	0.2834
	Cyclotetracosane	0.4135		
	Cyclohexane, 1,2-dimethyl-3-pentyl-4-propyl-	0.3913		
	Cyclotetradecane, 1,7,11-trimethyl-4-(1-methylethyl)-	0.3619		
	Cycloheptane, methyl-	0.3523		
	Cyclohexane, 1,2,3,5-tetraisopropyl-	0.3435		
	Cyclohexane, 1-(1,5-dimethylhexyl)-4-(4-methylpentyl)-	0.3425		
	Cyclohexane, 1-(1,5-dimethylhexyl)-4-(4-methylpentyl)-	0.3383		
	Cyclohexane, 1,2-dimethyl-3-pentyl-4-propyl-	0.3252		
	Cyclotetradecane, 1,7,11-trimethyl-4-(1-methylethyl)-	0.3159		
	Cyclotetradecane, 1,7,11-trimethyl-4-(1-methylethyl)-	0.3145		
	Cyclopentane, 1,2-dipropyl-	0.3141		
	Cyclopentane, 1,1'-ethylidenebis-	0.309		
	Cyclohexane, 1,2-dimethyl-3-pentyl-4-propyl-	0.4033		
	Dodecane, 3-cyclohexyl-	0.281		
	Cyclohexane, 2-propenyl-	0.2795		
	Total	14.18		6.06

Table D1E: Chemical composition of HPF bio-oil.

	Paraffin	**Area%**	**Olefin**	**Area%**
	Heptadecane	9.3587	1-Tetradecene	2.6867
	Pentadecane	4.6727	Hexadecanedinitrile	0.8061

Hydrotreated Poultry Fat Bio-oil	Hexadecane	2.9488	1-Hexacosene	0.79
	Heptadecane	1.8351	1-Docosene	0.6858
	Octadecane	1.5338	Z-5-Nonadecene	0.5661
	Tetracosane	1.0481	1-Tridecene	0.4579
	Nonadecane	0.9709	1-Nonadecene	0.4474
	Pentacosane	0.9464	17-Pentatriacontene	0.416
	Eicosane	0.9059	Pentadec-7-ene, 7-bromomethyl-	0.4061
	Tricosane	0.9035	3,4-Octadiene, 7-methyl-	0.3891
	Heptadecane	0.7947	17-Pentatriacontene	0.3709
	Heneicosane	0.7825	17-Pentatriacontene	0.3688
	Octadecane	0.7617	1-Nonadecene	0.3423
	Hexacosane	0.7396	2-Pentadecanone	0.3308
	Pentadecane	0.6828	1-Heptadecene	0.3066
	Octacosane	0.6119	Nonadecanenitrile	0.3065
	Nonacosane	0.5789	17-Pentatriacontene	0.3062
	Octadecane, 1-chloro-	0.4949	17-Pentatriacontene	0.2854
	Tridecane	0.4006		
	Heptacosane	0.3254		
	Cyclopentadecane	0.3088		
	Triacontane	0.3025		
	Total	***31.90***		***9.98***

Table D1F: Chemical composition of HPF bio-oil.

	Napthene and Aromatics	**Area%**	**Oxygenates**	**Area%**
Hydrotreated Poultry Fat Bio-oil	Cyclohexane, 1,1'-(1,3-propanediyl)bis-	0.9514	1-Eicosanol	1.9015
	Cyclohexane, 1,1'-(1,4-butanediyl)bis-	0.8846	Oxalic acid, cyclobutyl hexadecyl ester	1.2607
	Cyclohexane, octyl-	0.7048	1,2-Benzisothiazole, 3-(hexahydro-1H-azepin-1-yl)-, 1,1-dioxide	0.6823
	Cyclohexane, 1,2,4,5-tetraethyl-, (1.alpha.,2.alpha.,4.alpha.,5.alpha.)-	0.5974	1,2-Benzisothiazole, 3-(hexahydro-1H-azepin-1-yl)-, 1,1-dioxide	0.6364
	Cycloheptane, methyl-	0.5008	3-(6,6-Dimethyl-5-oxohept-2-enyl)-cyclohexanone	0.5354
	Cyclopentadecane	0.8451	E-14-Hexadecenal	0.5252
	Cyclotetradecane, 1,7,11-trimethyl-4-(1-methylethyl)-	0.4364	2,6,10,14-Tetramethylpentadecan-7-one	0.5173
	Benzene, 1-chlorodifluoromethoxy-4-nitro-	0.427	E-11-Methyl-12-tetradecen-1-ol acetate	0.4925
	Cyclopentadecane	0.414	Dichloroacetic acid, heptadecyl ester	0.4909
	Cyclohexane, 1-(1,5-dimethylhexyl)-4-(4-methylpentyl)-	0.3846	Oxirane, tetradecyl-	0.4712
	Cyclooctane, cyclohexyl-	0.3754	4-Chlorobenzenesulfonamide, N-methyl-	0.4678
	Cyclohexane, (1-methylethyl)-	0.3402	22-Tricosenoic acid	0.4668
	Benzene, 1-chlorodifluoromethoxy-4-nitro-	0.3378	2-Pentadecanone	0.4503
	1H-Indene, 2-butyl-5-hexyloctahydro-	0.314	Phenol, 2,2'-methylenebis[6-(1,1-dimethylethyl)-4-ethyl-	0.4476

	1H-Indene, 2-butyl-5-hexyloctahydro-	0.5776	Oxalic acid, cyclohexylmethyl isohexyl ester	0.4384
	Cyclohexane, 1-(1,5-dimethylhexyl)-4-(4-methylpentyl)-	0.2811	2-Dodecen-1-yl(-)succinic anhydride	0.4031
			1-Pentacosanol	0.3694
			1,2-Benzisothiazole, 3-(hexahydro-1H-azepin-1-yl)-, 1,1-dioxide	0.358
			1,2-Benzisothiazole, 3-(hexahydro-1H-azepin-1-yl)-, 1,1-dioxide	0.3562
			4H-Pyran-4-one, 2,3-dihydro-2-[1-(benzyloxy)ethyl]-	0.3552
			1,2-Benzisothiazole, 3-(hexahydro-1H-azepin-1-yl)-, 1,1-dioxide	0.3542
			2- Chloropropionic acid, octadecyl ester	0.3467
			.beta.-Resorcylic acid, 3-(3,7-dimethyl-2,6-octadienyl)-6-pentyl-, ethyl ester, (E)-	0.3331
			2,10-Dodecadien-1-ol, 3,7,11-trimethyl-, (E)-(.+/-.)-	0.3127
			Phenol, 2,2'-methylenebis[6-(1,1-dimethylethyl)-4-ethyl-	0.3041
			1,2-Benzisothiazole, 3-(hexahydro-1H-azepin-1-yl)-, 1,1-dioxide	0.2942
			1,2-Benzisothiazole, 3-(hexahydro-1H-azepin-1-yl)-, 1,1-dioxide	0.2923
			E-8-Methyl-9-tetradecen-1-ol acetate	0.2906
			E-10-Methyl-11-tetradecen-1-ol acetate	0.2897
			Oxirane, tetradecyl-	0.2772
	Total	***8.37***		***14.92***

Table D1G: Chemical composition of HSS bio-oil.

	Paraffins	**Area%**	**Olefins**	**Area%**
	Pentadecane	3.8064	1,4-Methanonaphthalene, 1,4-dihydro-	0.4278
	Heptadecane	3.4038	Phenanthrene, 1-methyl-	0.3063
	Tridecane	3.2103	Phenanthrene, 1-methyl-	0.3012
	Hexadecane	2.1451	4-Tetradecene, (E)-	0.2374
	Tetradecane	2.1069	Benzocycloheptatriene	
	Undecane	1.8301		
	Eicosane	1.477		
	Pentadecane	1.2676		
	Heneicosane	1.1086		
	Pentadecane, 2-methyl-	1.0535		
	Nonadecane	0.9836		
	Tetradecane	0.8526		

Hydrotreated HTL Sewage Sludge Bio-oil	Tridecane, 2-methyl-	0.8508		
	Octadecane	0.8		
	Octadecane	0.7597		
	Hexadecane	0.7192		
	Tricosane	0.6567		
	Pentacosane	0.6327		
	Tridecane, 7-propyl-	0.5414		
	Hexadecane, 2-methyl-	0.541		
	Undecane	0.5309		
	Docosane	0.5255		
	Heptadecane	0.5036		
	Undecane	0.4495		
	Undecane	0.4348	Phenol, 2,2'-methylenebis[6-(1,1-dimethylethyl)-4-ethyl-	0.3041
	Undecane	0.4082	1,2-Benzisothiazole, 3-(hexahydro-1H-azepin-1-yl)-, 1,1-dioxide	0.2942
	Tetracosane	0.3533	1,2-Benzisothiazole, 3-(hexahydro-1H-azepin-1-yl)-, 1,1-dioxide	0.2923
	Tridecane, 2-methyl-	0.3529	E-8-Methyl-9-tetradecen-1-ol acetate	0.2906
	Nonacosane	0.3444	E-10-Methyl-11-tetradecen-1-ol acetate	0.2897
	Pentadecane, 8-hexyl-	0.3437	Oxirane, tetradecyl-	0.2772
	Octacosane	0.3429		14.92
	Dodecane, 2-methyl-	0.3241		
	Dodecane	0.3213		
	Dodecane	0.3048		
	Pentadecane	0.2159		
	1,1,1,3,5,5,5-Heptamethyltrisiloxane	0.2225		
	Hexadecane	0.2281		
	Pentadecane, 3-methyl-	0.2312		
	Undecane	0.2391		
	Hexadecane	0.2439		
	Tridecane, 3-methyl-	0.2609		
	Hexacosane	0.2622		
	Methylene Chloride	0.2643		
	Total	***36.455***		***1.79***

Table D1H: Chemical composition of HSS bio-oil.

	Napthene and Aromatics	**Area%**	**Oxygenates**	**Area%**
	1H-Indole, 5,7-dimethyl-	1.4276	Disulfide, di-tert-dodecyl	1.7257
	1H-Indole, 2,3,5-trimethyl-	0.8338	(3H,6H)Thieno[3,4-c]isoxazole, 3a,4-dihydro-6-methyl-	0.8909
	1H-Indole, 2-methyl-	0.7523	3-Butenamide, N-1-(1-naphthyl)ethyl-	0.6692
	1H-Indole, 2,3-dimethyl-	0.6008	Cyclohexanecarboxylic acid, 1-naphthyl ester	0.4752
	Benzene, (3-methyl-2-butenyl)-	0.5951	Phenol, 2,5-dimethyl-	0.4704
	Indole, 1,7-dimethyl-	0.4754	1-Methyl-2-formylindole	0.4218

Hydrotreated HTL Sewage Sludge Bio-oil	Naphthalene, 1,4,6-trimethyl-	0.4401	1,8-Nonadien-3-ol	0.304
	Benzenamine, 3-methyl-	0.4382	Phenol, 4-methyl-	0.2951
	3-Isoquinolinamine	0.4087	1,8-Nonadien-3-ol	0.304
	1,4-Ethanoisoquinoline, 1,2,3,4-tetrahydro-2-methyl-	0.4086	Phenol, 4-methyl-	0.2951
	3-Methylpyridazine	0.3894	Isoquinoline, 3,4-dihydro-1,3,3-trimethyl-	0.3622
	Indole, 1,7-dimethyl-	0.3708	5-Methyl-2-trimethylsilyloxy-acetophenone	0.1998
	Naphthalene, 2,7-dimethyl-	0.3678	Phenol, 2-ethyl-6-methyl-	0.2096
	Cyclotetradecane	0.5156	Phenol, 2,2'-methylenebis[6-(1,1-dimethylethyl)-4-ethyl-	0.2128
	2,4'-Bipyridine	0.3353	Fluorene, 4-[1,2-dihydroxyethyl]-	0.2178
	Cyclotrisiloxane, hexamethyl-	0.3303	Phenol, 2-ethyl-4-methyl-	0.2196
	Cyclohexane, 1-ethynyl-1-isocyano-	0.326	1,8-Nonadien-3-ol	0.2182
	Benzene, 1-methoxy-3-methyl-	0.3253	5H-Dibenz[b,f]azepine-5-carboxamide, 10,11-dihydro-	0.2241
	1H-Indole, 2-methyl-	0.3228	n-Butanoic acid,methyl(tetramethylene)silyl ester	0.2259
	1H-Indene, 2,3-dihydro-1,3-dimethyl-	0.3224	Benzeneethanamine, 2-fluoro-.beta.,3-dihydroxy-4-methoxy-	0.2338
	Azulene, 4,6,8-trimethyl-	0.3123	4,4-Dimethoxy-6-pentyl-cyclohex-2-enone	0.2394
	1,4-Ethanoisoquinoline, 1,2,3,4-tetrahydro-2-methyl-	0.3025	Benzenepropanol, .gamma.-phenyl-	0.2441
	Phthalazine, 1-methyl-	0.2961	3,5-Cyclohexadiene-1,2-dione, 3,4,5,6-tetrachloro-	0.2483
	2-Ethyladamantane	0.2909	1,8-Nonadien-3-ol	0.2453
	Indolizine	0.7315	Cycloheptanol, 2-methylene	0.2504
	1-Phenyl-1-butene	0.5411	Silicic acid, diethyl bis(trimethylsilyl) ester	0.257
	Benzo[h]quinoline, 2,4-dimethyl-	0.2004	cis-8-Ethyl-bicyclo[4.3.0]non-3-ene	0.263
	3-Methylcarbazole	0.2084	Phenol, 2,4-dimethyl-	0.2685
	2,3,7-Trimethylindole	0.2077	N-Methoxy-2-carbomethoxy-2-carbethoxyaziridine	0.28
	5-(o-Tolyl)-1H-tetrazole	0.2023		
	1-Naphthalenol, 4-methyl-	0.2124		
	1H-Indole, 2-methyl-	0.2107		
	5H-Dibenz[b,f]azepine-5-carboxamide, 10,11-dihydro-	0.2241		
	2,3,7-Trimethylindole	0.2256		
	Naphthalene, 2,7-dimethyl-	0.2287		
	1H-Pyrrole-2-acetonitrile, 1-methyl-	0.2295		
	2,3,7-Trimethylindole	0.2311		
	Indolizine, 2,5-dimethyl-	0.237		
	1H-Indole, 2-methyl-	0.2382		
	5H-Dibenz[b,f]azepine, 10,11-dihydro-	0.2493		
	Phthalazine, 1-methyl-	0.2536		
	Indole, 1,7-dimethyl-	0.2585		
	1H-Indole, 1,2,3-trimethyl-	0.263		
	3-Methylcarbazole	0.28		
	Total	***16.612***		***10.471***

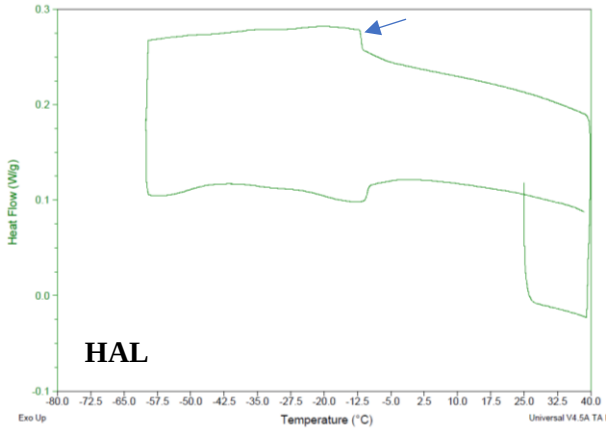
HAL
Heat Flow (W/g)
Temperature (°C)
Exo Up

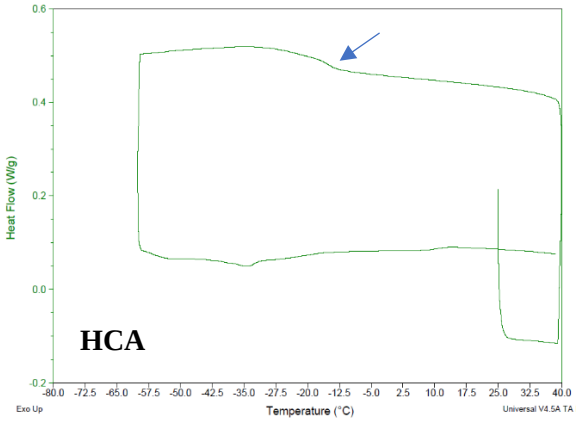
HCA
Heat Flow (W/g)
Temperature (°C)
Exo Up

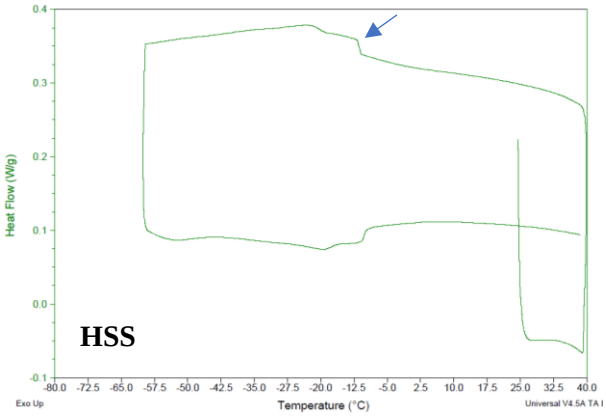
HSS
Heat Flow (W/g)
Temperature (°C)
Exo Up

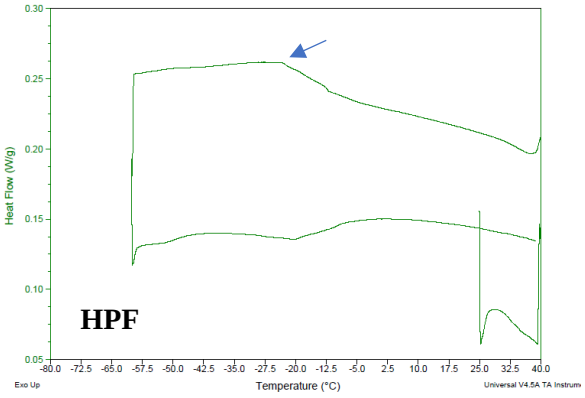
HPF
Heat Flow (W/g)
Temperature (°C)
Exo Up

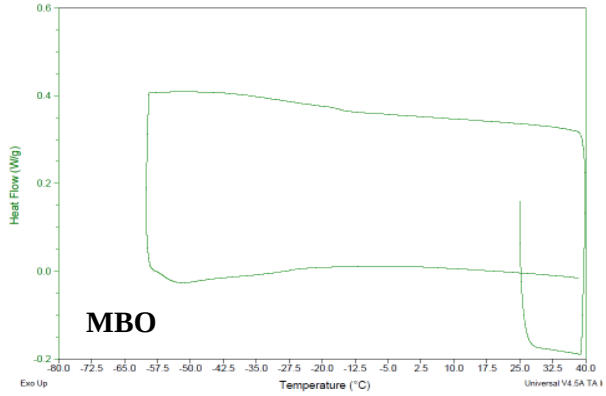
MBO
Heat Flow (W/g)
Temperature (°C)
Exo Up

Figure D 1. DSC thermograms for the hydrotreated bio-oils and mineral base oil for pour point measurement.

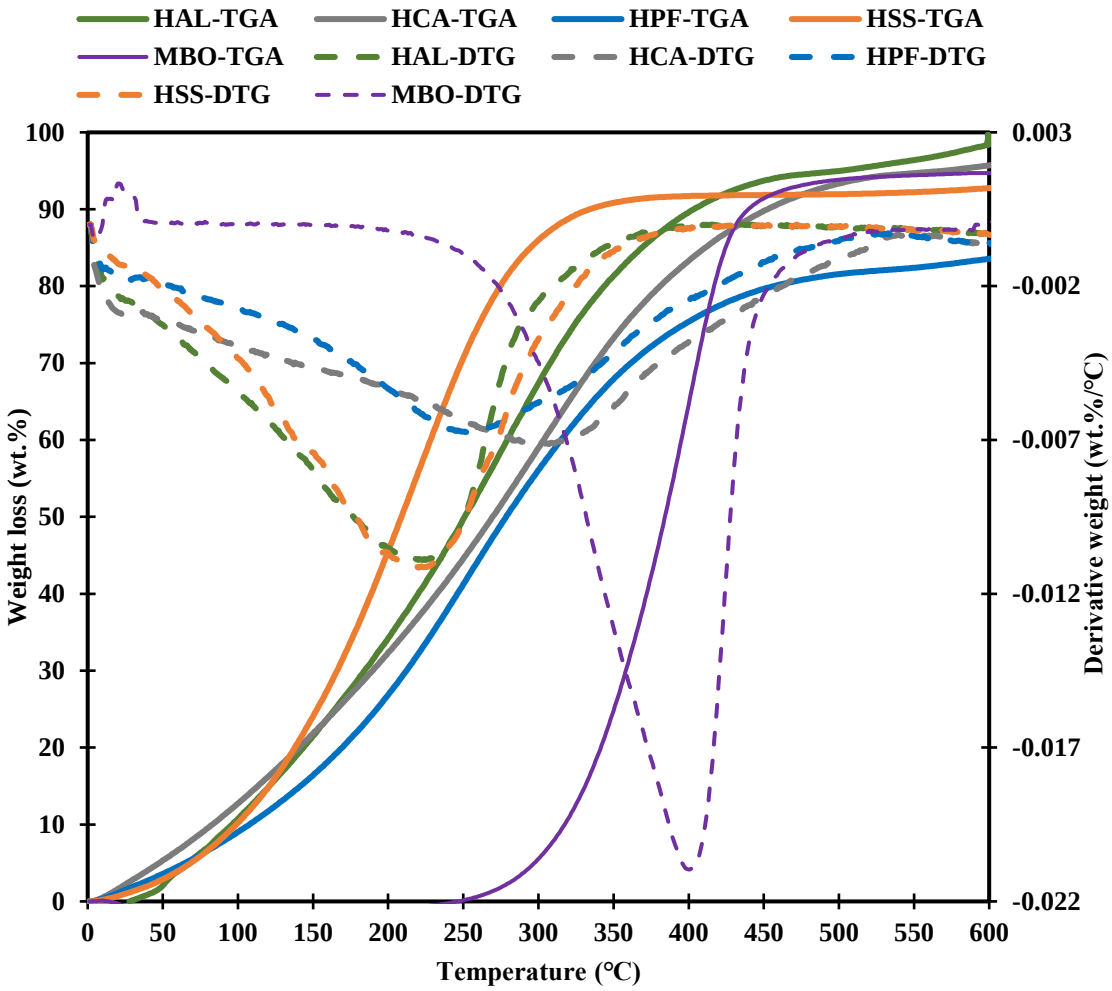

Figure D 2. TGA and DTG thermograms for the hydrotreated bio-oils and mineral base oil under inert atmosphere.